

To Pauline

BUBBLES IN FLUIDISED BEDS

A thesis submitted

by

STEPHEN PHILIP WATKINS

for the degree of
Doctor of Philosophy

Department of Chemical Engineering
University of Aston in Birmingham

March 1971

-5 MAY 71 157320

S U M M A R Y

The aim of the investigation was to measure accurately the growth rate of small bubbles in gas fluidised beds.

This was achieved by recording individually injected known volumes of gas into a bed operating in its particulate regime. The systems investigated were ballotini, catalyst and diakon fluidised with both air and carbon dioxide under ambient conditions.

The bubble volume, and hence growth rate, was measured by a capacitance technique and volumes from 0.1 to 8.0cm³ could be measured with an overall accuracy of better than $\pm 10\%$. The accuracy of the measurement of capacitance was ± 0.002 pF and the range over which capacitance measurements were made was 0.30 to 0.70pF. The instrument followed a square wave with no apparent time lag when using a galvanometer with a linear frequency response of up to 100Hz.

It was found that a meta-stable bubble phenomenon exists for all the systems investigated. That is, under given particulate conditions, a bubble greater than the stable size will grow and one smaller will shrink and vanish. It was found that meta-stable bubble volumes less than 4cm³ could be correlated with gas velocity by an equation of the form:

$$(\text{Meta-stable volume})(\text{gas velocity in excess of the minimum fluidising velocity})^n = \text{a constant.}$$

(where n is a constant for a given system.)

Growth rates measured covered the range -0.15 to +0.25 (cm³/cm travelled) and the growth rate constants were found to cover the range 10 to 70 (cm).

It is shown that the meta-stable phenomenon can be explained in terms of bubble shape, assuming the shape is a function of a bubble Reynolds Number.

C O N T E N T S

SUMMARY	i
LIST OF CONTENTS	ii
LIST OF FIGURES	viii
LIST OF TABLES	xi
ACKNOWLEDGEMENTS	xii
1 <u>INTRODUCTION</u>	1
2 <u>LITERATURE REVIEW</u>	3
2.1. Introduction	3
2.2. Fluidised bed properties	4
2.2.1. The two-phase theory	4
2.2.2. Velocity of a single bubble	8
2.2.3. Pressure in a bubble	11
2.2.4. Voidage above a bubble	12
2.2.5. Gas flow in and around a bubble	13
2.2.6. Coalescence of bubbles	15
2.2.7. Particle movement due to bubbles	15
2.2.8. Gas leakage from bubbles during formation	16
2.2.9. Viscosity	16
2.3. Transition region	18
2.3.1. Relationship between aggregative and particulate fluidisation	18
2.3.2. Expansion of particulate fluidised beds	19
2.3.3. Injected bubbles	21
2.3.3.1. Bubble stability in a gas fluidised bed behaving particulate	21
2.3.3.2. Bubble growth in a gas fluidised bed behaving particulate	29

2.3.3.3.	Conclusions from previous work on injected bubbles in a gas fluidised bed behaving particulatey	30
2.4.	Techniques for measuring bubble volumes in gas fluidised beds	31
3	<u>BUBBLE STABILITY THEORIES</u>	34
4	<u>APPARATUS</u>	47
4.1.	Air supply	47
4.2.	Bubble injector system	51
4.3.	Fluidised bed container	55
4.4.	Distributors for gas fluidised bed	58
4.4.1.	Sintered Bronze	58
4.4.2.	Filter paper	58
4.4.3.	Vyon	58
4.4.4.	Vyon and filter paper	59
4.5.	Distributor for liquid fluidised bed	60
4.6.	Closure of Section 4	61
5	<u>INSTRUMENTATION</u>	62
5.1.	Introduction	62
5.2.	General arrangement of instruments	63
5.3.	The bridge	65
5.4.	The autobalance	69
5.4.1.	The autobalance circuit	69
5.4.2.	The autobalance outputs	69
5.5.	The amplifier	72
5.5.1.	The amplifier circuit	72
5.5.2.	The DC power supply	73
5.6.	UV oscillograph S.E.Labs. Type 200 Mk.II	76
5.6.1.	Oscillograph specification	76
5.6.2.	Oscillograph galvanometers	76

5.7.	Oscilloscope teleequipment Type D43	78
5.8.	Transducer: S.E.Labs. Type 150/D	79
5.9.	Closure of Section 5	80
6	<u>CALIBRATION</u>	81
6.1.	Design of the probe	81
6.2.	Bridge calibration	86
6.2.1.	Steady state calibration	86
6.2.2.	Unsteady state calibration	87
6.3.	Integrator calibration	92
6.4.	Electrical interference	93
6.5.	Theory of capacitance	94
6.5.1.	Relationship between different dielectrics	94
6.5.2.	Shape of the electric field (single dielectric)	94
6.5.3.	Shape of the electric field (two dielectrics)	95
6.6.	Capacitance change created by a bubble passing between the plates	97
6.6.1.	Oscillograph bubble trace	97
6.6.2.	Discussion of blips x_p and x_p^1	97
6.6.3.	Discussion of the peak	99
6.7.	Readings required from the trace	100
6.7.1.	Capacitance equivalent to the bed voidage during the bubble ascent	100
6.7.2.	Basic capacitance at which the bubble was measured	100
6.8.	Injector calibration	102
6.9.	Investigation of the size of an injected bubble	103
6.10.	Fluidising gas flow measurements	108
6.10.1.	Introduction	108
6.10.2.	Variable area flow meter theory	108
6.10.3.	Effect of atmospheric pressure changes	109

6.10.4. Effect of bed pressure drop changes	110
6.10.5. Flow meter calibration	111
6.11. Determination of probe dimensions	112
6.11.1. Determination of plate gap	112
6.11.2. Determination of plate width	113
6.11.3. Determination of plate height	113
6.12. Factors affecting the basic capacitance reading	117
6.12.1. Outside interference	117
6.12.2. Depth of the probe in the bed	117
6.12.3. Capacitance change due to injector tube	117
6.12.4. Screening of the plates	119
6.13. Probe calibration	123
6.13.1. Calibration theory	123
6.13.2. Calibration materials	126
6.13.3. Calibration technique	127
6.13.4. Calibration results	128
6.14. Relationship between the dielectric constant and the voidage of the dense phase of a fluidised bed	133
6.14.1. Theory	133
6.14.2. Experimental	136
6.15. Closure of Section 6	143
7 <u>PARTICLES</u>	144
7.1. Required particle properties	144
7.1.1. Shape	144
7.1.2. Size	144
7.1.3. Uniformity of size	144
7.1.4. Density	144
7.1.5. Electrical properties	144
7.2. Choice of materials	146

7.2.1.	Glass	146
7.2.2.	Cracking catalyst	146
7.2.3.	Diakon	146
7.2.4.	Others	147
7.3.	Sieving of materials	148
7.3.1.	Glass	148
7.3.2.	Catalyst	148
7.3.3.	Diakon	149
7.4.	Density determination	154
7.4.1.	Glass	154
7.4.2.	Catalyst	156
7.4.3.	Diakon	157
8	<u>RESULTS</u>	161
8.1.	Determination of the incipient fluidising velocities	161
8.2.	Bed expansion	166
8.2.1.	Bed expansion at gas velocities in the range $U_o < U_s < U_{mb}$	166
8.2.2.	Bed expansion at gas velocities in the range $U_s > U_{mb}$	166
8.3.	Injection effect	170
8.4.	Bubble stability	174
8.4.1.	Procedure	174
8.4.2.	Results	174
8.5.	Velocity of a single bubble	185
8.6.	Rate of growth of single bubbles	187
9	<u>DISCUSSION OF RESULTS</u>	197
9.1.	Determination of incipient fluidising velocities	197
9.1.1.	Discussion of gradient in Figs. 8.1.(1-3)	197
9.1.2.	Discussion of discrepancy between theoretical and recorded bed pressure at U_o	198

9.2.	Discussion of bed expansion results	199
9.2.1.	Bed expansion for gas velocities in the range $U_o < U_s < U_{mb}$	199
9.2.2.	Bed expansion at gas velocities in the range $U_s > U_{mb}$	200
9.3.	Injection effect	201
9.4.	Bubble stability	202
9.4.1.	Limits of meta-stable bubble phenomenon	202
9.4.2.	Physical properties affecting the meta-stable volume	204
9.4.3.	Theoretical explanation of the meta-stable phenomenon	204
9.5.	Rate of rise of a bubble	210
9.6.	Rate of growth of single bubble	211
9.6.1.	Relationship between dV_b/dh_s and V_b	211
9.6.2.	Variation in K for different systems	212
9.6.3.	Relationship between K and V_b	212
10	<u>CONCLUSIONS</u>	214
11	<u>SUGGESTIONS FOR FUTURE WORK</u>	217
	<u>APPENDIX</u>	
A 1.	Derivation of the relationship between the gas flow rate at atmospheric pressure (G_a) and the flow rate indicated by the VA flow meter ^a (G_c)	219
A 2.	Relationship between the dielectric constant and the voidage of the dense phase of a fluidised bed	221
A 3.	Results of the injection effect investigation	224
A 4.	Results of the bubble stability investigation	226
	NOMENCLATURE	253
	BIBLIOGRAPHY	258

LIST OF FIGURES

Fig. 2.3.3.1.(1)	22
Fig. 2.3.3.1.(2)	22
Fig. 2.3.3.1.(3)	24
Fig. 2.3.3.1.(4)	24
Fig. 2.3.3.1.(5)	26
Fig. 2.3.3.1.(6)	26
Fig. 3.(1)	40
Fig. 3.(2)	45
Fig. 4.1.(1)	49
Fig. 4.1.(2)	50
Fig. 4.2.(1)	53
Fig. 4.2.(2)	54
Fig. 4.3.(1)	56
Fig. 4.3.(2)	57
Fig. 5.2.(1)	63
Fig. 5.2.(2)	64
Fig. 5.3.(1)	66
Fig. 5.4.1.(1)	70
Fig. 5.5.1.(1)	74
Fig. 5.5.1.(2)	75
Fig. 6.1.(1)	83
Fig. 6.1.(2)	84
Fig. 6.1.(3)	85
Fig. 6.2.2.(1)	88
Fig. 6.2.2.(2)	88
Fig. 6.2.2.(3)	90

Fig. 6.5.2.(1)	96
Fig. 6.5.3.(1)	96
Fig. 6.6.1.(1)	98
Fig. 6.6.2.(1A and 1B)	98
Fig. 6.6.3.(1)	99
Fig. 6.9.(1)	105
Fig. 6.9.(2)	106
Fig. 6.9.(3)	107
Fig. 6.11.3.(1)	114
Fig. 6.11.3.(2)	116
Fig. 6.12.2.(1)	118
Fig. 6.12.3.(1)	120
Fig. 6.13.1.(1)	124
Fig. 6.13.4.(1)	130
Fig. 6.13.4.(2)	131
Fig. 6.13.4.(3)	132
Fig. 6.14.1.(1)	133
Fig. 6.14.1.(2)	139
Fig. 6.14.2.(1)	140
Fig. 6.14.2.(2)	141
Fig. 6.14.2.(3)	142
Fig. 7.3.1.(1)	150
Fig. 7.3.2.(1)	151
Fig. 7.3.2.(2)	152
Fig. 7.3.3.(1)	153
Fig. 7.4.1.(1)	158
Fig. 7.4.1.(2)	159
Fig. 7.4.1.(3)	160
Fig. 8.1.(1)	163

Fig. 8.1.(2)	164
Fig. 8.1.(3)	165
Fig. 8.2.1.(1)	168
Fig. 8.2.1.(2)	169
Fig. 8.3.(1)	172
Fig. 8.3.(2)	173
Fig. 8.4.2.(1)	177
Fig. 8.4.2.(2)	178
Fig. 8.4.2.(3)	179
Fig. 8.4.2.(4)	180
Fig. 8.4.2.(5)	181
Fig. 8.4.2.(6)	182
Fig. 8.4.2.(7)	183
Fig. 8.4.2.(8)	184
Fig. 8.5.(1)	186
Fig. 8.6.(1)	189
Fig. 8.6.(2)	190
Fig. 8.6.(3)	191
Fig. 8.6.(4)	192
Fig. 8.6.(5)	193
Fig. 8.6.(6)	194
Fig. 8.6.(7)	195
Fig. 8.6.(8)	196
Fig. 9.1.1.(1)	198
Fig. 9.4.1.(1)	203
Fig. 9.4.3.(1)	205
Fig. 9.4.3.(2)	208
Fig. 9.4.3.(3)	209
Fig. 9.6.1.(1)	211

L I S T O F T A B L E S

Table 2.3.3.1.(1)	27
Table 3.(1)	41
Table 6.13.1.(1)	125
Table 6.13.2.(1)	126
Table 8.1.(1)	162
Table 9.2.1.(1)	199
Table A.3.(1)	225
Table A.3.(2)	225
Tables A.4.1.(1 - 12)	227 - 232
Tables A.4.2.(1 - 14)	233 - 239
Tables A.4.3.(1 - 13)	240 - 245
Tables A.4.4.(1 - 9)	246 - 250
Tables A.4.5.(1 - 4)	251 - 252

A C K N O W L E D G E M E N T S

I should like to acknowledge my debt to my supervisor, Dr. D. E. Creasy, for his guidance and support throughout this work.

I should like to thank Professor G. V. Jeffreys, Head of the Department of Chemical Engineering, University of Aston in Birmingham, for providing the research facilities; the Science Research Council and the University of Aston for their financial aid; Chief Technician, Mr. N. Roberts, and his staff for their assistance with equipment; Mrs. Linda Handley for typing the draft copy of this thesis and my wife for typing the final copy and assisting with its compilation.

I N T R O D U C T I O N

Gas fluidised beds have been used for many years as heat treatment baths and for both chemical and physical processing operations. It is known that the efficiency with which a fluidised bed performs its desired function is controlled by the number and size of the bubbles in the bed, but as yet comparatively little is known concerning the causes of bubble nucleation and the factors which control, and possibly limit, their growth. In order to discuss fluidised beds further, it is first necessary to define several of the commonly used expressions.

A fluidised bed is usually said to be at the point of incipient fluidisation when the bed pressure drop is just sufficient to support the weight of the particles comprising the bed. The superficial fluid velocity required to generate this pressure drop is the incipient fluidising velocity (U_0).

When a fluidised bed has a superficial fluidising velocity in excess of U_0 , then, if the excess fluid passes through the bed in the form of bubbles, the bed is said to be aggregatively fluidised, but if the bed merely expands uniformly to accommodate the excess fluid velocity, such that no bubbles form, the bed is said to be particulate fluidised.

It has been found that gas fluidised beds normally fluidise aggregatively, although in a few extreme cases they have been found to behave particulate over a limited range of fluidising air flow rates. Conversely, though normally particulate in behaviour, a few liquid fluidised beds have been found to behave aggregatively. From these observations it appears that there is

no fundamental difference between an aggregatively fluidised bed and a particulate fluidised one. Therefore, if a study were made of the properties of the beds which operate in the transition region between aggregative and particulate fluidisation, information might be obtained about the parameters controlling the nucleation and growth of bubbles.

L I T E R A T U R E R E V I E W

2.1. INTRODUCTION

This literature review discusses the papers on the general properties of gas fluidised beds with respect to the effect of these properties on bubbles; and then the work that has been carried out in the transition region between particulate and aggregative fluidisation is examined in more detail.

From the gaps in knowledge apparent from this review, it is concluded that further work should entail accurate measurement of bubble volumes and therefore the various methods of bubble size and bed voidage determination are also surveyed. It is shown that a capacitance technique has considerable advantages over other techniques, provided the capacitance change caused by a given bubble volume can be accurately predicted.

As there is some evidence of a meta-stable bubble size, the review concludes (Section 3) with a critical analysis of the published theories on bubble stability, in an attempt to determine if any can be used to predict the existence of this meta-stable bubble state.

2.2. FLUIDISED BED PROPERTIES

2.2.1. The Two-Phase Theory

Though it is now widely accepted that an aggregative fluidised bed consists of two "phases", a particulate phase of fluidised particles and a bubble phase virtually empty of particles, there is considerable argument as to the division of the fluidising gas between the two. In the initial "two-phase theory" it was suggested that the gas velocity in the dense phase was equal to the incipient fluidising velocity, that the dense phase voidage was therefore the voidage existing at incipient fluidisation (e_0), and that all the surplus gas above that required for incipient fluidisation passed through the bed in the form of bubbles. This theory was accepted by Davidson and Harrison⁽¹⁾, but in a later review by Harrison⁽²⁾ it is noted that several workers have reported that their experimental results disagree with this theory, especially near the distributor where a value as high as $6U_0$ has been suggested⁽³⁾.

This conflict between theory and experimental results prompted further study of the two-phase theory. Partridge and Rowe⁽⁴⁾ considered a bubbling fluidised bed when cloud formation occurs, i.e. when U_b , the rate of rise of a bubble, is greater than U_i , the interstitial gas velocity through the dense phase. They assumed that, excluding the bubble clouds, the voidage of the dense phase (e_i) in a freely bubbling bed was not significantly different from that at the incipient fluidisation condition, and that therefore the superficial gas velocity through the dense phase outside the bubble clouds was equal to U_0 . They then showed that the average superficial upward gas velocity in the cloud which encloses a bubble was also equal to U_0 . Hence, all the gas in

excess of that required for incipient fluidisation must pass through the bed as bubbles. Davidson and Harrison⁽⁵⁾ made the same initial assumption regarding the dense phase voidage but without any proviso concerning bubble clouds, and then proceeded to set up a model to allow for gas by-passing the dense phase via the bubbles, thereby implying that they were considering only bubbles without clouds, i.e. small bubbles. The gas flows through the dense and bubble phases were calculated from the pressure gradient through the bed for the case when the particles, and therefore the bubbles, were imagined to be held stationary by an external force. The increase in gas flow due to bubble movement was then considered and an expression for the total gas flow through the bed developed:

$$A_1 U_s = Q_d + B_1 + Q_b \quad - \quad 2.2.1.(1)$$

where A_1 = cross-sectional area of the bed

B_1 = flow per unit cross-section through bubbles at a given height in the bed

Q_d = fluid flow through the dense phase

Q_b = observed bubble flow (the product of frequency and volume)

U_s = superficial gas velocity

It was then shown that it was possible to reduce equation 2.2.1.(1)

to

$$A_1 U_s = A_1 k_1 U_o + Q_b \quad - \quad 2.2.1.(2)$$

where k_1 = constant.

They then simply stated that " k_1 is unlikely to be very different from unity unless the bubbles are extremely close together",

(thereby causing gas by-passing of the dense phase) and that

therefore the assumption that the excess gas above that required

for incipient fluidisation passes up as bubbles was approximately true.

Lockett et al.⁽⁶⁾ considered further the equation 2.2.1.(2) in an attempt to predict the value of k_1 . An idealised two-dimensional system was considered with stationary particles and a swarm of fixed, circular bubbles on a 45° triangular pitch. Assuming Darcy's law to hold, the value of k_1 was calculated for different values of e_b , where e_b is the ratio of the total bubble volume in the bed to the total bed volume. An approximately linear relationship was obtained between k_1 and e_b for $e_b < 0.45$, such that

$$k_1 = (1 + e_b) \quad - \quad 2.2.1.(3)$$

It was assumed that, even at high superficial velocities, the maximum likely value of e_b would not exceed 0.4, and hence over the practical range the result may be represented by equation 2.2.1.(3) for the two-dimensional system.

The next step was to extend the two-dimensional model to the three-dimensional system, but in order to accomplish this, it was first necessary to simplify the initial model. A single bubble only was therefore considered and it was assumed that the flow round a bubble was not influenced by neighbouring bubbles and that the particles were only just supported by the fluid velocity (i.e. $U_i e_i = U_o$). The value chosen for the average gas velocity (U_a) through a bubble relative to the bubble depended on the stream function used. If the stream function of Davidson and Harrison⁽¹⁾ were used, then

$$U_a = 2U_o \quad - \quad \text{two-dimensional system}$$

and

$$U_a = 3U_o \quad - \quad \text{three-dimensional system.}$$

Now comparison of 2.2.1.(1) and 2.2.1.(2) shows that

$$A_1 k_1 U_o = U_o A_1 (1 - e_b) + U_a A_1 e_b$$

$$\text{i.e. } k_1 = (1 - e_b) + \frac{e_b U_a}{U_o} \quad - \quad 2.2.1.(3)$$

Therefore, substitution of $U_a = 2U_o$ into 2.2.1.(3) yielded $k_1 = (1 + e_b)$ for the two-dimensional system, as previously obtained by the more rigorous model. This agreement was taken as justifying the simplified model which was therefore applied to the three-dimensional system. Substituting $U_a = 3U_o$ into 2.2.1.(3) yielded $k_1 = (1 + 2e_b)$ for the three-dimensional system. However, if the stream function of Murray⁽⁷⁾ favoured by Partridge and Rowe⁽⁴⁾ were used, then $U_a = U_o$ was obtained for both two- and three-dimensional systems which, on substitution, yielded $k_1 = 1.0$. Judd⁽⁸⁾ measured the maximum (as opposed to average) gas velocity through a two-dimensional bubble and found a value of $5.1U_o$, which was in much closer agreement with Davidson and Harrison's predicted value of $4U_o$ (maximum) than with Murray's predicted value of $2.2U_o$ (maximum). Lockett et al. therefore concluded that the stream function of Davidson and Harrison is nearer reality than that of Murray.

Grace and Harrison⁽⁹⁾ photographed two-dimensional bubbles and from the result of the least mean squares analysis that they used to correlate their data, they suggest that

$$U_i e_i = 0.95U_o \quad - \quad 2.2.1.(4)$$

and that k_1 must equal $(1 + 4.93e_b)$ before they could balance the air flows through their two-dimensional bed. They suggest that this velocity through the bubble ($5.93U_o$) would be possible if the bubbles were elongated, possibly due to accelerating in the wake of another

bubble. It must be noted, however, that velocities of this order are predicted only when the bubble axis ratio is greater than 2:1.

To summarise, Partridge and Rowe, Davidson and Harrison, and Lockett et al. concluded from experimental observations that $e_i \approx e_o$, and they therefore assumed $U_i e_i = U_o$ for the dense phase. Their assumption, however, seems open to question because Davies and Richardson⁽¹⁰⁾ have shown that in the dense phase

$$U_s = U_f e_i^{n_1} \quad - \quad 2.2.1.(5)$$

(U_f = the value of U_s at $e_i = 1.0$ and

n_1 = a constant for a given system)

Now $n_1 \approx 5$ for a gas fluidised bed and therefore from Newton's law of small errors

$$\frac{dU_s}{U_s} \approx \frac{5de_i}{e_i} \quad - \quad 2.2.1.(6)$$

i.e. a small change in e_i requires a large change in U_s , and it is difficult to measure voidage experimentally with any degree of accuracy. Grace and Harrison⁽⁹⁾ concluded that, if anything, $U_i e_i < U_o$ for the dense phase but again their treatment does not appear to be very rigorous, and therefore, it would seem that, as yet, there is no theoretical proof that $U_i e_i$ cannot be greater than U_o . In fact, from the experimental evidence of Pyle⁽³⁾ and Davies and Richardson⁽¹⁰⁾, $U_i e_i > U_o$ would seem the likely explanation of the observed discrepancy between U_s and $U_o + Q_b$.

2.2.2. Velocity of a Single Bubble

The equation for the rising velocity of a gas bubble in a fluidised bed is based on the analogous case of a gas bubble in a

liquid. Harrison and Davidson⁽¹⁾ state that a theoretical expression for the rate of rise of a single gas bubble in an inviscid liquid is:

$$U_b = 0.914(g D_e)^{\frac{1}{2}} \quad - \quad 2.2.2.(1)$$

(where D_e is the equivalent diameter of a bubble of volume V_b)

compared with

$$U_b = 0.711(g D_e)^{\frac{1}{2}} \quad - \quad 2.2.2.(2)$$

determined experimentally by Davies and Taylor⁽¹¹⁾. The difference between these two equations is due to the fact that a real liquid cannot be inviscid, and hence there will be a resistance to rise created by the bubble wake. Davidson et al.⁽¹²⁾ measured the rates of rise of single bubbles injected into a fluidised bed and found that their results could be correlated by the expression:

$$U_b = k_2(g D_e)^{\frac{1}{2}} \quad - \quad 2.2.2.(3)$$

(where $k_2 =$ a constant)

After correcting for wall effect, k_2 was found to be 0.655 as opposed to 0.711 (equation 2.2.2.(2)), but Davidson et al. assumed that this difference was due to experimental error, and that a fluidised bed behaved as an inviscid liquid. However, Harrison and Leung⁽¹³⁾ used a much larger bed to eliminate the need for wall correction and found the value of k_2 to be 0.64, in good agreement with the experimental results of Davidson et al.⁽¹¹⁾

Rowe and Partridge⁽¹⁴⁾ also measured the rate of rise of a bubble but expressed their results in the form:

$$U_b = k_3(g r_n)^{\frac{1}{2}} \quad - \quad 2.2.2.(4)$$

(where $r_n =$ radius of curvature of the nose of the bubble and $k_3 =$ a constant for a given material and particle size).

(k_3 was found to vary between 0.83 and 1.2, depending on the material being fluidised.)

The theory of Davies and Taylor⁽¹¹⁾ predicted that $k_3 = 0.667$ for a spherical cap bubble in a liquid, where the included angle of the bubble (w) was about 75° , (i.e. a lenticular-shaped bubble), but Rowe and Partridge⁽¹⁴⁾ were considering bubbles where $w \approx 230^\circ$ (i.e. wake angle 130°) which makes direct comparison suspect.

Harrison⁽²⁾ has shown that if the values of r_n , measured by Rowe and Partridge⁽¹⁴⁾ for their size ranges of spherical (ballotini) particles, are converted to D_e , then k_2 lies in the range 0.64 - 0.72. This is in reasonable agreement with the value obtained experimentally by Harrison and Leung⁽¹³⁾ ($k_2 = 0.64$), and theoretically by Davies and Taylor⁽¹¹⁾ ($k_2 = 0.711$). It is surprising that this volumetric method of correlation should bring together results on bubbles of such widely differing shape. The theory is based on a spherical cap bubble in an inviscid liquid and yet it agrees with fluidised bed results where the included angle of the bubble indicates a bed viscosity of about 10 Poise.

For two-dimensional beds, Pyle and Harrison⁽¹⁵⁾ have suggested that the rate of rise of a bubble can be predicted by

$$U_b = k_4 \sqrt[4]{15.9 A_b} \quad - \quad 2.2.2.(5)$$

(where A_b = the projected area of a bubble measured in a vertical plane and k_4 = a constant).

When air bubbles in a gas fluidised bed and in water were investigated in the same equipment, k_4 was found to have the values of 15.9 and 18.1 respectively.

Although the constant has a deviation of the order of $\pm 20\%$ for fluidised beds, it again shows that a bubble in a fluidised

bed rises more slowly than that in a liquid. This difference may be due to the fact that water has a viscosity of $0.01P$, whereas the values found for fluidised beds are in the range $4 - 20P^{(16)}$.

2.2.3. Pressure in a Bubble

Reuter⁽¹⁷⁾ examined bubbles by allowing them to rise against the slightly off-vertical flat wall of a bed, thus effectively slicing them in half. He measured the pressure variations as the bubbles passed a given point with a transducer placed in the wall. As would be expected, since the pressure in a bubble is constant, he found that at the nose of the bubble the pressure is higher than that in the undisturbed bed at the same level, and that in the lower part of the bubble it was lower than in the undisturbed bed at the same level. The height in the bubble at which the pressure was equal to that outside the bed at the same level was found to be above the bubble centre. He postulated that this pressure variation in the bubble must cause gas to flow upwards through it, and that for this increased pressure to exist at the top of the bubble there must be an arch of decreased voidage around the bubble nose, the dense arch giving the bubble its stability.

Stewart⁽¹⁸⁾ has compared the theoretical predictions of Davidson, Collins, Murray and Jackson with Reuter's observed results. He has concluded that Davidson and Collins predicted pressure changes of the right magnitude and that Jackson was correct in assuming that particle momentum and gas pressure are directly linked, because his, Jackson's, theory predicts zero pressure gradient close to the nose of the bubble. This appears to be the case in practice.

Rowe⁽¹⁹⁾ has shown mathematically that Reuter is apparently

incorrect in stating that there must be an arch of decreased voidage above the bubble to give it its stability and allow it to rise as a void. Rowe first considered the streamlines through a spherical void in a fluidised bed if the particles were all prevented from moving. These streamlines were therefore the description of the initial pattern of movement of the particles if the restraint were removed.

The streamlines for a solid sphere rising in an inviscid liquid were considered next and shown to be the same as for the streamlines through the bubble in a fluidised bed. Therefore, if the restraint on the particles was lifted, the spherical void would accelerate upwards similar to a sphere in a liquid. When the void has reached its terminal velocity the theory predicts that above the void the particle motion is virtually identical to the flow of a fluid around a solid sphere, but below the void the drag forces oppose the ideal motion and there is a net upward force, which presumably supports the particles in the wake. It would therefore seem unlikely that Reuter's prediction of decreased voidage above a bubble is correct.

2.2.4. Voidage above a Bubble

Lockett and Harrison⁽²⁰⁾ used a capacitance technique in a two-dimensional bed to measure the voidage in the particulate phase near a rising bubble. They found an increase in voidage up to one bubble diameter above a bubble when fluidising a wide particle size range and for a smaller distance when a narrow cut was used. This increased voidage above the bubble is predicted by Jackson (but to a lesser extent than found experimentally), and also by Murray who confines it to a thin boundary layer round the bubble.

Stewart⁽²¹⁾ comments on Lockett and Harrison's⁽²⁰⁾ paper, and suggests that there was better correlation between Jackson's theory and the experimental results if, instead of taking the theoretical value of k_3 in equation 2.2.2.(4) (i.e. 0.5 for the two-dimensional case), the value was calculated from experimental results. Stewart's method was to combine the results of Pyle and Harrison⁽¹⁵⁾ (equation 2.2.2.(5)) with the ratio:

$$\frac{\text{bubble height}}{\text{bubble diameter}} = 0.83$$

found by measuring the bubble photographs published by Rowe et al.⁽²²⁾ and hence obtain the value $k_3 = 0.65$. He next showed that the voidage measurements of Lockett and Harrison⁽²⁰⁾ with the narrow particle size range can be correlated by equation 2.2.2.(4) if $k_3 = 0.7$, which he considers to be not significantly different from $k_3 = 0.65$ predicted above.

It must be noted that, due to the different bed viscosities and the spread of data in Pyle and Harrison's⁽¹⁵⁾ results ($+20\%$), the predicted value of $k_3 = 0.65$ would be expected to have an accuracy of at best $+20\%$, that is, the minimum range would be 0.5 - 0.8. This method cannot therefore be expected to discriminate between 0.65 and 0.7 or, indeed, between 0.7 and the theoretical value of 0.5. It would therefore appear that the theory still predicts less voidage change than found experimentally by Lockett and Harrison⁽²⁰⁾, and that further work is required to explain their results.

2.2.5. Gas Flow in and around a Bubble

Davidson and Harrison⁽¹⁾ have shown theoretically that the form of the fluid streamlines around a bubble in a fluidised bed

depends on whether U_i is greater or less than U_b . If $a = U_b/U_i$ then when $a < 1.0$ the fluid simply passes in through the bubble base and out through the nose to become entrained in the faster flowing gas outside the bubble. When $a > 1.0$ the gas flowing out through the nose of the bubble is dragged down by the particles surrounding the bubble and re-enters at the base. There is therefore recirculation of the gas through the bubble. The thickness of the gas cloud surrounding the bubble when $a > 1.0$ is inversely related to the value of a , and hence when a is large there is very little contact between the gas in the cloud and the bed particles.

Rowe and Partridge⁽²³⁾ have confirmed experimentally by the use of NO_2 in a two-dimensional bed that this gas cloud does exist, but they found a smaller cloud size than predicted by Harrison and Davidson. Rowe et al.⁽²²⁾ compared the experimental results on cloud formation with those predicted by the theories of Davidson and Murray. They showed that Murray's predictions were in better agreement with the cloud size found above the bubble. No comparison below the bubble was possible because both theories ignore the bubble wake. Rowe et al.⁽²²⁾ also noted that cloud shedding occurs by small regions of cloud breaking away from near the wake. Partridge and Rowe⁽²⁴⁾ continued their experimental investigations of bubble clouds and found from X-ray photographs that the ratio of the volume of cloud in the dense phase (V_c) to the bubble volume (V_b) is given by

$$\frac{V_c}{V_b} = \frac{1.17}{(a-1)}$$

If V_b , a and e_i are known, then assuming the cloud voidage is the same as the bed voidage, the value of $e_i V_c$ can be determined.

As this is the volume of gas in contact with particles, it can be used when calculating the degree of contact between the gas and particles.

Stewart⁽¹⁸⁾ compared his theory with those of Davidson, Collins, Murray and Jackson and showed that the predicted cloud thickness may vary by a factor of two, depending on which theory was used. He also showed that the theories of Jackson and Murray are in best agreement with the available experimental data, suggesting that they were correct in assuming that particle momentum determines the motion of the fluidising gas.

2.2.6. Coalescence of Bubbles

Harrison and Leung⁽²⁵⁾ investigated bubble coalescence by injecting two bubbles, one behind the other, in a gas fluidised bed. They found that the rear bubble was accelerated and drawn into the leading bubble as long as the bubbles were not separated by more than one bubble diameter. Grace and Harrison⁽⁹⁾ extended this work by considering swarms of bubbles, but approximately the same results were found.

Further investigation of bubble coalescence was carried out by Rowe and Partridge⁽¹⁴⁾, who recorded injected bubbles by an X-ray technique. Their results suggest that even at low bubble concentrations a bubble may spend up to 40% of its life splitting into two and 10% re-coalescing. It was also noted that the frequency of coalescence increases rapidly as bubble concentration increases.

2.2.7. Particle Movement due to Bubbles

It has been shown by Rowe and Partridge⁽²⁶⁾ that bubbles drag up particles in their wake, but that crescents of particles are

regularly shed from their wake, such that a bubble displaces about two-thirds of its volume in particles upwards through an average height of one bubble diameter. The intake of particles would appear to be a continuous process and bubbling therefore contributes strongly to the bulk circulation of particles in a fluidised bed.

2.2.8. Gas Leakage from Bubbles during Formation

Many workers have injected gas into fluidised beds and the majority have merely assumed that the volume of the bubble formed was equal to the volume of gas injected. Harrison and Leung⁽²⁷⁾ did consider leakage of gas from a bubble on formation, but concluded that for normal fluidised systems the leakage was not likely to exceed 15% of the volume injected. Unfortunately, there would appear to be some element of doubt on the validity of their calculations because their initial assumption was that the gas leakage would be small. Rowe and Partridge⁽¹⁴⁾ attempted to check Harrison and Leung's assumption using an X-ray technique, and in fact they found that for a given volume of injected gas, the volume of the bubble formed was both directly related and very sensitive to the background air rate. They therefore concluded that only under unique conditions will the size of bubble produced be equal to the volume of injected gas.

2.2.9. Viscosity

Several workers have attempted to measure the viscosity of a fluidised bed, but it is considered that the results of Schugerl et al.⁽²⁸⁾ are the most reliable because their method, using a rotating cylinder, created the least disturbance in the bed. They found that the viscosity (μ_a) of a fluidised bed decreases with

decreasing particle size and generally lies in the range 15 - 3P.

Grace⁽¹⁶⁾ has suggested that the viscosity of a fluidised bed can, in fact, be predicted by considering the included angle of a bubble as it rises in the fluidised bed, because it is known that the included angle of a bubble rising in a liquid increases with liquid viscosity. From published data Grace⁽¹⁶⁾ obtained a plot of Re_b versus w , where

$$Re_b \equiv \frac{D_e U_b \rho_f}{\mu_f} \quad - \quad 2.2.9.(1)$$

(ρ_f = density of the fluid)

(μ_f = viscosity of the fluid)

He used this plot to obtain the values of Re_b equivalent to the values of w published by Rowe and Partridge⁽¹⁴⁾ from their work on bubbles in a fluidised bed. Then by substituting these values of Re_b into equation 2.2.9.(2)

$$Re_b = \frac{D_e U_b \rho_p (1 - e_i)}{\mu_a} \quad - \quad 2.2.9.(2)$$

(ρ_p = density of the particles)

he was able to calculate values of μ_a for the systems used by Rowe and Partridge⁽¹⁴⁾. Good agreement was found between the values of μ_a calculated in this manner and the values obtained by Schugerl et al.⁽²⁸⁾.

2.3. TRANSITION REGION

2.3.1. Relationship between Aggregative and Particulate Fluidisation

Simpson and Rodger⁽²⁹⁾ have fluidised seven different solids with four different gases at pressures between 0 and 100 psig, and also glass, steel and lead spheres with water. They found it possible to represent the wide range of gas and liquid results obtained by a single, though rather complex, correlation which indicated that there is no fundamental difference between gas and liquid fluidised systems.

Harrison, Davidson and de Kock⁽³⁰⁾ have also considered the nature of aggregative and particulate fluidisation, but instead of concentrating on the bed voidage as did Simpson and Rodger, they have approached the problem from the point of view of a bubble size. Their theory is that a bubble can exist only if the particles in its wake are not entrained by the circulating gas in the bubble. If they are, the bubble will fill with particles and cease to exist. In order to fit figures to this theory, the assumption was made that the gas velocity through the bubble due to the internal circulation of the gas is equal to the bubble rising velocity. The expression for the rising velocity of a bubble was then equated to the terminal velocity of the particles being fluidised. From this the maximum bubble size that can exist was calculated. In a liquid fluidised bed, the terminal velocity of a given particle is much lower than in gas fluidised beds, whereas the bubble rate of rise is approximately equal for both types. According to this theory, therefore, only very small bubbles should exist in a liquid fluidised bed, and this indeed is found in practice, suggesting that the difference between the two types of fluidisation is, in fact, only one of degree. A tendency to fluidise particulately would be expected, the smaller

the particle size and density difference and the higher the viscosity. Harrison et al.⁽³⁰⁾ fluidised lead shot, steel, glass and resin particles (to alter the density difference) with aqueous solutions of glycerol of various concentrations (to alter principally the viscosity). Their results supported their theory qualitatively.

Qualitatively, support was also given by the work of Leung⁽³¹⁾, who fluidised phenolic spheres with CO₂ at different pressures. In all the experimental work, the observations were purely visual as to the uniformity of the bed; no actual bubble measurements were made. The theory predicts that for gas fluidisation of light spheres, there should be only very small bubbles, and though this is not found in practise at high multiples of U₀, at low multiples of U₀ a gas fluidised bed of small, light particles does behave particulatesly. It is therefore possible with such a bed to vary the fluidising gas rate over a limited range in excess of U₀ without producing bubbles and to study bed expansion and the properties of single (injected) bubbles.

2.3.2. The Expansion of Particulatesly Fluidised Beds

Richardson and Zaki⁽³²⁾ showed that for liquid fluidised beds, the expansion (expressed as the bed voidage) could be related to the superficial liquid velocity by

$$\frac{U_s}{U_f} = e_i^{n_1} \quad - \quad 2.3.2.(1)$$

(n₁ is a constant for a given system and is a function of the Reynolds number with respect to a particle (Re_p).)

$$\text{Where } Re_p = \frac{U_t d_p \rho_f}{\mu_f} \quad - 2.3.2.(2)$$

(d_p = diameter of a particle)

(U_t = terminal falling velocity of a particle)

U_t is related to U_f by

$$\text{Log } U_t = \text{Log } U_f + \frac{d_p}{D_c} \quad - 2.3.2.(3)$$

(D_c = diameter of bed container)

Davies and Richardson⁽¹⁰⁾ investigated a gas fluidised bed using small, light particles and found that over the gas range for which the bed behaved particulate, the bed expansion could be correlated by

$$U_s = A_2 e_i^{n_2} \quad - 2.3.2.(4)$$

(where A_2 and n_2 are constants for a particular system.)

This is of the same form as that found by Richardson and Zaki. The index n_2 only corresponds with the value of n_1 in liquid fluidisation when spherical particles are fluidised. Irregular shapes give higher values of n_2 than predicted by Richardson and Zaki's work for uniform spheres. It was also noted that A_2 only approaches U_t for a close cut of particles, A_2 tending to be smaller than U_t for wide size distributions.

Davies and Richardson's work has been extended by Godard⁽³³⁾ for higher velocities by working under pressure, but similar results were found.

2.3.3. Injected Bubbles

2.3.3.1. Bubble Stability in a Gas Fluidised Bed Behaving Particulately

Davies and Richardson⁽¹⁰⁾ fluidised a bed of cracker catalyst particulately up to the minimum bubbling velocity (U_{mb}) of about $2.8U_o$. At a given air rate between U_o and $2.8U_o$ gas bubbles of known volumes in the range $15 - 200\text{cm}^3$, were injected singly into beds of different heights (h_c) and the bubble volumes as they left the bed estimated by the decrease in the bed volume. They assumed that for a given background air rate the bubble growth rate was independent of its depth below the surface. The results for different bubble volumes and bed heights were then combined by adjusting the ordinates to give a single graph of predicted bubble volume versus distance travelled (h_s). The correlating curves of their results for three background air rates are shown in Fig. 2.3.3.1. (1), (p. 22). It must be noted that the curves are not extrapolated to the axes. The growth with distance was then deduced and plotted against bubble volume (Fig. 2.3.3.1.(2), (p. 22) with the correlating lines extrapolated through the origin. This, however, would appear to be in error since, when the work on bubble streams reported later in the same paper, and also the work published by Godard and Richardson⁽³⁴⁾ is considered, it would appear that $\frac{dV_b}{dh_s}$ can be negative for small bubbles.

Davies and Richardson continued their investigation by injecting continuous streams of gas (instead of individual bubbles) into the bed. They reported that at a background air velocity of $1.2U_o$ there was a net transfer of gas from the bubble phase to the continuous phase for an injection rate as high as $444\text{cm}^3/\text{s}$. However,

Fig. 2.3.3.1.(1).

Results of Davies and Richardson: catalyst-air system

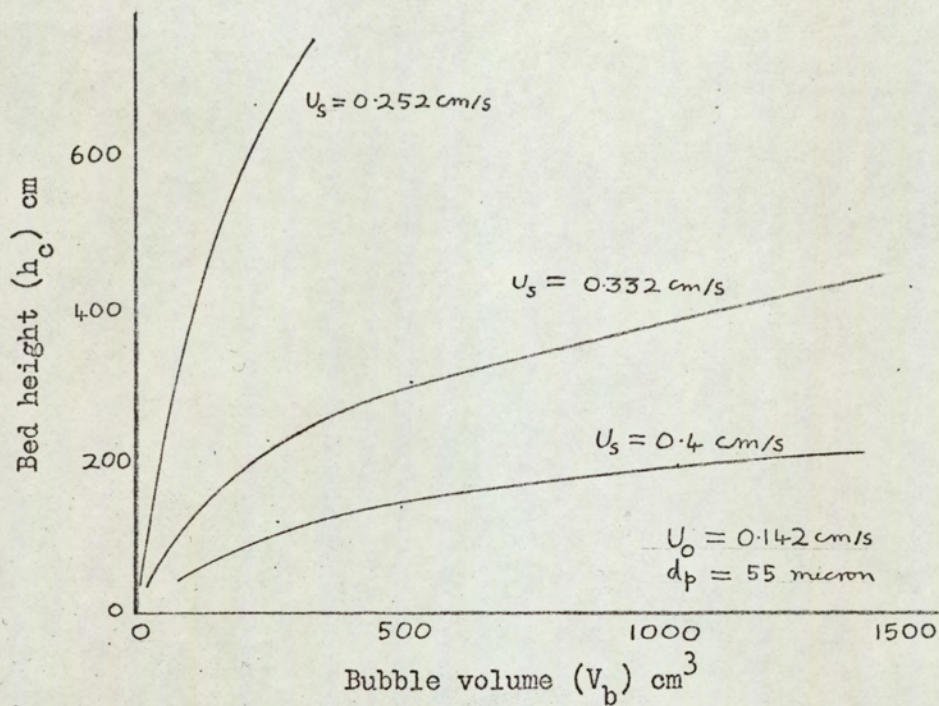
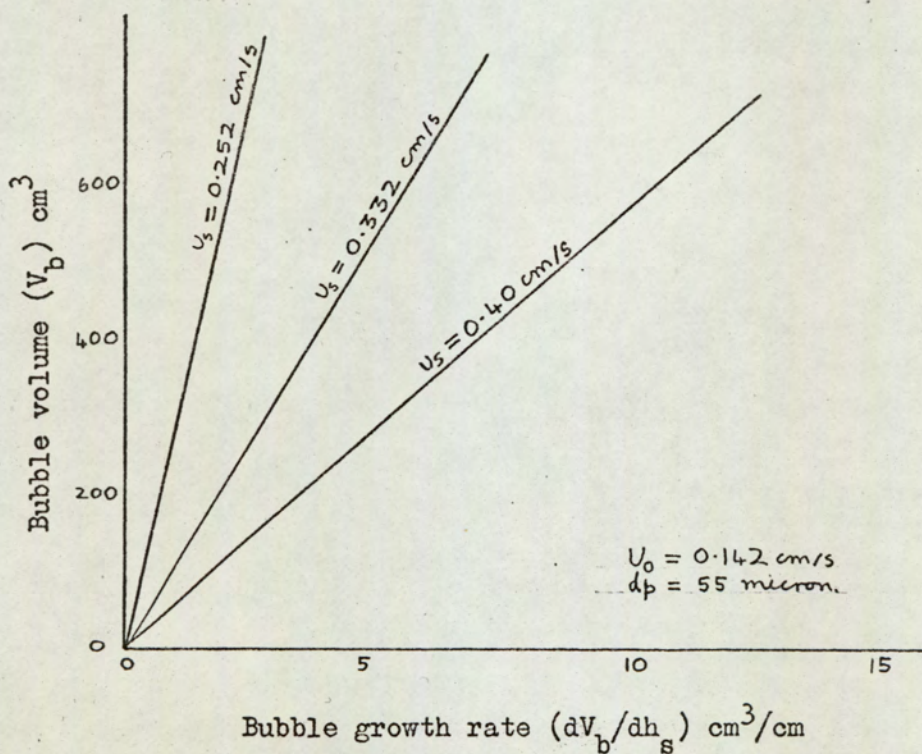


Fig. 2.3.3.1.(2).

Results of Davies and Richardson: catalyst-air system



when the background air velocity was increased to $1.7U_0$, bubble shrinkage occurred only when the injection rate was reduced to about $16.6\text{cm}^3/\text{s}$. This indicates that there is a meta-stable bubble size which is inversely related to the background air rate; this possibility is also supported by the results of Godard and Richardson⁽³⁴⁾, using a different experimental technique. It would therefore appear that the graph of Davies and Richardson, reproduced as Fig. 2.3.3.1.(1), should be altered to the form shown in Fig. 2.3.3.1.(3), (p.24) and Fig. 2.3.3.1.(2) should be altered to the form shown in Fig. 2.3.3.1.(4), (p.24). Fig. 2.3.3.1.(4) indicates that bubble shrinkage can occur, which Davies and Richardson⁽¹⁰⁾ could not investigate because their technique was geared to large bubbles. Their error was in extrapolating their results at the lower end.

As has been mentioned already, Godard and Richardson⁽³⁴⁾ have also considered this meta-stable bubble region, though they were able only to measure bubbles that were below the stable size, i.e. ones that were shrinking. Their technique was to inject known volumes of air and record the injected bubble volume that just reached the surface of a bed of known height, fluidised at a fixed background air rate. By altering the bed height, they were able to relate the minimum injected volume to reach the bed surface (V_m) to the bed height at constant background air rates. Their results are reproduced in Fig. 2.3.3.1.(5), (p.26). They concluded from their results that

- i) the meta-stable bubble volume for a background air rate of $2.04U_0$ was 0.08cm^3 because the results at that air rate gave a virtually constant bubble volume indicating no bubble shrinkage;

Fig. 2.3.3.1.(3).

Trend suggested by the results of Davies and Richardson

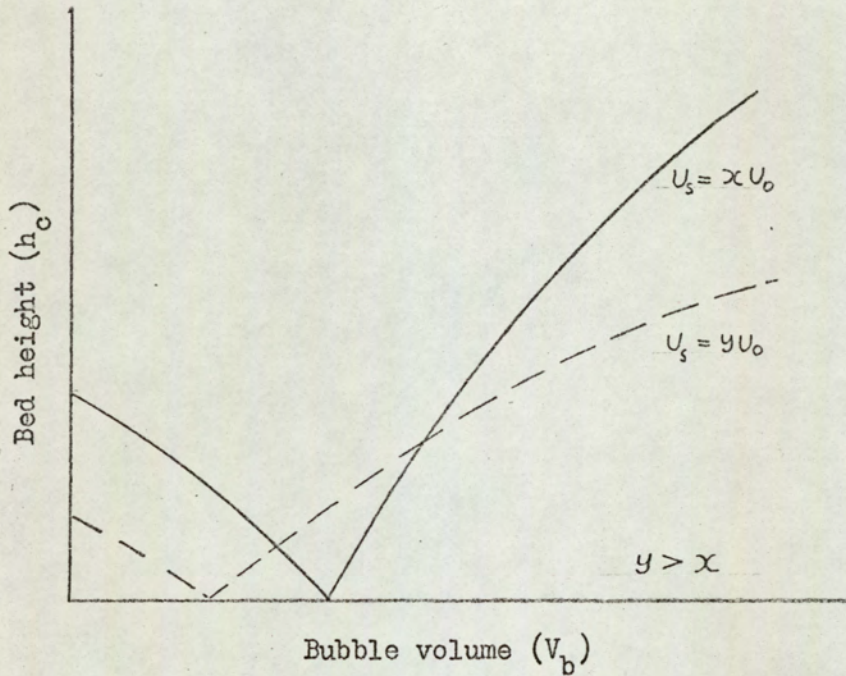
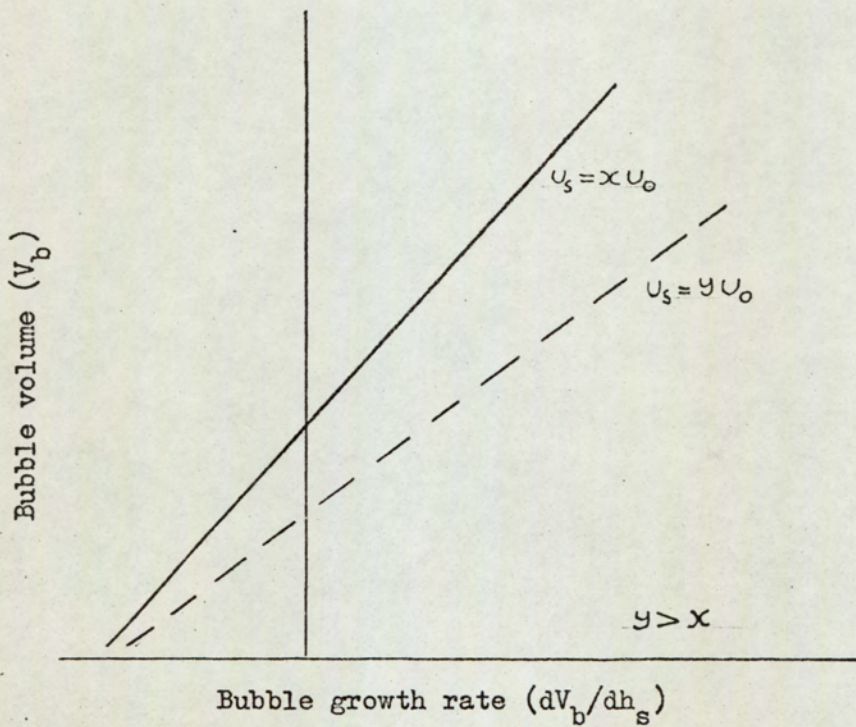


Fig. 2.3.3.1.(4).

Trend suggested by the results of Davies and Richardson



ii) the rate of loss of air from a bubble just smaller than the meta-stable bubble volume was linear with respect to distance travelled, i.e. independent of bubble volume. The rates were given as $0.037 \text{ cm}^3/\text{cm}$ travelled at a background air rate of U_0 to $0.0002 \text{ cm}^3/\text{cm}$ travelled at a background air rate of $2.04U_0$.

Fig. 2.3.3.1.(6), (p.26) is a qualitative graph representing the trend shown by the results of Godard and Richardson in Fig. 2.3.3.1.(5). The parameter is again background air rate as multiples of U_0 .

Let h_m be defined as the minimum distance a bubble of volume just less than the meta-stable volume, V_{bs} , must travel to be completely absorbed, in a bed fluidised at a given value of U_s . Then from Fig. 2.3.3.1.(6) it can be seen that the values of h_m , for the four lower values of U_s , are greater than the maximum bed height used by Godard and Richardson. They were therefore unable to determine the values of V_{bs} at these air rates. When $U_s = 2.04U_0$ it can be seen that their minimum bed height was greater than h_m and therefore, though they obtained a value for V_{bs} , they were unable to determine the value of h_m .

As it was assumed that the rate of collapse of a bubble with distance was linear, their calculations of the net rate of gas transfer from bubble to continuous phase were correct, except for the rate at the background air velocity of $2.04U_0$. The results for this air rate are shown in Table 2.3.3.1.(1).

Fig. 2.3.3.1.(5).

Results of Godard and Richardson

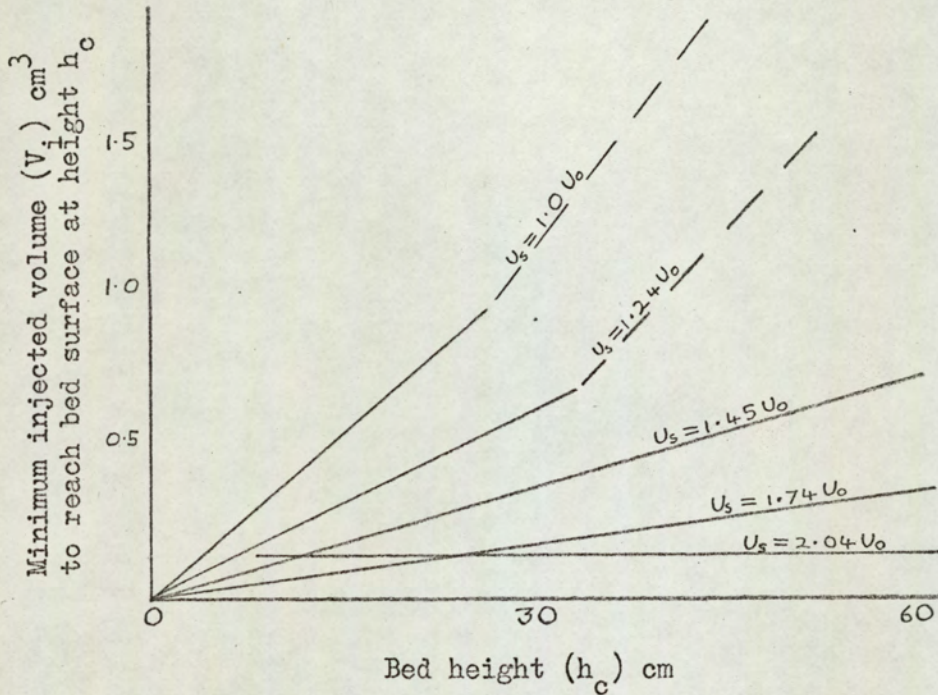


Fig. 2.3.3.1.(6).

Trend suggested by results of Godard and Richardson (Fig. 2.3.3.1.(5))

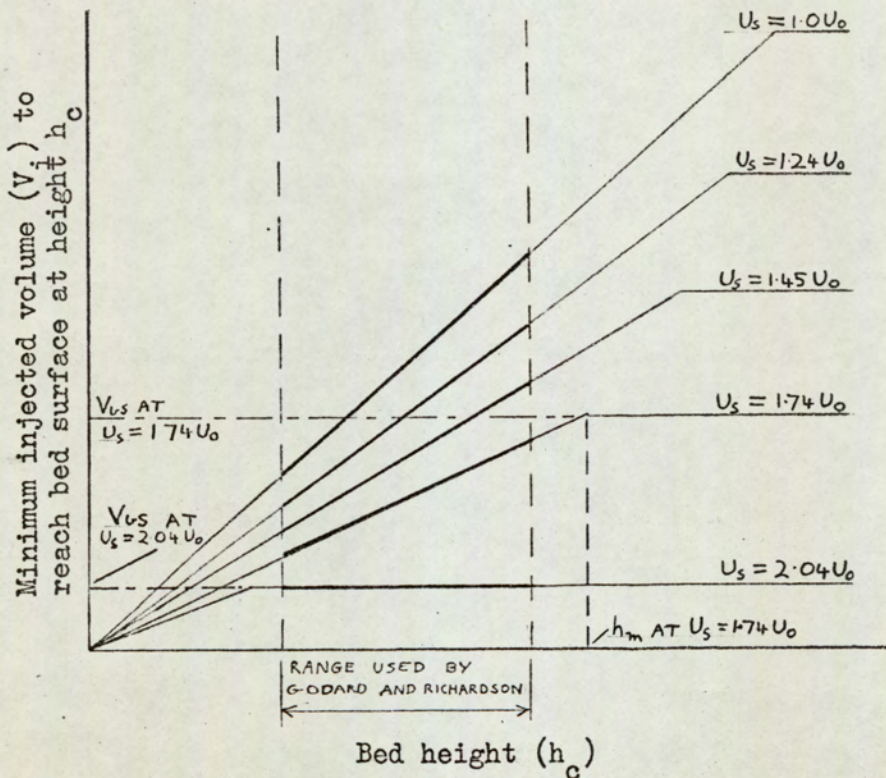


Table 2.3.3.1.(1)

The results of Godard and Richardson for a background

air rate = $2.04U_0$

Bed weight g	625		1,250		1,875		2,500	
Gas velocity cm s^{-1}	V_m cm^3	h_c cm	V_m cm^3	h_c cm	V_m cm^3	h_c cm	V_m cm^3	h_c cm
$2.04U_0$	0.08	12.85	0.08	25.60	0.08	38.51	0.09	51.20

It can be seen that the bubble volume was constant, except for the last reading where it had increased by 0.01cm^3 which is within the stated injection accuracy at this bubble size of $\pm 0.02\text{cm}^3$ (and this was therefore not a significant change). The gas transfer rate was stated as 0.01cm^3 in 51.2cm travelled, i.e. $0.0002\text{cm}^3/\text{cm}$. This was erroneous because (referring to Fig. 2.3.3.1.(6)) all their other rates referred, correctly, to the gradients of the lines $OA_{(1-4)}$ which pass through the origin. Now, either the line for the air rate $2.04U_0$ should have been drawn passing through the origin, when the gas transfer rate would have been in excess of $0.0002\text{cm}^3/\text{cm}$, or the line should have been drawn horizontal and hence the measured rate of gas transfer would have been zero. The latter case would seem to be the true explanation and the minimum rate of gas transfer possible, when bubbles are small enough to shrink, can therefore be calculated for this

air rate by assuming that a 0.07cm^3 bubble only just disappeared in the minimum bed height used, 12.85cm . Thus the minimum transfer rate = $(0.07/12.85)\text{cm}^3/\text{cm} = 0.00545\text{cm}^3/\text{cm}$ which is close to the value found ($0.0046\text{cm}^3/\text{cm}$) for the background air rate of $1.74U_0$, and a factor of 25 greater than the stated value. The error can be confirmed by showing that a minimum bubble size of 0.08cm^3 at a bed height of 13cm and a rate of gas transfer of $0.0002\text{cm}^3/\text{cm}$ are incompatible: if 0.08cm^3 is the smallest bubble to reach the bed surface when the bed height is 13cm , then a 0.07cm^3 bubble must disappear in less than 13cm , but with a gas transfer rate of $0.0002\text{cm}^3/\text{cm}$ it would require a bed height of 350cm .

Two other points that seem rather open to question are:

- i) a quoted bubble volume refers to an injected volume rather than the bubble volume formed by the injection;
- ii) the assumption that the rate of loss of gas from a bubble is a constant, irrespective of the bubble size since their results (reproduced in Fig. 2.3.3.1.(5)) tend to be curves and Davies and Richardson⁽¹⁰⁾ found bubble growth to be very definitely related to bubble volume.

It would therefore appear that although the work of Godard and Richardson suggests the presence of a meta-stable bubble with a volume inversely related to the background air velocity, not too much weight should be given to the numerical values, as they unfortunately depend to a certain extent on the extrapolation of curves.

2.3.3.2. Bubble Growth in a Gas Fluidised Bed Behaving
Particulately

As stated in the previous section, Davies and Richardson⁽¹⁰⁾ investigated single bubble growth rates and the gas transfer between the continuous phase and an injected stream of bubbles. Although their presented correlation should be modified for small bubbles, as suggested by Fig. 2.3.3.1.(4), for large bubbles their results can still be represented by

$$V_b \simeq K \frac{dV_b}{dh_s} \quad - \quad 2.3.3.2.(1)$$

(where K is a constant dependent on the material being fluidised and the background air rate.)

Hence,

$$\ln (V_{b2}/V_{b1}) = \frac{\Delta h_s}{K} \quad - \quad 2.3.3.2.(2)$$

and therefore, for a given value of K, the size of a bubble after it has travelled a distance (h_s), can be calculated if its initial size is known. Davies and Richardson also noted that a plot of $\log K$ versus $\log (U_s - U_o)$ gave a linear relationship so that values of K at different air rates could be found by interpolation of their results. Their growth rate results with streams of injected bubbles appear to agree well with their results from the single bubbles. They showed that if V_{b1} and V_{b2} were expressed in cm^3/s for the injected streams of bubbles and K was found from the single bubble data for the correct background air rate, then the predicted rate of gas transfer, using equation 2.3.3.2.(2), agreed very closely with that found experimentally. As has been discussed in Section 2.3.3.1., this prediction of bubble stream gas transfer rates from single bubble data will hold only when

there is a net loss from the continuous to the bubble phase, because the correlation of their single bubble results does not allow for bubble shrinkage.

2.3.3.3. Conclusions from previous work on Injected Bubbles in a Gas Fluidised Bed Behaving Particulately

The conclusions that can be drawn from Davies and Richardson's and Godard's work are:

- i) that there is evidence that a meta-stable bubble may exist and its size is apparently inversely related to the background air velocity;
- ii) at a given background air rate, bubbles larger than the meta-stable size grow at a rate directly related to their size, and for a given bubble size this rate is directly related to the background air rate;
- iii) bubbles smaller than the meta-stable size shrink but insufficient evidence is available to predict the rate of collapse with any degree of accuracy.

2.4. TECHNIQUES FOR MEASURING BUBBLE VOLUMES IN GAS FLUIDISED BEDS

In Section 2.3.3.1. it was suggested that further results were necessary before the existence of a meta-stable bubble could be proved to exist, but assuming that it does exist, it will be necessary to relate its volume to the physical and dynamic properties of the bed.

There are several methods which have been used to investigate fluidised bed perturbations, but all of them have inherent disadvantages when it is required to measure bubble volumes in three-dimensional beds.

Of the methods that do not entail probes placed inside the bed, only X-rays are at all satisfactory. Photographing the top surface of the bed yields only information on the bubbles as they burst, and cine films of bubbles rising against a bed wall have the disadvantage that they have been influenced by the wall all the way up the bed. X-rays do yield useful information as demonstrated by Rowe⁽¹⁴⁾ but are not so practical when looking at bubbles smaller than 2cm^3 , when the hazy fringe of the X-ray photograph leads to large errors. The equipment is also expensive and requires special operating facilities. For these reasons, many workers have placed probes inside the bed, the great disadvantage in this case being that the probes must disturb the bed to a certain extent. Probes can be split into different categories depending on the physical property being measured. Ashton et al.⁽³⁵⁾ and Winter⁽³⁶⁾ used a light source and a photo-electric cell to record density fluctuations, but because only a thin layer of particles is necessary to obscure completely the source from the sensor, a light probe would only be able to measure bubbles whose diameter

was nearly the same as the gap between the source and the sensor. This method, therefore, would be of little use for measuring a range of bubble sizes. Ostergaard⁽³⁷⁾ used the change in electrical resistance, caused by a gas bubble passing between two wires in a water-sand fluidised bed, to determine bubble frequency. However, using the change in electrical resistance to measure bubble volume in a gas fluidised bed is feasible only when the particles are conductors, so that a bubble passing between the plates causes an increase in resistance.

There are very few conducting materials readily available in the form of small, low density particles, which is one of the pre-requisites for a gas fluidised bed to behave particulate over a reasonably large voidage range. This effectively eliminates the use of resistance probes for investigating the properties of a gas fluidised bed.

The use of non-conducting particles allows a capacitance technique to be used to record bed properties and many workers have, in fact, done so. Morse and Ballou⁽³⁸⁾ and Dotson⁽³⁹⁾ measured a "bed uniformity" by averaging the recorded capacitance fluctuations due to the rising bubbles. Lanneau⁽⁴⁰⁾, Ormiston et al.⁽⁴¹⁾ and Angelino et al.⁽⁴²⁾ used two sets of plates and measured the rate of rise of bubbles. Bakker and Heertges⁽⁴³⁾ showed that the Wiener equation appears to relate correctly the dense phase voidage and the bed dielectric constant, and they also investigated^(44, 45) the steady state variation of the dense phase voidage at different heights above the distributor, using a capacitance technique. A similar method was used by Lockett and Harrison⁽²⁰⁾ to determine the voidage above a bubble in a two-dimensional bed.

Now, though no one appears to have done so, it seems likely that, if, instead of merely indicating a voidage change, a capacitor consisting of two plates could be calibrated for bubble size, it would be much cheaper than X-ray equipment and more versatile, as there would be no restrictions on operating conditions, bed size or bubble volume. The probe would cause interference in the bed but it would be unlikely to cause any interference in the bed below the plates, and once a bubble has been recorded then it is of no concern if it passes into a region above the plates where the bed is disturbed.

BUBBLE STABILITY THEORIES

In Section 2.3.3.3. it was concluded that a meta-stable bubble may exist and in view of this, the existing bubble stability theories are examined to determine if they could be used to explain this phenomenon.

Two different approaches to the problem of predicting bubble stability were used by the early workers in this field. Jackson⁽⁴⁶⁾ considered the general equations of motion for a fluidised assembly of identical particles. He showed that a fluidised bed is always unstable and that the initial rate of growth of a disturbance of several particle diameters in length could vary from one system to another, being very small in those systems normally described as particulate and very large in those described as aggregative. There is, however, no proof that these disturbances will continue to grow until they form bubbles, but it is suggested that this could be the case. Harrison et al.⁽³⁰⁾, on the other hand, considered the fully developed bubble. They suggested that a bubble would be filled in by the particles in its wake when the gas velocity through the bubble exceeded the terminal falling velocity of the particles. By assuming the velocity through the bubble equalled the rate of rise of the bubble, they were able to relate maximum bubble size to the particle size and the density difference between the fluid and the particles: this model shows reasonably good agreement with that found in practice. These two theories are almost complementary to each other; the former considers the initial disturbance that creates the bubble and

the latter considers the maximum size to which the bubble can grow, once it is formed, but provides no reason why a bubble should form in the first place. Anderson and Jackson⁽⁴⁷⁾ have, in fact, found good agreement between the two theories when both were used to predict the type of fluidisation found with several different experimental systems. Rice and Wilhelm⁽⁴⁸⁾ considered the interface between the dense bed phase and the particle free fluid phase, and in particular developed a theory to predict the effect of instabilities, at the distributor on bubble generation, and at the upper surface of a bubble on bubble growth. For a simplified model, their theory showed that the interface at the distributor is inherently unstable, and that the interface at the upper surface of a bubble is inherently stable, i.e. that bubbles could always be generated at the distributor and that they would be stable throughout the bed. They also suggested that whether the bed behaves particulate or aggregative is in part dependent on the rate of growth of disturbances in the bed, which is related to the physical properties of the system. The effect of bed viscosity is investigated in some detail and their theory predicts that the lower the viscosity, the more likely is the bed to fluidise particulate.

In an attempt to suggest a criterion to differentiate between particulate and aggregative fluidisation, Wilhelm and Kwauk⁽⁴⁹⁾ postulated that the Froude Number (where $Fr = U_o^2/g d_p$) increases with decreasing bed stability and that the transition point from particulate to aggregative fluidisation occurs at $Fr = 1$. This holds for fluidised systems with a large or small Froude Number $Fr > 1.0$ but does not predict the type of fluidisation found in more recent work where systems with a Froude Number in the range $0.1 < Fr < 1.0$ have been used.

Romero and Johanson⁽⁵⁰⁾ used Rice and Wilhelm's⁽⁴⁸⁾ work as a basis from which they attempted to derive a new criterion of bubble stability to fit all the observed results. They suggested that for fluidisation it may depend on the following dimensionless groups:

$$\text{Fr}, \text{Re}_p, \frac{(\rho_p - \rho_f)}{\rho_f}, \text{ and } \frac{d_p}{D_c} \text{ or } \frac{h_o}{D_c}$$

(h_o = bed height at incipient fluidisation)

Insufficient data was available to weight any particular group by the use of exponents, and therefore the criterion obtained was:

$$\left[\text{Fr} \text{Re}_p \left(\frac{(\rho_p - \rho_f)}{\rho_f} \right) \left(\frac{M}{d_c} \right) \right]$$

(where $M = d_p$ or h_o)

This fits the observed results better than the Froude Number alone and the dividing limit between particulate and aggregative fluidisation is between 1 and 4 when $M = d_p$ and about 100 when $M = h_o$. However, it was noted that the minimum fluidisation velocity appeared to be in itself a good criterion of fluidisation, a value of about 6cm/s being the transition velocity, with lower velocities indicating particulate fluidisation and higher velocities aggregative.

Rowe⁽⁵¹⁾ considers the effect particles in the path of a rising bubble will have on the bubble as a method of establishing a criterion for bubble stability. He suggests that if the particles cannot move out of the bubble path, then the bubble will become filled with particles and disappear, and the bed will therefore behave particulate. Now the ease with which a particle can move

when above a bubble is shown to be inversely proportional to the fluid viscosity, μ_f , and proportional to the density difference ($\rho_p - \rho_f$). The suggested parameter is therefore $(\rho_p - \rho_f)/\mu_f$, and from experimental data it would appear that the transition value is approximately 10^3 s/cm^2 , lower values indicating particulate fluidisation and higher values aggregative.

Ruckenstein and Muntean⁽⁵²⁾, like Romero and Johanson⁽⁵⁰⁾, also developed one of Rice and Wilhelm's⁽⁴⁸⁾ theories in order to predict the size to which a perturbation must grow before it could leave the distributor in the form of a bubble. They suggested that a bubble can only leave the distributor when its buoyancy forces are sufficient to overcome the bed resistance opposing its growth and the inertia of the bed. They were thus able to develop an equation for D_e in terms of the fluid viscosity and density, and the bed viscosity and density, where D_e is the minimum size that can just rise from the distributor. D_e was calculated at different gas velocities for the system of air-glass beads with a particle diameter of 100 micron and a particle density of 2.43 g/cm^3 . For an increase in background air rate of five times, the value of D_e increased only by a factor of about 1.3 for a bed at constant viscosity and for an increase in bed viscosity of four times, the value of D_e increased only by a factor of two at a given background air rate. This theory therefore predicts that for the stated air-glass system, the minimum bubble diameter is about $0.5 - 1.0 \text{ cm}^3$, irrespective of background air rate and bed viscosity.

Rietema⁽⁵³⁾ also suggested a model to predict whether a bed will behave aggregatively or particulate. His argument is based on the fact that the flow of gas due to bubbles passing through

the bed must be less than the total gas input to the bed. He stated that a void must have a certain minimum volume before it can be recognised as a bubble, and that therefore there must be a minimum value of bubble voidage in a bubbling fluidised bed (e_{bm}). The minimum total volume of fluid transported by bubbles can therefore be related to a superficial velocity (U_m) which equals ($e_{bm} U_b$). The interstitial gas velocity (U_s) can be calculated from Ergun's equation, and by stating that U_s/U_m must be ≥ 1.0 , and assuming an arbitrary value for e_{bm} , an equation was derived for the minimum value of ρ_p/ρ_f for bubbling to be possible. Rowe⁽⁵⁴⁾ attempted to explain the phenomenon of a gas fluidised bed of small, light particles behaving particulate over a limited range of background gas velocity. He considered the minimum flow rate of gas, above that required to fluidise the bed incipiently, that could support a stream of bubbles if the minimum feasible bubble diameter was 0.5cm. For an average bed size and an air-solid system of light, small particles, he showed that a 20% increase in gas rate is required above U_0 before there is sufficient excess gas to support a stream of bubbles. He therefore concluded that the reason for a bed of fine particles behaving particulate is that there is insufficient air to generate even the smallest bubbles, whereas with bigger, heavier particles a 1% or 2% increase in air flow rate above U_0 would produce the extra gas flow necessary to support bubbling. Molerus⁽⁵⁵⁾ commenced in a similar manner to Jackson⁽⁴⁶⁾, in that he considered the growth of perturbations in a fluidised system, but, unlike Jackson, he considered that particulate fluidisation is due to the initial perturbations decaying away, i.e. a negative growth rate. Jackson's theory is that in a particulate system, the perturbations increase,

but only very slowly. Thus, Molerus stated that when fluidising particulates a fluidised bed is in a stable state, and when fluidising aggregatively it is in an unstable state. This he expressed mathematically by the equation:

$$S_a = \frac{f(e_i) q_f A_3}{3\pi(e_i^3 (1-e_i)(1-A_3) d_p^3 \xi)^{\frac{1}{2}}} \quad - \quad 3.(1)$$

(S_a = measure of stability)

($f(e_i)$ = function of bed voidage)

(A_3 = ρ_f/ρ_p)

(q_f = kinematic viscosity of the fluid)

High values of S_a signify stability and low values instability. From equation 3.(1) there is therefore a critical value of S_a , (S_{ac}) which defines the stability boundary, i.e. above S_{ac} the perturbations decrease, below S_{ac} the perturbations increase.

For a given fluid q_f and ρ_f are constants and Molerus next states that S_{ac} = constant for a given fluid and that therefore the line S_{ac} = constant can be plotted on a graph of e_i versus $1/A_3$ with d_p as the parameter. Before it is possible to do this, it would appear to be necessary to know the value of S_{ac} and $f(e_i)$, neither of which is given.

If equation 3.(1) is considered for a given fluid with a bed at constant voidage then the equation reduces to:

$$S_a = \frac{k_5 A_3}{((1-A_3) d_p^3)^{\frac{1}{2}}} \quad - \quad 3.(2)$$

where $k_5 = \frac{f(e_i) q_f}{3\pi (e_i^3 (1-e_i) g)^{\frac{1}{2}}} = \text{constant}$

If the value of S_a is taken as S_{ac} , i.e. the bed at its stability boundary, then as $S_{ac} = \text{constant}$

$$\frac{A_3}{((1-A_3) d_p^3)^{\frac{1}{2}}} = \text{constant} \quad - \quad 3.(3)$$

Molerus' Figure 2 has been reproduced in the present work as Fig. 3.(1), (p.40) and data extracted from it at $e_i = 0.6$. The results are tabulated in Table 3.1. From which it can be seen that the left hand side of equation 3.(3) is indeed a constant.

Fig. 3.(1)

Molerus' Stability Graph for Gas Fluidisation

- | | |
|------------------------------|-----------------------------|
| Line A - $d_p = 5000$ micron | Line D - $d_p = 200$ micron |
| Line B - $d_p = 1000$ micron | Line E - $d_p = 100$ micron |
| Line C - $d_p = 500$ micron | Line F - $d_p = 50$ micron |

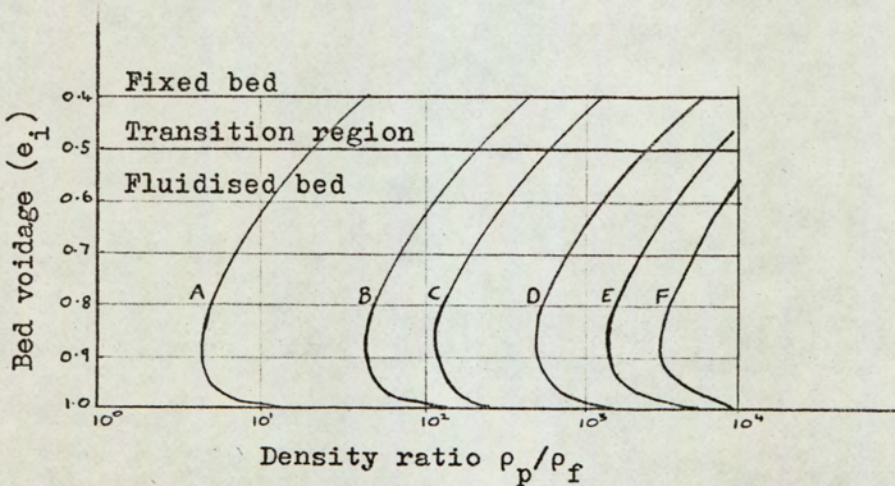


Table 3.(1).

Data extracted from Molerus' Graph (Fig. 3.(1))

$1/A_3$	d_p mm	k_9	$1-A_3$
13	5.0	0.00719	0.923
140	1.0	0.00719	0.9928
370	0.5	0.00754	0.997
1500	0.2	0.00738	0.9993

As can be seen in Table 3.(1), the values of $(1-A_3)$ can be approximated to 1.0 when fluidising with a gas and therefore for a bed fluidised with a given gas at a given voidage

$$S_{ac} = \frac{k_5 A_3}{(d_p^3)^{\frac{1}{2}}} = \text{constant.} \quad - 3.(4)$$

As $A_3 = \rho_f / \rho_p$ where ρ_f is a constant in this case

$$\text{then, } \rho_p (d_p^{\frac{1}{2}})^3 = \frac{k_5 \rho_f}{S_{ac}} = \text{a constant,} \quad - 3.(5)$$

but as neither S_{ac} nor $f(e_i)$ is known, the only method of comparison between Molerus' ⁽⁵⁵⁾ predicted results and experimental results is by direct plotting of experimental results onto Molerus' stability graphs. Fortunately, several workers have reported the maximum superficial fluidising velocity (U_{mb}) for given systems to behave particulates and the corresponding voidage (e_{mb}).

The results of (a) Davies and Richardson⁽¹⁰⁾

$$\rho_p/\rho_f = 784$$

$$d_p = 55 \text{ micron}$$

$$e_{mb} = 0.63$$

$$\rho_p = 0.945 \text{g/cm}^3$$

and (b) Godard⁽³³⁾

$$\rho_p/\rho_f = 985$$

$$d_p = 128 \text{ micron}$$

$$e_{mb} = 0.51$$

$$\rho_p = 1.184 \text{g/cm}^3$$

were plotted on Molerus' Figure 2, and it was noted that Molerus' theory predicted that for case (a) the bed should always behave particulates and for case (b) the bed should normally behave particulates at voidages below 0.8 but might behave aggregatively at a voidage of about 0.85 before behaving particulates again when the voidage reached 0.9. As in both cases the beds behaved aggregatively at voidages in excess of 0.62, Molerus' model does not seem to give a very accurate prediction of the results found in practice. This discrepancy would not appear to be the results of agglomeration (suggested by Molerus as a reason why beds of fine particles are sometimes found to behave aggregatively) because in case (a) the bed behaved particulates up to a voidage of 0.6, whereas if agglomerations had occurred, the fluidised bed would have behaved aggregatively at all voidages.

Thus far the stability theories considered have predicted that:

- i) there is a maximum size of bubble which is related to the physical properties of the bed and which decreases with $(\rho_p - \rho_f)$ and d_p (Harrison et al.⁽³⁰⁾);

- ii) all fluidised beds are unstable but that the perturbations grow very quickly in aggregative beds but only slowly in particulate ones (Jackson⁽⁴⁶⁾);
- iii) there is a minimum bubble volume that can exist because one smaller than this minimum size would be unable to leave the distributor (Ruckenstein and Muntean⁽⁵²⁾);
- iv) there is a critical value of ρ_p/ρ_f , below which bubbles cannot exist because they would remove more air from the bed than was fed into it, assuming a minimum size of bubble (Rietema⁽⁵³⁾);
- v) a fluidised bed behaving particulate is in a stable state and therefore perturbations shrink, whilst one behaving aggregatively is in an unstable state and the perturbations grow (Molerus⁽⁵⁵⁾);
- vi) the reason for the large difference between U_o and U_{mb} when fluidising fine particles with a gas is that the gas flow rate required to support a stream of bubbles, assuming a minimum bubble size, is well in excess of U_o (Rowe⁽⁵⁴⁾);
- vii) though there have been several attempts to establish a theoretical criterion for bubble stability, examination of experimental results suggests that one of the best criteria would appear to be simply U_o (Romero and Johanson⁽⁵⁰⁾).

Hence, only Ruckenstein and Muntean⁽⁵²⁾ have postulated that there may be a minimum bubble size, but their theory considers only bubble formation, and the suggested expression for the minimum bubble size is very insensitive to changes in background gas velocity. Therefore their theory is not applicable to the

phenomenon of the meta-stable bubble which the results of Davies and Richardson⁽¹⁰⁾, and Godard and Richardson⁽³⁴⁾, indirectly suggest exists. Only Rietema⁽⁵⁶⁾, using a soil mechanics approach, has a model which predicts results of a similar form to those postulated by Godard and Richardson⁽³⁴⁾. He considered that continuous interaction between particles occurs in a gas fluidised bed and suggested a model for relating the degree of particle interaction to the minimum bubble size that can rise through the bed. His model is an adaptation of the work done by Richmond and Garner⁽⁵⁷⁾ on the limiting span for arching of bulk materials in vertical two-dimensional channels. The main difference between the theory of Richmond and Garner, and Rietema, is that the former considered the arches formed by compressive forces between particles of wet clay in packed beds and the latter considered an arch formed in a fluidised bed by the tensile forces of attraction between particles. Rietema's theory is that in a gas fluidised bed it could be possible for the particles to form a stable or free arch above a bubble, and if the bubble were too small, then the gas flow out of its top would be insufficient to force the particles apart and break up the arch. The bubble would therefore be held stationary in the bed by the arch above it.

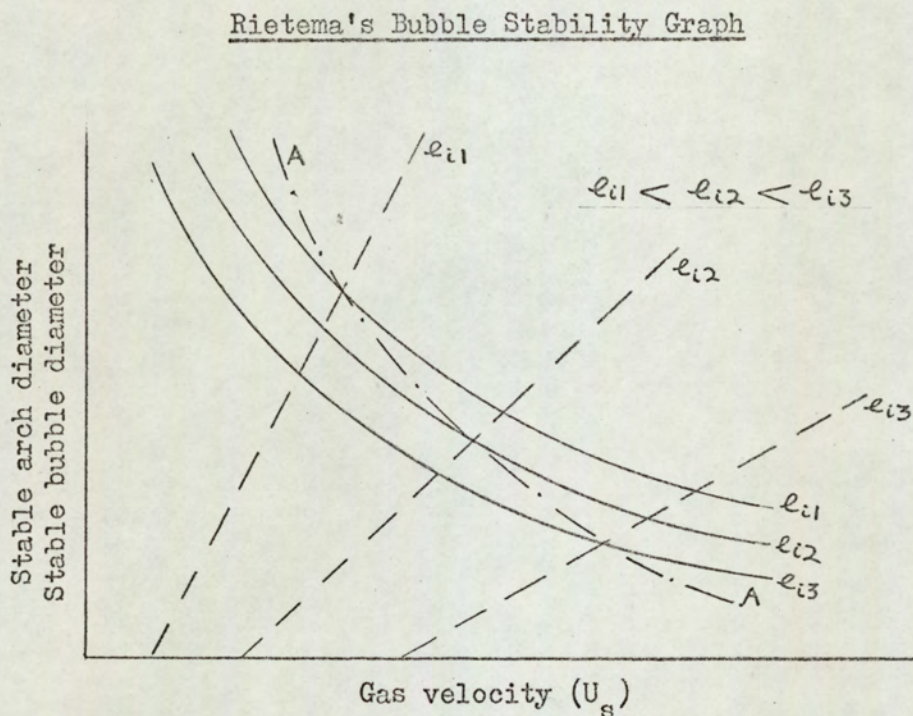
By making the same assumptions as Richmond and Garner, concerning the stresses in the vicinity of a free arch, Rietema was able to extend their mathematical theory for the limiting size of stable arch, from a packed bed system to a fluidised bed system. He determined that there is an inverse relationship between the gas velocity (U_i) through a stable arch of particles and the maximum stable arch diameter (D_s):

$$U_i = \frac{k_6}{D_s} \quad - 3.(6)$$

(where k_6 is a constant at constant bed voidage.)

In fact, k_6 is inversely related to voidage and hence the maximum stable arch diameter is also inversely related to the bed voidage. Rietema was therefore able to plot qualitatively the solid lines on the graph shown in Fig. 3.(2).

Fig. 3.(2).



(Line A is the locus of the stable bubble diameter)

He was unable to plot them quantitatively because it was impossible to evaluate k_6 which is also a function of the cohesion constant, and the angle of internal friction of the bed of particles. He considered next the gas flow through a bubble at a given bed voidage, and stated that the larger the bubble, the stronger the gas flow through it, and also for a given bubble size the higher

the bed voidage, the stronger the gas flow through it. Both these relationships are shown qualitatively on Fig. 3.(2) by the dotted lines, and the co-ordinates of the intersections of the dotted lines and a solid line of the same voidage give the bubble diameter which has just sufficient gas flow through it to break open a stable arch at that voidage. The dotted lines are, in fact, drawn straight in Rietema's paper, indicating that there is a direct relationship between bubble diameter and superficial gas velocity, but there would seem to be no published data to support this assumption. The results predicted by Rietema's model can be qualitatively summarised by the line A, Fig. 3.(2).

The weak point in this model is that a theory has been taken, with all its inherent assumptions, which was developed for a packed bed with gravitational forces causing the free arching, and it has been applied to a fluidised bed where these forces are negligible. The assumptions made by Richmond and Garner may therefore not hold when applied to a fluidised system, and because of this, though Rietema's theory does predict a type of critical bubble which increases in size with decreasing bed voidage, as suggested by Godard and Richardson⁽³⁴⁾, some doubt must be placed on the validity of this model.

The conclusion from Section 3 is that no theory predicts with any degree of certainty the existence of a meta-stable bubble phenomenon. The apparatus design therefore had to allow for the maximum possible range and number of variables because there was no indication as to which physical properties would be the most important.

A P P A R A T U S

4.1. AIR SUPPLY

The air for the fluidised bed was supplied by the compressor at between 80 - 100psig and the flow diagram is shown in Fig. 4.1.(1), (p.49). Dust and moisture were removed by the aerox filter and the Birlec minisorber respectively. The air humidity was then measured by the sensing element of a Wayne Kerr meter so that it was possible to check if the dryer became saturated. The air pressure was reduced to 40psig by a Hamilton pressure controller and this also reduced the pressure fluctuations considerably. The bubble injection off-take was positioned after this reducer.

Next came a Manostat pressure reducer which reduced the pressure at its outlet to 10psig, and pressure fluctuations below a detectable level. The valve at the Manostat inlet was set such that the maximum possible flow was just less than the maximum permitted rate for the Manostat to avoid diaphragm vibration. The outlet of the Manostat fed into an inlet manifold which supplied a bank of variable area flow meters. The outlet manifold was connected via a valve to the fluidised bed air box. Fig. 4.1.(2), (p.50) is a photograph showing the general arrangement of the apparatus.

The flow meters used were metric type Rotameters and Fischer and Porter tri-flat meters. It was possible to meter flows between $6\text{cm}^3/\text{s}$ and $1.7 \times 10^3\text{cm}^3/\text{s}$.

Each meter had its own inlet and outlet valves and

where possible the inlet was of the needle valve variety and the outlet was of the rubber diaphragm type. This meant that the air flow could be controlled accurately by the inlet valves, without the likelihood of the flow altering due to deformation of the rubber. The outlet valves were used for isolating any meter not in use as their rubber internals ensured a definite seal. The needle valve at the inlet to the fluidised bed was to enable the meters to be operated under pressure if it was found necessary to increase their range and to reduce float oscillation.

Fig. 4.1.(1).

Air Flow Diagram

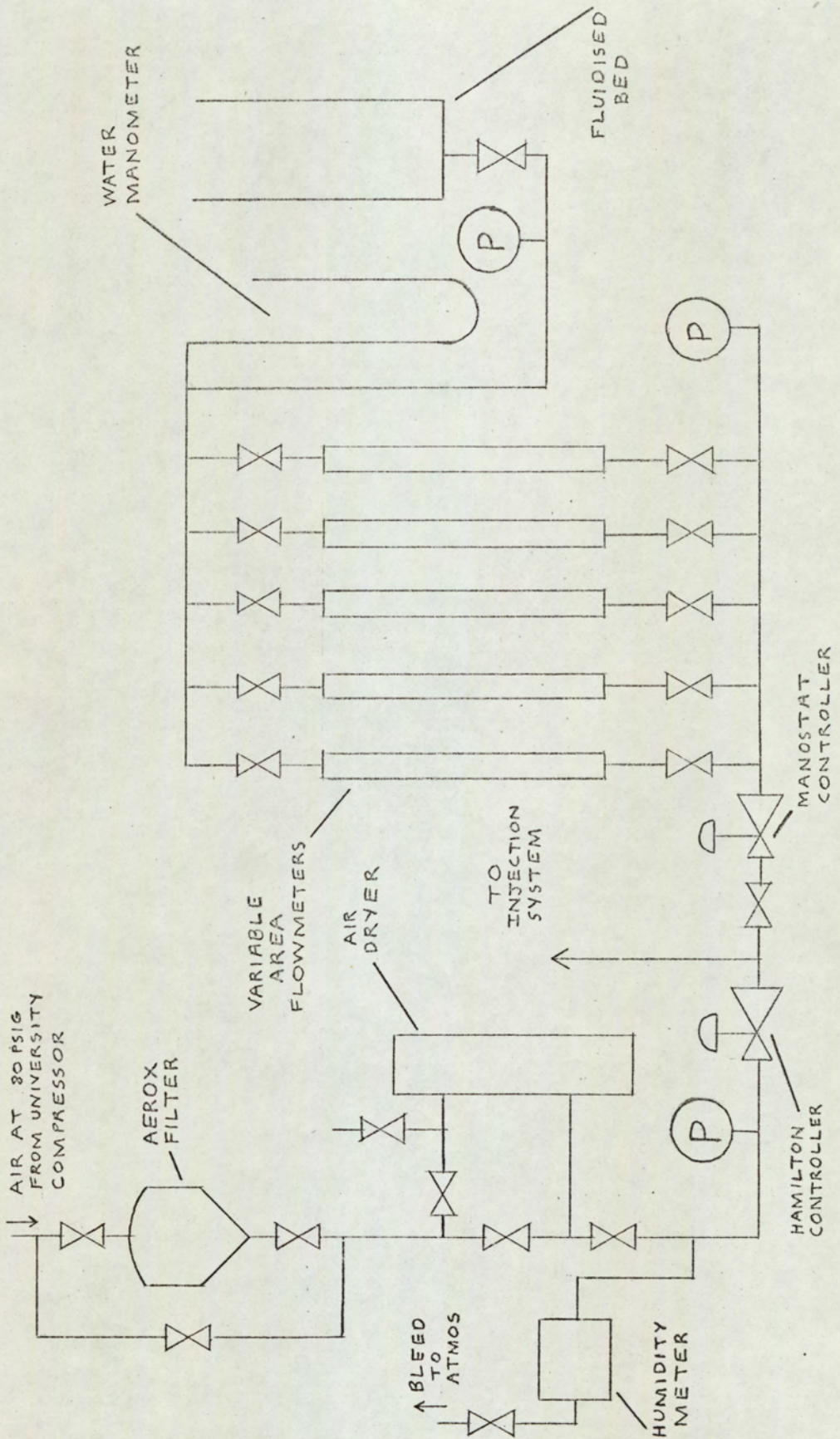


Fig. 4.1.(2).

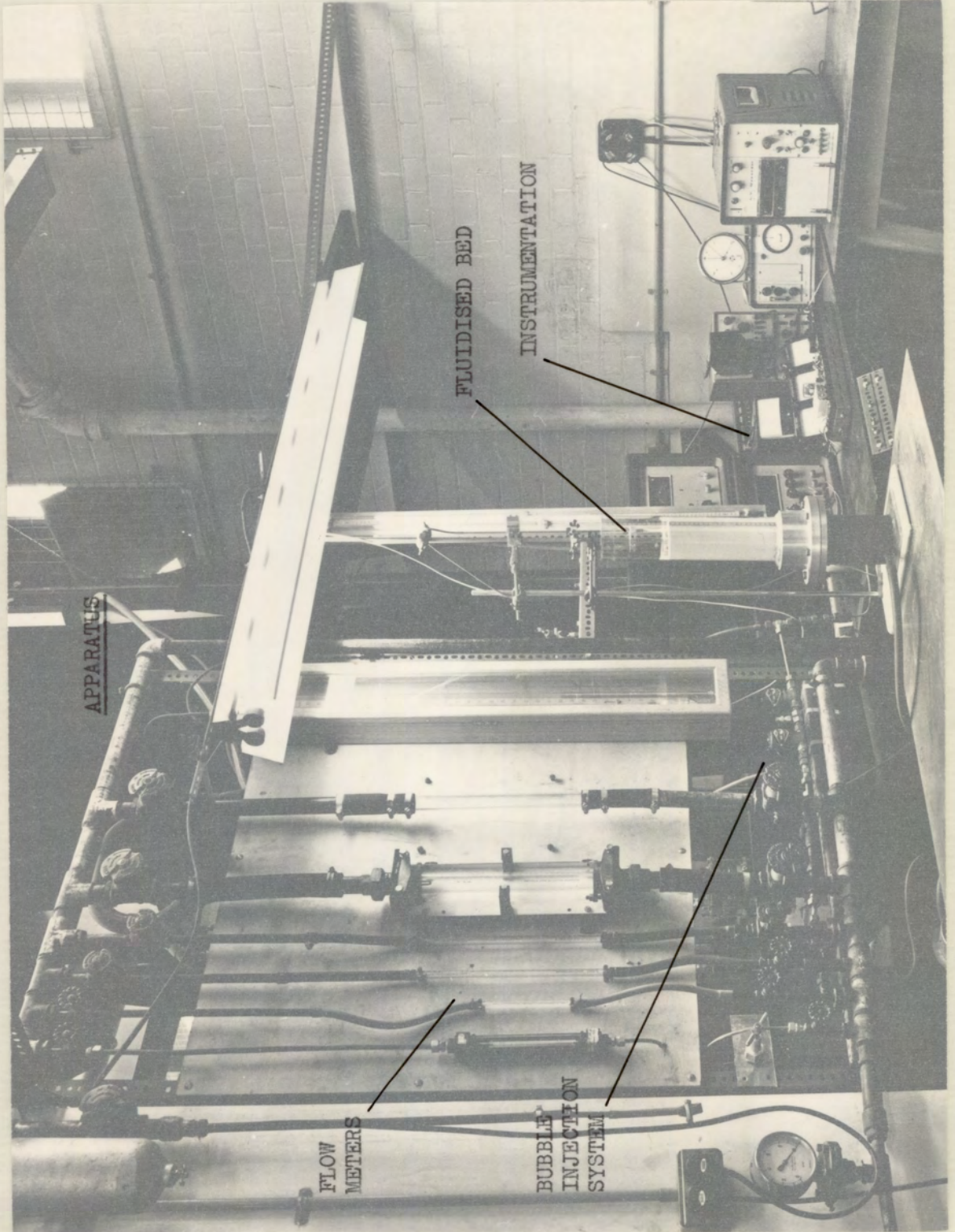
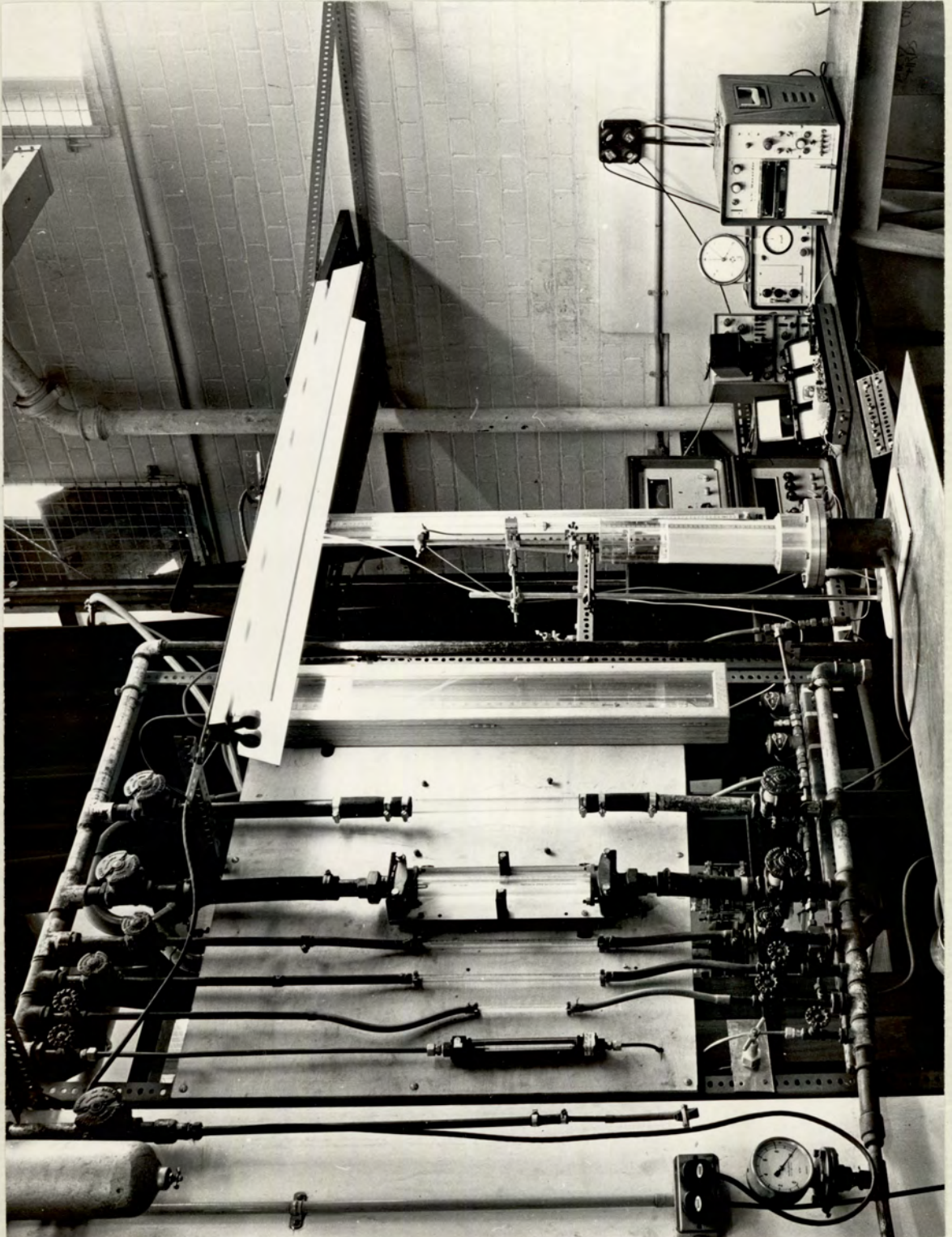


Fig. 4.1.(2).



4.2. BUBBLE INJECTOR SYSTEM

It was noted that several workers^(14, 10, 34) had, by virtue of their experimental technique, been unable to predict the volume of gas they had injected into a fluidised bed until after the injection. In fact, about ten injections had to be made and the average volume per injection determined from the air supply pressure drop.

This was felt to be a disadvantage, and therefore, for this work an injection system was built such that a variable predetermined volume of gas could be injected, using two solenoid valves, one on either side of a small pressure vessel, (Fig. 4.2.(1), (p.53) and Fig. 4.2.(2), (p.54)). The injector system tapping was before the Manostat inlet (see Fig. 4.1.(1)) to prevent the injector causing any surging in the supply to the bed when very low fluidising rates were being used. The air pressure was therefore at 40psig, and this was reduced to about 10psig by a Negretti and Zambra controller which damped out all noticeable pressure fluctuations.

After the controller there was a variable bleed to atmosphere and then a mercury manometer. Then came the first of the two Alcon solenoid valves, which were in series and joined by the pressure vessel (a copper pipe approximately 6cm in length and 1cm in diameter). The outlet of the second solenoid valve then split to the calibration equipment and also to the bubble injector tube. The bubble injector tube was a 0.3cm diameter glass tube with a 350 mesh gauze glued over its outlet, to prevent backflow of particles which would reduce the velocity of the injected air.

The solenoid valves were operated by biased toggle switches which were suppressed with 0.1 μ F capacitors. The switch for the

second solenoid valve was also wired such that when the switch was closed a mark was recorded on the oscillograph trace.

The injector calibration system was an inverted burette placed inside a measuring cylinder filled with water.

Fig. 4.2.(1).

Bubble Injector System

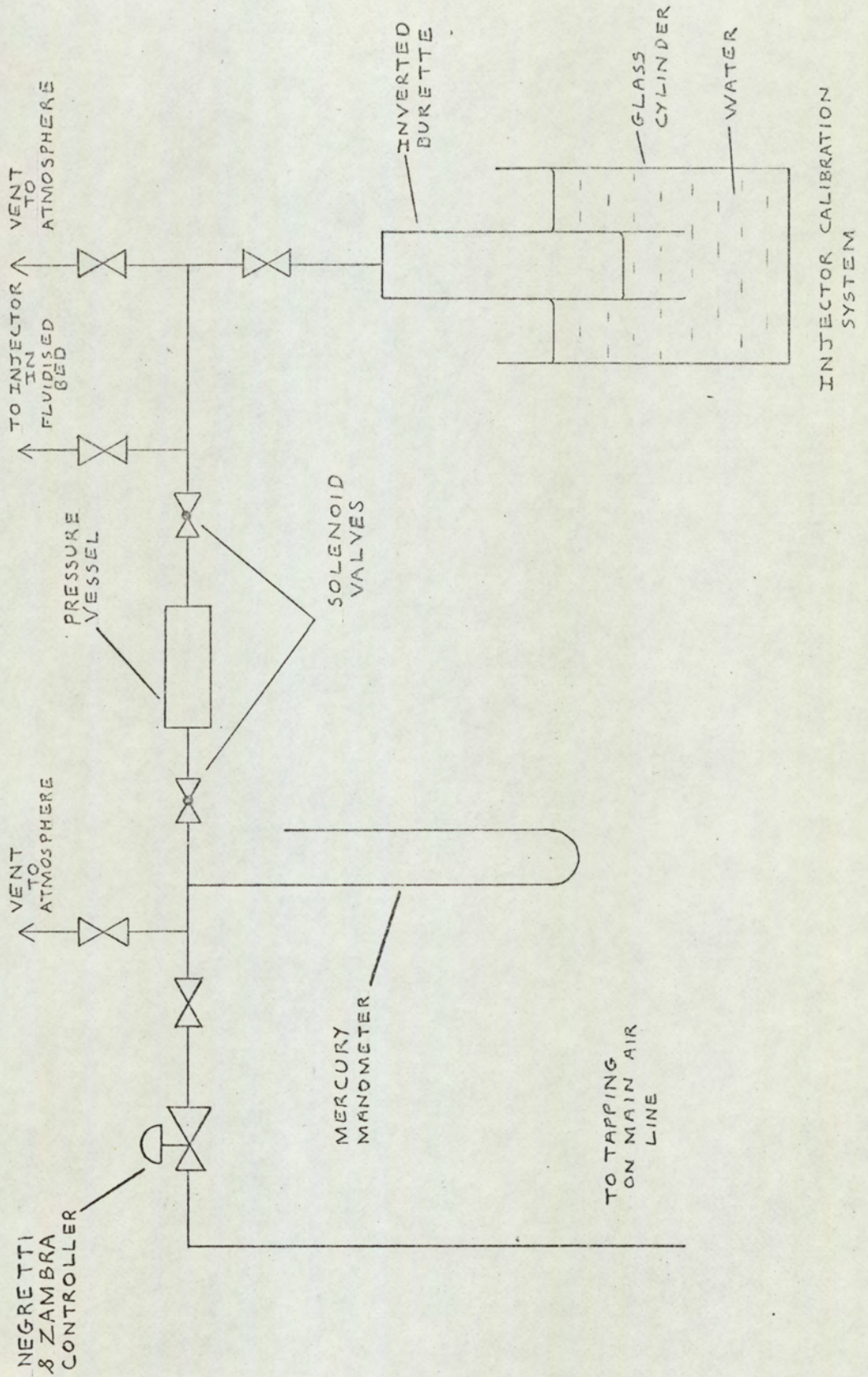


Fig. 4.2.(2).

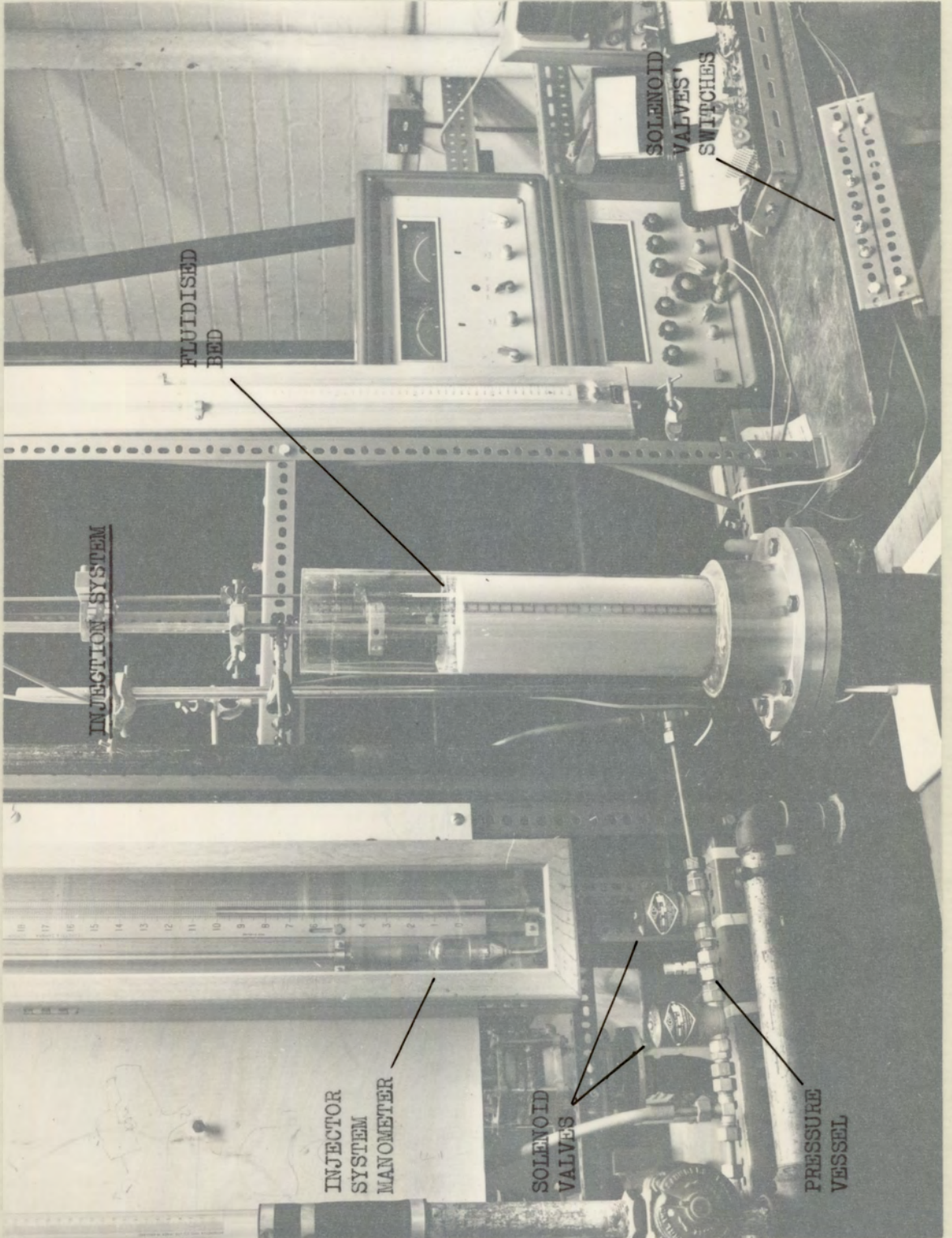
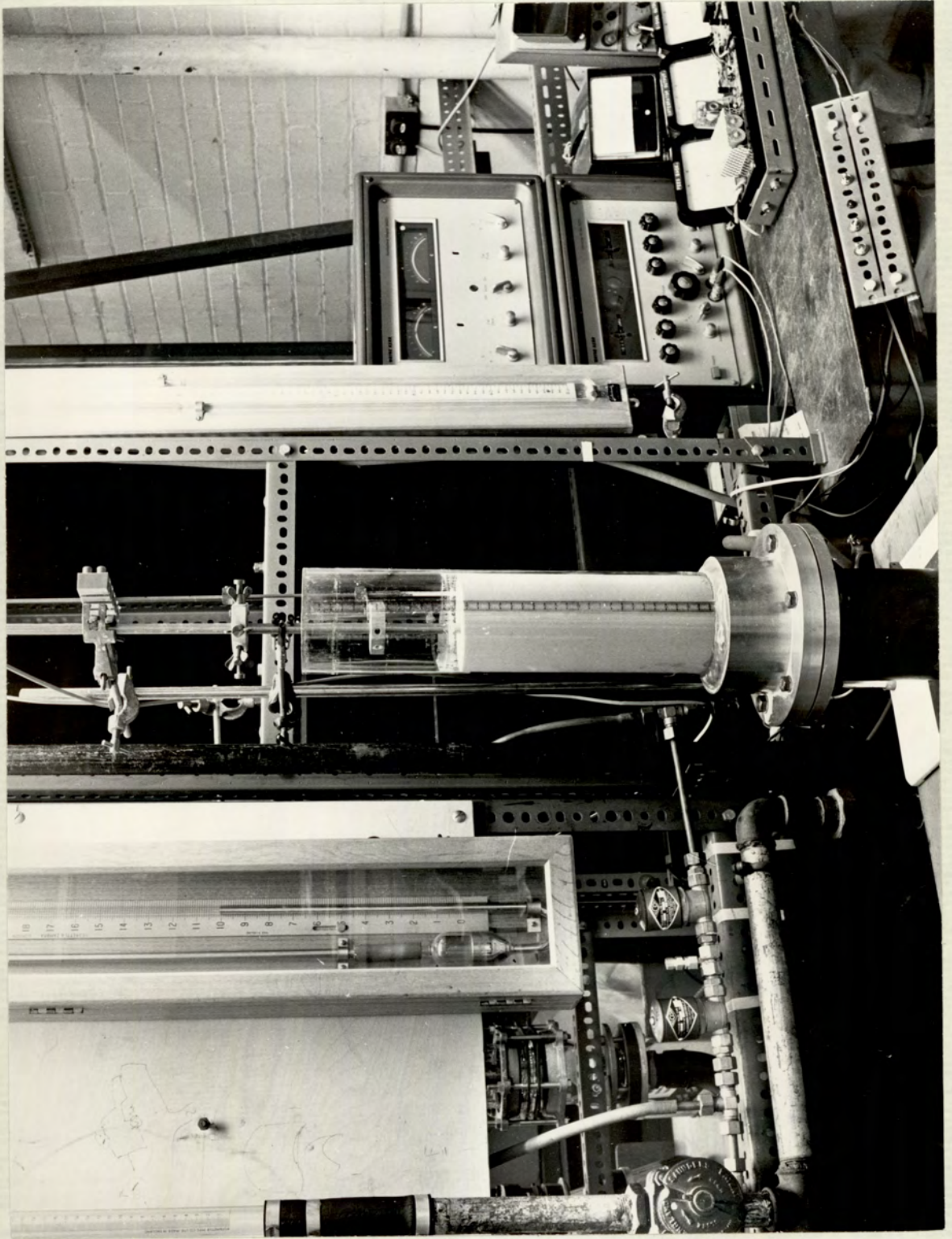


Fig. 4.2.(2).



4.3. THE FLUIDISED BED CONTAINER

It was considered that, though the experiments might ultimately have to be carried out at raised pressures and temperatures, the apparatus would be operated initially at ambient conditions to facilitate commissioning and calibration. Two glass containers were therefore built, one for gas fluidisation and the other for liquid fluidisation.

Both containers were glass tubes about 50cm in length, 9cm inside diameter and with a wall thickness of 0.3cm. A recess was turned in the duralumin bases for porous plate distributors and the apparatus assembled as shown in Fig. 4.3.(1), (p.56) and Fig. 4.3.(2), (p.57). Earlier designs had an additional flange to assist in changing distributors, but this was unnecessary once the type of distributor had been chosen.

The difference between the gas and the liquid fluidised beds was that the former had a stronger flange. It was considered that the liquid fluidised bed would only be used occasionally and therefore a small flange would, with care, suffice; whereas the gas fluidised bed would be in almost continuous use and the glass therefore needed a much greater degree of support (Fig. 4.2.(2)).

Fig. 4.3.(1).

Gas Fluidised Bed Container

(All dimensions in centimetres. Scale: $\frac{1}{2}$ full size)

List of Materials

- | | |
|---------------------------------|---|
| A - Duralumin | F - 0.32cm thick Vyon covered with a filter paper |
| B - Glass | G - 0.16cm thick rubber gasket |
| C - 10cm diameter copper tube | H - Alignment tape |
| D - 0.95cm diameter copper tube | I - Araldite |
| E - 0.65cm diameter copper tube | J - 6 x 0.8cm diameter bolts |

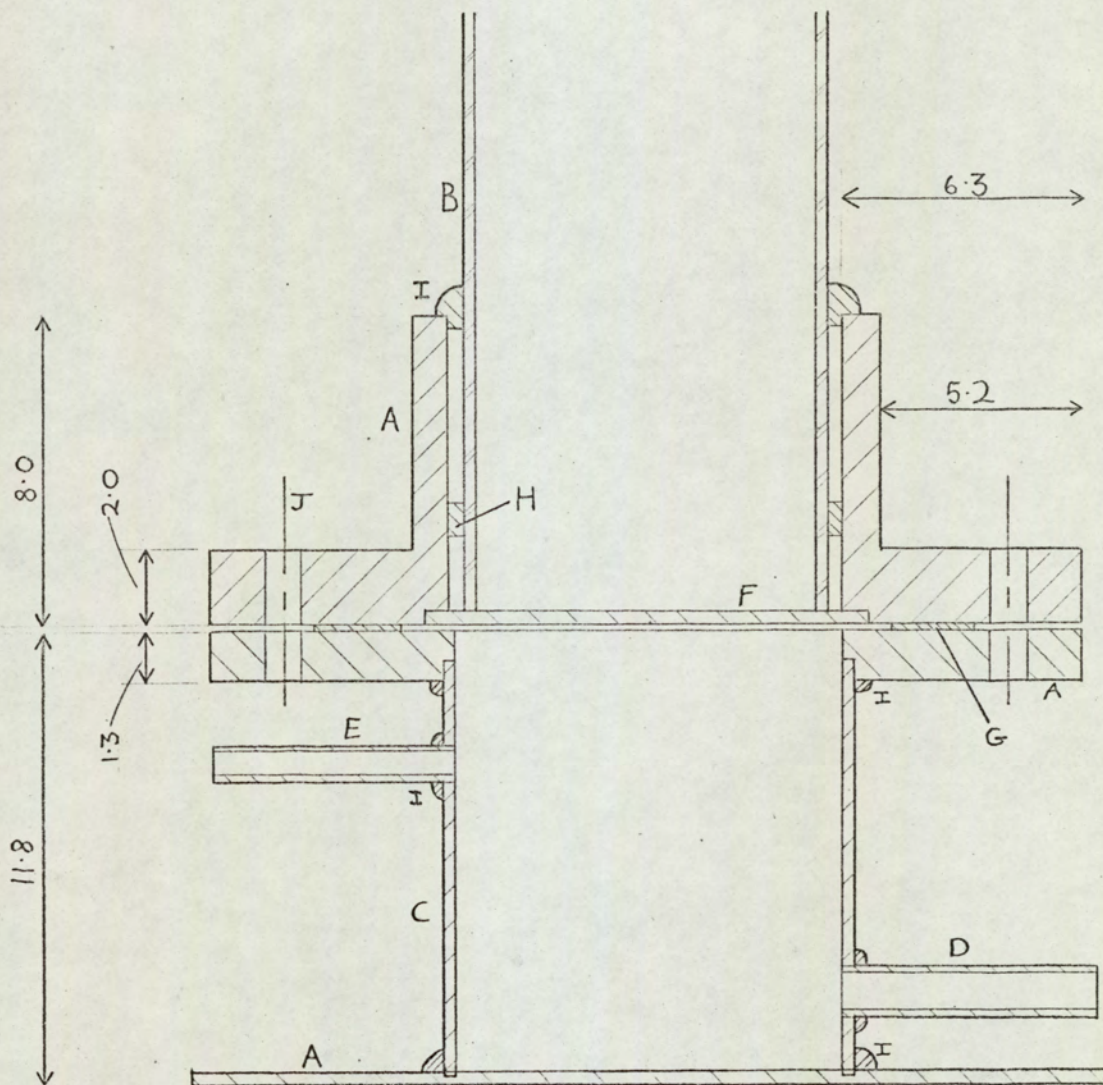


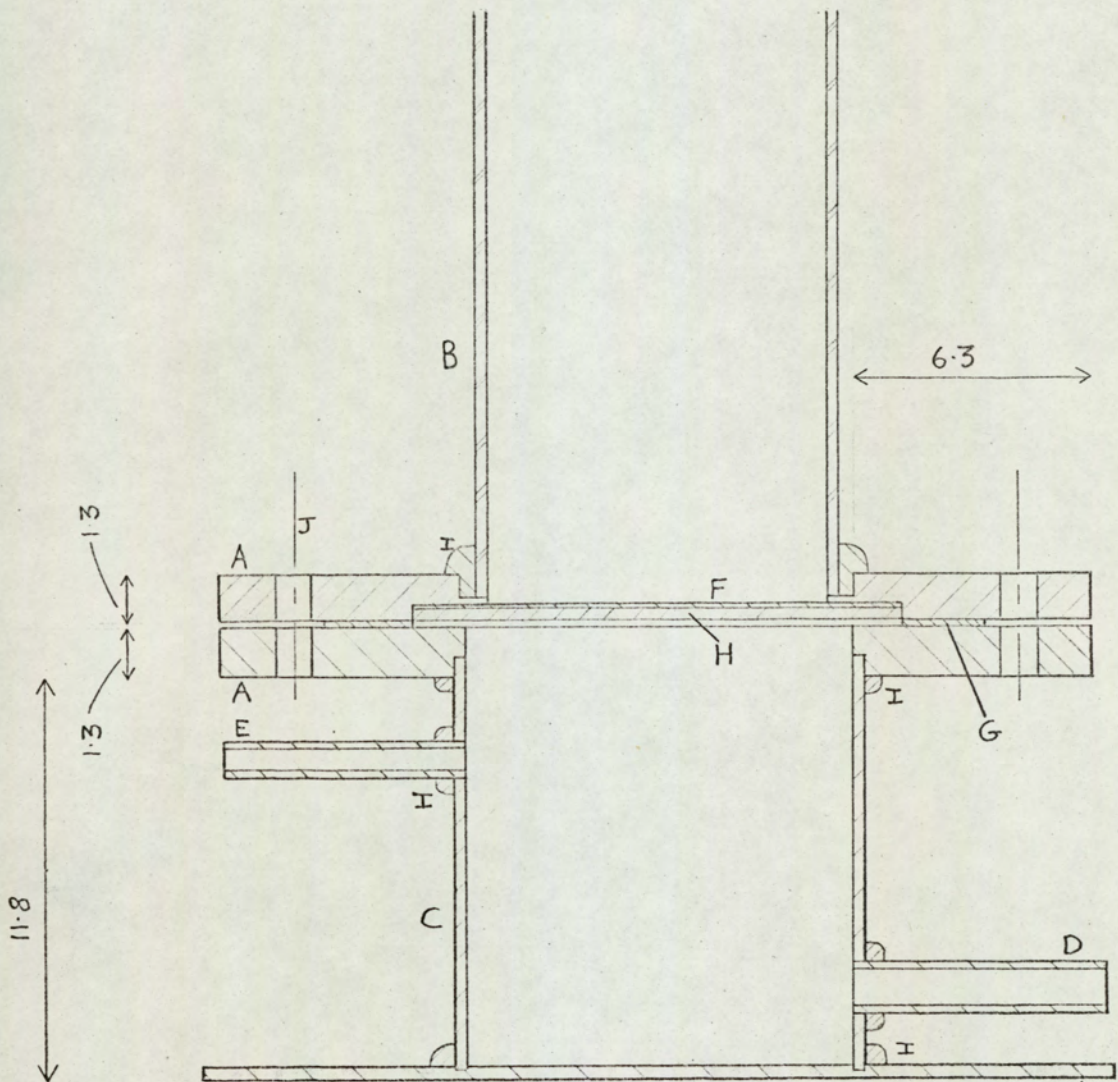
Fig. 4.3.(2).

Liquid Fluidised Bed Container

(All dimensions in centimetres. Scale: $\frac{1}{2}$ full size)

List of Materials

- | | |
|---------------------------------|--------------------------------|
| A - Duralumin | F - 200 BS Mesh gauze |
| B - Glass | G - 0.16cm thick rubber gasket |
| C - 10cm diameter copper tube | H - Perforated metal disc |
| D - 0.95cm diameter copper tube | I - Araldite |
| E - 0.65cm diameter copper tube | J - 6 x 0.8cm diameter bolts |



4.4. DISTRIBUTORS FOR GAS FLUIDISED BED

4.4.1. Sintered Bronze

A sintered bronze distributor was tried but it was found to have weak points so that it produced several jets of air rather than even distribution. It was therefore felt that some medium with very fine pores was required.

4.4.2. Filter Paper

Filter paper was an obvious example of a porous medium, but a base had to be designed to prevent the paper from distorting upwards when the air pressure was applied. The filter paper was glued onto a rubber gasket and an expanded metal disc placed above and below to support it. It was found that the expanded metal disc above the paper tended to generate bubbles, but without it the distortion was too great at the flow rates required to fluidise large particles.

4.4.3. Vyon

From the work with filter papers, it was concluded that for high flow rates a rigid distributor would have to be used. A disc of Vyon (a porous plastic material obtained from Porous Plastics Ltd.) was cut to the required diameter and found to give better distribution than sintered bronze. To select a portion of Vyon without weak spots, the complete sheet was mounted in an air box, a shallow covering of fine particles added and the air turned on. It was then possible to determine the areas giving the most uniform distribution and to cut out these portions for distributors. The Vyon disc was mounted as shown in Fig. 4.3.(1).

4.4.4. Vyon and Filter Paper

Though Vyon distributors selected by the method described in 4.4.3. were adequate for particles whose diameter was greater than 150 micron, it was felt that for smaller diameters the uniformity of distribution provided by filter paper was required.

After measuring the pressure drop and comparative mechanical strength of several filter papers, a Whatman Number 1 was chosen. The paper was then cut to the same size as the Vyon disc and glued to its periphery. This was found to be adequate for fluidising particles with a diameter of less than 100 micron and a density of less than 3g/cm^3 . For larger particles it was necessary to glue the paper to the Vyon in the centre, creating a dead patch of approximately 0.3cm in diameter. The effect of this dead patch was only visually apparent for about 3cm above the distributor.

4.5. DISTRIBUTOR FOR LIQUID FLUIDISED BED

The distributor pressure drop even when fluidising with liquids of very low viscosity such as white spirit or pentane, was too high with a Vyon distributor, and therefore a 200 mesh gauze distributor was used.

An expanded metal disc was cut to act as support for the gauze, but as the disc had an uneven surface it was first necessary to form a 1.25cm wide rim of mounting plastic round the periphery to which the gauze could be glued. This was done by oiling the distributor recess in the liquid fluidised bed flange, placing the disc in the recess and pouring in mounting plastic, ensuring that the plastic went through the disc perforations. The disc was then removed, the smooth surface of the plastic degreased and glued to the 200 mesh gauze and mounted as shown in Fig. 4.3.(2).

4.6. CLOSURE OF SECTION 4

The fluidisation apparatus has facilities for metering a wide range of gas flow rates, for changing of distributors and for injecting single bubbles of predetermined volumes. Attention was therefore turned to the instrumentation necessary to record bubble volumes, bearing in mind the conclusions drawn in Section 2.4.

I N S T R U M E N T A T I O N

5.1. INTRODUCTION

Some work had previously been carried out by Lea⁽⁵⁸⁾, who used a Wayne Kerr Bridge fed by an external oscillator. The bridge output passed through an amplifier to an ultra-violet oscillograph, acting as an external detector. The capacitance being measured was that existing between the two plates of a probe which was connected to the bridge with screened leads. This system was perfectly satisfactory when used to measure a non-varying capacitance, the bridge being adjusted to give the minimum deflection on the galvanometer. At this minimum deflection the bridge was at its balance point and the capacitive and conductive values could be read from the bridge dials.

This method of measurement, however, is fundamentally sound only when the bridge is in balance, though in practice the bridge can be calibrated for change in capacitance versus out-of-balance current, as long as there is no change in the conductance value of the system being examined. Unfortunately, when the probe was placed in a fluidised bed, it was found that a change in capacitance was accompanied by a small but significant change in conductance, the ratio of the two changes depending on the material being fluidised and the fluidising medium.

This varying conductance ruled out the use of Lea's apparatus because in the present work it was required to measure the capacitance change with some degree of precision, and therefore to overcome this inherent error a more accurate system was developed.

5.2. GENERAL ARRANGEMENT OF INSTRUMENTS

The system (Fig. 5.2.(1), (p.63) and Fig. 5.2.(2), (p.64)) consisted of a Wayne Kerr Bridge coupled to an Autobalance, the output from which fed through a differential amplifier to an oscilloscope wired in parallel with a UV oscillograph.

Fig. 5.2.(1).

Diagramatic arrangement of instruments

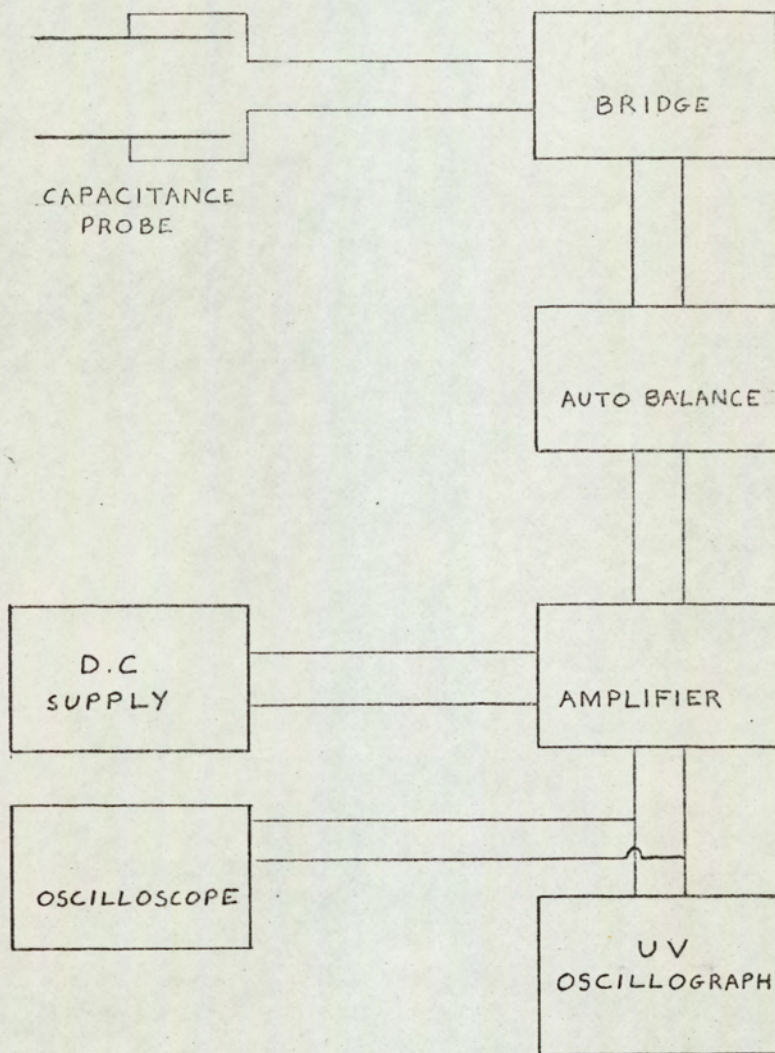


Fig. 5.2.(2).

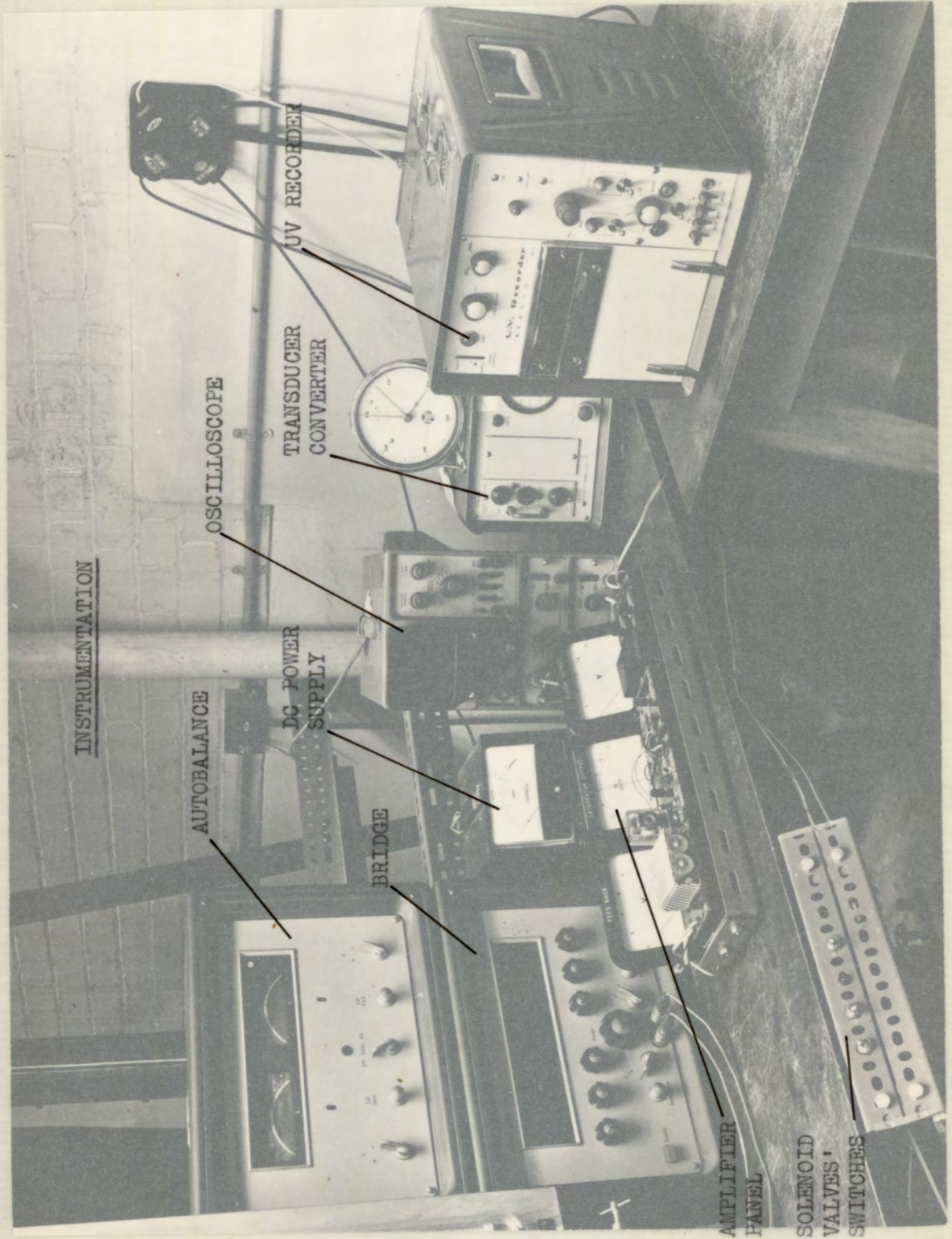
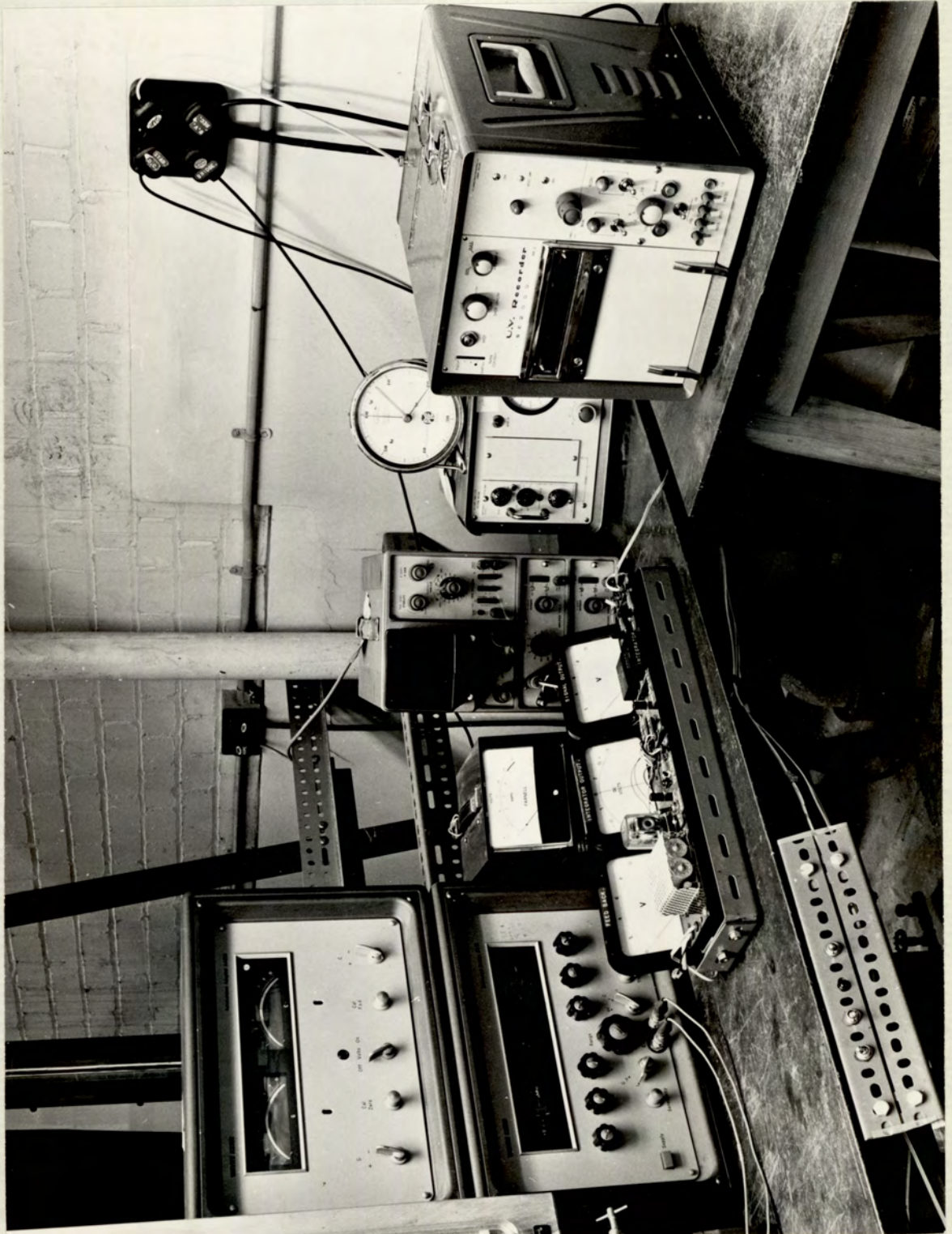


Fig. 5.2.(2).



5.3. THE BRIDGE

The Bridge used was a Wayne Kerr Universal Bridge, type B221. This was an A.C. bridge operating with an internal source of 1592Hz, but it could be operated at any frequency using an external source and detector. It was capable of measuring capacitance values from $10\mu\text{F}$ to 0.002pF with an accuracy of $\pm 0.001\text{pF}$, irrespective of the length of connecting cables.

To ensure that the final output from the instruments was directly proportional to the capacitance existing between the plates of the probe, the circuits in the bridge and the other instruments were studied in some detail.

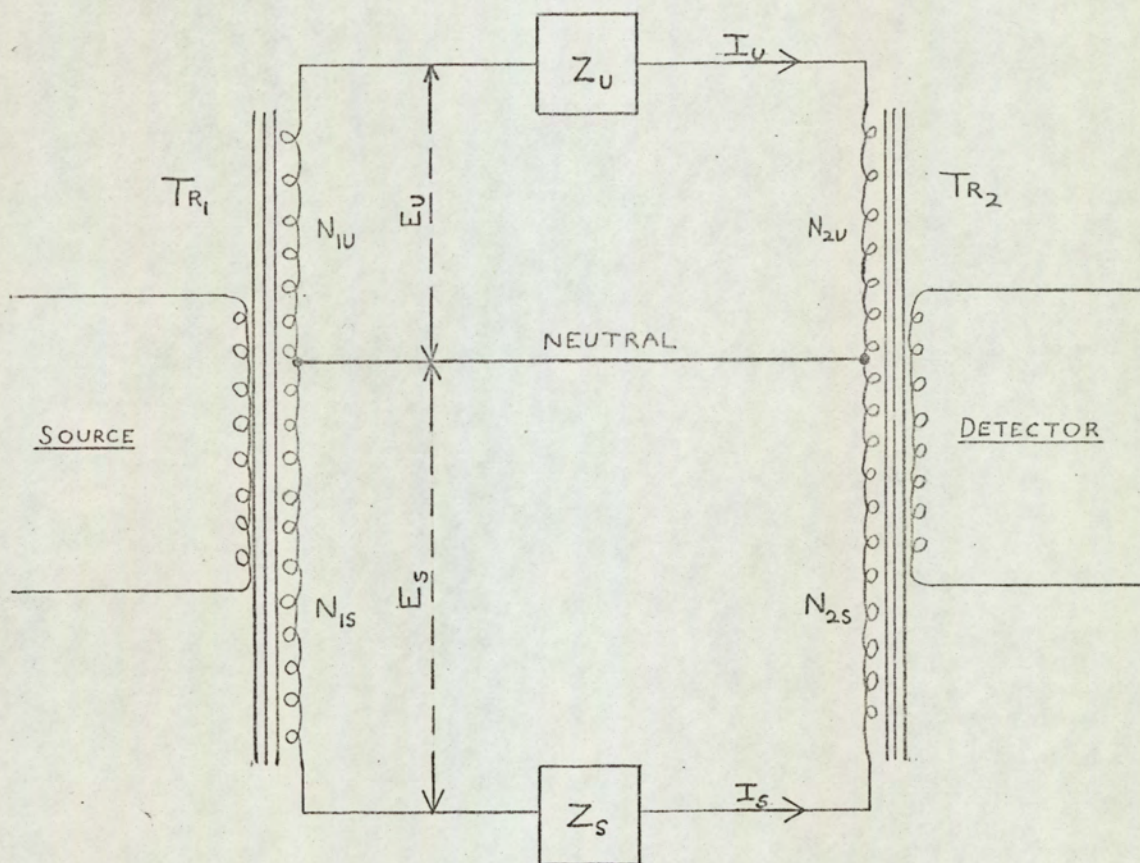
A simplified circuit diagram of the bridge is shown in Fig. 5.3.(1), (p.66), in which the subscripts 1 and 2 refer to the voltage and current transformer respectively, and the subscripts u and s refer to the unknown and standard side of the bridge respectively.

The source voltage was provided by the 1592Hz internal oscillator and this was fed into the primary winding of the voltage transformer, Tr_1 . The secondary of Tr_1 was tapped to give two sections of N_{1u} and N_{1s} turns.

The primary winding of the current transformer, Tr_2 , was tapped to give N_{2u} and N_{2s} turns, and the secondary was connected to the detector. Referring to Fig. 5.3.(1), if the impedance, Z_s , is adjusted to give zero deflection in the detector then, under these conditions, zero flux is produced in the current transformer and there is therefore no voltage drop across its windings. The detector side of both the unknown, Z_u , and the standard, Z_s , impedances are therefore at neutral potential. The voltages across the unknown and the standard are then E_u and E_s respectively.

Fig. 5.3.(1).

Simplified Bridge Circuit



Tr - Transformer

Z - Impedance

E - Voltage

I - Current

N - Number of turns on a transformer

Subscripts 1 and 2 refer to the voltage and current transformers respectively

Subscripts u and s refer to the unknown and standard sides of the bridge respectively

Therefore from Ohm's Law:

$$I_u = E_u / Z_u \quad - 5.3.(1)$$

$$I_s = E_s / Z_s \quad - 5.3.(2)$$

(where I_u and I_s are the currents flowing through Z_u and Z_s respectively.)

In order that the core flux in the current transformer be zero the sum of the ampere-turns for the standard side and the unknown side must equal zero,

$$\text{i.e. } I_u N_{2u} = I_s N_{2s} \quad - 5.3.(3)$$

Substituting for I_u and I_s in 5.3.(1) and (2) gives:

$$\frac{E_u N_{2u}}{Z_u} = \frac{E_s N_{2s}}{Z_s}$$

$$\text{i.e. } Z_u = \frac{E_u N_{2u} Z_s}{E_s N_{2s}} \quad - 5.3.(4)$$

For an ideal transformer the voltage ratio is equal to the turns ratio; therefore:

$$Z_u = \left(\frac{N_{1u} N_{2u}}{N_{1s} N_{2s}} \right) Z_s \quad - 5.3.(5)$$

Equation 5.3.(5) shows the advantage to be gained by using a transformer bridge over a conventional bridge, because there are two ratios available (N_{1u}/N_{1s} and N_{2u}/N_{2s}) which can be varied

as opposed to the one ratio of impedances with a conventional bridge.

When the bridge was operated without an external detector the current was tapped from the secondary of the current transformer, fed through an amplifier and then to two magic eyes. If an external detector were plugged in across the secondary of Tr_2 , the internal amplifier was automatically disconnected. Since the bridge was to be used with a varying input, it was necessary to have the capacitance and conductance terms separated, such that the capacitance change could be measured without interference from conductance variations. The bridge output was therefore fed into an autobalance.

5.4. THE AUTOBALANCE

5.4.1. The Autobalance Circuit

The Autobalance, which was coupled to the B221 bridge, was the Wayne Kerr Adaptor type AA221. It included its own source and detector operating at 1592Hz and allowed the bridge to be operated without any manual balancing. It had outputs available for recording conductive and capacitive components simultaneously, as can be seen from Fig. 5.4.1.(1), (p.70).

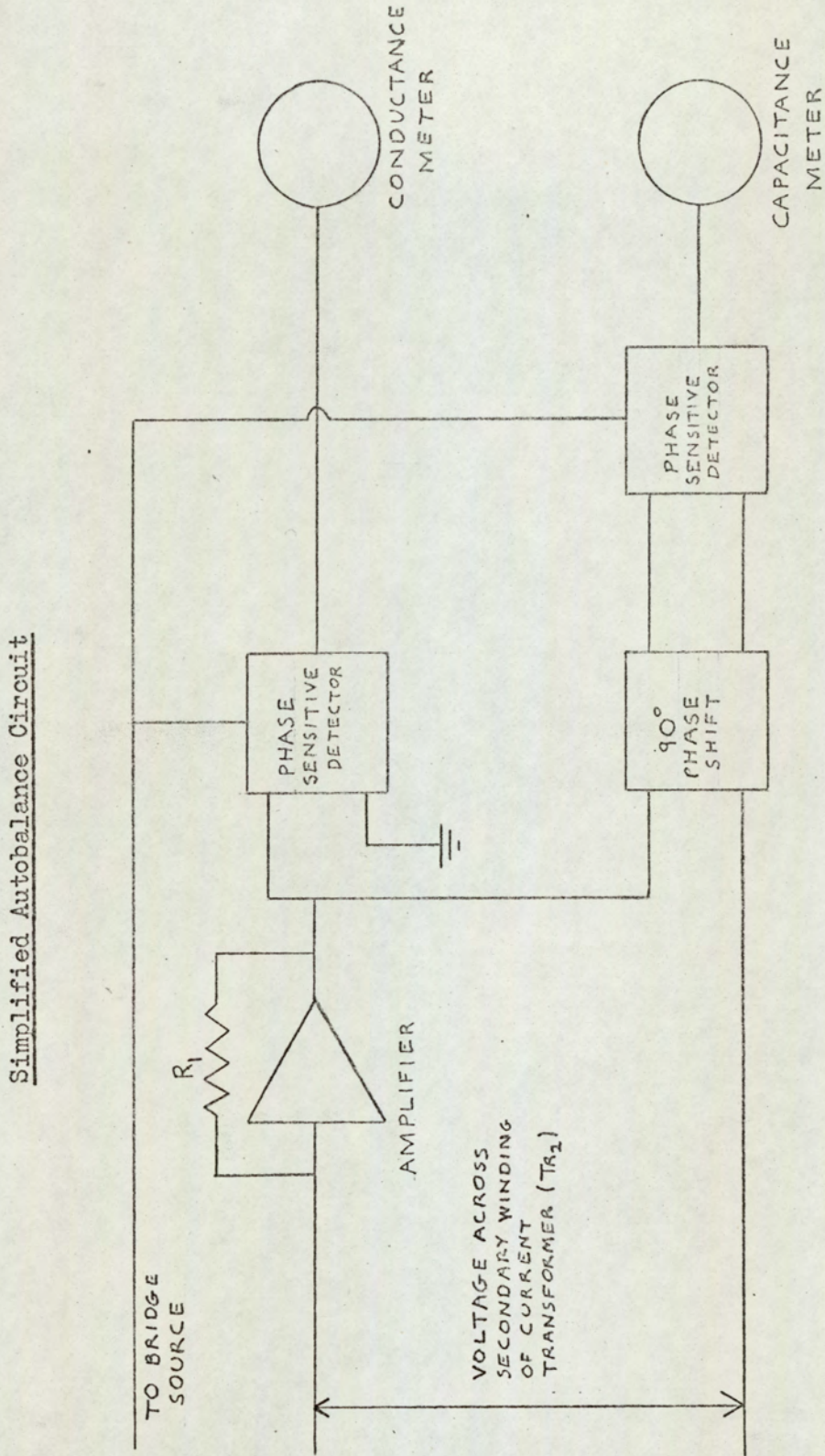
Considering Fig. 5.4.1.(1), any out-of-balance in the bridge circuit causes a current to flow in the current transformer, Tr_2 . The input to the autobalance is connected across the secondary winding of Tr_2 , so any current flowing in this secondary winding passes through the autobalance amplifier. The negative feedback from the amplifier produces a current in opposition, so reducing to zero the net core flux in the current transformer. The output signal is derived by measuring the voltage developed across the feedback resistor, R_1 . This voltage is applied to two phase-sensitive detectors, one of which is preceded by a 90° phase-shifting circuit. Both detectors are followed by meters which display the in-phase and quadrature terms of the unknown.

5.4.2. The Autobalance Outputs

The output signal from the autobalance was a differential A.C. signal which had been passed through a full wave rectifier and modulated by the degree of out-of-balance of the bridge. A current output and a voltage output were provided for an external detector and both outputs were considered:

- i) The current output provided $100\mu\text{A}$ into a resistance of

Fig. 5.4.1.(1).



less than 10Ω . If this resistance value were exceeded, then the bridge accuracy was affected. The most sensitive available galvanometer (the S.E. Labs. type A35) had a sensitivity of $0.8 \mu\text{A}$ per cm scale deflection but required a damping resistance of 350Ω . Therefore even with the maximum value of 10Ω shunted across the autobalance output, the maximum galvanometer deflection possible was only about 3cm, i.e. 20% of FSD. This output was therefore of little use in the present work.

- ii) The voltage output provided 0 - 100mV with a source impedance of approximately $10\text{k} \Omega$, and to prevent overloading of the bridge, the detector had to have an input impedance of at least $200\text{k} \Omega$. As the galvanometers had to look into an impedance of less than $1\text{k} \Omega$, it was therefore clear that the signal had to be amplified before going to the galvanometer, and that the amplifier had to have a pre-amplifier, based on a field effect transistor, in order to produce the required high input impedance and low output impedance.

The autobalance output was a differential output, such that neither side could be earthed and this created difficulties when attempting to obtain a suitable amplifier.

5.5. THE AMPLIFIER

5.5.1. The Amplifier Circuit

Initially, an attempt was made to design and build a suitable amplifier from component parts, but difficulty was experienced in obtaining matching transistors and in current stabilisation. Professional assistance was therefore sought and the circuit shown in Fig. 5.5.1.(1), (p.74) was built after discussions with the British Scientific Instrument Research Association⁽⁵⁹⁾, and Ancom Limited⁽⁶⁰⁾. It consisted of a balanced input differential amplifier, type 15A - 3a, with a very high input impedance. The output from this amplifier was fed in parallel to a galvanometer and to another amplifier, type 15A - 3, which acted as an integrator. The output from the 15A - 3 was fed to another galvanometer.

The integrator amplifier 15A - 3 had one input to common and the other one was connected to the output of the 15A - 3a via a large resistance (R_2). The amplifier was shunted with a capacitor C_3 , and varying the value of the product of R_2 and C_3 , varied the time constant of the integrator circuit. It was also possible to feed a constant negative voltage into the integrator input from the potentiometer, R_5 , so that only voltages above the value of the negative feed were integrated. This allowed the bridge to be set out of balance without the signal being integrated.

The minimum gain of the 15A - 3a was 100, and with the 0 - 100mV input from the bridge, this gave an amplifier output of 0 - 10V. As this was perfectly adequate, the base of the amplifier was wired as shown in Fig. 5.5.1.(2), (p.75). The closed loop gain was stated to be $((R_6 + 10K\Omega)/200)$ and the required value of R_6 was therefore $10K\Omega$, to produce the minimum gain of 100.

The 15A - 3a amplifier was set up as follows:

- i) Terminals 1 and 2 were shorted to common and R_7 adjusted for no output.
- ii) Terminals 1 and 2 were shorted. 1 volt DC above common was applied to them and R_8 adjusted for zero change in output.
- iii) Terminals 1 and 2 were shorted and 1 volt AC at 50Hz applied to them. C_4 was trimmed for minimum output.

From the data sheet on the 15A - 3a, which merely stated the input and output impedances and the closed loop gain, it would appear that the amplifier consisted of a differential field effect transistor amplifier as a pre-amplifier. This would provide the high input impedance and the low output impedance and have a gain of approximately 0.98. The output from the pre-amplifier would be matched to the input of a differential operational amplifier which would carry out the actual amplification of the signal.

5.5.2. The DC Power Supply

The power to drive the Ancom amplifiers was provided by a Farnell Type L30 stabilised voltage supply, with the 30V supply being split to $\overset{+}{-}15V$ by the circuit, shown in Fig. 5.5.1.(1).

Fig. 5.5.1.(1).

Amplifier Circuit Diagram

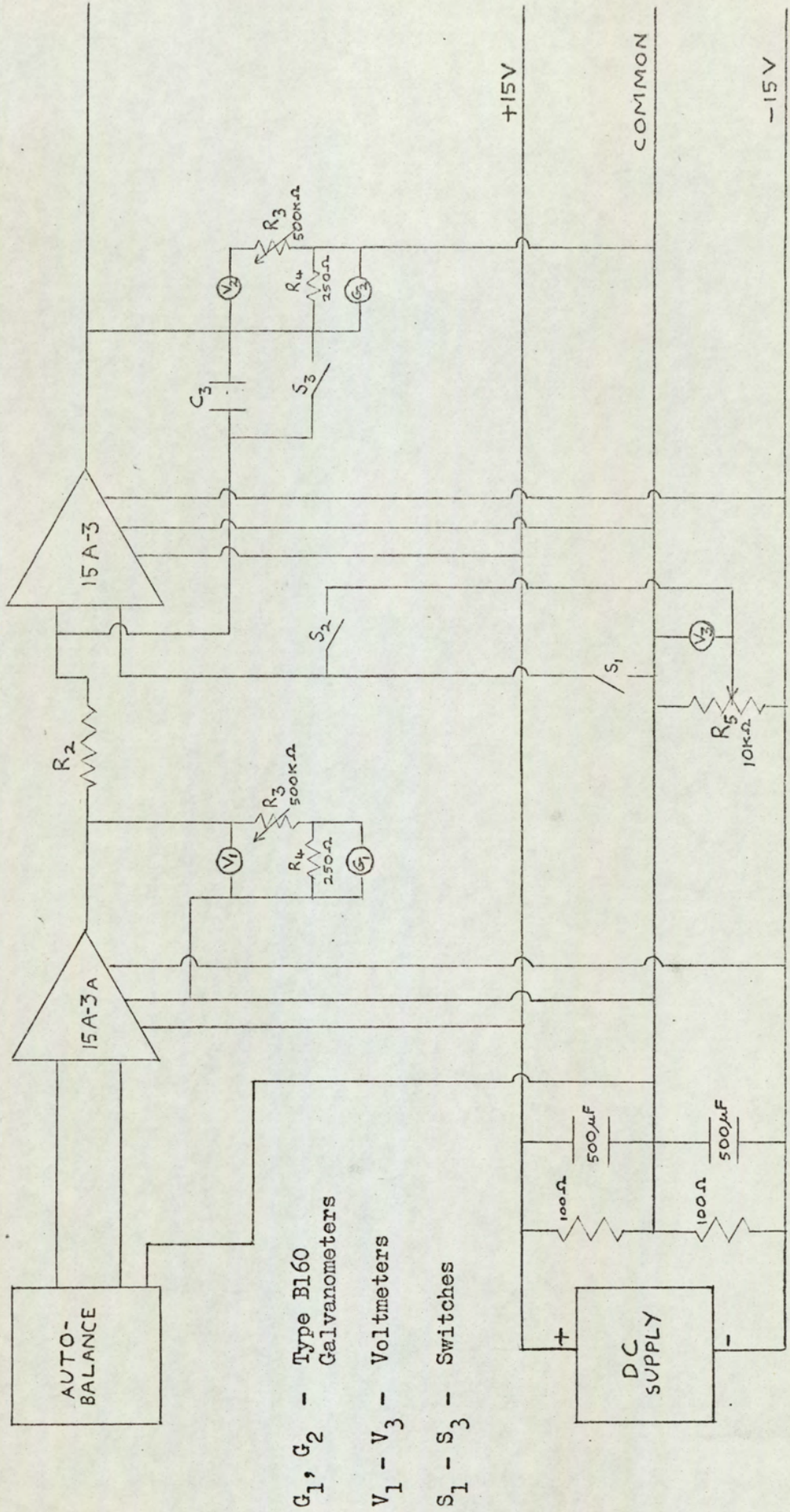
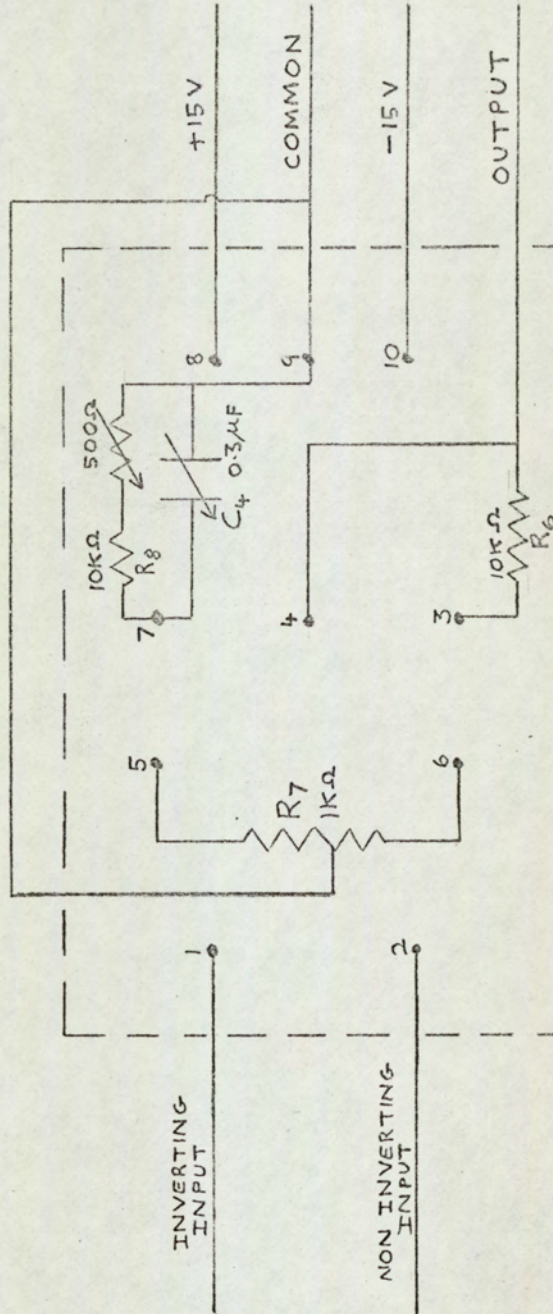


Fig. 5.5.1.(2).

External Wiring of 15A - 3a Amplifier



5.6. UV OSCILLOGRAPH S.E. LABS. TYPE 2000 Mk II

5.6.1. Oscillograph Specification

The UV oscillograph had provision for 12 galvanometers and a maximum paper speed of 200cm/s. Timing lines could be printed up to a maximum of one every 0.015s, and there was also a pulse recorded every second. An additional marker was provided which was operated manually by the second solenoid valve of the bubble injection system.

The UV paper used was Kodak Linagraph direct print paper which developed in daylight in a few seconds. It was not found necessary to stabilise the traces chemically.

5.6.2. Oscillograph Galvanometers

Both galvanometers were S.E. Labs. type B160 with a linear frequency response up to 100Hz and an internal resistance of 90 Ω . Their sensitivity was 0.5mV/cm which meant that for a 10cm deflection they required an input of 5mV. As the amplifier produced 10V this signal was reduced by a 500K Ω variable resistor (R_3) to the required value. Due to the value of R_3 , the source resistance (R_s) was much higher than that required for the galvanometer damping, and therefore the galvanometer required a resistor shunted across it (R_4).

The damping resistance required (R_d) can be expressed as:

$$R_d = \frac{R_s R_4}{R_s - R_4}$$

Now as $R_s \gg R_4$

Therefore $R_d \approx (R_s R_4)/R_s = R_4$

Therefore the value of the resistor (R_4) to be shunted across the galvanometers was R_d which, for a galvanometer type B160, was 250Ω .

5.7. OSCILLOSCOPE TELEEQUIPMENT TYPE D43

This was a double beam oscilloscope and the 0 - 10V signal from the Ancom amplifier was fed into one channel through a Teleequipment type A amplifier.

5.8. TRANSDUCER: S.E. LABS. TYPE 150/D

A 0 - 5psig transducer was linked to an S.E. 905 transducer converter. The output from the converter was fed into the oscillograph so that a permanent record of any measured pressure fluctuations could be obtained.

5.9. CLOSURE OF SECTION 5

The various instruments, their modes of operation and the necessary circuits to link them together have been discussed in this section. The next logical step was to fabricate a suitable capacitance probe and then calibrate the complete apparatus.

C A L I B R A T I O N

6.1. DESIGN OF THE PROBE

The probe had to be designed so that:

- i) it could operate under moderate temperature and pressure;
- ii) it could measure single bubbles;
- iii) it had adequate electrical screening;
- iv) it caused the minimum interference in the fluidised bed;
- v) it had adequate mechanical strength;
- vi) it could be easily raised and lowered in the bed.

To measure single bubbles it was considered that the probe should be inside the bed, local to the point of interest. The physical operating conditions suggested a single vertical rod, as a simple gland would give an adequate seal. To satisfy the other requirements it was found that a 0.95cm OD, 0.64cm ID steel rod was the smallest diameter rod that could incorporate the two screened wires and still be perfectly rigid when subjected to the stresses in a fluidised bed.

These considerations led to the probe design shown in Fig. 6.1.(1), (p.83). Probes of this type were used for some of the plate size experiments, but it was found that:

- i) capacitance fluctuations could be induced by relative movement of the unscreened portions of the leads in the probe (necessary for making electrical connections);
- ii) mechanical fracture of the insulation occurred due to lack of rigidity in the plate mounting;
- iii) fracture of the internal soldered joints occurred;

iv) the unscreened portion of the wires made accurate comparison of the theoretical capacitance with bridge reading impossible, the unscreened section having a capacitance of about 3pF and the plates themselves only about 0.2pF.

These disadvantages were overcome by redesigning the probe which is shown in Fig. 6.1.(2), (p.84) and Fig. 6.1.(3), (p.85).

The screened wire could be replaced if any breakage occurred. The two inner wires were always screened from each other and involved no joints. With the cable screen connected to the neutral of the bridge the measured and theoretical capacitances of the probe compared favourably. The probe was connected to the bridge and the bridge output characteristics were next examined.

Fig. 6.1.(1).

Initial Probe Design

(All dimensions in centimetres. Scale: twice full size)

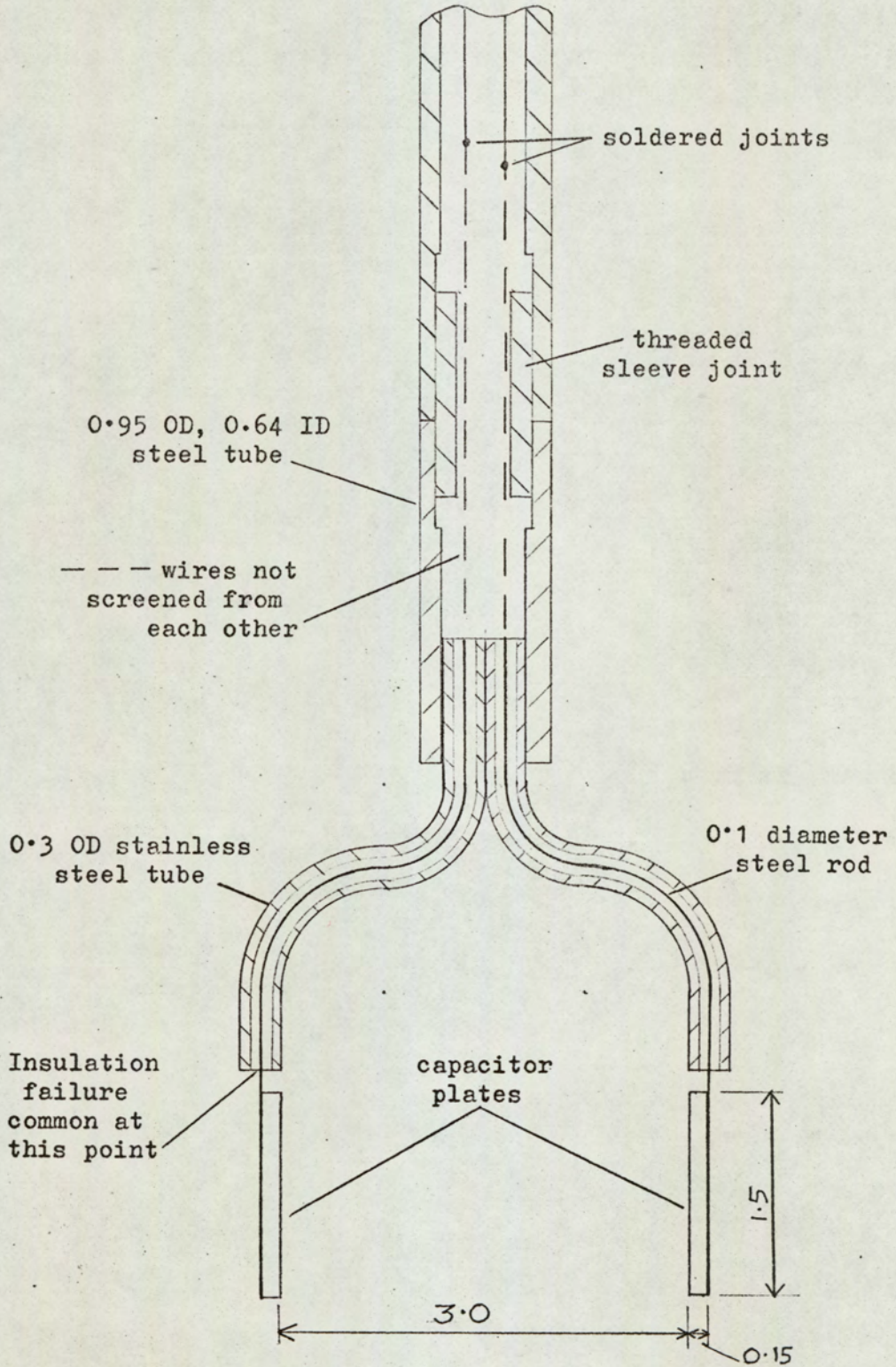


Fig. 6.1.(2).

Final Probe Design

(All dimensions in centimetres. Scale: twice full size)

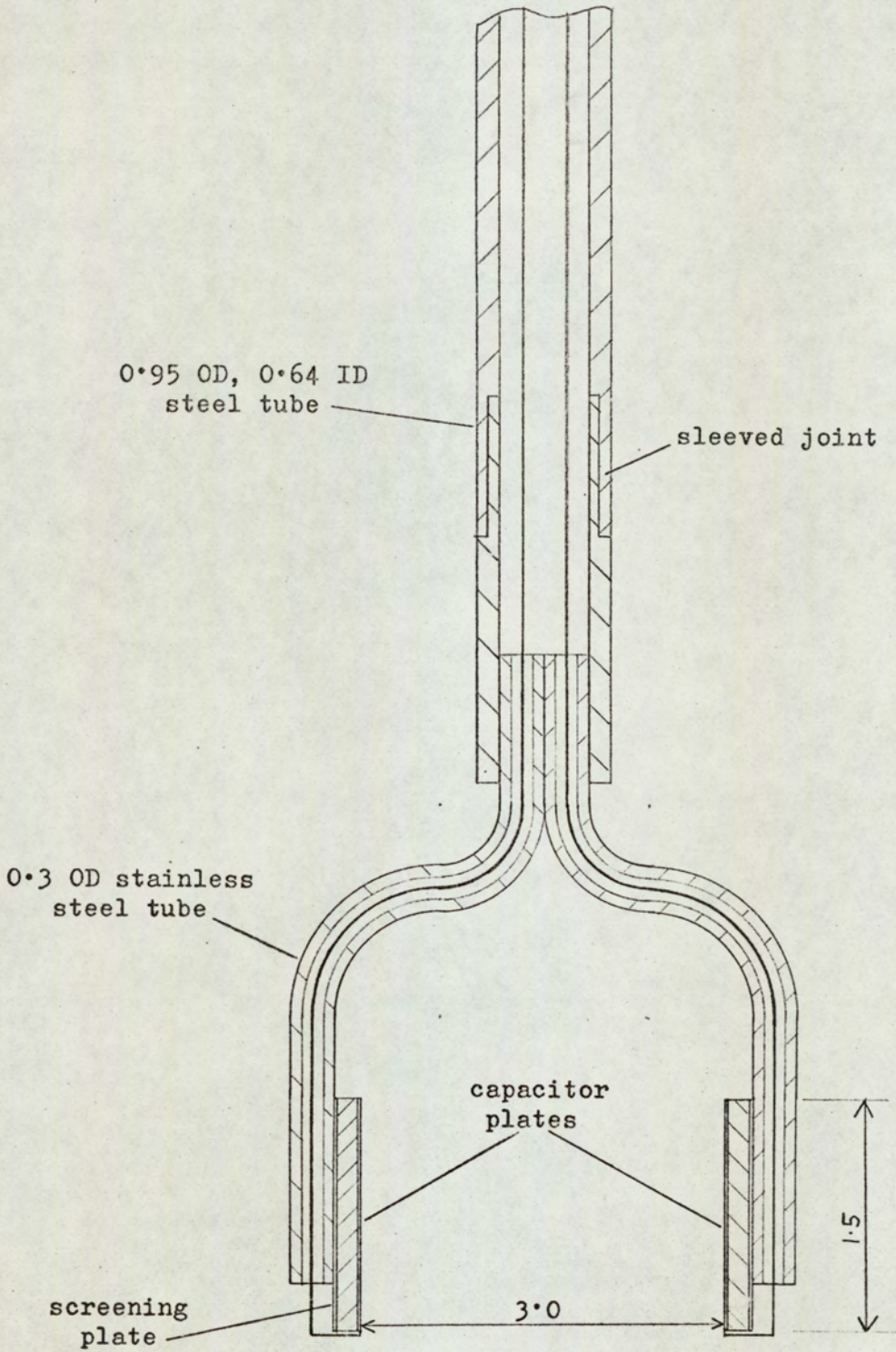


Fig. 6.1.(3).

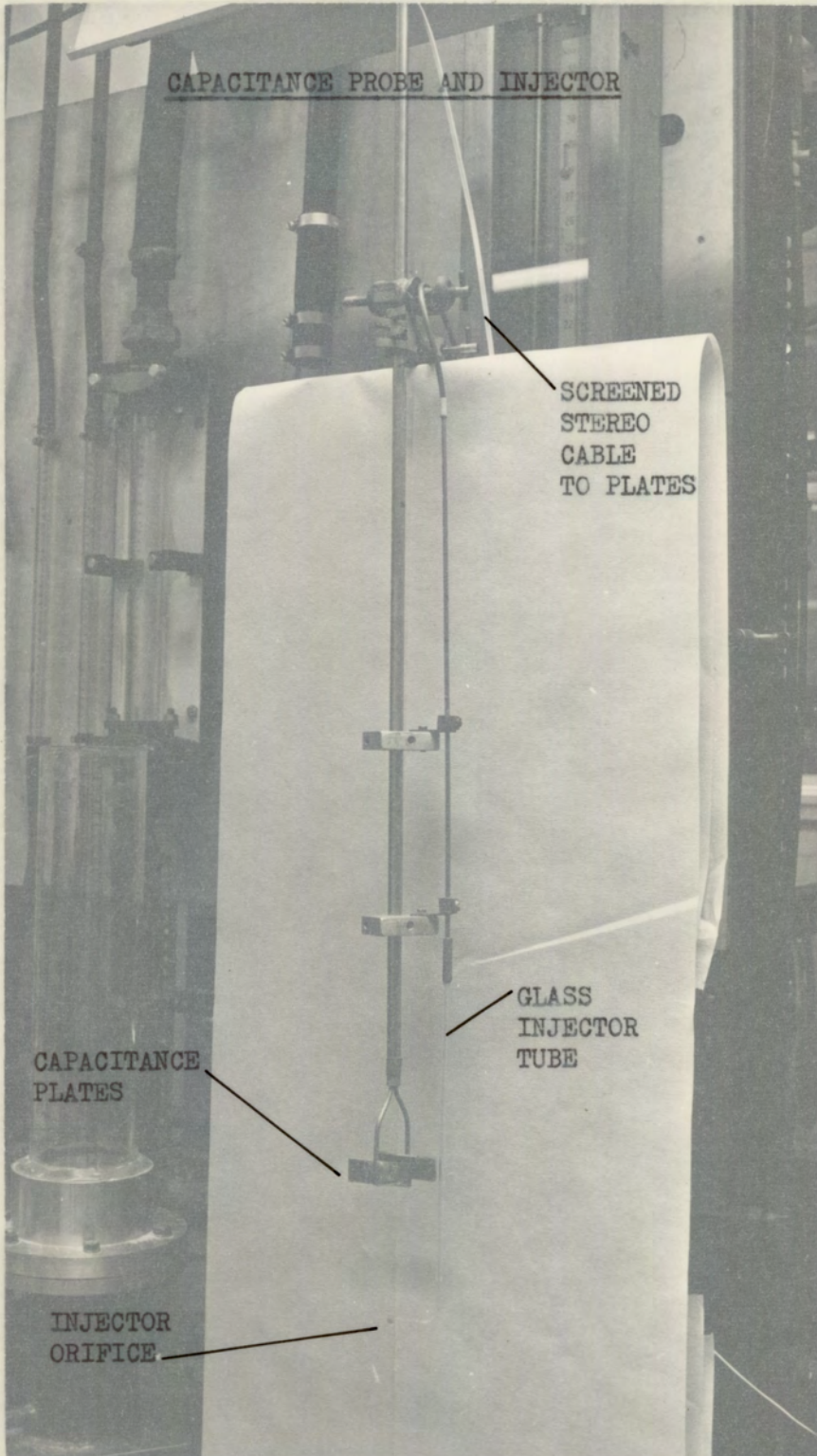
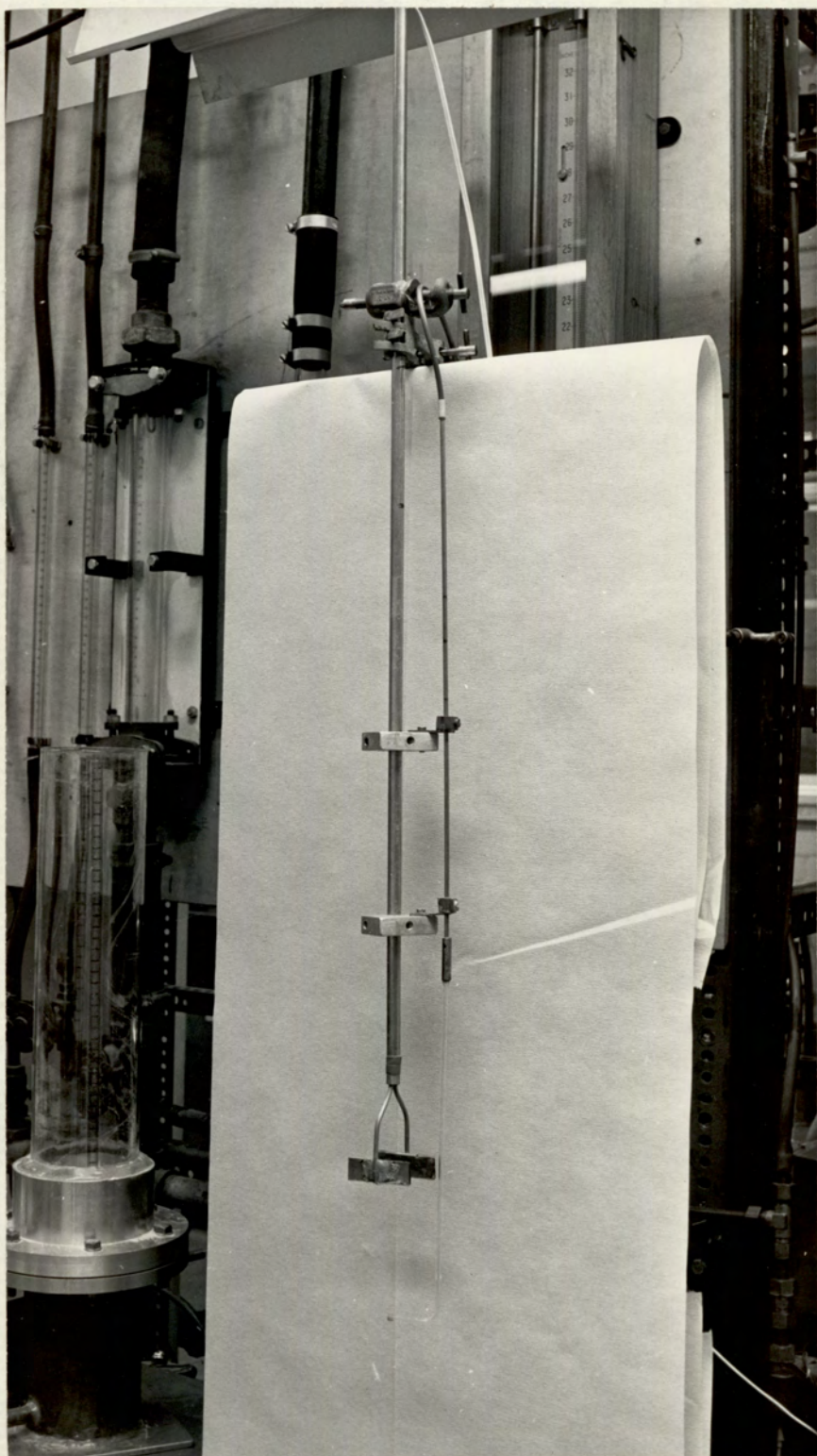


Fig. 6.1.(3).



6.2. BRIDGE CALIBRATION

6.2.1. Steady State Calibration

To obtain maximum accuracy the low capacity cables were used for all measurements. The neutrals of the two leads were linked together and the various trimming potentiometers adjusted, as suggested in the handbook. With the bridge set to maximum sensitivity (Scale 1) and switched to give a voltage output, the mechanical zero of the B160 galvanometer was adjusted to 2cm on the 0 - 14cm scale with no bridge signal. The bridge was then put out of balance by 0.1pF which produced a FSD of the autobalance capacitance meter.

The voltage output from the autobalance equivalent to the FSD of the meter was 100mV, which, after amplification, was increased to 10V and fed to the 500K Ω resistance, R_3 (Fig. 5.5.1. (1), (p.74)). This 500K Ω variable resistance was adjusted to give a galvanometer deflection of 10cm, i.e. the trace from the B160 was aligned on the 12cm mark on the scale.

The bridge decade switch which was used to create the 0.1pF signal change was returned to the balanced position and the vernier control altered instead. The vernier control was divided into 0.002pF increments and comparison between the vernier value and the galvanometer displacement showed that the latter was directly proportional to capacitance change.

Having shown that the circuit gave a linear response for a steady state change in capacitance, the next step was to determine whether the bridge would accurately follow a varying signal, such as would be created by a bubble passing between the probe plates in a fluidised bed.

6.2.2. Unsteady State Calibration

When a step change in capacitance was fed into the bridge, using a small capacitor in series with a reed switch operated by a solenoid, the galvanometer overshoot wildly before slowly returning to its correct value. In an attempt to find the cause of this frequency sensitivity, a rig was built to generate an oscillating capacitance change, so that the output signal amplitude could be compared at frequencies from 0 - 40Hz.

The variable capacitance was produced by an eccentrically mounted steel disc passing between the two plates of the probe and driven by a variable speed motor (Fig. 6.2.2.(1), (p.88)). The indirect drive was incorporated to reduce vibration.

The maximum and minimum steady state readings given by the stationary disc are shown as lines A and B in Fig. 6.2.2.(2), (p.88). The disc was rotated at various speeds between 2Hz and 40Hz, the speed being recorded by a tachometer and the maximum and minimum output signals being recorded on the chart. The results are shown qualitatively on Fig. 6.2.2.(2), from which it can be seen that the output was frequency sensitive at all frequencies. It was also noted that for input frequencies greater than 7Hz, the output frequency was always much less than the input frequency.

Tests were therefore carried out to determine which of the instruments was producing this frequency sensitive output.

Fig. 6.2.2.(1)

Apparatus for unsteady state calibration

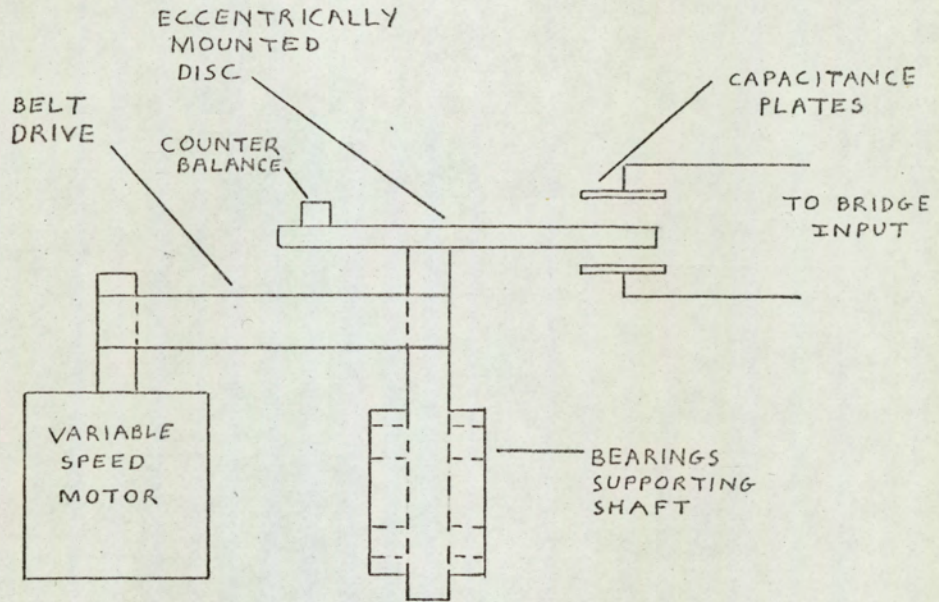
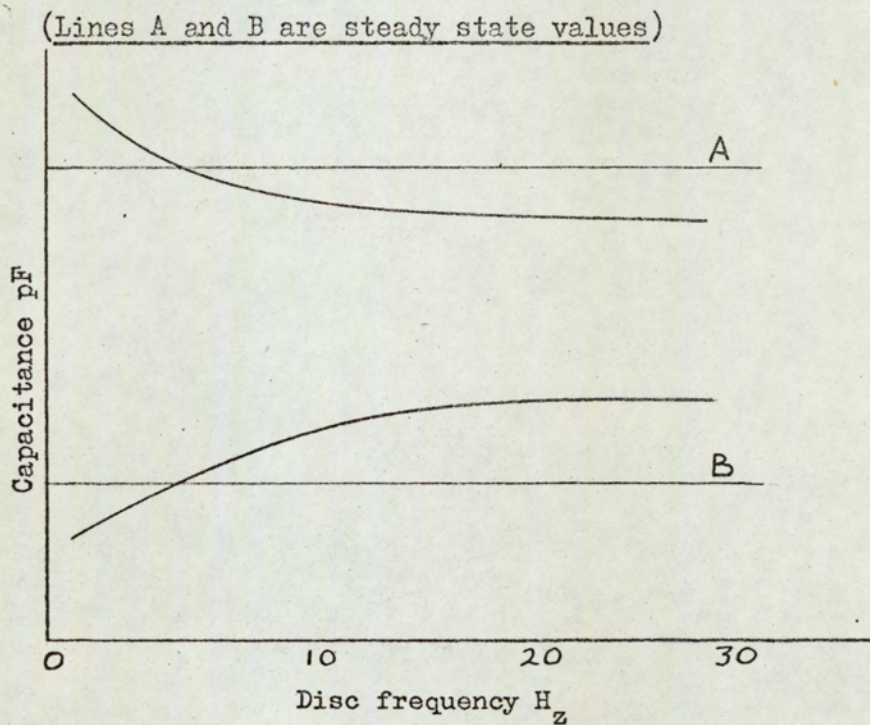


Fig. 6.2.2.(2).

Maximum and minimum capacitance readings for unsteady state calibration



Amplifier Test

Since similar results were obtained using the current output circuit which does not use an amplifier, it was concluded that the fault was not in the amplifier circuit. Therefore, either the bridge, the autobalance or the oscillograph was at fault.

Oscillograph Test

The UV oscillograph was eliminated by feeding into it a sine wave signal from an audio frequency oscillator instead of the signal from the autobalance. The recorded amplitude was independent of frequency and the input number of cycles was faithfully reproduced on the chart.

Autobalance Test

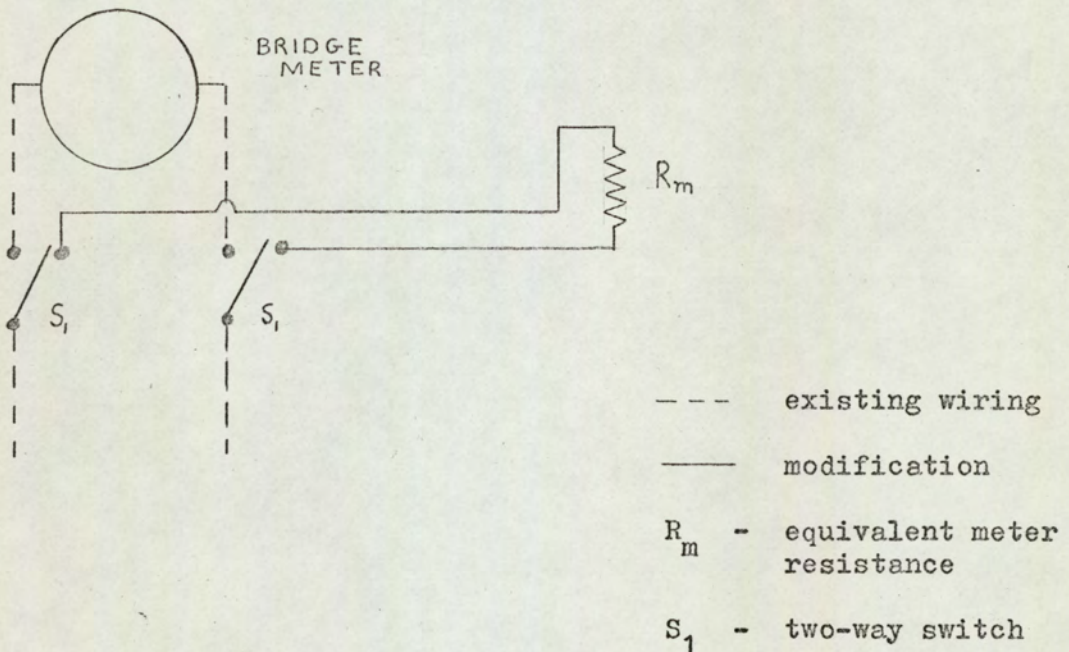
The meter reading of the autobalance was compared with the rate at which the metal disc was rotating, and it was noticed that the meters oscillated wildly up to about 10Hz. Above this frequency the needle just vibrated at an approximately constant reading. As it was at about 10Hz when the amplitude of the galvanometer deflection became independent of frequency (see Fig. 6.2.2.(2)), it was thought that it could be the meters which were causing the non-linearity, and should therefore be replaced with resistors.

The value of the resistance, R_m , (Fig. 6.2.2.(3), (p.90)) equivalent to the internal resistance of each meter was found accurately by setting up the bridge with the meter in circuit to give a known deflection on the UV oscillograph. The meter was then replaced by a variable resistor, which was adjusted until the galvanometer deflection was the same as with the meter in circuit. The variable resistor was then removed, its value

measured, and replaced with an equivalent fixed resistor. Using two-way switches the bridge was then checked to see that there was no difference in reading on the galvanometer whether the meter or the resistor was in circuit.

Fig. 6.2.2.(3)

Modification to bridge meter circuit



The Checking of Unsteady State Response

With the meters replaced by their equivalent resistors, the apparatus was again tested with the rotating disc, and the output signal amplitude was then found to be constant to within $\pm 1\%$, and the maximum and minimum readings were to within $\pm 0.5\%$ of their respective steady state values. The number of input cycles per second was also faithfully reproduced on the chart up to the motor maximum of 40Hz.

As a further check, a capacitance step change was again fed into the bridge, and the square wave output had no apparent

time lag or overshoot when using a galvanometer with a linear frequency response up to 100Hz. It was therefore felt that the area under the trace could be used to record bubble volume. An integrator was included in the electrical circuit in case this area was required, either to compare with the work by Dotson⁽³⁹⁾ or as a check on the peak height reading.

6.3. INTEGRATOR CALIBRATION

The integrator was an Ancom type 15A - 3 differential amplifier with the one input fed from the output of the 15A - 3a amplifier, and the other input linked to common, as can be seen in Fig. 5.5.1.(1), (p.74).

The integrator was checked by feeding in a constant voltage and noting that the voltage output increased linearly with respect to time.

The autobalance output was switched such that a decrease in capacitance (which would occur when a bubble passed between the probe plates in the fluidised bed) produced an increase in output signal, otherwise the integrator showed a small change in a large value when recording a bubble. To allow for the variations that occur in the capacitance value of a non-bubbling fluidised bed, due to small voidage changes, the bridge had to be set slightly out of balance all the time, thereby generating a small output signal.

To prevent this signal being integrated, another signal of the same value was fed into the integrator input linked to common, as described in Section 5.5.1., so the integrator output was purely the integration of the signal variation created by the bubble. Finally, the values of R_2 and C_3 (Fig. 5.5.1.(1), (p.74)) were adjusted such that the product gave the required time constant for the integrator circuit. The instruments having been commissioned and calibrated, attention was turned to the actual oscillograph trace and the readings produced by the capacitance variations in the fluidised bed.

6.4. ELECTRICAL INTERFERENCE

From the oscillograph trace it was obvious that, even though all the wiring was screened, a considerable amount of mains interference was being picked up. This was partly reduced by screening the glass fluidised bed with a copper shield and connecting the copper to the neutral of the bridge. The interference was reduced to less than 1% of FSD when a motor with a loose brush holder in the laboratory was located and repaired.

The copper shield connected to neutral also served to screen the probe in the fluidised bed from any outside variations in capacitance. The copper shield was made by cutting in half longitudinally a 10cm ID copper tube. Two small protrusions were soldered to one longitudinal edge of one half. This meant that there was a small gap created when the two halves were clamped round the bed so it was possible to measure the bed height visually without removing the shield.

With the reduction in interference effected by the copper shield, it was possible to study the response when a bubble passed between the plates in a fluidised bed, but to interpret these results it was necessary to make an elementary study of the theoretical capacitance of a composite system of two dielectrics.

6.5. THE THEORY OF CAPACITANCE

6.5.1. The Relationship between Different Dielectrics

When two conducting bodies, separated by a dielectric, are charged, an electric field is set up in the dielectric. The amount of charge created between the bodies by a unit of potential difference is called the capacitance of the system and is measured in coulombs per volt. The property controlling the magnitude of the charge developed for a given applied voltage is called the permittivity or the dielectric constant, and is defined as the ratio of the charge taken by the dielectric to the charge taken by a vacuum, for the same applied voltage.

i.e.:

$$\text{Dielectric Constant } (D_k) = \frac{\text{charge created by } x \text{ volts in dielectric}}{\text{charge created by } x \text{ volts in a vacuum}}$$

As the charge generated by a unit of potential difference is called capacitance then,

$$D_k = \frac{\text{capacitance of the dielectric}}{\text{capacitance of vacuum}}$$

6.5.2. The Shape of the Electric Field (Single Dielectric)

The shape of an electric field between two plates for a single dielectric is shown in Fig. 6.5.2.(1), (p.96). When a positive charge is moved away from a negative charge the "tubes" of electric force are stretched, i.e. they are in tension. Similarly, the cross sectional area of a tube is determined by the presence of other such tubes which gives rise to a lateral compressive force.

With an arrangement as in Fig. 6.5.2.(1), the tension tends to keep the lines of force as short as possible and in the middle

of the plates the compressive forces cancel each other. At the edges of the plates the compressive forces act outwards only and the lines of force therefore curve outwards until equilibrium is reached between the compressive and tensile forces.

6.5.3. The Shape of the Electric Field (Two Dielectrics)

Fig. 6.5.3.(1), (p.96) illustrates the refraction of the lines of force created by two different dielectrics in the same capacitor. The lines of force bend such that they appear to be attracted to the dielectric with the higher dielectric constant.




Fig. 6.5.2.(1).

The shape of an electric field

(Single dielectric)

--- lines of force

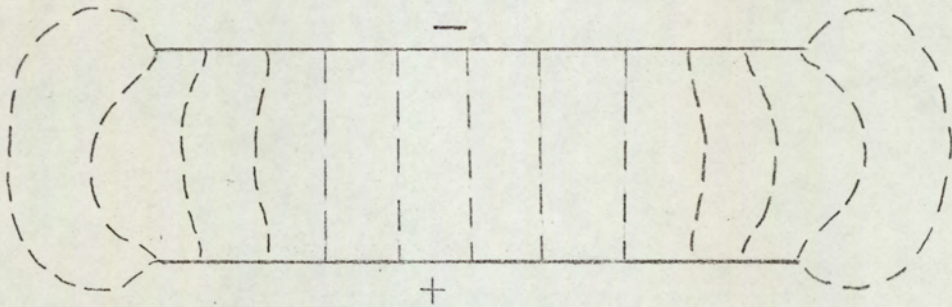
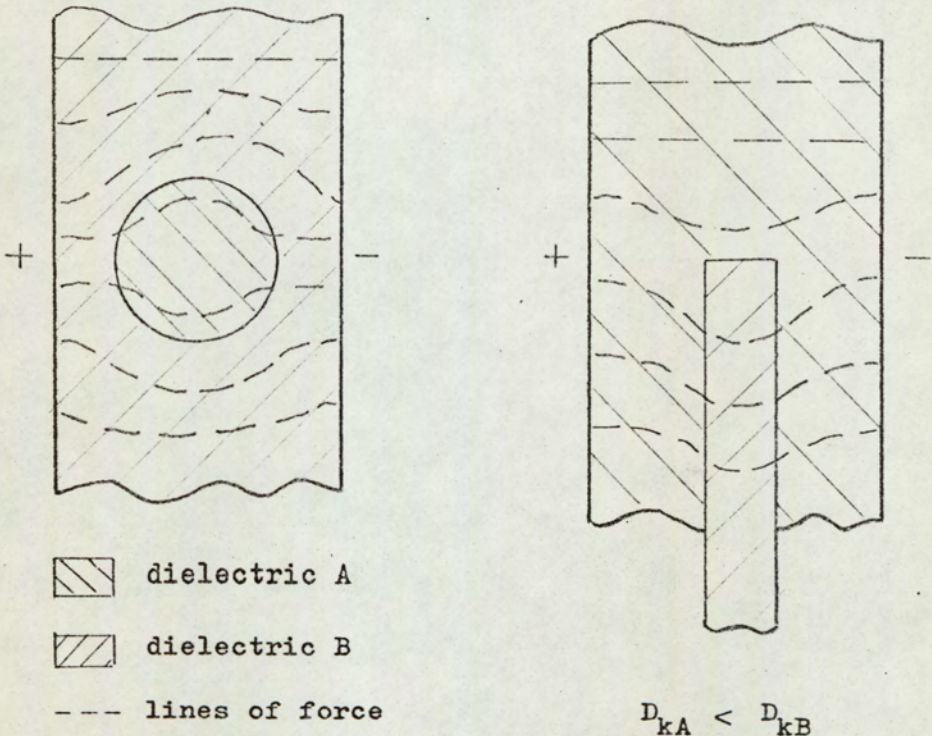


Fig. 6.5.3.(1).

The shape of an electric field

(Two dielectrics A and B)



6.6. CAPACITANCE CHANGE CREATED BY A BUBBLE PASSING BETWEEN THE PLATES

6.6.1. Oscillograph Bubble Trace

When a gas bubble passed between the plates of the probe in a non-conducting fluidised bed, the trace drawn by the UV oscillograph was as shown in Fig. 6.6.1.(1), (p.98). The trace shows that there are four heights that could be measured because h_p is not necessarily equal to h_p^1 and x_p is not necessarily equal to x_p^1 .

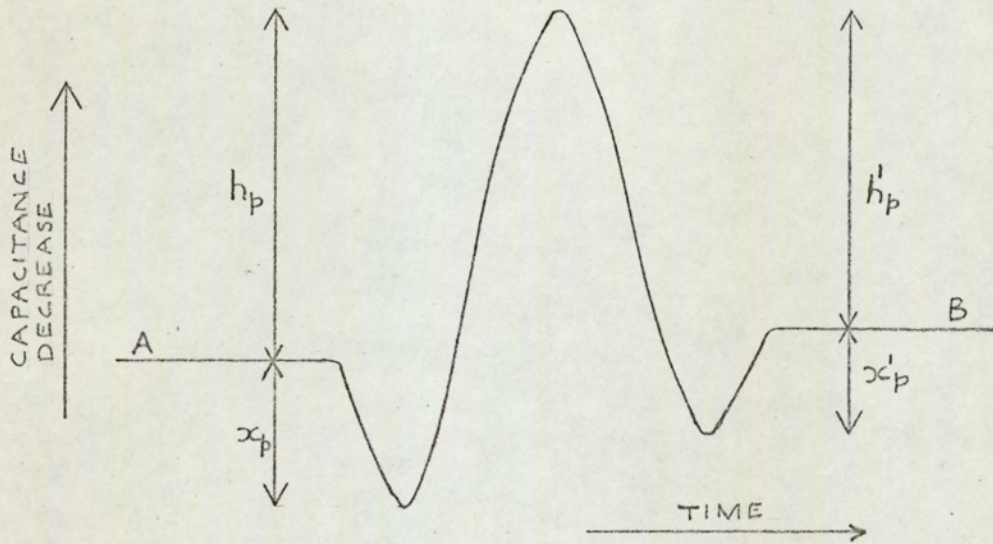
6.6.2. Discussion of Blips x_p and x_p^1

From Fig. 6.6.1.(1). it was seen that the two blips of height x_p and x_p^1 were increases in capacitance. These were either complex capacitance changes or large decreases in the voidage of the dense phase. The latter seemed unlikely as it occurred just before and after a bubble and was therefore the opposite of the effect found by Lockett and Harrison⁽²⁰⁾. To clarify this point the probe was placed in a non-conducting liquid and an air bubble injected. The same type of trace was observed and in this case the blips must have been due to an electrical rather than a physical change because the liquid could not have become more dense or its dielectric constant increased. Hence it would appear that the blips recorded for a fluidised bed must also be at least in part due to an electrical change.

The lines of electric force are shown for the plates in a fluidised bed of constant voidage in Fig. 6.6.2.(1A), (p.98). When a bubble approaches the plates the lines of force will be refracted, as shown in Fig. 6.6.2.(1B) and as discussed in Section 6.5.2.

Fig. 6.6.1.(1).

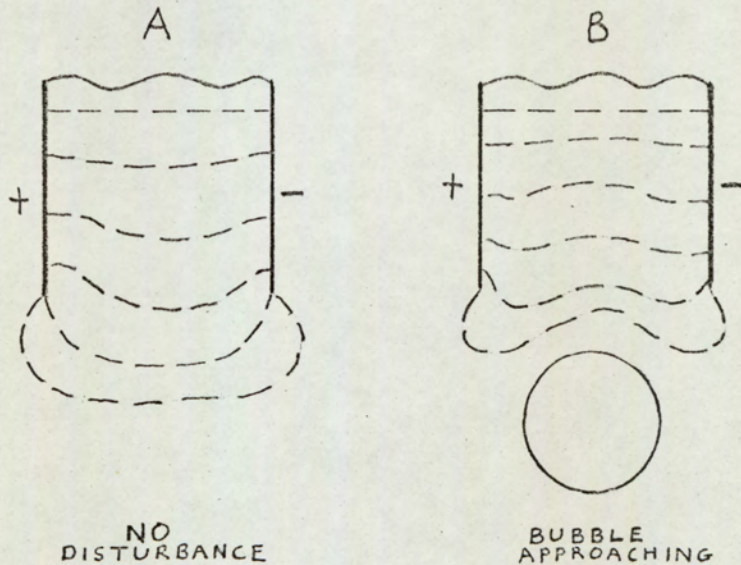
Oscillograph trace for a gas bubble
recorded in a non-conducting fluidised bed



Line A is equivalent to dense phase capacitance before passage of bubble.
Line B is equivalent to dense phase capacitance after passage of bubble.

Fig. 6.6.2.(1).

Refraction of the lines of force owing to a gas bubble
rising between the plates of a capacitance probe in a fluidised bed



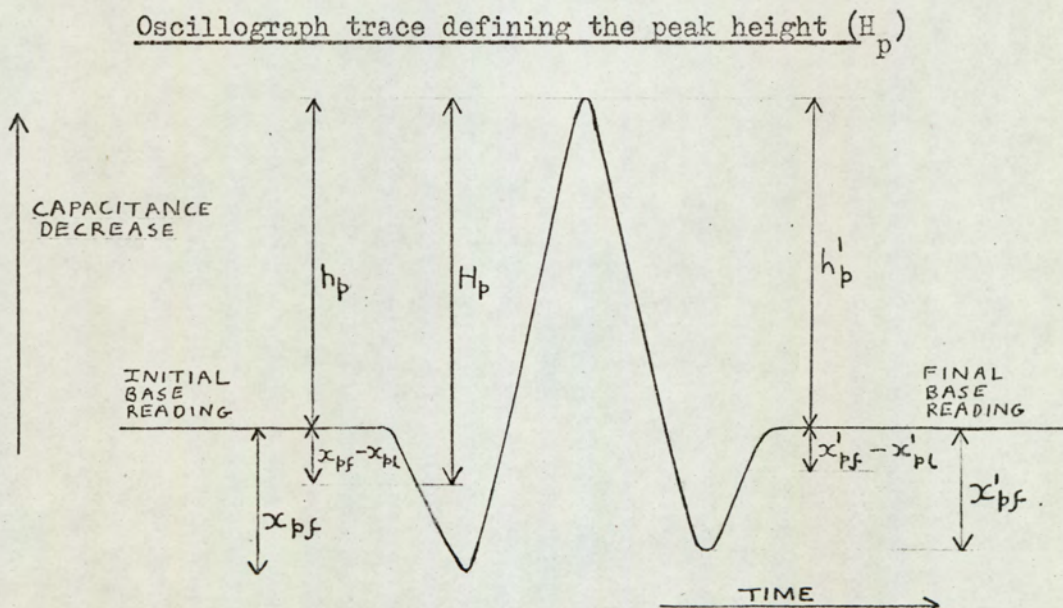
--- lines of force

In Fig. 6.6.2.(1B) it can be seen that the lines of force have been compressed together and this is equivalent to having a medium of a higher dielectric constant between the plates. The net effect of a bubble of gas in a fluidised bed approaching the plates is therefore to produce an increase in the observed capacitance. The same effect is, of course, produced when the bubble leaves the plates, and these two increases are recorded on the trace as at least part of the blips of height x_p and x_p^1 . These two blips cannot therefore be directly related to any change in bed voidage.

6.6.3. Discussion of the Peak

Once the bubble is between the plates the lines of force are as shown in Fig. 6.5.3.(1A), (p. 96), and there is therefore a decrease in the capacitance reading owing to the density of the lines of force having been reduced. This reduction is recorded as the peak in the trace in Fig. 6.6.3.(1), (p.99).

Fig. 6.6.3.(1).



6.7. READINGS REQUIRED FROM THE TRACE

6.7.1. The Capacitance Equivalent to the Bed Voidage During the Bubble Ascent

The initial and final base readings on the chart (Fig. 6.6.3. (1)) corresponded to the voidage above and below the bubble respectively. As it was considered that the bed above the bubble exerted a stronger influence on the bubble than the bed below, the initial base line was taken as the datum from which the bed voidage was found.

6.7.2. The Basic Capacitance at which the Bubble was Measured

When a bubble was recorded in a liquid, two blips of height x_{pl} and x_{pl}^1 were found before and after the peak respectively; these were increases in capacitance due to the refraction of the lines of force. Now when the blips x_{pf} and x_{pf}^1 (Fig. 6.6.3.(1)) were measured for a bubble in a fluidised bed of approximately the same dielectric constant as the liquid, they were found to be greater than x_{pl} and x_{pl}^1 respectively for the same size bubble. The increase from x_{pl} to x_{pf} and x_{pl}^1 to x_{pf}^1 could not be due to refraction, because both media had the same dielectric constant, and could not be due to refracting and cutting the lines of force at different rates, because the bubble velocities in the fluidised bed and in the liquid were comparable. Therefore, the increases must have been caused by physical changes in the bed structure near the probe.

It was considered that though the voidage decrease causing the change from x_{pl} to x_{pf} was present whilst the bubble passed between the plates and therefore affected the response, the change x_{pl}^1 to x_{pf}^1 only occurred after the bubble had been recorded and

so could be disregarded.

The basic capacitance at which the bubble was measured was therefore larger than the capacitance equivalent to the initial base line by an amount equivalent to the distance $(x_{pf} - x_{pl})$ and the capacitance change created by the bubble was equivalent to the distance $(h_p + x_{pf} - x_{pl})$. This distance is defined in Fig. 6.6.3.(1) as the peak height (H_p) .

6.8. INJECTOR CALIBRATION

In order to measure bubble growth it was desirable to know the volume of gas initially injected (V_i). The bubble injection system was therefore calibrated with the apparatus shown in Fig. 4.2.(1), (p.53).

The controller (K) was set to deliver 80in Hg pressure. This effectively damped out the pressure oscillations from the mains supply. The Negretti and Zambra controller then regulated the pressure, so that fluctuations were not detectable, and supplied air at any desired pressure from 0 - 32in Hg.

A constant gas volume was created by charging the pressure vessel at a given pressure and then discharging it. The calibration was effected simply by displacing water from the inverted burette and noting the displaced volume at atmospheric pressure. The gas volume was varied by adjusting the Negretti and Zambra outlet pressure, as indicated by the reading of the mercury manometer. The reading was then plotted against the gas volume generated.

As would be expected for an isothermal expansion, it was found that the calibration was linear, and in fact 2.5in increments of the mercury manometer were equivalent to a 1cm^3 change in the injected gas volume. As the manometer scale was graduated in 0.1in increments, the gas volume injected was therefore known to be $\pm 0.02\text{cm}^3$.

6.9. INVESTIGATION OF THE SIZE OF AN INJECTED BUBBLE

From the injector calibration the volume of gas being injected was known, but it was thought that due to injection effects the volume of a bubble formed in a fluidised bed would be different from the volume of air injected, as reported in Section 2.2.8. (14, 27). This difference was investigated by recording the rate of change of the pressure in the pressure vessel when a bubble was injected, using a pressure transducer.

The plot of pressure (p) versus time (t) obtained from the transducer when 4cm³ of air was injected is shown in Fig. 6.9.(1), (p.105) and the results were converted to give a plot of free volume of gas injected versus time (Fig. 6.9.(2), (p.106)). From the slope of this curve the relationship between the gas volume injected and the injection rate was plotted as line A in Fig. 6.9. (3), (p.107). Line B on the same Figure is a plot of the theoretical relationship,

$$V_b = 1.138 G_v^{6/5} / g^{3/5} \quad - \quad 6.9.(1)$$

suggested by Davidson and Harrison⁽¹⁾, between the bubble volume (V_b) formed from a constant gas flow rate (G_v); i.e. V_b is the volume a bubble will grow to before it leaves the orifice and a new bubble starts to form. It is accepted that the rate of gas supply is not constant for the case being considered, but after the bubble has grown to about 2.5cm³ the rate of growth does not change rapidly (see Fig. 6.9.(2)). Therefore the intersection of lines A and B (Fig. 6.9.(3)) at a bubble volume of about 3cm³ does suggest that when 4cm³ of air is injected in this way, the main bubble so formed will leave the injection orifice before it has

grown to 4cm^3 . Allowing for one or two small bubbles to be entrained into the wake of the main bubble and then rapidly coalescing, a reasonable estimate of the main bubble size would seem to be about 3.5cm^3 when 4cm^3 is injected. A similar percentage reduction (say 10%) would be expected for different injected volumes.

Further work on the injection effect, reported in Section 8.3, suggests that injected volumes of less than 2cm^3 may in fact initially grow and that though injected volumes in excess of 3cm^3 will initially shrink, as predicted, the percentage gas loss may be considerably less than 10%, for injected volumes between 3cm^3 and 4.5cm^3 .

Fig. 6.9.(1).

3 The rate of change of pressure in the pressure vessel when a 4cm bubble was formed by injection (initial pressure = 10 in Hg)

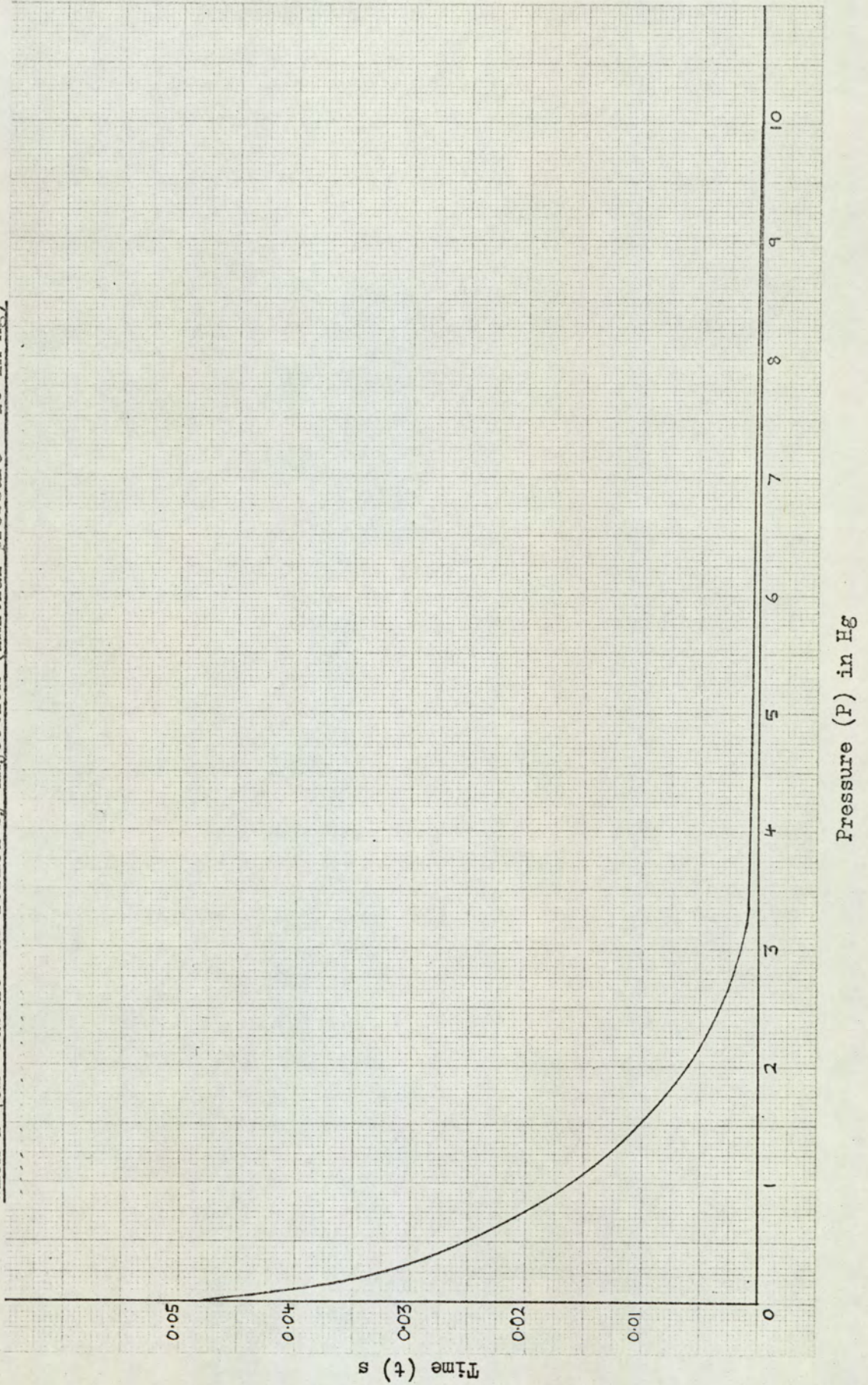


Fig. 6.9.(2).

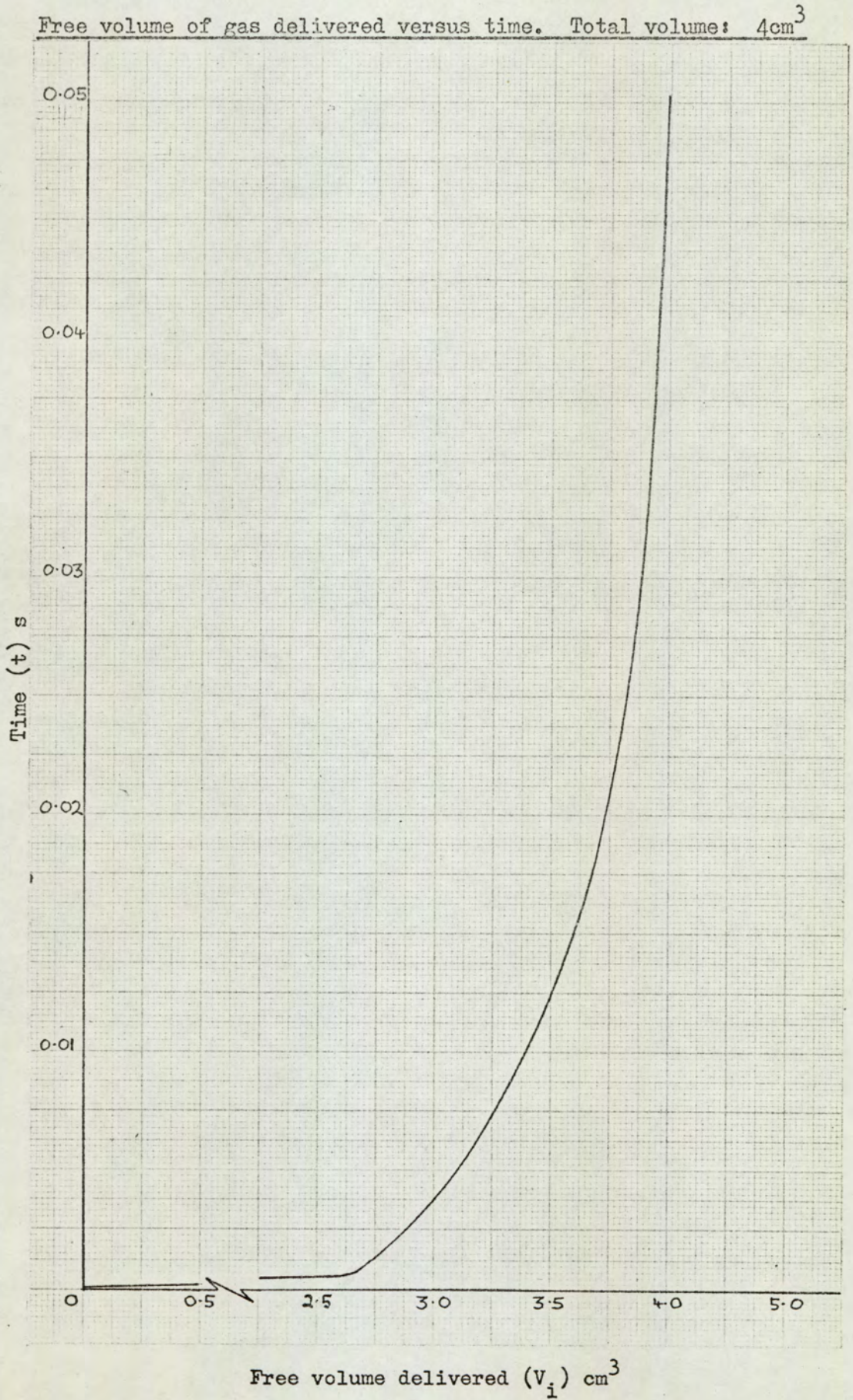
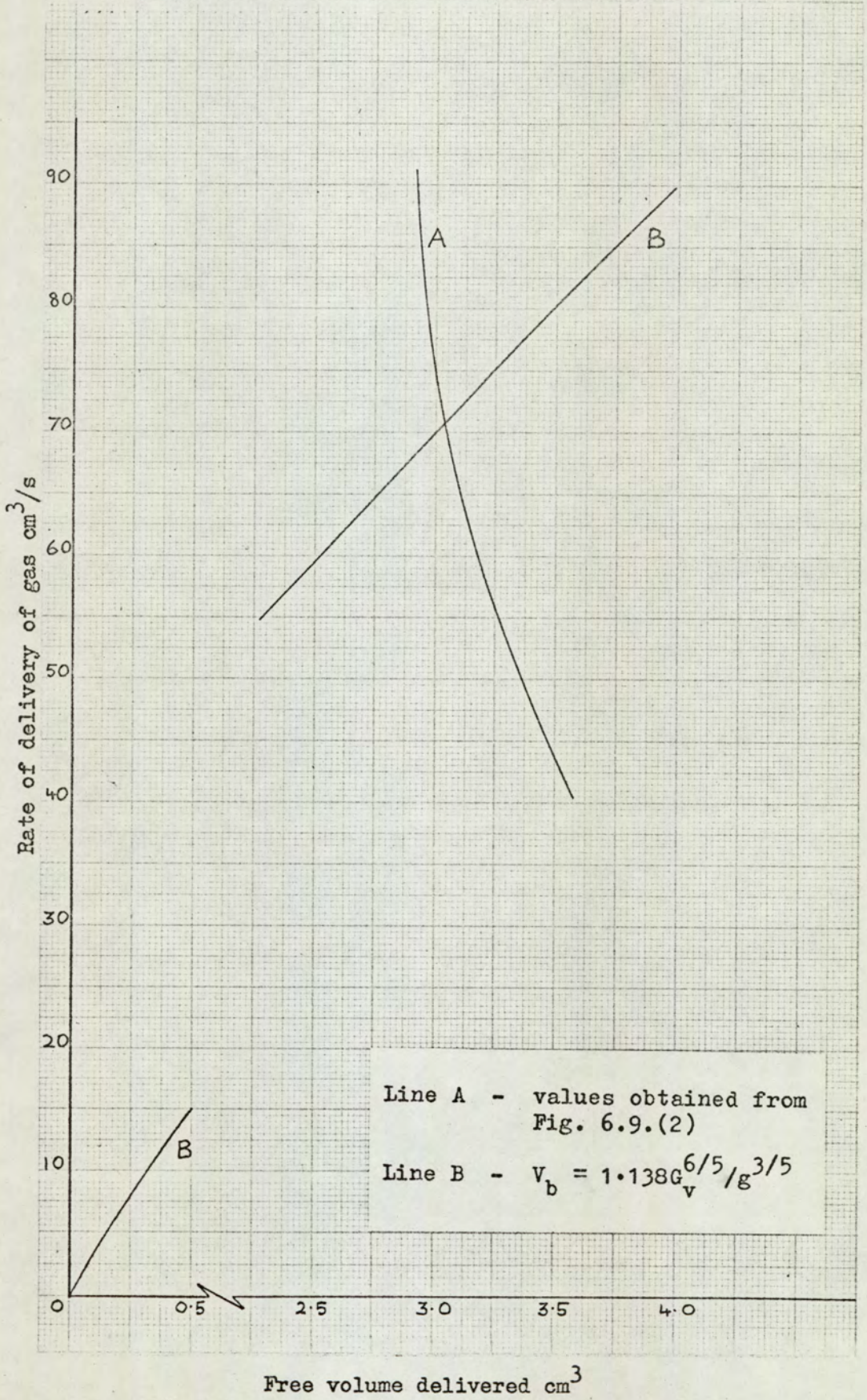


Fig. 6.9.(3).

Free volume of gas delivered versus rate of delivery of gas



6.10. FLUIDISING GAS FLOW MEASUREMENTS

6.10.1. Introduction

In all fluidisation work it is necessary to measure the flow rates of the fluidising fluid. Variable area flow meters were chosen in this work, in view of their rapid response and convenience in use. (In the following text "Variable area" has been abbreviated to VA.)

6.10.2. Variable Area Flow Meter Theory

From basic fluid dynamics

$$G_v = \frac{k_{10}}{P_r^{1/2}} \quad - \quad 6.10.2.(1)$$

and in the Appendix Section A1 it has been shown that equation 6.10.2.(1) can be rewritten as:

$$G_a = \frac{G_c k_{10} (P_a + \Delta P)^{1/2}}{P_a} \quad - \quad 6.10.2.(2)$$

(where G_v = Volumetric flow rate)

(P_r = Pressure in the VA flow meter)

(k_{10} = A constant)

(G_a = Volumetric flow rate at pressure P_a)

(P_a = Prevailing atmospheric pressure when operating)

(G_c = Volumetric flow rate in the VA flow meter at pressure P_c)

(P_c = Pressure in the VA flow meter tube at calibration)

(ΔP = Bed pressure drop)

All pressures are in absolute units.

6.10.3. The Effect of Atmospheric Pressure Changes

Consider a small change in P_a , δP_a which would cause a change in G_a , δG_a . Then from equation 6.10.2.(2):

$$\frac{dG_a}{dP_a} = G_c k_{10} \frac{d}{dP_a} ((P_a + \Delta P)^{\frac{1}{2}} P_a^{-1})$$

$$dG_a = -dP_a G_c k_{10} \left[\frac{\Delta P + P_a/2}{P_a^2 (\Delta P + P_a)^{\frac{1}{2}}} \right] \quad - 6.10.3.(1)$$

Dividing equation 6.10.3.(1) by equation 6.10.2.(2):

$$\frac{dG_a}{G_a} = \frac{-dP_a}{P_a} \frac{(\Delta P + P_a/2)}{(\Delta P + P_a)} \quad - 6.10.3.(2)$$

The expected maximum and minimum atmospheric pressures were 765mm Hg and 735mm Hg respectively. The average value of P_a was therefore 750mm Hg and the maximum value of $\delta P_a = 750 - 735 = +15\text{mm Hg}$, i.e. a 2% change in P_a .

When controlling the air flow with a VA flow meter inlet valve, the average value of ΔP was 20mm Hg and substituting this value into equation 6.10.3.(2), the fractional change in G_a caused by a pressure change can be calculated.

For a pressure change from 750mm Hg to 735mm Hg:

$$\frac{dG_a}{G_a} = -0.0103$$

i.e. a +2% change in P_a would cause a -1% change in G_a .

However, if the air flow were controlled at the fluidised bed inlet valve, the value of ΔP would be 507mm Hg, and substituting this value into equation 6.10.3.(2), a +2% change in P_a would

cause a -1.4% change in G_a . It was therefore concluded that for a VA flow meter calibration chart calculated at $P_a = 750\text{mm Hg}$, the changes caused by variations in atmospheric pressure were negligible compared with other experimental errors. This conclusion was directly applicable to the Rotameters used in this work, but not to the Fischer and Porter tri-flat flow meters, due to the difference in float shape and internal meter design. However, from the calibration procedure stated in the Fischer and Porter handbook, it was again concluded that the fluctuations in atmospheric pressure could be neglected.

6.10.4. The Effect of Bed Pressure Drop Changes

Consider a small change in ΔP , $\delta \Delta P$ which would cause a change in G_a , δG_a . Then from equation 6.10.2.(2):

$$\frac{dG_a}{d\Delta P} = \frac{d}{d\Delta P} \left(\frac{G_c k_{10} \sqrt{(P_a + \Delta P)}}{P_a} \right) \quad - \quad 6.10.4.(1)$$

$$\text{therefore } \frac{dG_a}{G_a} = \frac{d\Delta P}{\Delta P} \cdot \frac{\Delta P}{2(P_a + \Delta P)} \quad - \quad 6.10.4.(2)$$

The maximum and minimum values of ΔP were 25mm Hg and 2.5mm Hg respectively. The average value of ΔP was therefore 14mm Hg and the maximum value of $\delta \Delta P = 25 - 14 = 11\text{mm Hg}$. The average value of P_a was 750mm Hg and substituting into equation 6.10.4.(2):

$$\frac{dG_a}{G_a} = 0.007$$

i.e. a +80% change in ΔP would only cause a +0.7% change in G_a .

It was therefore considered that for a calibration chart calculated at $\Delta P = 14\text{mm Hg}$, the effect of variations in bed pressure drop

was negligible when compared with other experimental errors, for both Rotameters and Fischer and Porter flow meters.

6.10.5. Flow Meter Calibration

The flow meters were individually calibrated against positive displacement meters. This was found necessary since at the same air flow rate there was a difference in indicated flow rates of 2.8% between the 7A and 10K Rotameters and 6% between the 10K and 18A Rotameters.

After first leak testing the apparatus at 10psig, calibration was carried out at atmospheric conditions. Low flow rates were measured using a Parkinson Cowan wet meter type E40, with a stated accuracy of $\pm 0.25\%$ and a maximum throughput of $0.3 \times 10^3 \text{ cm}^3/\text{s}$. Higher flow rates were measured with a Parkinson Cowan dry meter type D1 with a stated accuracy of $\pm 0.5\%$ and a maximum flow rate of $1.4 \times 10^3 \text{ cm}^3/\text{s}$. The two meters were first compared against each other by passing air through them in series. After an hour the type E40 displayed 0.741 m^3 and the type D1 0.745 m^3 , a discrepancy of 0.5%. This error was found to be constant for several lower flow rates, so assuming that the wet meter was more accurate, all flows metered by the dry meter were reduced by 0.5%.

The VA meters were calibrated in this way and the flows calculated at 19.5°C and 750mm Hg. The calibration of Rotameter type 7A showed that a fault had occurred in the manufacture of the tube, such that at a scale reading of 13, the indicated flow was $108 \text{ cm}^3/\text{s}$, whereas the true flow was $120 \text{ cm}^3/\text{s}$, an error of about 10%.

6.11. DETERMINATION OF PROBE DIMENSIONS

6.11.1. Determination of Plate Gap

The final aim of this development work was to design an instrument for measuring accurately the volume of small bubbles in a fluidised bed. To reduce to a minimum the amount of physical interference from the plates they had to be as far apart and as small as possible whilst still being able to detect a bubble. This determined that the bridge would have to be operated in its most sensitive range (Scale I). With the bridge on Scale I the maximum capacitance change which the autobalance will record is about 0.13pF. The galvanometer was therefore adjusted to give a 10cm deflection for a 0.1pF change in capacitance.

A compromise had then to be reached between minimum bed interference and signal strength, to design a probe which gave a 0.1pF change when the maximum size of bubble passed between the plates.

It has been shown⁽¹⁾ that slugging occurs when $D_b > D_c/3$, where D_b = maximum bubble diameter. At $D_b = D_c/3$ the wall effect on the bubble is still considerable, but Uno and Kintner⁽⁶¹⁾ have shown that if $(1 - D_b)/D_c > 0.75$, then $U_b/U_{b\infty} > 0.95$ (where $U_{b\infty}$ is the velocity of a bubble in a vessel with $D_c = \infty$). i.e. the rate of rise of a bubble is only decreased by a maximum of 5%.

It was arbitrarily decided that a wall effect creating up to a 5% reduction in $U_b/U_{b\infty}$ would be acceptable in this work. In a 10cm diameter bed this gives a maximum bubble diameter of 2.5cm, and therefore a maximum value of $V_b = 8\text{cm}^3$. Therefore, the gap (h_g) between the plates must be at least 3cm.

The maximum size of bubble that the probe must measure was

therefore fixed at 8cm^3 . It was realised that this was probably larger than would be required, but it was felt that the larger size would ease the determination of the calibration techniques, and when these were developed, plates with a smaller gap could be easily calibrated to cater for a smaller bubble size range.

6.11.2. Determination of Plate Width

An increase in the plate width (h_w) should not affect the change in capacitance created by a given bubble as long as the plate width was greater than the bubble diameter. Thus, the factors affecting the width of the plates were the necessity of all the bubbles to pass between the plates, and the need to create the minimum interference with the fluid dynamics of the bed. Since bubbles tend to be self-centering in these small beds it was considered that the minimum plate width necessary should be twice the maximum bubble diameter, i.e. 5cm.

6.11.3. Determination of Plate Height

The plate height (h_t) required was found by considering the theoretical response expected from a given size of bubble for a given plate height.

If the bubble height were less than the plate height, then the bubble would be completely covered by the plates at some stage, and therefore the response would be related to the bubble volume.

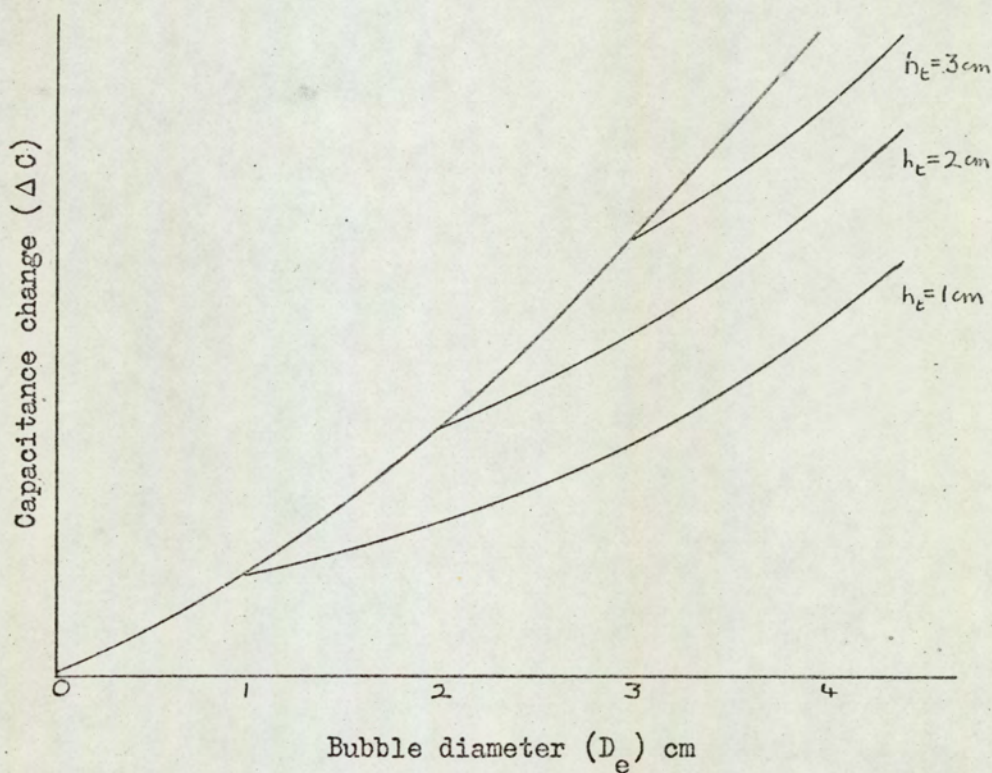
If, however, the bubble height were much greater than the plate height, the bubble would overlap greatly above and below the plates. The response expected would then be related to D_b^2 because if the bubble size were increased from D_{b1} to D_{b2} , there would be

an increase in the bubble volume between the plates in the horizontal directions but not in the vertical direction, assuming that the plate gap and width were greater than D_b . Assuming that $D_e \simeq$ the bubble height, then the expected shape of a plot of ΔC versus D_e would be as shown in Fig. 6.11.3.(1), (p.114), provided the plate width was greater than the bubble diameter.

Fig. 6.11.3.(1).

Theoretical plot of capacitance change versus bubble diameter

(Parameter is plate height)



The parameter h_t is the plate height and the graph predicts that for a given bubble size the response increases with plate height until the whole bubble is covered by the plates, when the response reaches a constant and remains at this value for any further

increase in plate height.

From previous sections it has been shown that the minimum plate width should be 5cm, the minimum gap 3cm, and that for negligible curvature of the lines of electric force, the response, i.e. capacitance change, for a given bubble diameter increases to a maximum when the plate height and bubble diameter are equal. However, for maximum sensitivity this capacitance change must be less than 0.1pF. Since in fact the lines of force "bell out" considerably, the optimum plate height had to be found experimentally using probes of different heights and measuring the response for different volumes injected into an air-ballotini system, 180 - 150micron diameter particles, (Fig. 6.11.3.(2), (p.116)).

It must be noted that, at the time, there was no method of determining the volume of a bubble formed by injecting a known volume of gas. It was therefore assumed that no growth or shrinkage occurred.

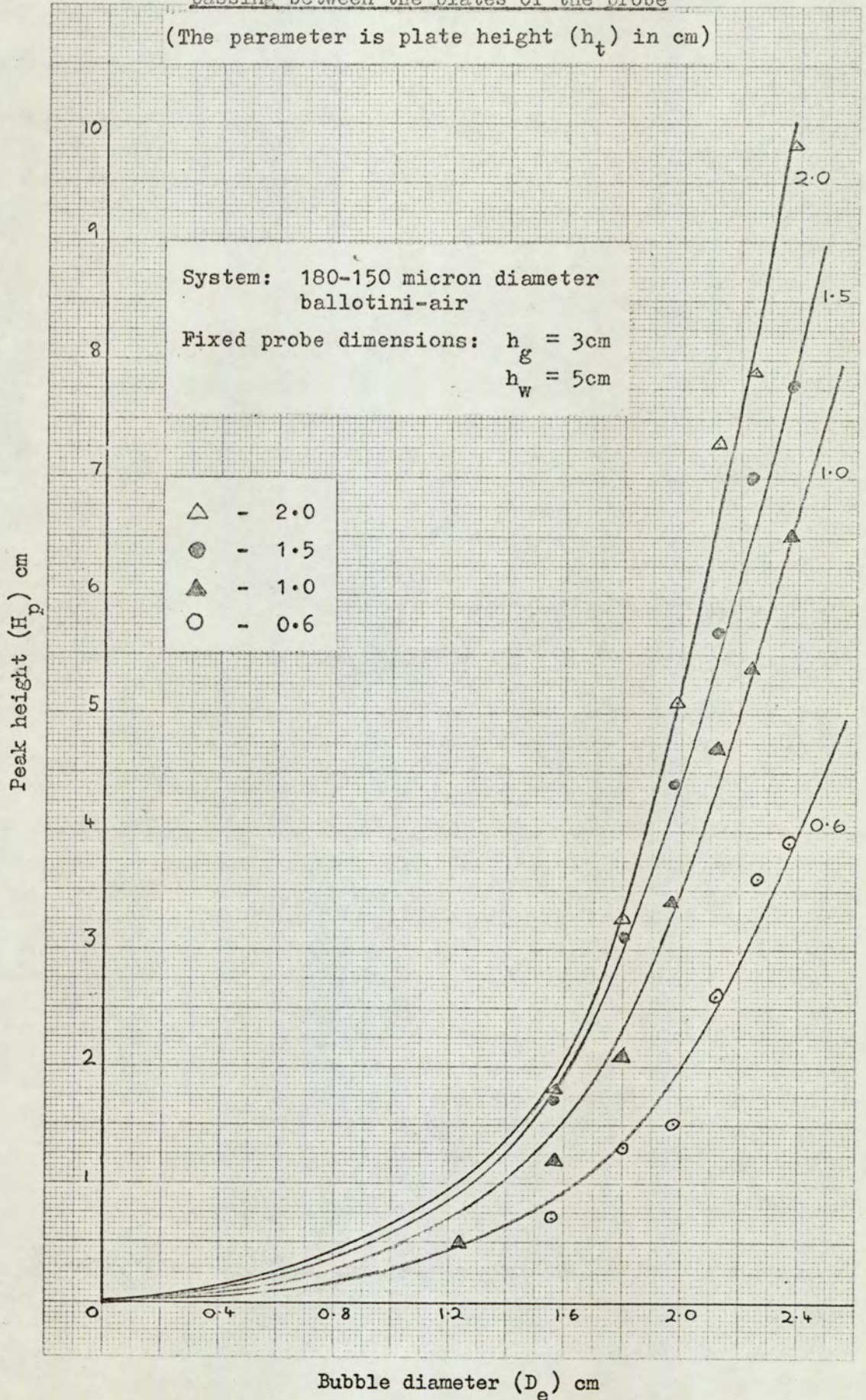
From these tests a plate height of 1.5cm was chosen, as it gave a capacitance change of approximately 0.09pF for an injected volume of 8cm^3 . It was realised that the maximum size of bubble that could be recorded in a catalyst system would be less than 8cm^3 , but it was considered that the sensitivity in a ballotini system should not be reduced.

The probe dimensions having been fixed, it was then necessary to investigate the capacitance changes that were caused by the proximity of other objects in the fluidised bed container.

Fig. 6.11.3.(2).

Peak height caused by a bubble of diameter D_e
passing between the plates of the probe

(The parameter is plate height (h_t) in cm)



6.12. FACTORS AFFECTING THE BASIC CAPACITANCE READING

6.12.1. Outside Interference

The copper screen described in Section 6.4. (p.93) also eliminated the capacitance variations caused by bodies outside the bed. Without the copper screen a hand placed on the outside of the bed container created a 0.15pF change, i.e. 1.5 times galvanometer FSD, whereas with the screen in position no change was detectable.

6.12.2. The Depth of the Probe in the Bed

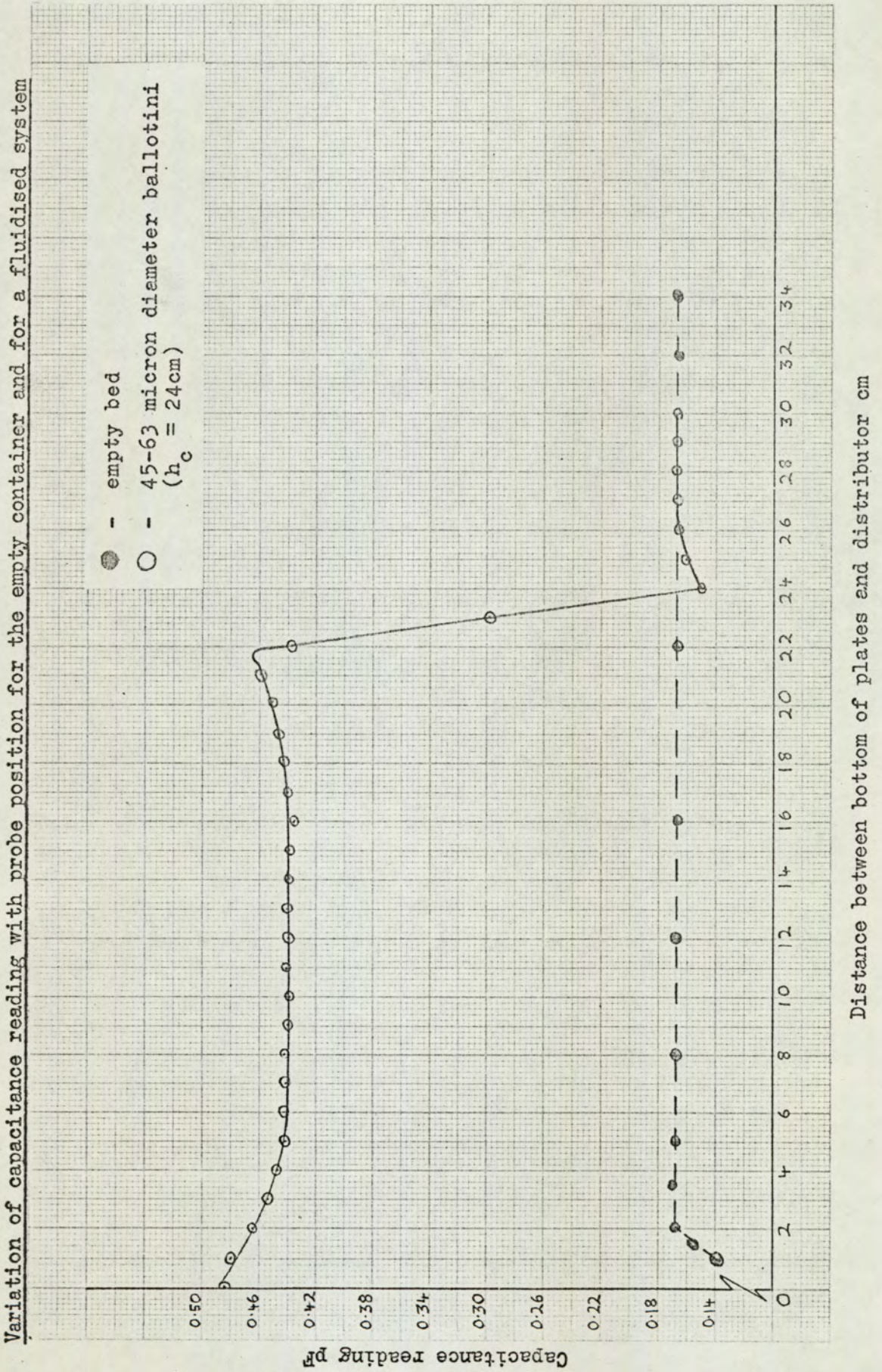
Even with the screen, a variation in the capacitance reading was noticed as the probe was raised and lowered in the bed, and there was also a small but definite horizontal effect. Tests were therefore carried out with the screen in place, the probe symmetrically positioned, and the base of the bed and the screen connected to the neutral of the bridge.

The tests were made with an empty container and then with the container filled to different heights with particles. The results were plotted and are shown for the empty and full container in Fig. 6.12.2.(1), (p.118). From the Figure it can be seen that for a full container, the capacitance value is constant as long as the probe is more than 4cm above the distributor, and at least 6cm below the bed surface. Between these limits all capacitance changes can be directly compared because the basic reading of capacitance in the empty bed is also a constant between the same limits.

6.12.3. Capacitance Change due to the Injector Tube

The effect of the injector tube on the capacitance reading

Fig. 6.12.2.(1).



was initially investigated in an air-ballotini system. The prototype metal injector tube was placed in the fluidised bed with the orifice below the plates and pulled upwards. The capacitance change (ΔC) it created as it passed between the plates was greater than 0.1pF and its effect was noticeable for 5cm above and below the plates (line A, Fig. 6.12.3.(1), (p.120)).

This was very undesirable as the capacitance change for a given bubble volume would depend on the location of the injector, so further tests were performed. A vertical steel tube and a horizontal nylon tube were joined to form a new injector and the maximum capacitance change it created was 0.01pF (line B, Fig. 6.12.3.(1)). This change was sufficiently low for the initial calibration work, but the nylon tube caused too much physical interference. So for the final calibration and the experimental investigations, a metal-glass injector was used (see Fig. 6.1.(3), (p.85)), which created less physical disturbance and a negligible capacitance change, in both air-ballotini (line C, Fig. 6.12.3.(1)) and air-catalyst systems.

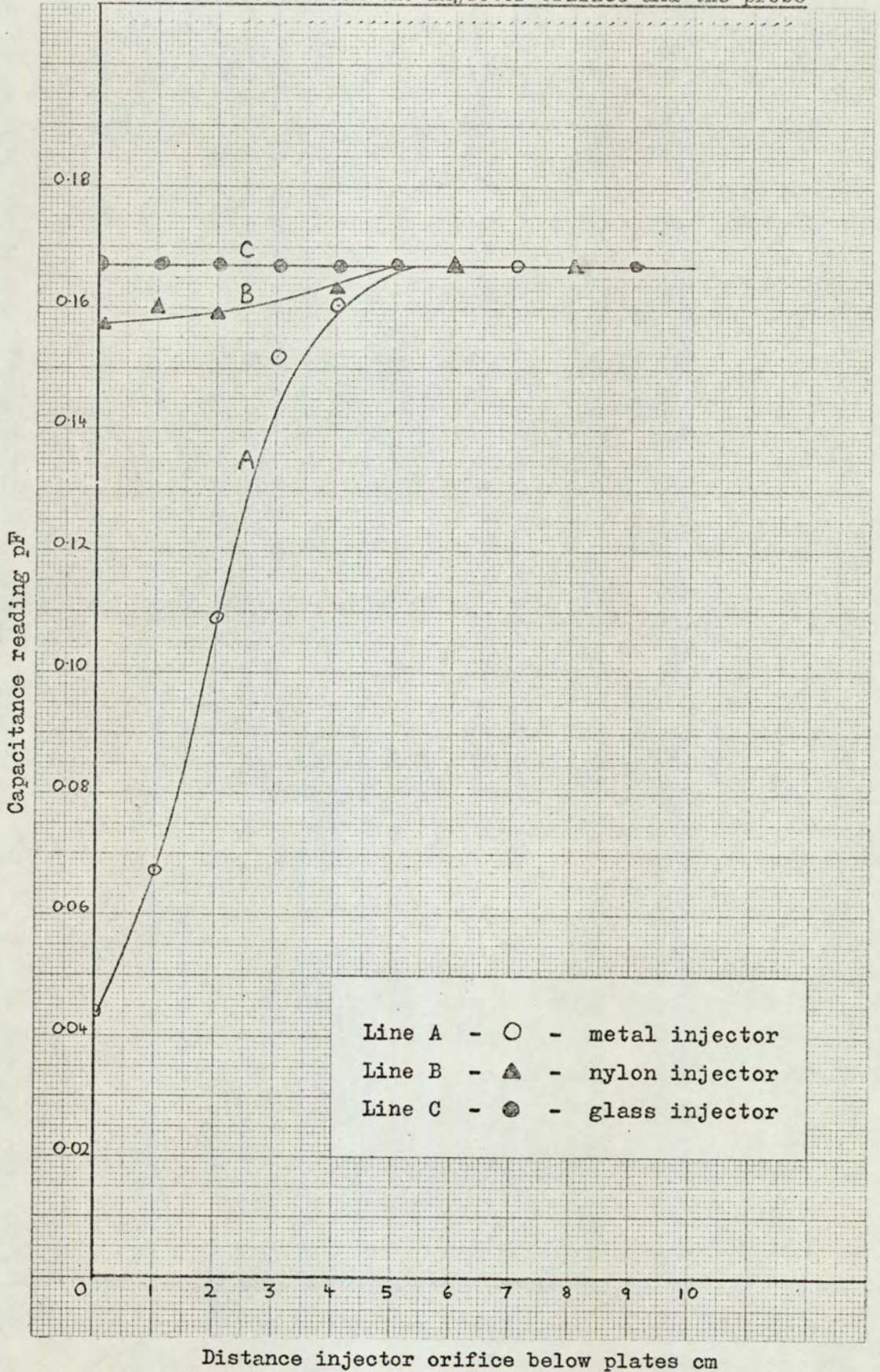
6.12.4. Screening of the Plates

With unscreened plates, a bubble rising anywhere in the bed would be recorded, but the response for a given size of bubble would depend on its position relative to the plates. A bubble passing behind one of the plates would cause only about a third of the change that it would cause if it passed between the plates. The plates were therefore screened by making them of two strips of shim brass separated by a sheet of mica insulation and then wired as shown in Fig. 6.1.(2), (p.84).

A very small response was still noticed with this arrangement

Fig. 6.12.3.(1).

Variation of probe capacitance reading
with distance between the injector orifice and the probe



when a bubble passed behind a plate. To ensure that the plates were completely screened, the screening plates for the probe size used would have to be 10.5cm high and 14cm wide⁽⁶²⁾. These were obviously far too large to place in the bed, so the plates were therefore constructed as described above.

A bubble rising to one side of the plates was still recorded. Two methods were considered to reduce this effect:

- i) Curved Plates: Though probably effective, these would have the disadvantage of producing a different flux density at different points between the plates. The response would depend on the position of the bubble between them, and therefore were not investigated experimentally.
- ii) Boxed Plates: Boxed plates were constructed by linking the ends of the screening plates with brass strip, such that a rectangular screen was formed (3cm x 5cm x 1.5cm high). This proved successful in eliminating any response from a bubble not between the plates, but it was thought that the box would impede the particles' movement and the method was therefore discarded.

This problem of bubbles rising behind the plates is more apparent than real since the bubbles tend to rise up the centre axis of the bed in any case. Screening the plates reduced the recorded capacitance value slightly but also reduced the variation in capacitance when they were moved off centre, making accurate centering unnecessary.

The interference created by objects inside and outside the bed had therefore been reduced to a minimum and the distance in the bed over which the probe could be used had been fixed. The

next step was therefore to calibrate the probe.

6.13. PROBE CALIBRATION

6.13.1. Calibration Theory

When an air bubble is injected in a fluidised bed, the capacitance change, as it passes between the two plates of a capacitor, is related to the dielectric constant of the bed material. The larger the dielectric constant of the dense phase, the larger the capacitance change will be when a given volume of air passes between the plates of the probe, because air has virtually the smallest possible dielectric constant. Hence, if different materials were used and known sizes of bubbles injected, it should be possible to obtain a calibration graph of capacitance change versus dielectric constant of the dense phase (D_{km}), with bubble volume as the parameter, qualitatively shown in Fig. 6.13.1. (1), (p.124).

In theory, the capacitance value of two plates of a given size with a given air gap between them is a constant. However, in practice the value was found to vary depending on the surroundings, and it was found that the reading in air varied considerably when the probe was in the empty bed container, depending on whether the copper screen was present or not, and also whether or not this screen was connected to the neutral of the bridge. Now this effect also occurred when the probe was in a bed of material but the variations in the readings for the material were not in the same ratio as the variations in the air readings. Therefore, on calculating the dielectric constant of the material, three different values were found, as can be seen in Table 6.13.1.(1), (p.125).

Fig. 6.13.1.(1).

Theoretical plot of capacitance change
versus dense phase dielectric constant
(Parameter is bubble volume)

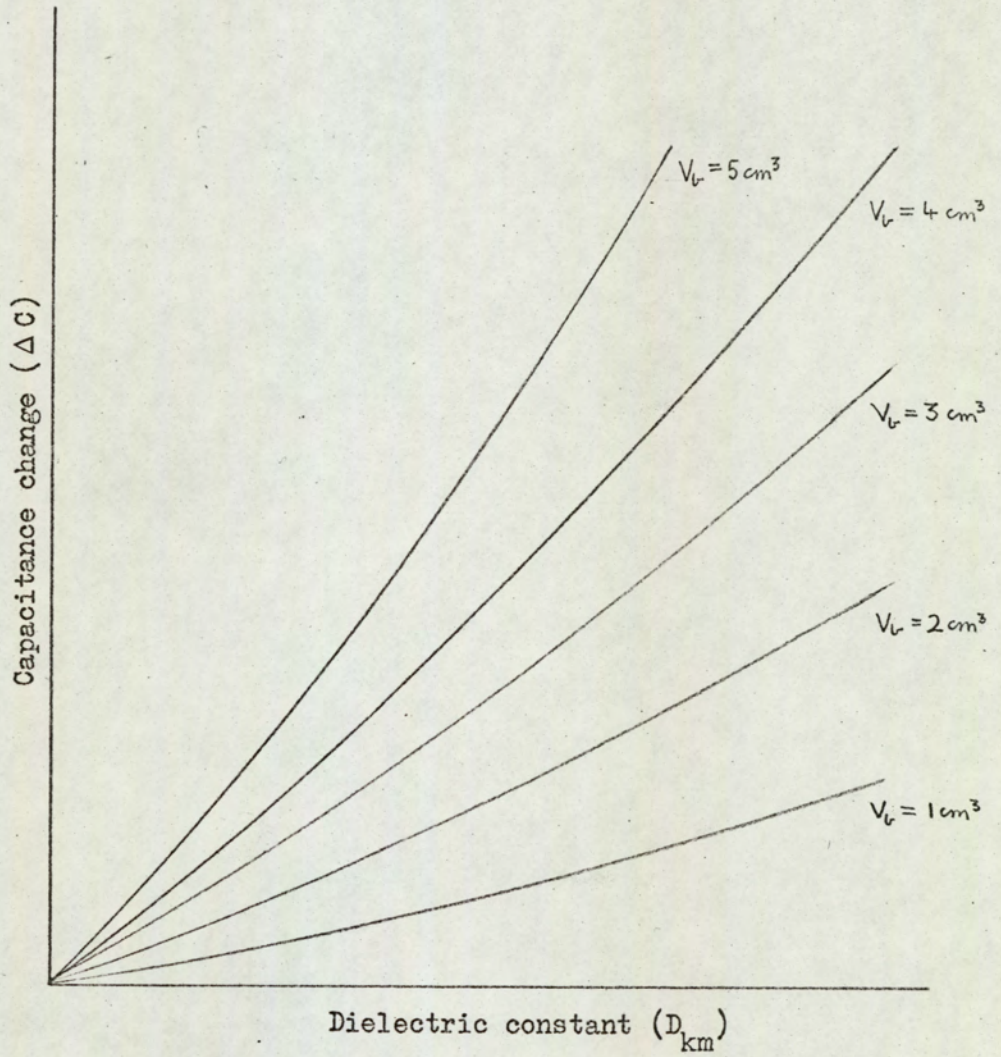


Table 6.13.1.(1).

Values of the Apparent Dielectric Constant of White Spirit obtained with Different Bed Screening Arrangements

Screening Arrangements	Without Screen	Screen Insulated from the Bridge	Screen Shorted to the Bridge Neutral
Capacitance Reading in White Spirit pF	0.416	0.369	0.336
Capacitance Reading in Air pF	0.186	0.169	0.159
Apparent Dielectric Constant of White Spirit	2.24	2.18	2.12

This is, of course, theoretically impossible and the error is probably caused by the lines of force between the plates being closer together for a higher dielectric and therefore the change in the screening arrangement causes a different percentage change in the capacitance, compared to that of air. Due to this variation in the measurement of dielectric constants, it was decided that the calibration would apply only to a given bed container, and that therefore there was no point in converting the capacitance values to dielectric constants.

The abscissa of the calibration graph will therefore be calibrated in pico-Farads and the lines of constant bubble size on the calibration graph will now all intercept the abscissa at the capacitance reading for air in the screened container, with the screen connected to the bridge neutral.

It has been shown (Section 6.9.) that the volume of an injected bubble may be different from the volume of injected gas.

Since in a fluidised bed there is no method of determining this difference, the use of non-conducting liquids appeared to be the method most likely to give reproducible and accurate results, because as long as the liquids used were transparent, the volume of the trailing bubbles could be estimated.

6.13.2. Calibration Materials

In Section 6.14.1. it will be shown that, assuming the minimum bed voidage for a fluidised bed to be 0.4, then the value of the dielectric constant of a fluidised bed must lie between 1.0 and 5.5. Liquids with dielectric constants in the range 1.0 to 5.5 were therefore required for the calibration, but preliminary tests showed that the liquid viscosity was also important; too low a viscosity gave multiple bubbles. The most suitable liquids, considering their dielectric constants⁽⁶³⁾, viscosity⁽⁶⁴⁾ and availability were chosen, and are listed in Table 6.13.2.(1), together with their properties.

Table 6.13.2.(1).

Liquids used in Calibration

Substance	Temperature T °C	Dielectric Constant D _k	Temperature T °C	Viscosity μ _f cP
Rape seed oil	16	2.85	20	163
Olive oil	20	3.11	20	101
Linseed oil	13	3.35	30	33
Castor oil	11	4.67	20	986

These oils provided four points on the calibration chart which were considered to be insufficient, so five different mixtures of castor oil and olive oil were made up to provide liquids with dielectric constants between 3.35 and 4.67. Liquids with dielectric constants in the range 1.5 - 2.8 were also required, but the only available liquids had such low viscosities that they were discarded.

6.13.3. Calibration Technique

The glass container for the air fluidised bed was fitted with an impervious plastic disc immediately below its distributor. This was to prevent the air box filling with liquid which might have affected the capacitance readings.

As stated in Section 6.12.2, the probe had to be positioned centrally in the container more than 4cm above the distributor and more than 6cm below the surface of the bed material. For calibration the liquid height was always 30cm, (the approximate bed height anticipated), and the probe was always positioned 13.5cm above the distributor, i.e. within the stated calibration limits.

At the start of a run, the probe was placed in the empty bed container, the copper shield clamped in position and connected to the neutral of the bridge. The capacitance reading was then noted. Provided it lay between 0.165pF and 0.169pF the probe was considered to be correctly positioned. The oil under test was poured in to a height of 30cm and the capacitance value again noted. The autobalance was set to give a 2cm datum deflection and it was visually checked that injected bubbles passed centrally between the plates. Different known sizes of bubbles ranging from

0.5cm^3 - 7cm^3 were then injected and the response recorded by the oscillograph. The oil was then changed and the process repeated.

6.13.4. Calibration Results

The variation of the basic capacitance reading in the empty container was found to vary over a period of days by 3% (0.165pF - 0.169pF). This variation was neglected since the capacitance range in the presence of oils was 0.5pF - 0.8pF .

In constructing the calibration curve it was necessary to make a correction to the bubbles larger than 4cm^3 (injected volume) since it was found that even in oil of viscosity 100cP one or two trailing bubbles of about 0.2cm^3 were formed. These small bubbles rose slowly and therefore did not affect the main probe response. Their volume was estimated by extrapolation of the results for bubbles smaller than 4cm^3 and the corrected volumes were then plotted against peak height for each oil (Fig. 6.13.4.(1), (p.130)). It can be seen that the peak height would appear to be directly proportional to the bubble volume over the range investigated, and that the scatter of points about each line was less than $\pm 2\%$. By replotting the results as peak height versus capacitance with bubble volume as parameter the required calibration graph was obtained (Fig. 6.13.4.(2), (p.131)). It appeared that the lines of constant bubble volume were approximately straight and therefore the best straight line was drawn through each set of points, by the least mean squares technique, having first weighted the results such that all the lines intersected the abscissa at the value of 0.167pF . These lines were interpolated in order to obtain a graph of peak height versus bubble volume with capacitance as parameter (Fig. 6.13.4.(3), (p.132)), i.e. similar to Fig. 6.13.4.(1), but

with a line for every 0.02pF increment in capacitance.

Though bubble volume could be accurately measured, the capacitance value of the dense phase had not yet been calibrated against the dense phase voidage. This was necessary if the probe was to be used in a metal fluidised bed container in which no direct bed height measurements would be possible. The variation in the capacitance reading with dense phase voidage was therefore considered to determine if the instrument was sufficiently sensitive to measure this variation with any degree of accuracy.

Fig. 6.13.4.(1).

Peak height (H_p) versus bubble volume (V_b)
for different dielectric liquids

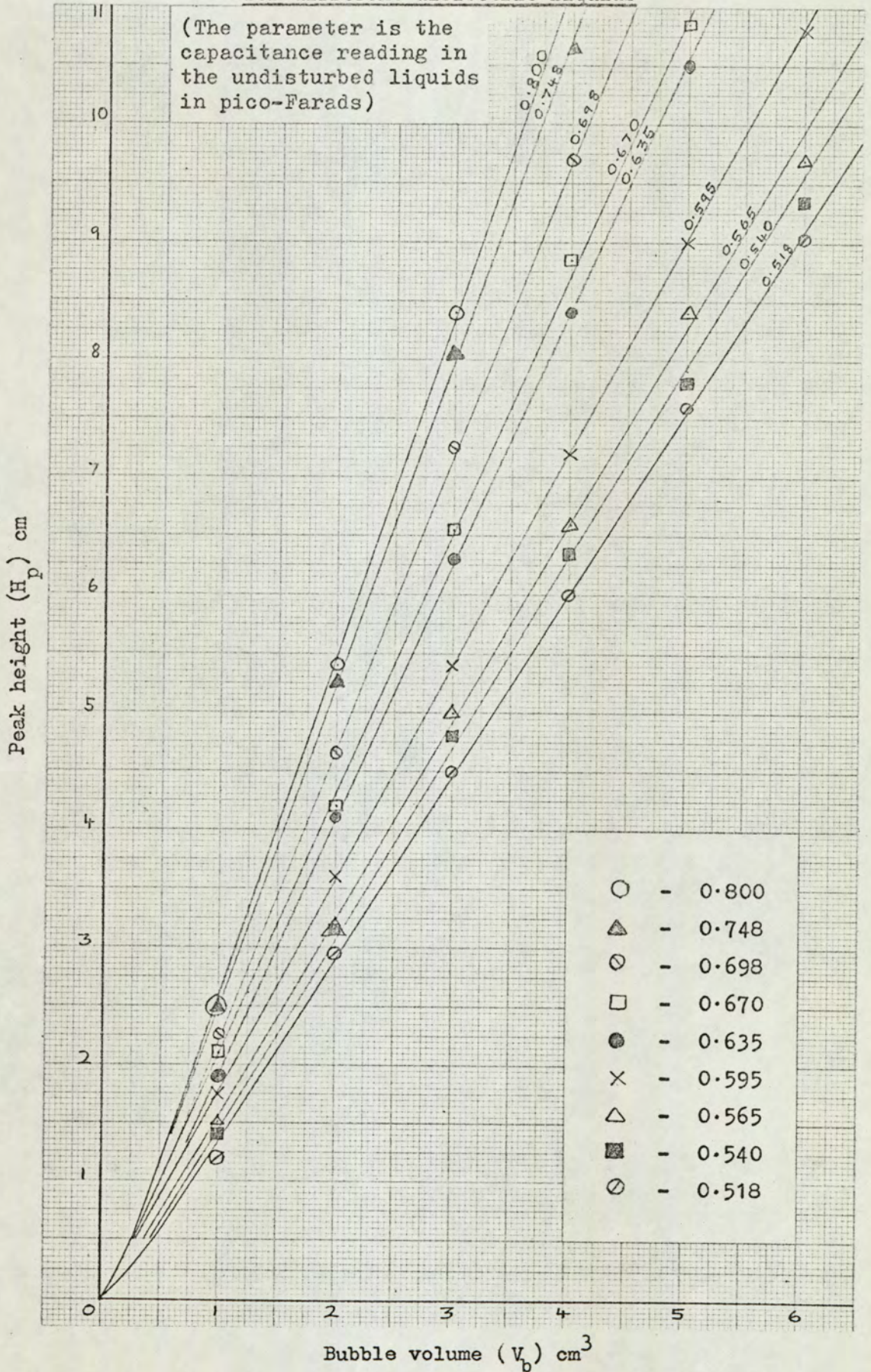


Fig. 6.13.4.(2).

Peak height (H_p) versus capacitance reading of the undisturbed liquid

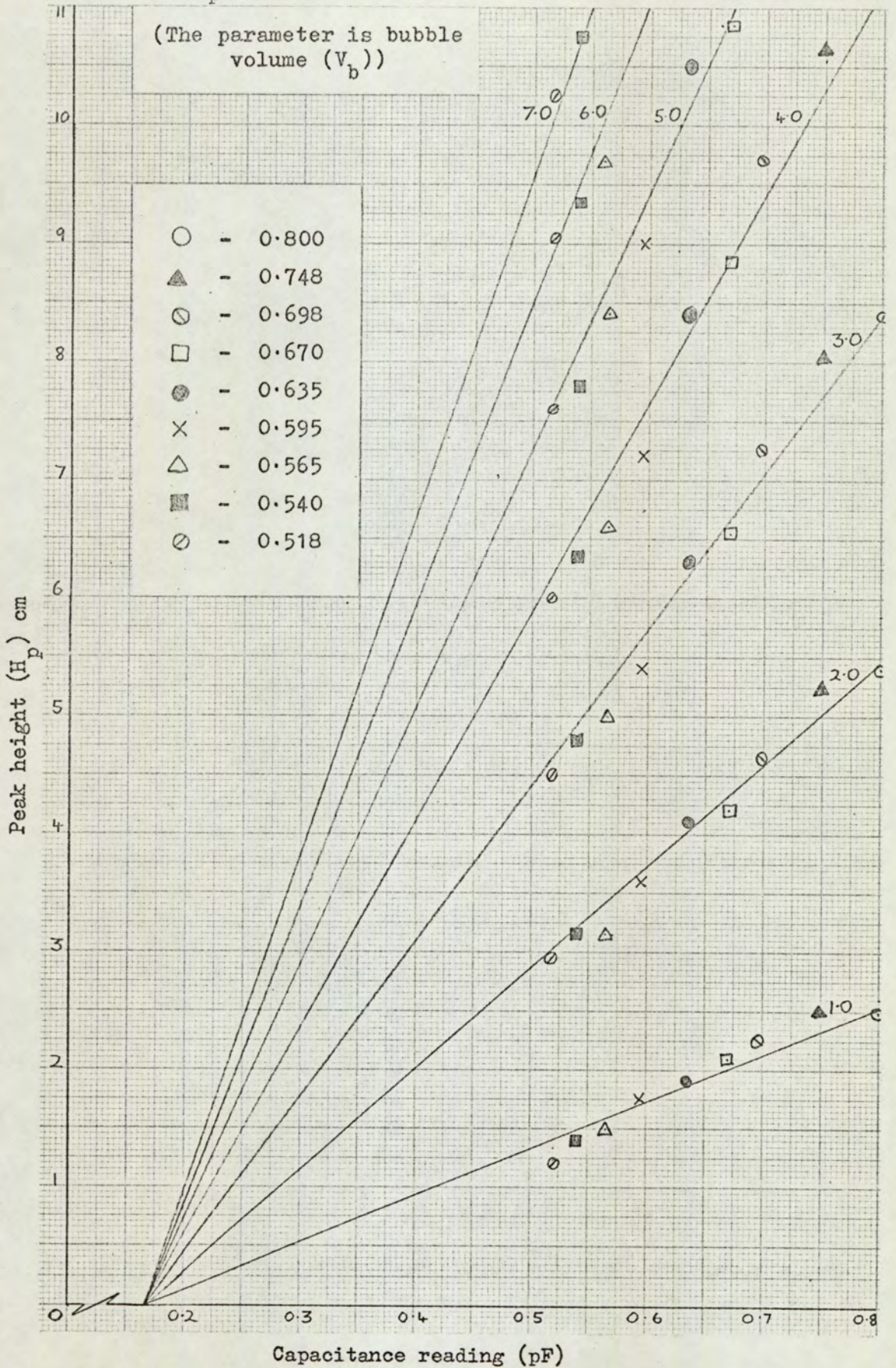
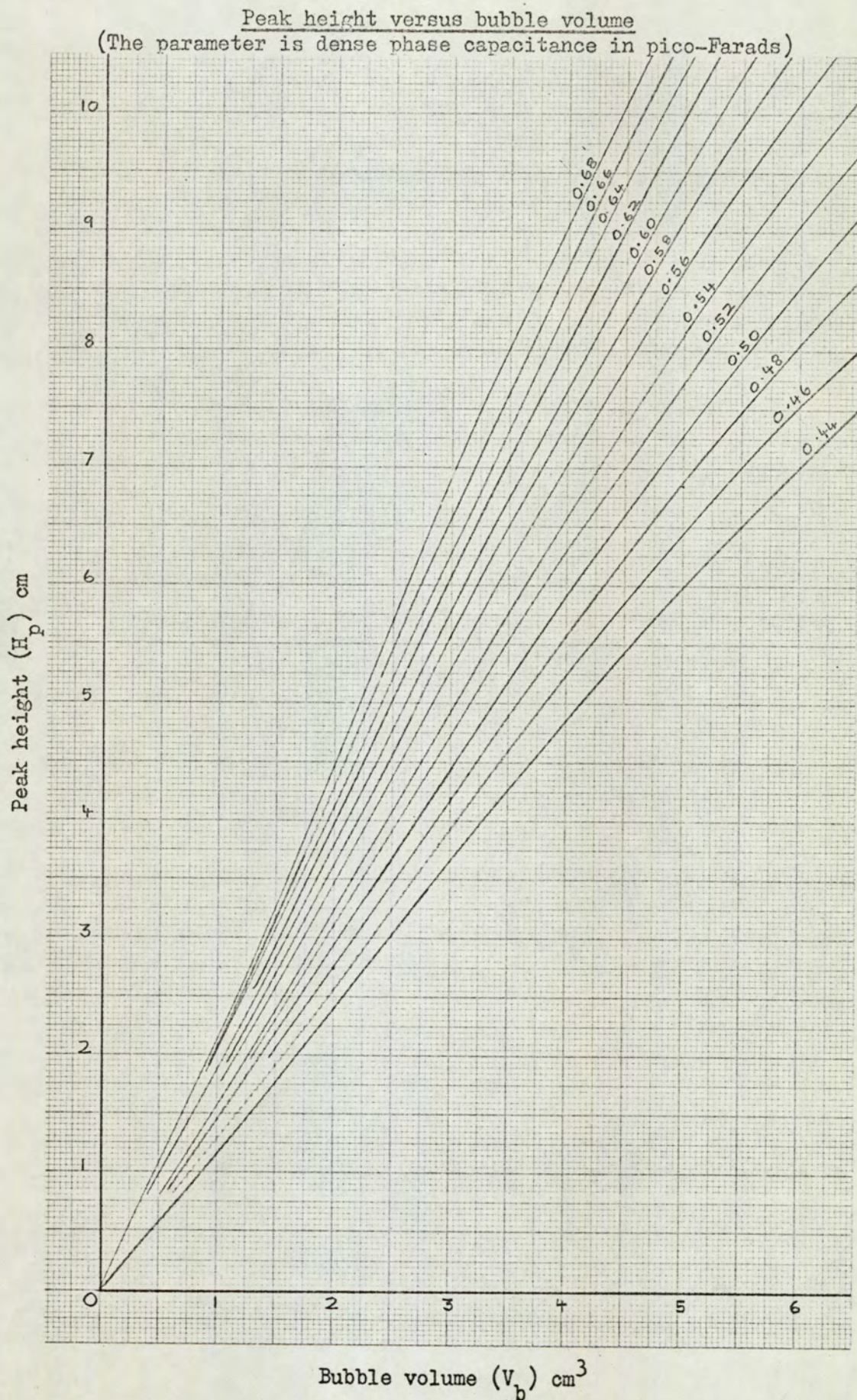


Fig. 6.13.4.(3).



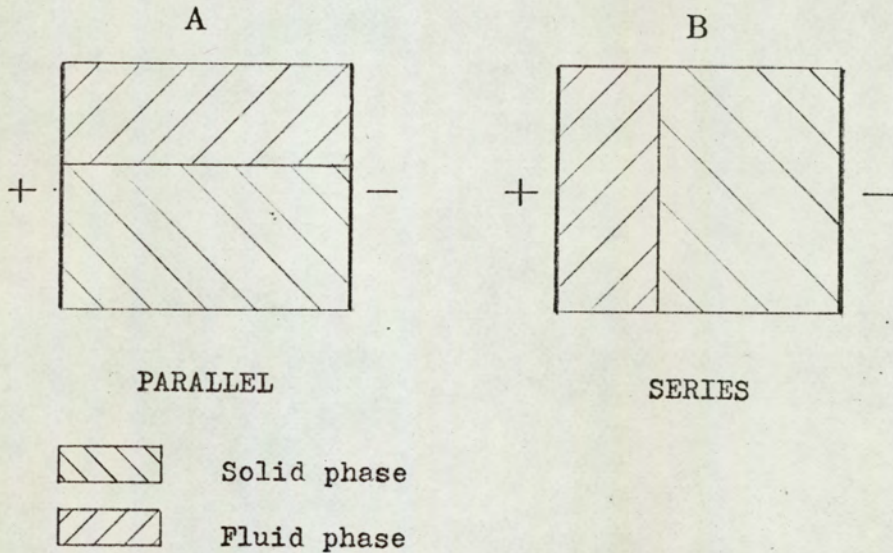
6.14. RELATIONSHIP BETWEEN THE DIELECTRIC CONSTANT AND THE VOIDAGE OF THE DENSE PHASE OF A FLUIDISED BED

6.14.1. Theory

When the dielectric constant of a mixture of a fluid and a solid is considered, two extreme values can be calculated for a given voidage from the expressions for (i) Parallel and (ii) Series Capacitance, if it is assumed that the solid phase can form a compact mass of zero voidage as shown in Fig. 6.14.1.(1), (p.133).

Fig. 6.14.1.(1).

The two extreme cases for a mixture of a fluid and a solid between the plates of a capacitor



Let:

the subscript 1 refer to the discontinuous phase, i.e. solid phase;

the subscript 2 refer to the continuous phase, i.e. fluid phase;

the subscript T refer to the summation of both phases;

$$e_k = \frac{\text{volume of component 2}}{\text{total volume}} \quad - \quad 6.14.1.(1)$$

In the Appendix Section A2 it has been shown that the expression for the total capacitance of the two components (D_{kT}) is as stated below, for the two extreme cases:

i) Parallel Capacitance

$$D_{kT} = D_{k1} (1 - e_k) + D_{k2} e_k \quad - 6.14.1.(2)$$

ii) Series Capacitance

$$\frac{1}{D_{kT}} = \frac{(1 - e_k)}{D_{k1}} + \frac{e_k}{D_{k2}} \quad - 6.14.1.(3)$$

In an ideal, non-bubbling fluidised bed a homogeneous mixture of particles and fluid exists and therefore the value of the dielectric constant should lie between the values predicted by the parallel and series cases. Several authors have attempted to derive a general equation for the dielectric constant of a solid-fluid mixture (D_{km}), as the voidage changes from one extreme to the other. Bakker and Heertjes⁽⁴³⁾ considered the expressions from about eight of these investigations, and found that the Wiener equation

$$\frac{D_{km} - D_{k2}}{D_{km} + 2D_{k2}} = \frac{(1 - e_i)(D_{k1} - D_{k2})}{D_{k1} + 2D_{k2}} \quad - 6.14.1.(4)$$

gave the best agreement with their experimentally determined values for glass-air mixtures.

If the Wiener equation is rearranged such that

$$\frac{D_{km} - D_{k2}}{D_{km} + 2D_{k2}} \frac{1}{(1 - e_i)} = \frac{D_{k1} - D_{k2}}{D_{k1} + 2D_{k2}} \quad - 6.14.1.(5)$$

then for a given solid and fluid the right hand side is a constant, k_8 .

i.e. $D_{k1} - D_{k2} = k_8 (D_{k1} + 2D_{k2})$ - 6.14.1.(6)

Now if the fluid is air, $D_{k2} = 1.0$ and hence $D_{k1} > D_{k2}$

Therefore $0 < k_8 < 1.0$,

and when $k_8 = 0$, $D_{k1} = 1.0$

and when $k_8 = 1$, $D_{k1} = \infty$.

Hence substituting into 6.14.1.(5)

$$0 < \frac{D_{km} - 1}{D_{km} + 2} \frac{1}{(1 - e_i)} < 1.0 \quad - 6.14.1.(7)$$

i.e. $0 < (D_{km} - 1) < (D_{km} + 2)(1 - e_i)$

Therefore $1 < D_{km} < \left(\frac{3}{e_i} - 2\right)$ - 6.14.1.(8)

Hence for $e_i = 0.6$ $1 < D_{km} < 3.0$

$e_i = 0.4$ $1 < D_{km} < 5.5$

and as $e_i \rightarrow 0$ $D_{km} \rightarrow D_{k1}$

A plot of the maximum value of D_{km} versus e_i

(i.e. $D_{k1} = \infty$ and $D_{km} = (3/e_i - 2)$) is given as line D in Fig. 6.14.1.(2), (p.139).

The values found for D_{km} for an air-ballotini fluidised bed when $D_{k1} = 7.86$ are given below.

when $e_i = 0.6$, $D_{km} = 2.1$

and when $e_i = 0.4$, $D_{km} = 3.2$

If it is assumed that the Wiener equation holds for a gas fluidised bed behaving particulatesly, then from the above it can

be seen that:

- i) the value of the bed dielectric constant (D_{km}) for a given bed voidage is only approximately doubled, when the value of D_{k1} is increased from 7 to ∞ ;
- ii) the amplitude of a peak for a given probe measuring a given bubble size can only change by a factor of about three for an infinite change in D_{k1} , because the minimum value of D_{km} likely to be encountered in a gas fluidised bed is about two (diakon fluidised, $D_{km} \simeq 1.9$) and the maximum value is about 5.5.

This suggests that a single calibrated probe could be used to investigate a very wide range of gas fluidised materials.

6.14.2. Experimental

As it was possible to obtain larger voidage changes with a liquid fluidised bed than with a gas fluidised bed, a white spirit-soda glass ballotini system was used to determine whether the Wiener equation held for the apparatus being used in this work.

As has been mentioned in Section 6.13.1., the apparent value of the dielectric constant of a material depended on the physical conditions prevailing at the time of measurement, and therefore values of the dielectric constant of the white spirit and the glass recorded in the bed container were required, rather than the manufacturers' quoted values. The value of the dielectric constant for the white spirit was of course easily measured but there was no obvious method of determining that of the glass. The method suggested by Bakker and Heertjes⁽⁴³⁾ was attempted but considerable difficulties were experienced, perhaps due to ionisation of the aniline.

The procedure used was to calculate the value of the left hand side of the equation 6.14.1.(5)

$$\frac{D_{km} - D_{k2}}{D_{km} + 2D_{k2}} \cdot \frac{1}{(1 - e_i)}$$

for each measured pair of values of voidage and dielectric constant, the measured value of D_{k2} being 2.1.

Over a voidage range of 0.442 - 0.644 the value of the above expression was found to be constant at $k_8 = 0.475 \pm 1\%$ which was taken as proof that the Wiener equation did hold for the apparatus being used. Substitution of the average value of k_8 and the measured value of D_{k2} (2.1) into the right hand side of the equation 6.14.1.(6) gave an apparent value of $D_{k1} = 7.86$.

Using this value of D_{k1} the theoretical Wiener equation was plotted as shown in Fig. 6.14.2.(1), (p.140), and the experimental results superimposed to demonstrate the lack of scatter.

Having shown that the Wiener equation could be used to predict voidages over a fairly wide voidage range, attention was turned to gas fluidised beds. Soda glass ballotini (45 - 63 micron diameter) was fluidised with air, and the values of voidage and dielectric constant were recorded over the voidage range for which the bed behaved particulatesly. Using the same procedure as described for the liquid fluidised bed, the value of D_{k1} was again found to be 7.86 (but for this system $D_{k2} = 1.0$).

Using the values of $D_{k1} = 7.86$ and $D_{k2} = 1.0$, substituting in equations 6.14.1.(2), (3) and (4) gave the theoretical curves for the parallel, series and Wiener cases which are shown in Fig. 6.14.1.(2) as lines A, B and C. For comparison, the plot of voidage versus bed dielectric constant when $D_{k1} = \infty$ and $D_{k2} = 1.0$, is also included on the same Figure (line D).

From Fig. 6.14.2.(2), (p.141), it can be seen that the Wiener equation approximates to a straight line over the voidage range available with a soda glass ballotini-air fluidised bed, and that the scatter of experimental results is only $\pm 0.2\%$. The two points at the lowest gas rates were ignored because it was suspected that the high recorded values of capacitance were due to jamming of particles between the plates, causing a local decrease in voidage and therefore apparently high bed dielectric constants. A similar effect was noted with the liquid fluidised bed (Fig. 6.14.2.(1)).

The catalyst-air results are presented in a similar fashion, Fig. 6.14.2.(3), (p.142), but it must be noted that the average value of k_g in equation 6.14.1.(6) is 0.993, which is too close to 1.0 for an accurate determination of the dielectric constant of the catalyst. The line given in Fig. 6.14.2.(3) is therefore for $D_{k1} = \infty$ ($k_g = 1.0$) and the scatter of experimental results is of the order of $\pm 1\%$.

Fig. 6.14.1.(2).

Theoretical dielectric constant of a mixture of two components (1 and 2) versus voidage

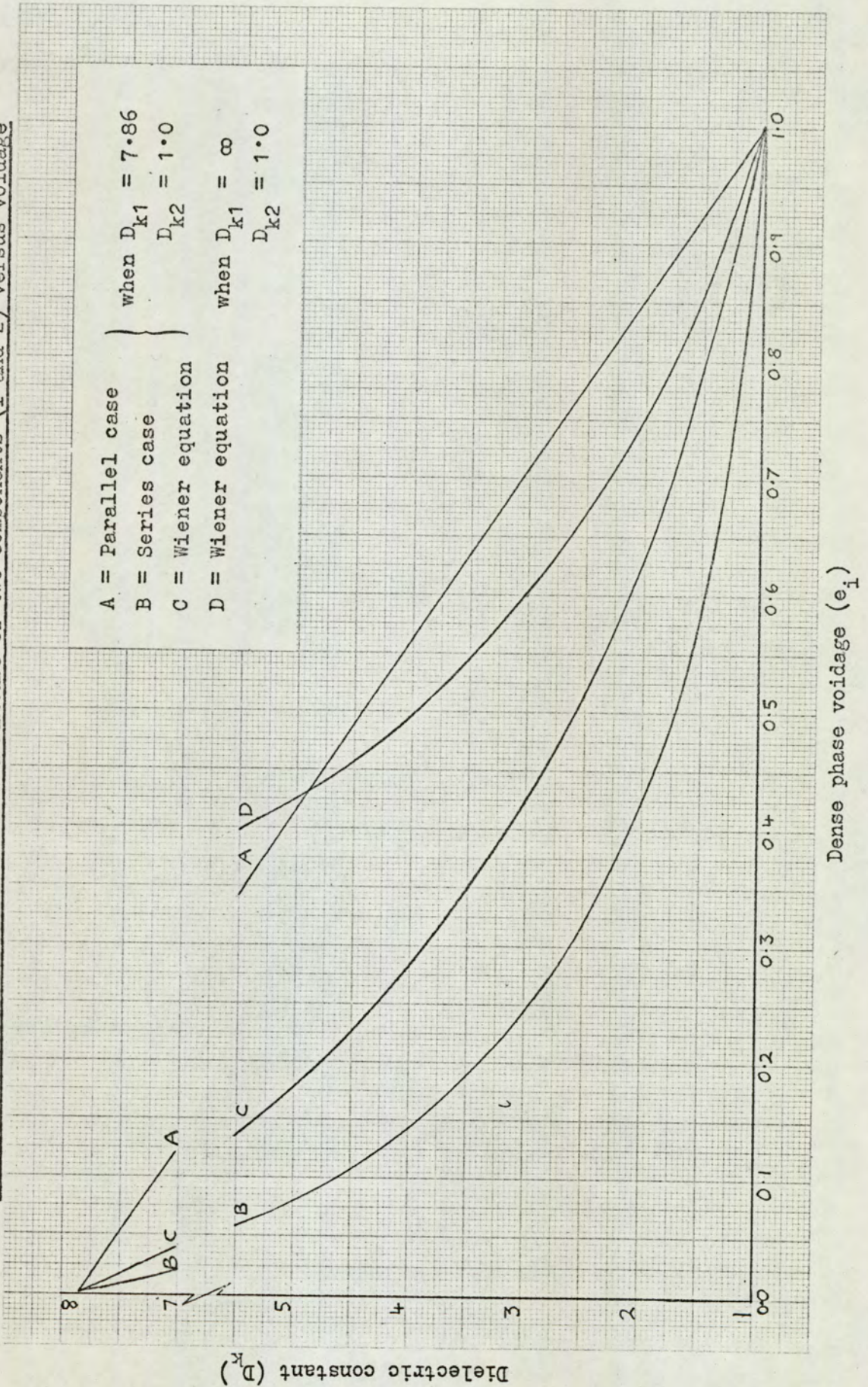


Fig. 6.14.2.(1).

Dielectric constant of a fluidised bed for a ballotini ($D_{k1} = 7.86$)-white spirit ($D_{k2} = 2.1$) system versus dense phase voidage

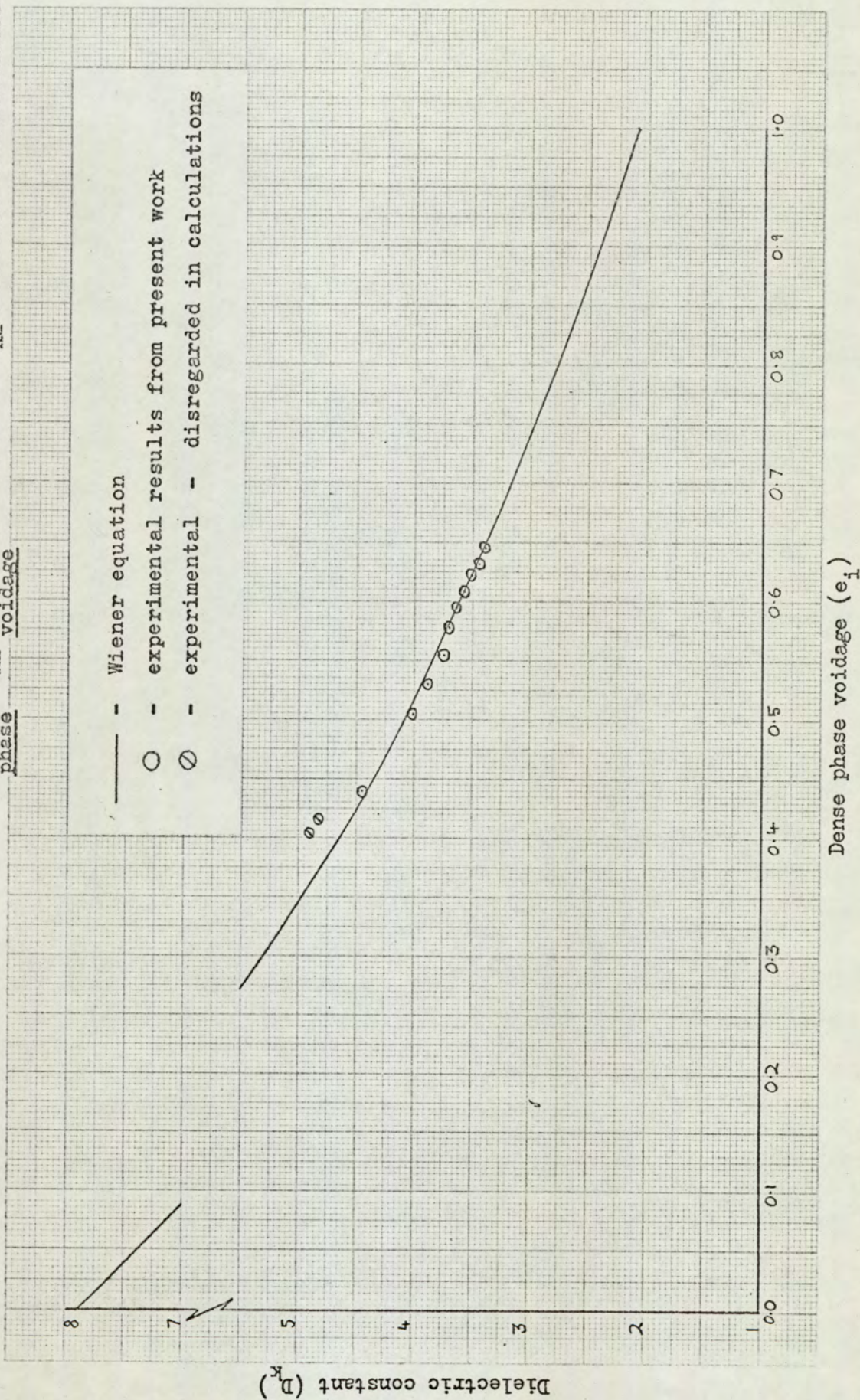
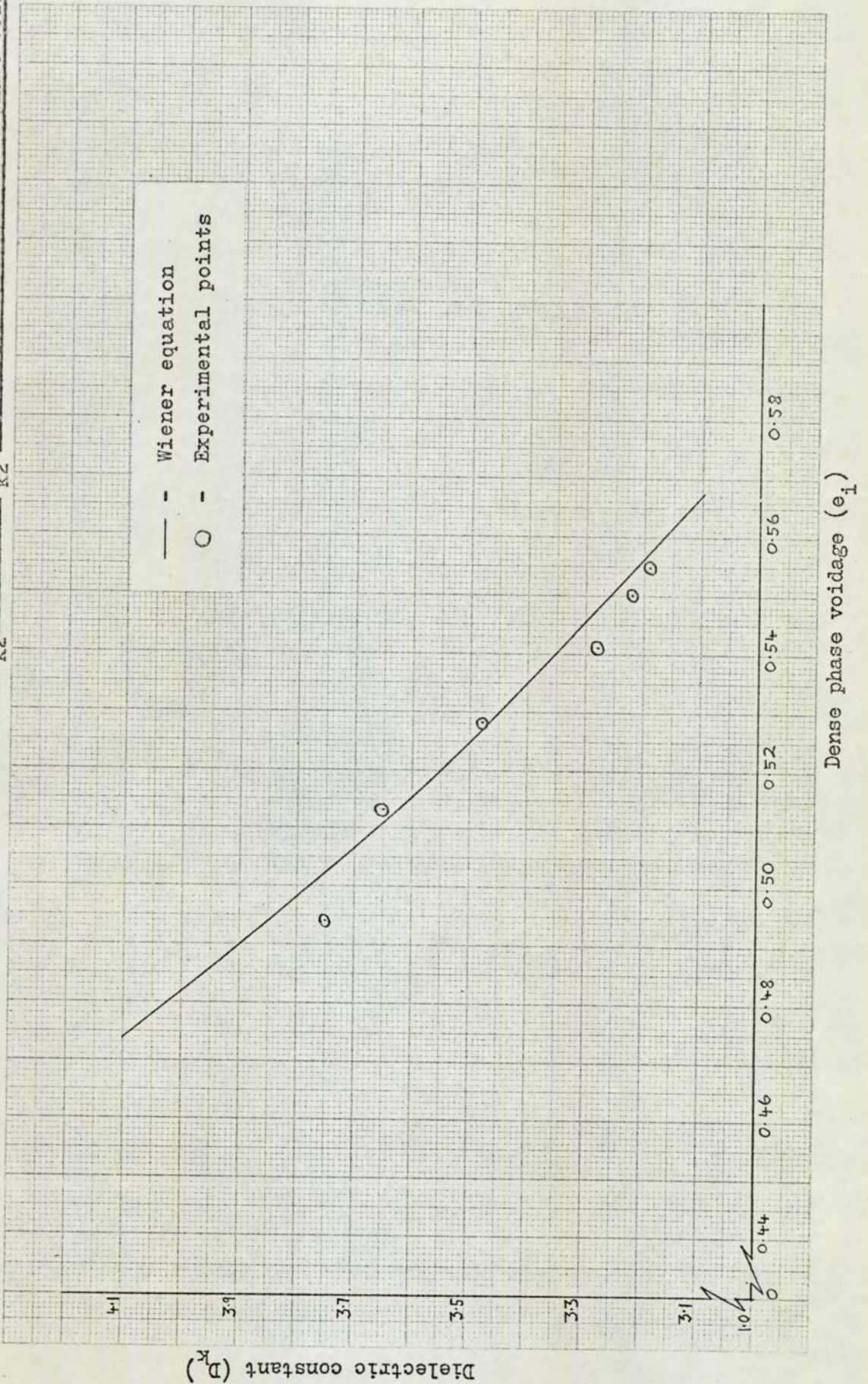


Fig. 6.14.2.(3).

Dielectric constant of a fluidised bed for a catalyst ($D_{k2} \approx \infty$)-air ($D_{k2} = 1.0$) system versus dense phase voidage



6.15. CLOSURE OF SECTION 6

In this Section the calibration of the instruments, and the development and calibration of the probe have been reported with, where possible, the theoretical explanations for the practical problems that were encountered.

Having successfully developed a sensitive instrument, the physical properties of the media available for fluidising were investigated before commencing the experimental study of the properties of fluidised beds.

PARTICLES

7.1. REQUIRED PARTICLE PROPERTIES

7.1.1. Shape

Spherical particles were required for ease of fluidisation and correlation of results with published theories.

7.1.2. Size

In order to work in the transition region between particulate and aggregative fluidisation with gas fluidisation, it was preferable to have particles with a diameter of the order of 50micron.

7.1.3. Uniformity of Size

With small particles it is often difficult to determine the point of incipient fluidisation with any degree of accuracy, probably due to the wider size range normally obtained. It was therefore preferable to work with as small a size range of particles as possible, in an attempt to reduce to a minimum the error in measuring the incipient velocity.

7.1.4. Density

Material with a low density was required because, from the literature, it appeared that particles of low density tended to fluidise particulately over a larger voidage range than high density particles, all other factors being equal.

7.1.5. Electrical Properties

The particles had to be non-conductors and, for accurate

work in gas fluidised beds, have a value of D_{km} greater than about 2.3. If it is assumed that an average voidage for a gas fluidised bed is about 0.47, then substitution of $D_{km} = 2.3$, $e_i = 0.47$ and $D_{k2} = 1.0$ into the Wiener equation (6.14.1.(4)) shows that the material dielectric constant (D_{k1}) should be greater than about 5. A gas bubble in a fluidised bed with a bed dielectric constant of less than 2.3 would still be recorded, but the response is related to the bed dielectric constant and at values below 2.3 the response for small bubbles is such that the errors in the chart measurement become significant.

7.2. CHOICE OF MATERIALS

7.2.1. Glass

Glass was chosen because the suppliers⁽⁶⁵⁾ stated that the glass spheres (ballotini) were available from 1×10^3 micron diameter to less than 53 micron diameter with a density of 2.9g/cm^3 (lead glass), and for any specified size range (normally alternate BS sieves) 80% of the spheres would be between the two limits. The disadvantage of the rather high density was outweighed by the small size and close cuts available and the dielectric constant of lead glass which is about 7.

7.2.2. Cracking Catalyst

The alumina catalyst used was a dusty powder with an initial size range of 0 - 100 micron. Its advantages were that:

- i) it was easy to sieve;
- ii) it had a particle density of about 0.9g/cm^3 ;
- iii) its particle dielectric constant was greater than 100, giving an expanded bed dielectric constant of about 3.8.

These advantages outweighed the fact that the particles were not spherical.

7.2.3. Diakon

This is an acrylic polymer and was available as spheres with an average diameter of 270 micron, a particle density of about 1.2g/cm^3 and a dielectric constant of about 3.5. The low dielectric constant and the ease with which the particles became charged with static electricity made this a far from ideal material, and therefore only a limited number of tests were carried out with it.

Rubbish

7.2.4. Others

PVC spheres and stearic acid spheres were available but both had disadvantages similar to diakon.

7.3. SIEVING OF MATERIALS

(In this text "BS Mesh size" has been abbreviated to M.)

7.3.1. Glass

The sieving of ballotini with a diameter greater than about 150 micron was carried out by machine. Microscope checks showed that this method was sufficiently accurate, although the percentage of ballotini outside the given size range of the "as supplied" material was considerably more than the 20% quoted by the suppliers. When fine ballotini, stated size range 80% less than 240M (63 micron) was machine-sieved, the fraction retained between the 240M (63 micron) and the 350M (45 micron) sieves was checked with an image shear microscope and the results are shown as line A in Fig. 7.3.1.(1), (p.150). This indicated that the machine-sieving was inaccurate for fine particles so a fresh sample was hand-sieved (as BS 1796) and the fraction between the 240M and 350M sieves again checked with the microscope (line B, Fig. 7.3.1.(1)).

It can be seen that:

- i) hand-sieving is more accurate than machine-sieving for fine particles;
- ii) even with hand-sieving, a relatively high percentage (4%) of smaller particles will be retained when dealing with particle diameters of less than 100 micron.

7.3.2. Catalyst

The catalyst was hand-sieved and the fraction retained between the 240M (63 micron) and 350M (45 micron) examined by microscope, (Fig. 7.3.2.(1), (p.151)). In order to calculate the cumulative %w/w undersize it was assumed that the particles were spherical.

This is, of course, not true, as can be seen from the photomicrograph (Fig. 7.3.2.(2), (p.152)). The large %w/w of particles with a dimension greater than 63 micron is probably due to the fact that the mono layer required for microscope analysis ensured that the majority of the particles presented their largest dimension for measurement, whereas during sieving a smaller dimension could be presented to the sieve aperture allowing the particles to pass through the mesh.

7.3.3. Diakon

The large size range of the diakon and the effect of static made it uneconomic from the time point of view to separate a close cut. All particles larger than 250 micron were removed, leaving a size range of 125 - 250 micron (see Fig. 7.3.3.(1), (p.153)). From microscope analysis the sauter diameter was 194 micron. If it had been necessary to achieve a close cut then the best method might well have been to coat the spheres with silver to reduce the static problem, a technique used by McCoy and Madden⁽⁶⁶⁾.

Fig. 7.3.1.(1).

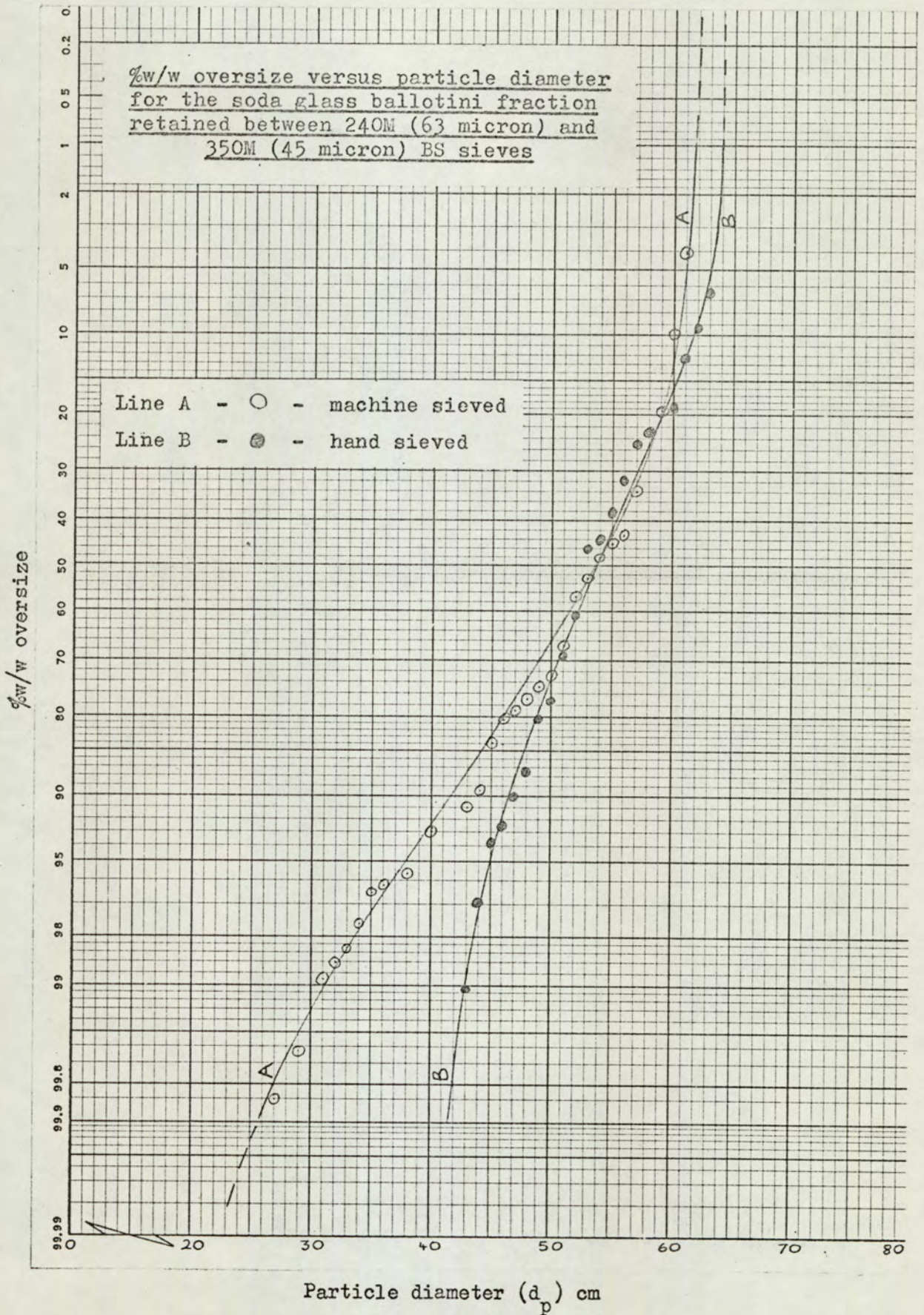


Fig. 7.3.2.(1).

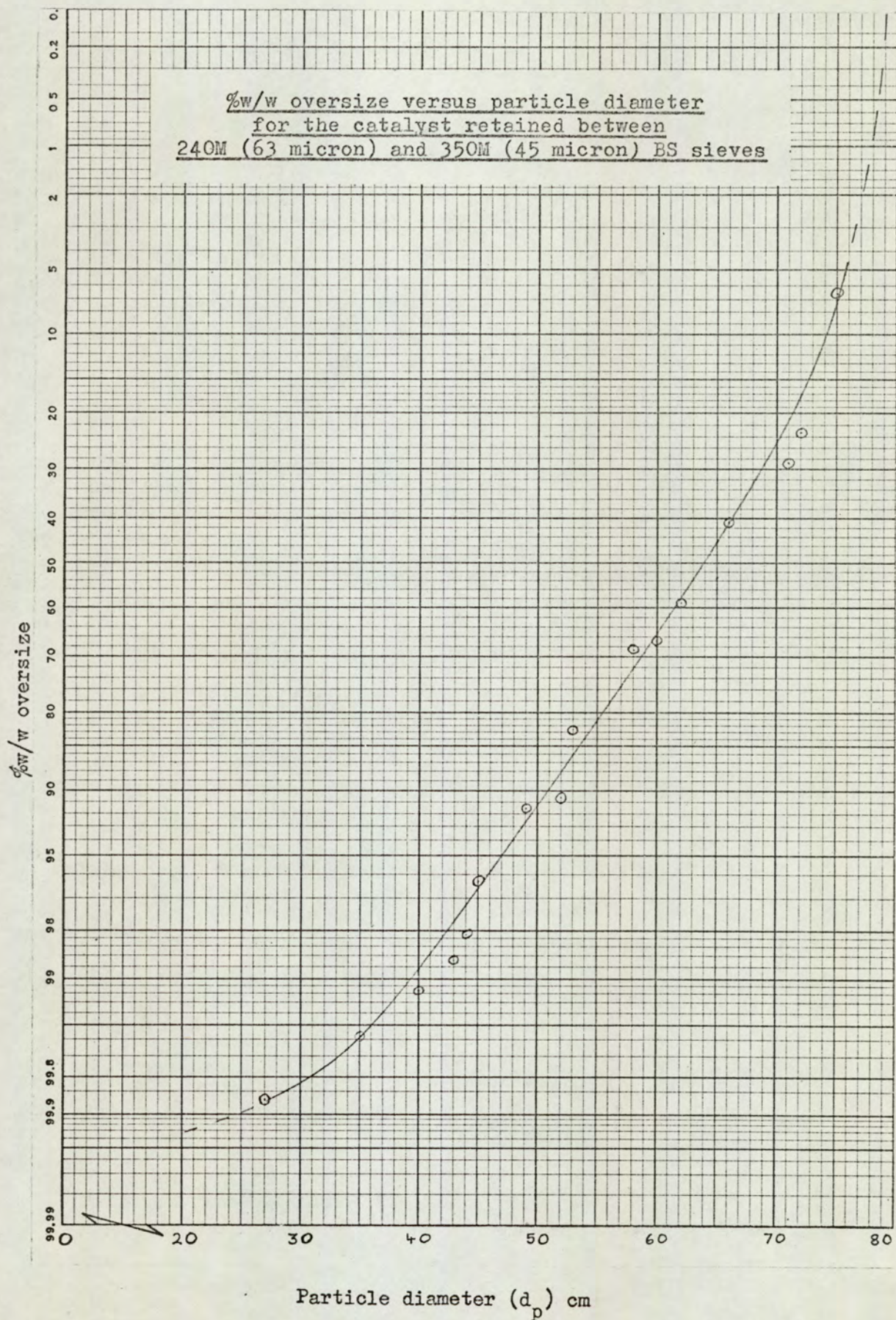
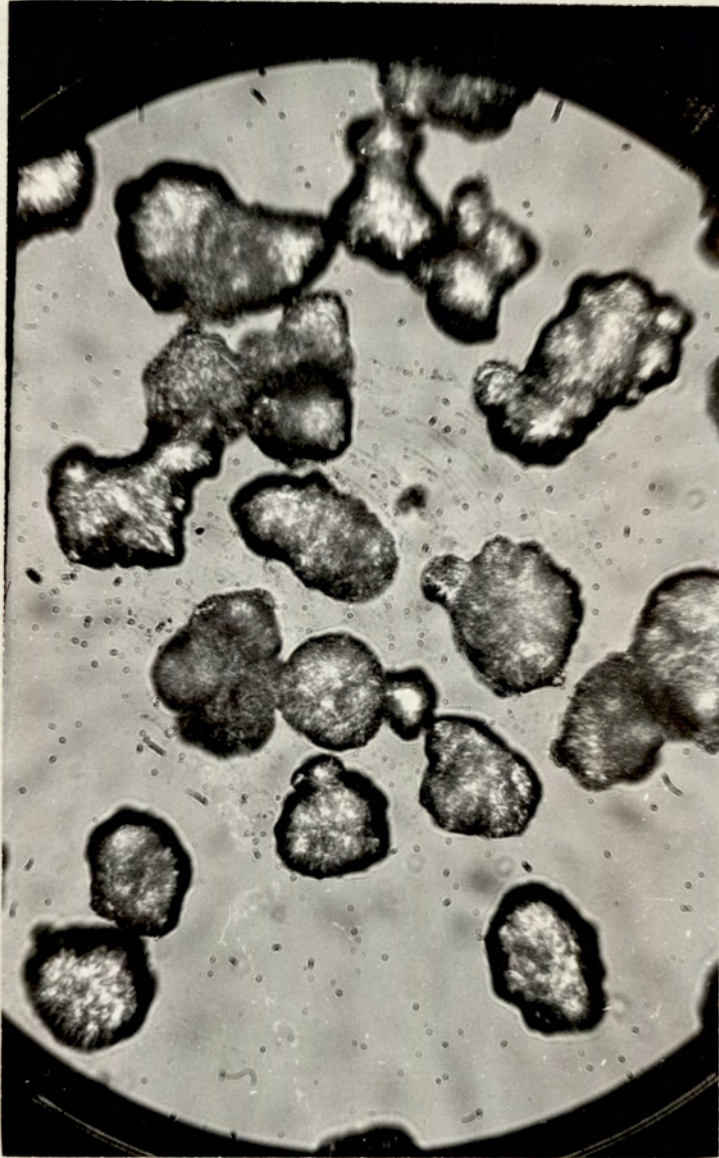


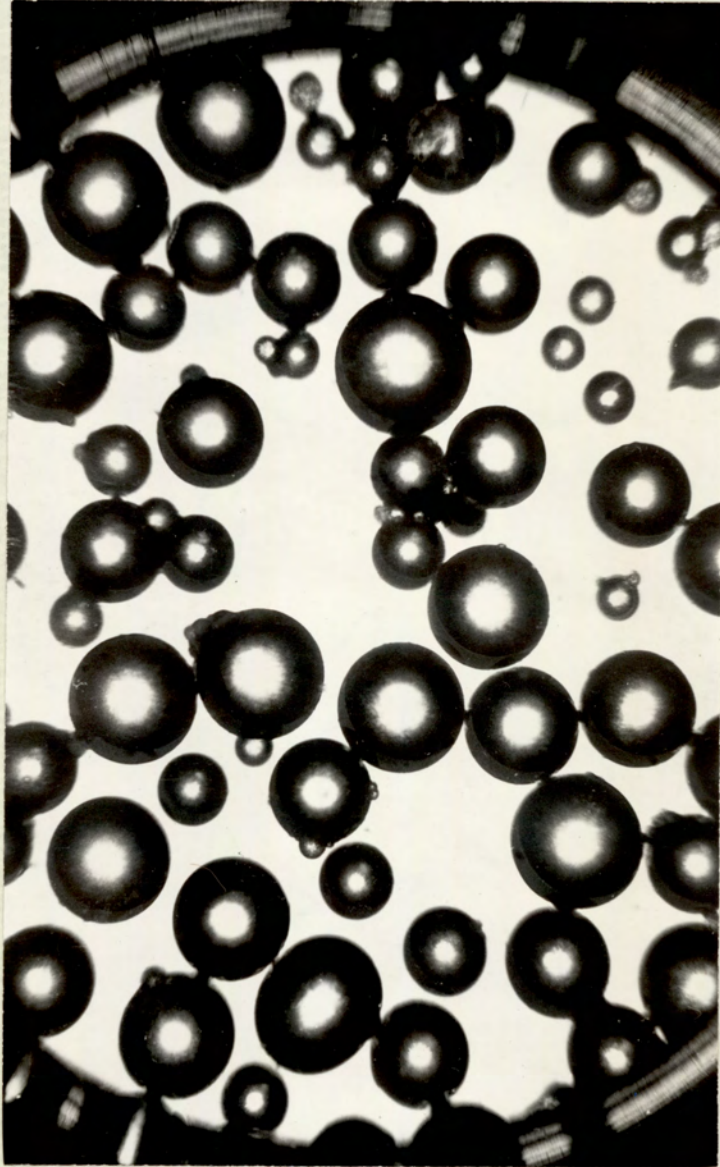
Fig. 7.3.2.(2).



Catalyst, nominally 45-63 micron diameter.

Magnified 300 times.

Fig. 7.3.3.(1).



Diakon, 125-250 micron diameter

Magnified 80 times

7.4. DENSITY DETERMINATION

7.4.1. Glass

The supplier⁽⁶⁵⁾ stated that all ballotini smaller than 3×10^3 micron diameter in the sieve graded sizes was supplied in lead glass only. To overcome the problem of measuring the density of very fine particles it was decided to use ballotini with a diameter of about 500 micron and take this value as the density for all sizes. The density of the ballotini thus found was 2.96g/cm^3 which was within 2% of the suppliers' figure. However, when this density value was used to determine the voidage at incipient fluidisation of a bed of particles with a size range 45 - 63 micron diameter, the voidage predicted was 0.58 which was clearly too large.

Now it had been noticed that when 250 - 300 micron diameter ballotini was fluidised with white spirit (while checking the Wiener equation), two different layers had formed in the bed, the top 10% being much whiter than the rest of the bed. Samples from the top and the bottom of the bed were taken and added to bromoform ($\rho_f = 2.84\text{g/cm}^3$). The sample from the top floated whilst that from the bottom sank, suggesting that a mixture of lead and soda glass had been supplied in this particular size range. Water fluidisation was therefore used to segregate the two types for all size ranges and the top layer discarded from any bed that settled into two layers.

The 45 - 63 micron diameter ballotini had not formed two layers and it had therefore been assumed that it was all lead glass, until the high calculated value for bed voidage suggested that, in fact, the ballotini was soda glass, which has a considerably lower density. This was confirmed with a flame test, the ballotini

remaining white and fusing together, whereas lead glass at the same temperature turned black and did not melt.

The discrepancies found between the catalogue and the actual product were such that it seemed better to attempt to measure the density of the fine ballotini directly, rather than measure the density of some larger diameter soda glass ballotini and assume that the glass composition would be the same for all sizes. The main practical difficulty was that even with a surfactant such as Nonidet P40, the water displacement method was unsatisfactory, as there were minute bubbles of air trapped between the submerged particles and there was always about 3% of the spheres floating on the surface.

It was considered that a better method would be to pour a known volume of bromoform into a glass vessel containing some of the ballotini. This, being soda glass, would of course float. If carbon tetrachloride ($\rho_f = 1.60\text{g/cm}^3$) was then added with a burette, the density at which the ballotini sank would be known, assuming bromoform and carbon tetrachloride form an ideal mixture. Unfortunately, though some of the spheres sank when the density of the liquid reached about 2.4g/cm^3 , many of them still floated and the liquid density had to be lowered to 2.1g/cm^3 before the majority of the spheres had sunk. About 5% were still floating on the surface and about another 10% were suspended in the liquid.

This was unsatisfactory so, after taking a photo-micrograph of a random sample of the ballotini (Fig. 7.4.1.(1), (p.158)), attention was again turned to the water method. This time the density bottle and its contents were heated until the water boiled, in an attempt to drive off all the entrapped air. On cooling, about 2% of the spheres still floated, so a sample of these was

removed and compared under a microscope with a sample from the ones that had sunk. It was noted that all the floating sample appeared as thin black rings with grey centres (Fig. 7.4.1.(2), (p.159)). The more dense phase sample, however, appeared as black circles with white centres, like the majority of the spheres in the photo-micrograph of the sample prior to the flotation (Fig.7.4.1.(1)). This suggested that the floating sample was, in fact, hollow spheres, and this was proved by the ease with which they could be crushed (Fig. 7.4.1.(3), (p.160)). Measurement with the microscope showed that in some cases the wall thickness was a mere 2 micron, accounting for the fact that some floated in water.

To reduce the problem of having hollow spheres of varying wall thickness, which meant having, in effect, a considerable density range, the ballotini was fluidised vigorously for 24 hours in an attempt to remove at least the very thin wall spheres. A random sample was then taken from the remainder and the density determined by the displacement of benzene ($\rho_f = 0.878\text{g/cm}^3$). In the benzene less than 1% floated and the average density was found to be 2.2g/cm^3 , which was taken as the ballotini density.

7.4.2. Catalyst

It was noted that the catalyst particles were porous and that therefore the particle density required was the value that would be obtained if all the pores could be plugged with a solid of the same density as air and a normal density determination in water then carried out. This density value was obtained by measuring the skeletal density of the particles by the water method, and then correcting this value by the pore volume per unit mass determined on a sample of the sieved catalyst⁽⁶⁷⁾.

$$\text{Skeletal density} = 2.18\text{g/cm}^3$$

$$\text{Pore volume} = 0.68\text{cm}^3/\text{g}$$

$$\text{Skeletal specific volume} = \frac{1}{2.18} = 0.46\text{cm}^3/\text{g}$$

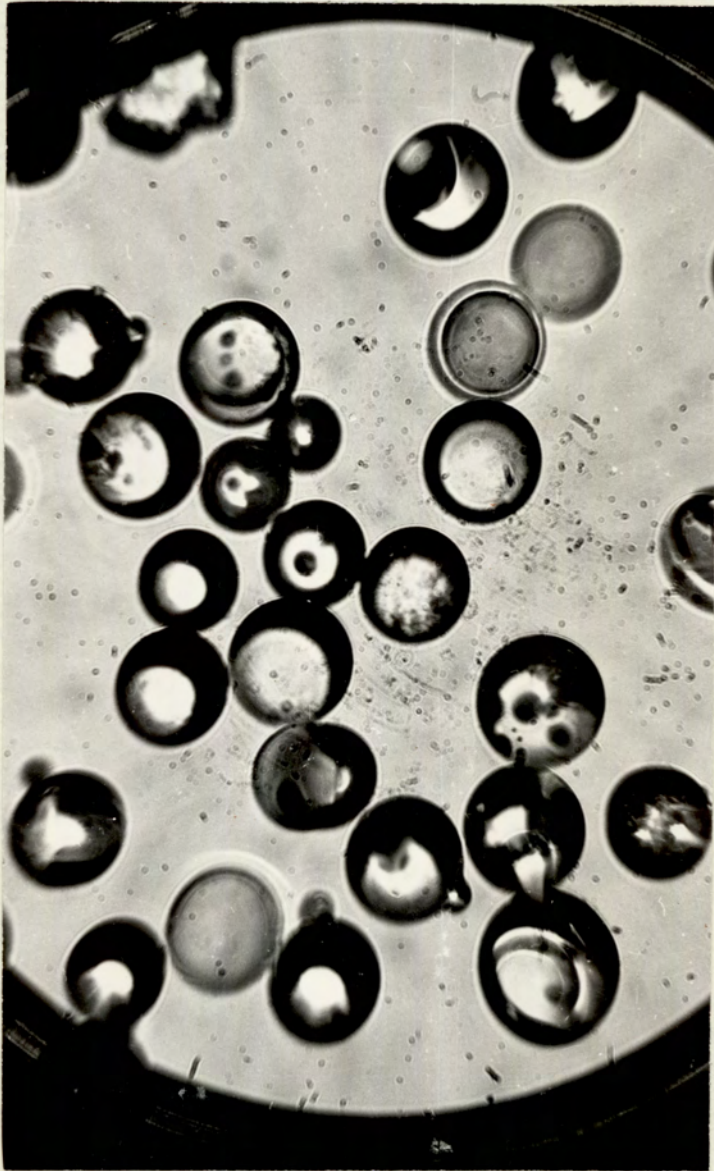
$$\text{Therefore total volume per gramme} = 0.46\text{cm}^3 + 0.68\text{cm}^3$$

$$\text{Therefore particle density} = \frac{1}{1.14} = 0.88\text{g/cm}^3$$

7.4.3. Diakon

The density of the diakon was determined using the water displacement method and found to be 1.17g/cm^3 , which agrees with the figure quoted by Davies and Richardson⁽¹⁰⁾.

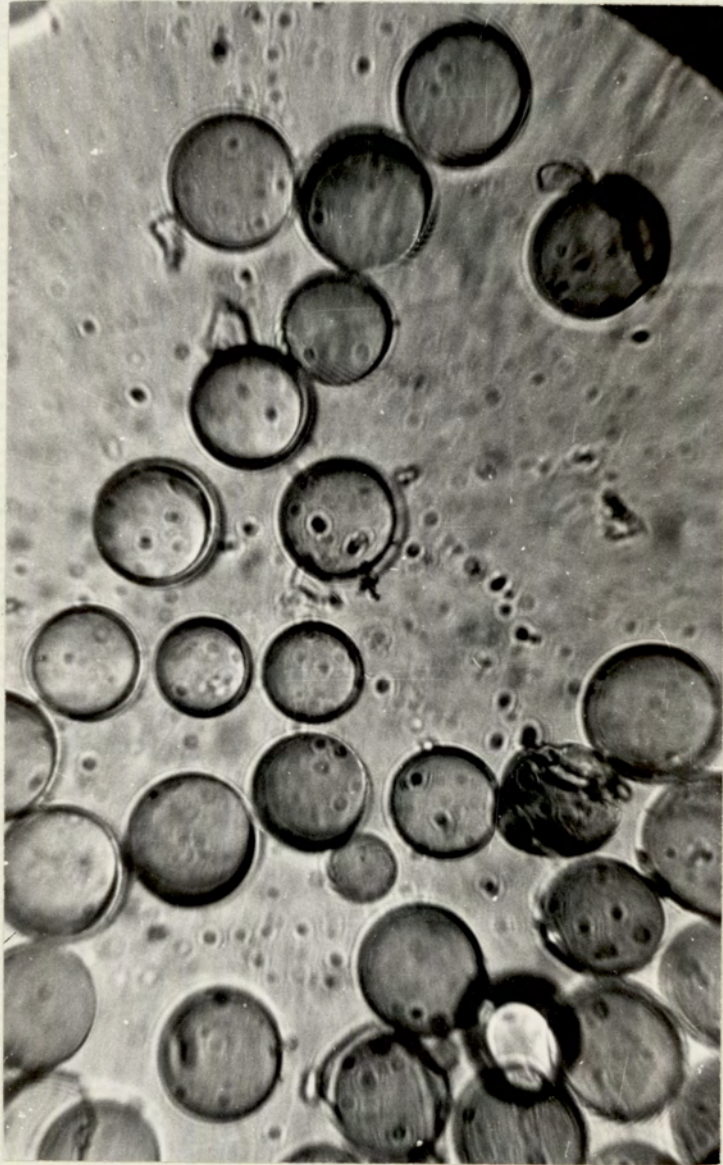
Fig. 7.4.1.(1).



Soda glass ballotini, 45-63 micron diameter: a
random sample before segregation by flotation

Magnified 300 times

Fig. 7.4.1.(2).



Soda glass ballotini, 45-63 micron diameter: a
sample of the particles less dense than water
Magnified 350 times

Fig. 7.4.1.(3).



Soda glass ballotini, 45-63 micron diameter: a
sample of the particles less dense than water,
crushed to show that they were hollow
Magnified 350 times

R E S U L T S

8.1. DETERMINATION OF THE INCIPIENT FLUIDISING VELOCITIES

The incipient fluidising velocity was determined for the following systems:

- i) 45-63 micron diameter soda glass ballotini - air;
- ii) 45-63 micron diameter soda glass ballotini - CO₂;
- iii) nominal 45-63 micron diameter catalyst - air;
- iv) nominal 45-63 micron diameter catalyst - CO₂;
- v) 125-250 micron diameter diakon - air.

The bed pressure drop (ΔP) was plotted against decreasing fluidising gas velocity for each system (Figs. 8.1.(1-3), (pp.163-165). In Section 1 it was stated that a fluidised bed is generally said to be at the point of incipient fluidisation when the bed pressure drop is just sufficient to support the weight of the particles comprising the bed. This critical point should correspond to an abrupt change of gradient in the pressure drop versus background gas velocity. However, for the systems being considered in this work, where the particles were small and of low density, there was no discontinuity and therefore the conventional constructional method was used to determine U_0 . This is the same procedure as adopted by Godard⁽³³⁾ and the pressure drop corresponding to U_0 is generally 2-3% less than the weight of the bed (Table 8.1.(1), (p.162).

The determination of the value of U_0 for the ballotini-air system was carried out twice, once with the probe present and once without it. No difference in the value of U_0 was noted, and therefore the value of U_0 for the other systems was determined without

the probe being present.

Another method sometimes used to determine the value of U_0 for gas fluidised beds is to plot bed height versus gas velocity and take as the value for U_0 the minimum velocity at which the bed height is a constant. This method could not be employed for the present work because the change in the rate of bed expansion with gas velocity was significant at velocities well in excess of U_0 .

Table 8.1.(1).

Pressure Drop Data at Incipient Fluidisation

System	1	2	3	4	5
	U_0 Determined Graphically cm/s	Grid Pressure Drop at U_0 cm H ₂ O	Bed Pressure Drop at U_0 cm H ₂ O	Bed Weight cm H ₂ O	% Difference between Columns 3 & 4
Air- ballotini	0.360	5.5	34.5	35.4	2.7
Air- catalyst	0.235	3.5	14.9	15.2	2.5
CO ₂ - ballotini	0.410	5.6	34.5	35.4	1.9
CO ₂ - catalyst	0.292	4.0	14.9	15.2	2.5
Air- diakon	2.570	31.5	20.9	20.9	0

Fig. 8.1.(1).

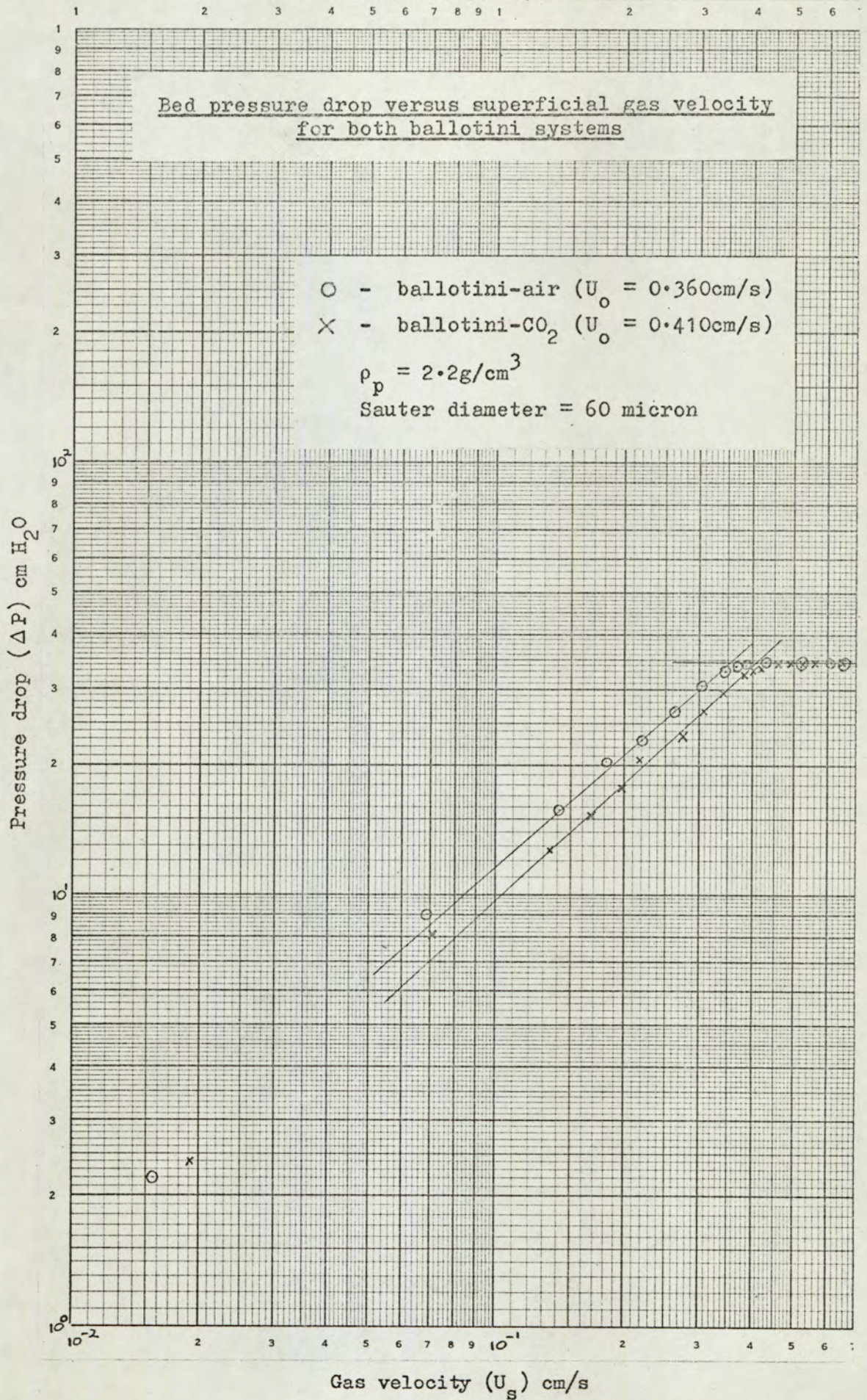


Fig. 8.1.(2).

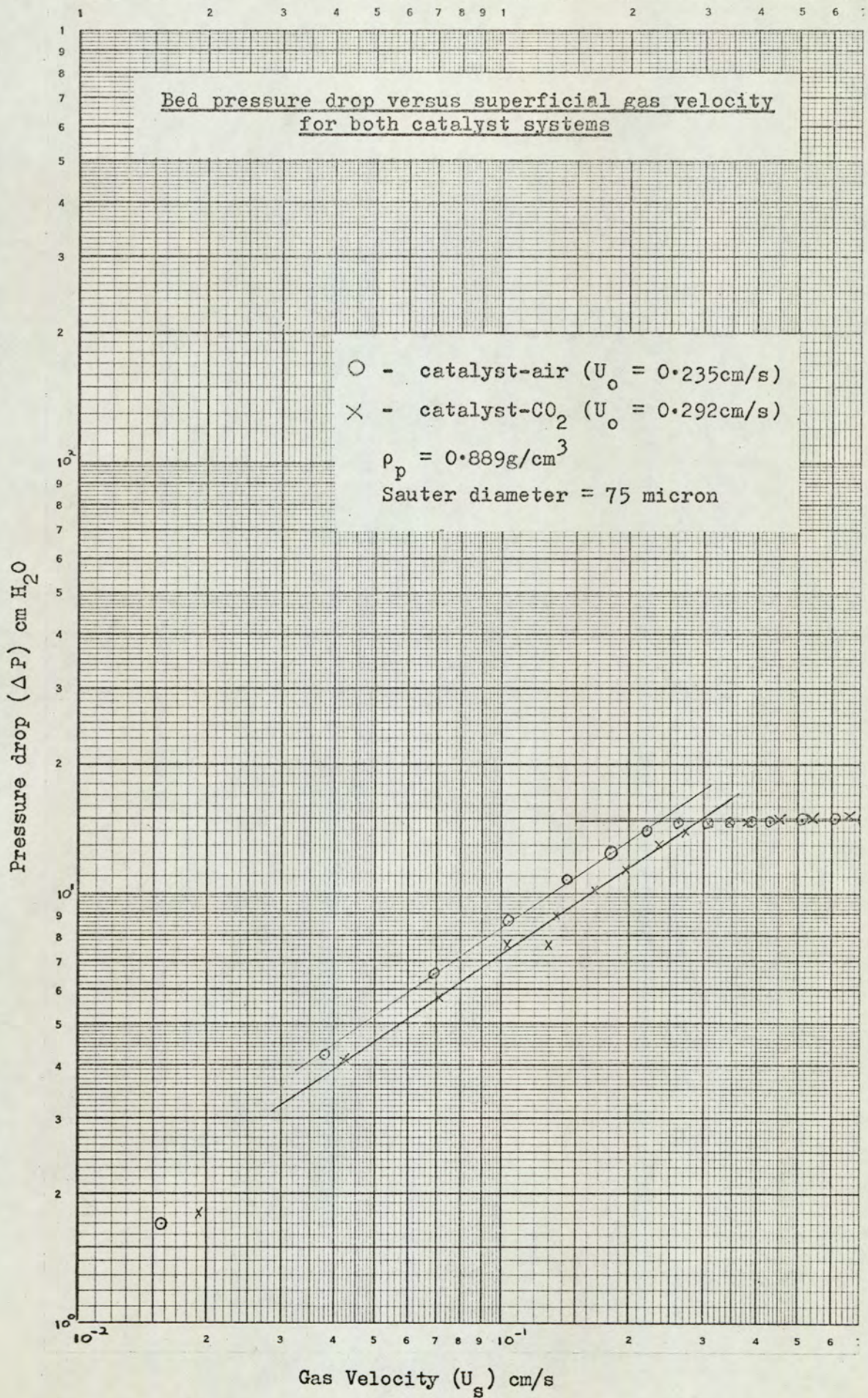
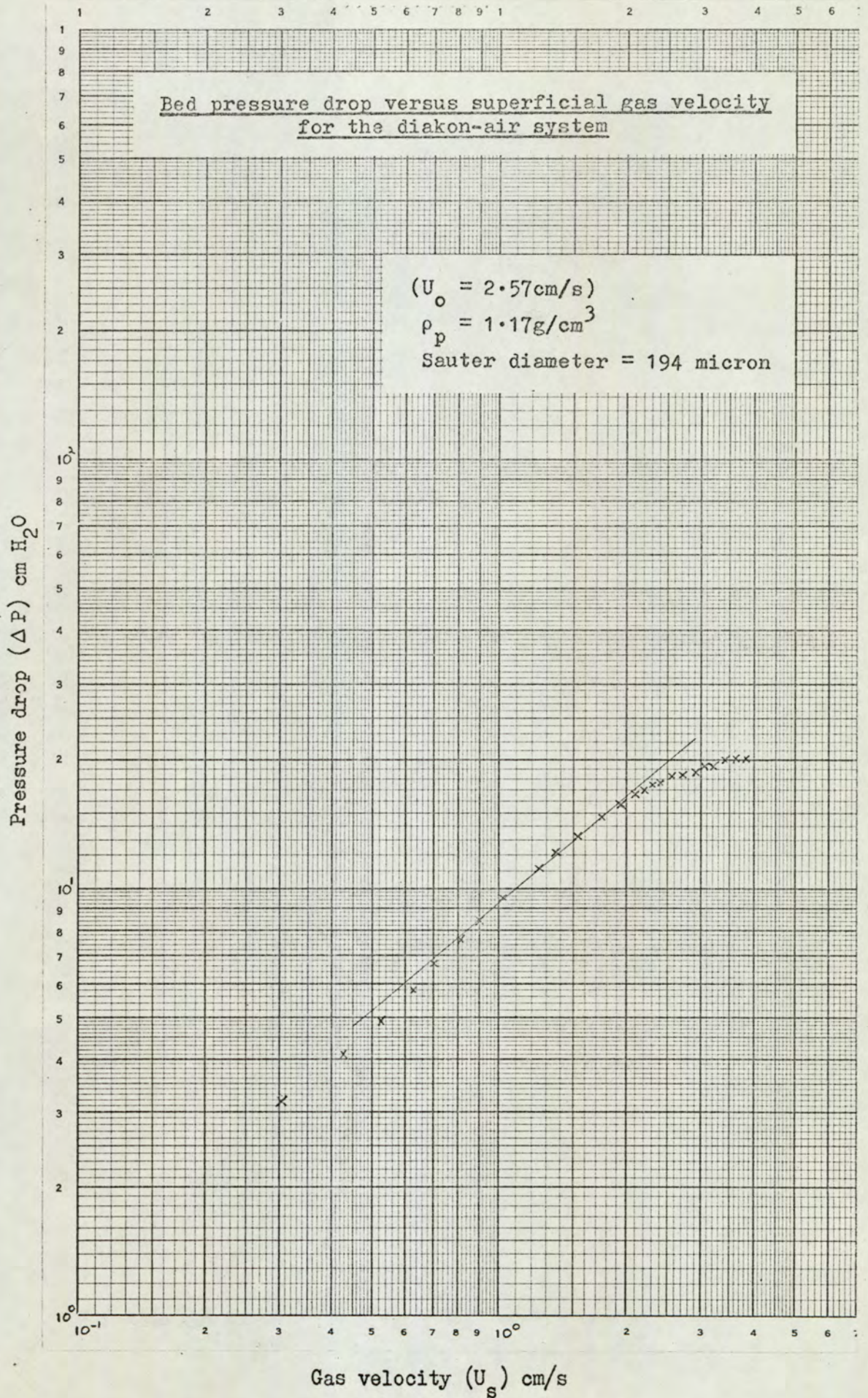


Fig. 8.1.(3).



8.2. BED EXPANSION

8.2.1. Bed Expansion at Gas Velocities in the Range $U_o < U_s < U_{mb}$

Fig. 8.2.1.(1), (p.168) is a plot of bed height versus gas velocity for the air-catalyst system, and was obtained both by increasing and decreasing the background gas velocity. It can be seen that the bed expanded uniformly with change in gas velocity at velocities well above U_o , and this was also noted with the other systems investigated. Fig. 8.2.1.(2), (p.169) is a log-log plot of voidage (e_i) versus gas velocity (U_s) for the air-catalyst system. It can be seen that the relationship between e_i and U_s can be expressed in the form

$$U_s = A_2 e_i^{n_2} \quad - \quad 2.3.2.(4)$$

for $U_o < U_s < U_{mb}$, and determining the values of A_2 and n_2 for the present work gave

$$U_s = 6.6e_i^{4.5} \quad - \quad 8.2.1.(1)$$

The results of Davies and Richardson⁽¹⁰⁾ for a similar system are included in Fig. 8.2.1.(2). for comparison.

8.2.2. Bed Expansion at Gas Velocities in the Range $U_s > U_{mb}$

When the ballotini and catalyst systems were fluidised at velocities in excess of U_{mb} , it was found that the bed height oscillated between two limits, represented by lines A and B on Fig. 8.2.1.(1).

It was also noted that:

- i) these oscillations had a period of between 10 and 30 seconds at velocities close to U_{mb} ;
- ii) the decrease in bed height from A to B was virtually

- instantaneous;
- iii) when the maximum height had been reached the bed degassed by bubbles apparently forming instantaneously throughout the bed;
 - iv) as the gas velocity approached $2U_{mb}$ the oscillations had become negligible, the bed behaving as a normal bubbling gas fluidised bed;
 - v) the collapsed bed height (line B) was always greater than the height at U_0 .

Fig. 8.2.1.(1).

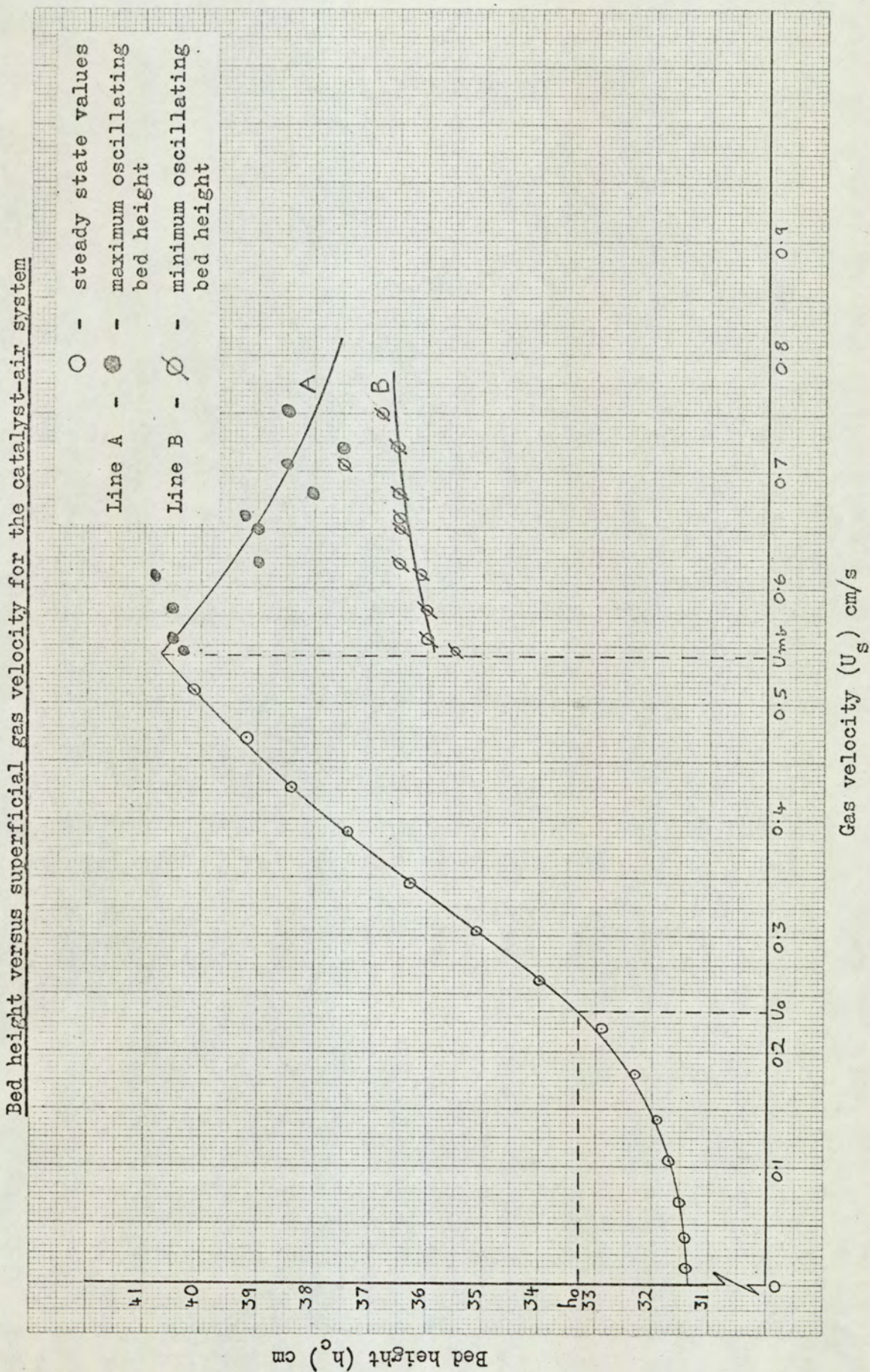
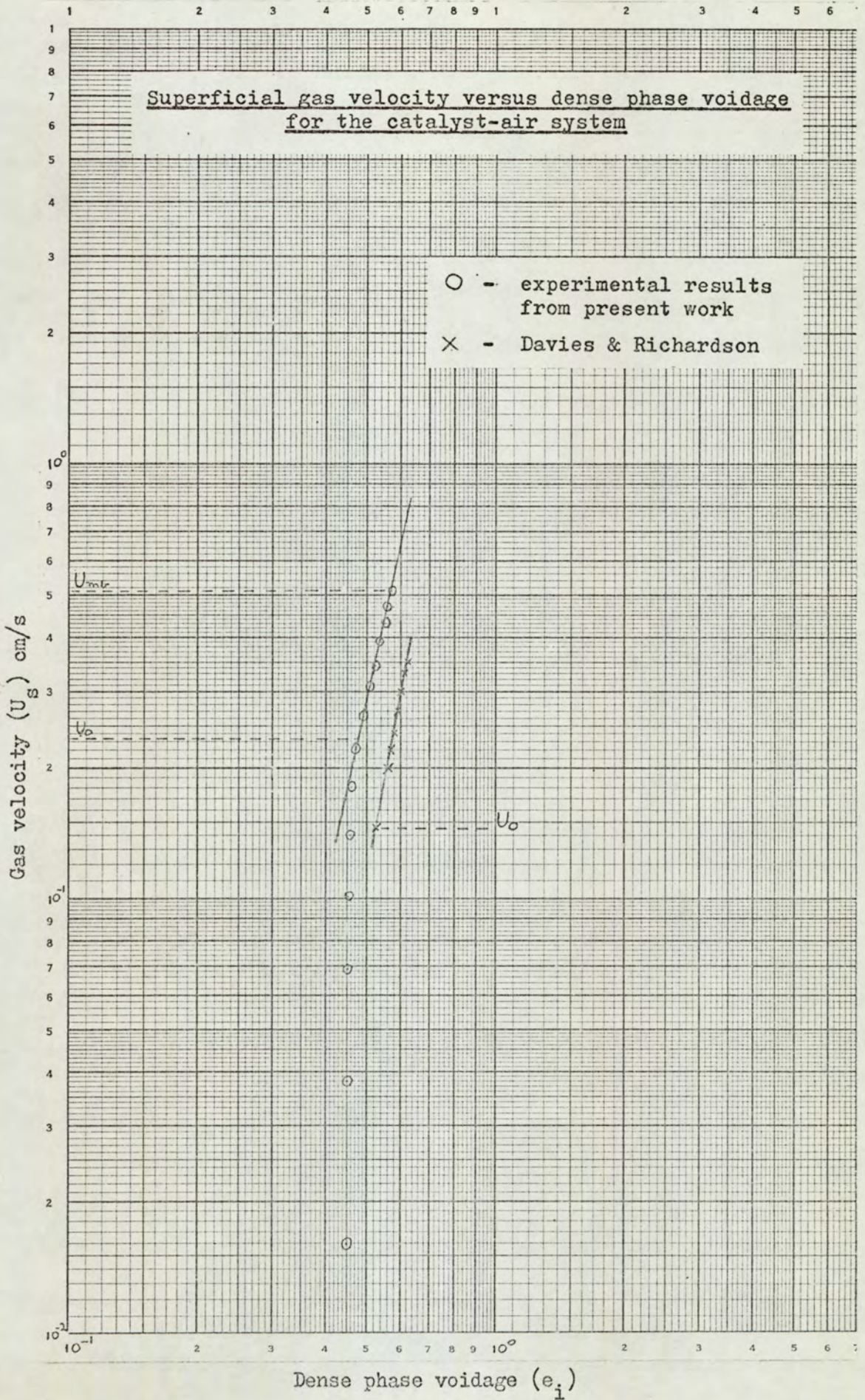


Fig. 8.2.1.(2).



8.3. INJECTION EFFECT

An injection effect was suspected from previous work carried out during calibration of the apparatus (Section 6.9.) and from the literature^(14, 27). Its existence was confirmed by the results of the initial investigations reported below. A known volume of air was injected into an air-ballotini bed and fluidised at a known background air rate. The volume of the bubble formed was measured with the probe 10cm above the injector orifice. The experiment was repeated for different background air rates and injected volumes. The results were plotted as shown in Fig. 8.3.(1), (p.172), where the parameter is the volume of air injected. On this graph, line A shows the locus of the intersections of the points when the injected gas volume equals the measured bubble volume. This indicates that there are two stable bubble sizes at any given background gas rate in excess of some critical value, instead of the one stable size expected.

However, if it is assumed that about 10% of the injected volume is lost on injection (as suggested in Section 6.9.), then line A can be replaced by line B in Fig. 8.3.(1). Now although it appears that line B may be asymptotic to U_0 , as expected, it nevertheless predicts that stable bubbles in the range $1 - 5\text{cm}^3$ should exist in an unfluidised bed, suggesting that the injection correction was in error over that bubble size range. Therefore, further investigation of the injection effect was made by injecting a known volume of air into an air-ballotini system, fluidised at a known background air rate. The volume of the bubble formed was recorded at increments of 1cm height above the injector orifice between the limits of 2cm and 10cm. No readings were taken closer than 2cm to the injector as it was considered that the bubbles

would not have formed their stable shape and therefore the readings could be in error.

The run was then repeated for two other background air rates and then the complete experiment was repeated for several different volumes of injected gas (see the Appendix Section A3). The results for one background air rate only are plotted in Fig. 8.3.(2), (p.173), the results for the two other air rates being omitted for clarity. Each point represents the average of three bubble injections.

From Fig. 8.3.(2) it can be seen that:

- i) for injected volumes greater than 3cm^3 the initial bubble volume is smaller than the injected volume and for injected volumes less than 2cm^3 the initial bubble volume is greater than the injected volume;
- ii) after approximately 7cm above the injector orifice, the gradients of the lines appear to stabilise.

It would therefore appear that the true plot of meta-stable bubble volume versus background air rate (Fig. 8.3.(1)) is of the form indicated qualitatively by line C, where an allowance has been made for injected volumes less than 2cm^3 initially growing and for injected volumes greater than 3cm^3 initially shrinking.

Thus, it was concluded that because of these injection effects it was not possible to accurately predict the bubble volume formed from a known volume of injected gas, and that a different procedure was required for accurate bubble growth investigation.

Fig. 8.3.(1).

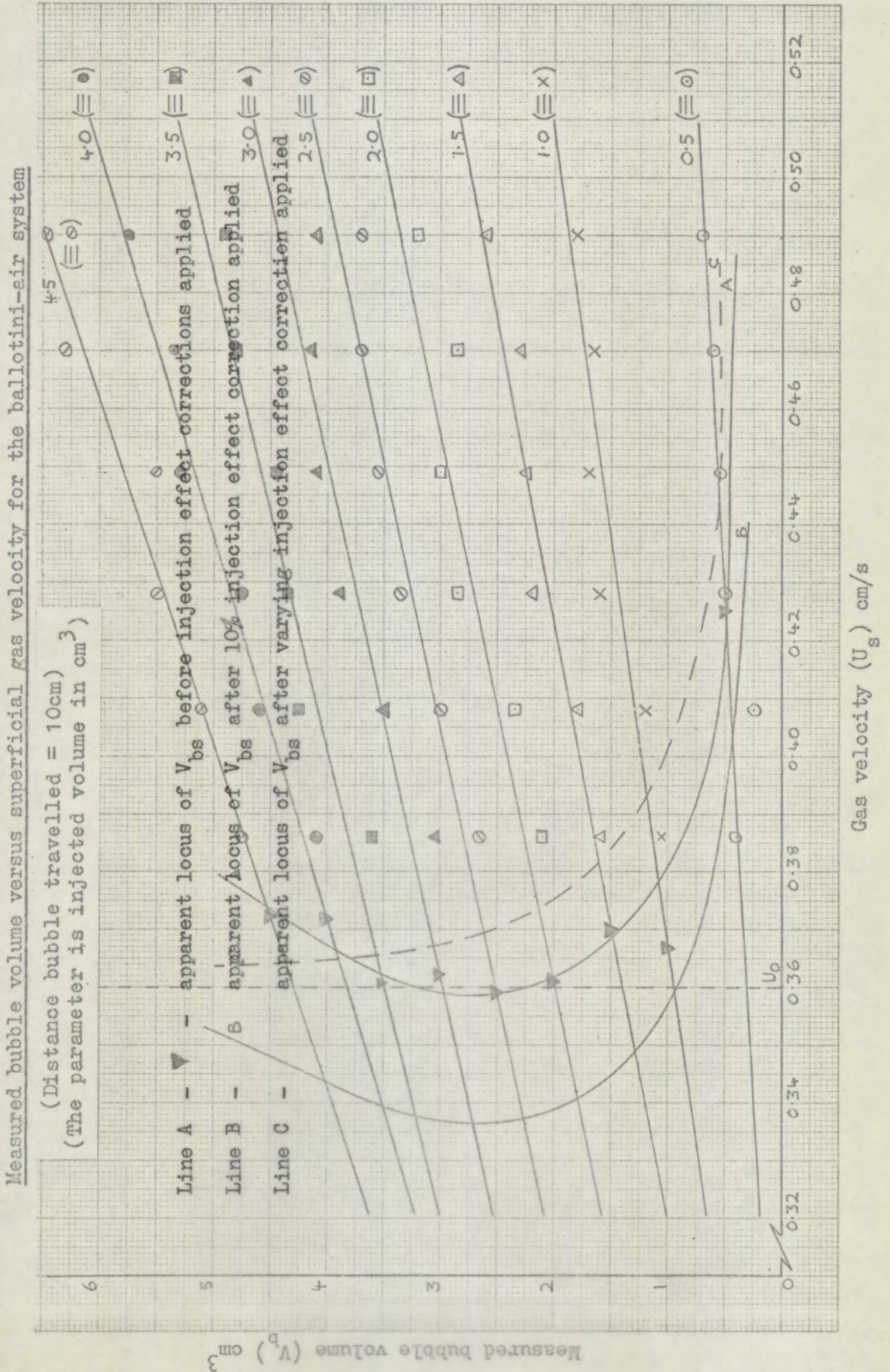
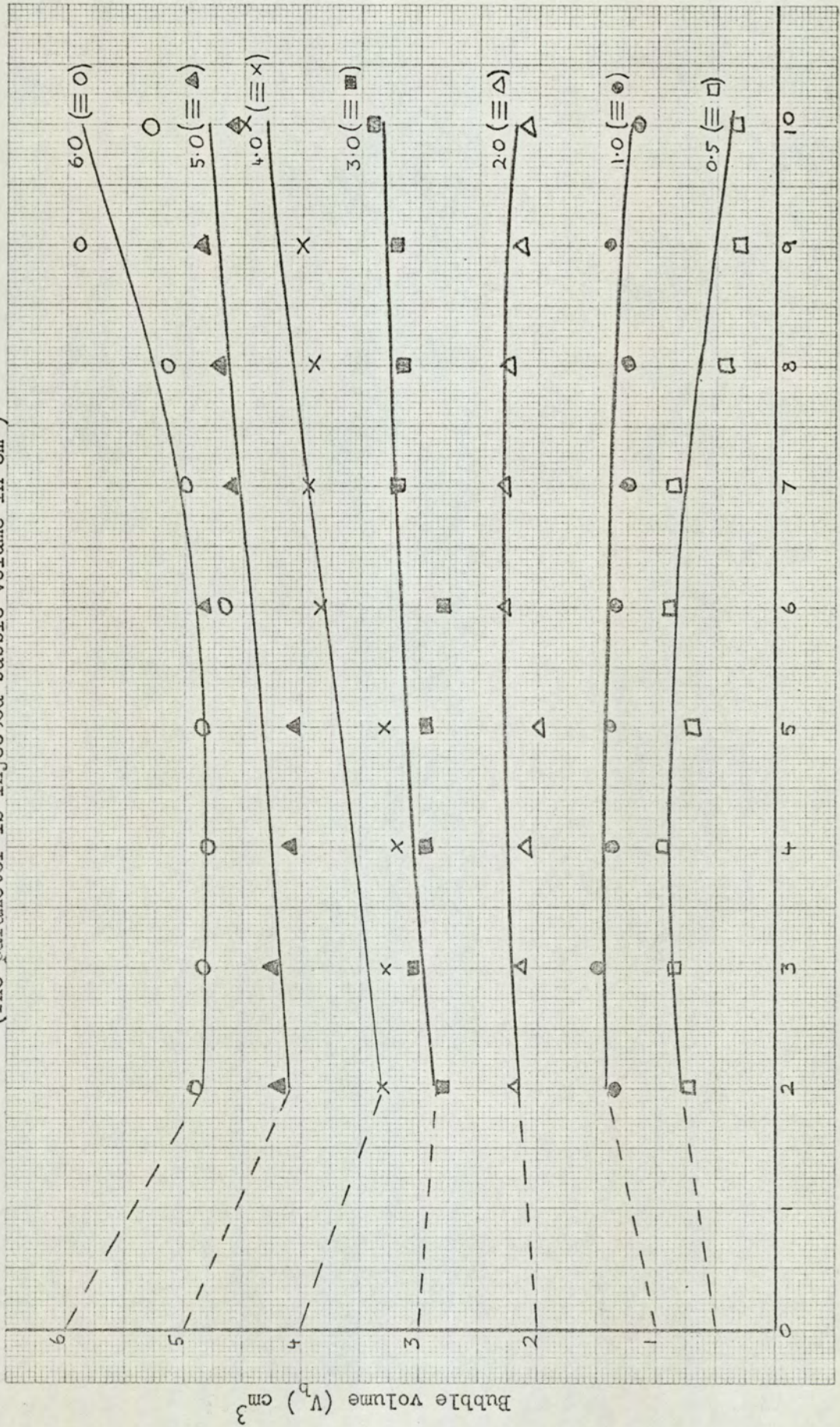


Fig. 8.3.(2).

Measured bubble volume versus distance bubble travelled for the ballotini-air system ($U_s = 0.386 \text{ cm/s}$)

(The parameter is injected bubble volume in cm^3)



Distance bubble travelled (h_s)

8.4. BUBBLE STABILITY

8.4.1. Procedure

The results of the preliminary investigation into the injection effect suggested that bubble volumes must be recorded at least 7cm above the point of injection. To obtain data on bubble stability it was decided to record bubble volumes at distances of 8, 11, 15 and 18cm above the injection point. From Section 6.12.2., it has been shown that there must be at least 6cm of bed above the plates and therefore the height of the bed was always greater than 24cm and normally about 31cm. The same systems as were investigated in the incipient fluidising velocity work (Section 8.1.) were studied at various background gas rates.

The bed was fluidised at a preset background gas rate, the probe placed in the bed with the plates 18cm above the injector orifice and the capacitance value of the dense phase noted. Then a fixed volume of gas was injected several times, a 30 second interval being left between each injection to reduce the likelihood of bed channelling forming and affecting succeeding bubbles (as was noted by Godard and Richardson⁽³⁴⁾). The volume of the bubble formed by each injection was recorded as a peak height by the UV oscillograph. This process was then repeated with different injected gas volumes. This procedure was repeated at the other injector to plate distances, and then the complete procedure was repeated at different values of background gas rates.

8.4.2. Results

An example of a set of results obtained at one background gas rate by the procedure described above is shown in Fig. 8.4.2.(1), (p.177), each point plotted being the average of three recordings.

Similar graphs were obtained for each background gas rate and they show that the smaller bubbles decrease in size and the larger ones increase. The bubble volumes cannot be read directly from the graphs but may be obtained by using Fig. 6.13.4.(3), (p.132). The complete set of results is tabulated in the Appendix, Section A4.

For each background gas rate, the minimum recorded peak height equivalent to a bubble volume that will grow, and the maximum recorded peak height equivalent to a bubble volume that will shrink, were both noted. These results were converted to bubble volumes and plotted (lines A and B respectively), versus the background gas rate, (Figs. 8.4.2.(2-6), (pp.178-182)). The increments between the injected volumes were not infinitely small so it was necessary to interpolate between lines A and B in order to obtain the plot of meta-stable bubble volume (V_{bs}) versus the gas velocity ratio U_s/U_o .

The interpolation procedure was to assume that the meta-stable bubble volume was the average volume (of lines A and B) for given values of the background gas rate, and these interpolated results are shown in Figs. 8.4.2.(7 and 8), (pp.183-184) for the ballotini and catalyst systems respectively. (The ballotini results have been repeated on Fig. 8.4.2.(8) for comparison.) The points superimposed on the above graphs are the values of V_{bs} determined from equation 8.6.(2) when $dV_b/dh_g = 0$.

The results of the diakon-air system have not been included with the ballotini and catalyst systems because great difficulty was experienced with this system. As can be seen from Fig. 8.4.2.(6), (p.182) the meta-stable bubble volume phenomenon appears to exist for the diakon-air system but the tendency of the particles to agglomerate (presumably due to static) and the poor sensitivity

(due to the low dense phase capacitance of approximately 0.295pF)
combined to make it impossible to obtain accurate results.

Fig. 8.4.2.(1).

Peak height versus distance bubble travelled for the ballotini-air system ($U_s = 0.449 \text{ cm/s}$)
(The parameter is gas volume injected in cm^3)

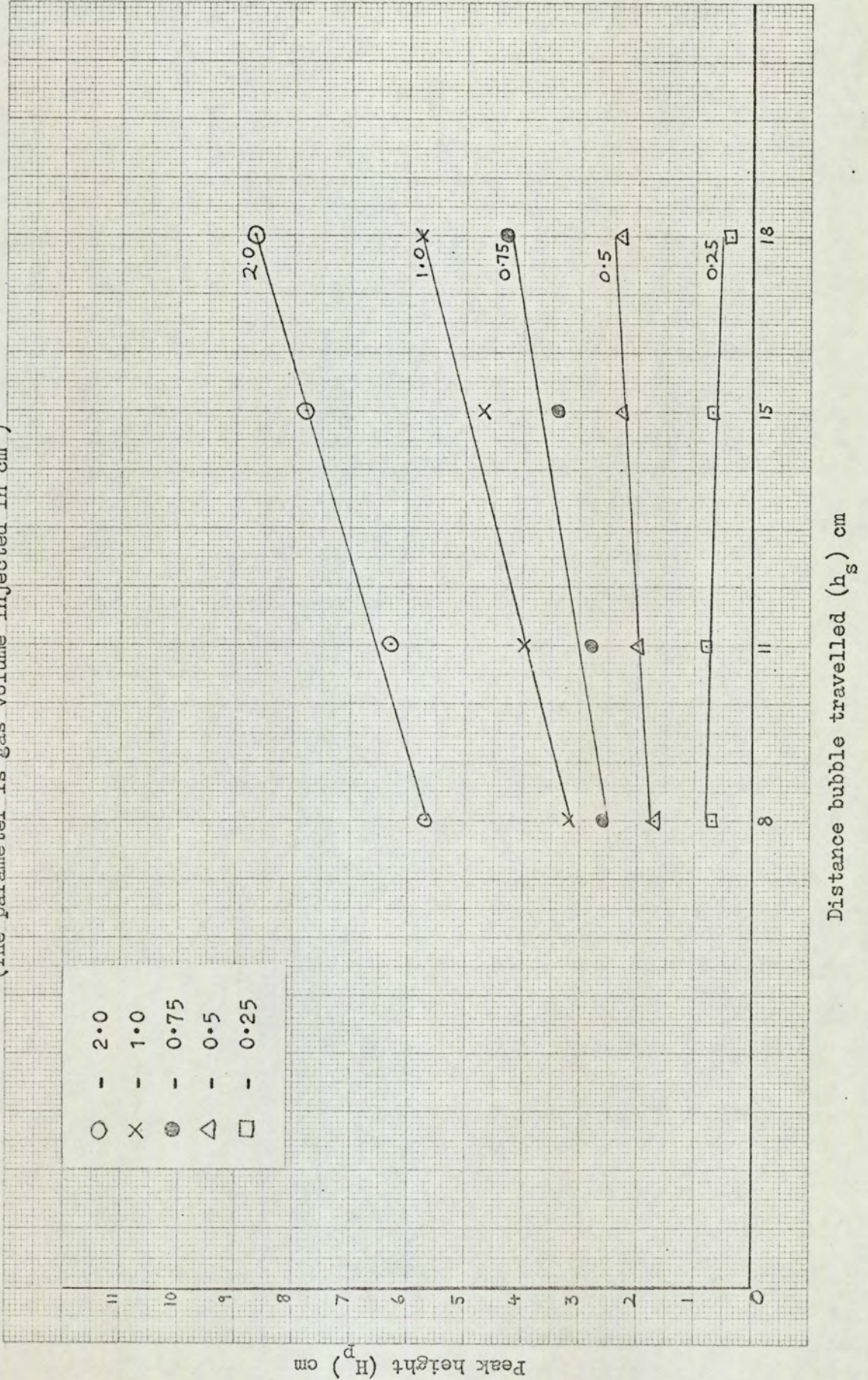


Fig. 8.4.2.(2).

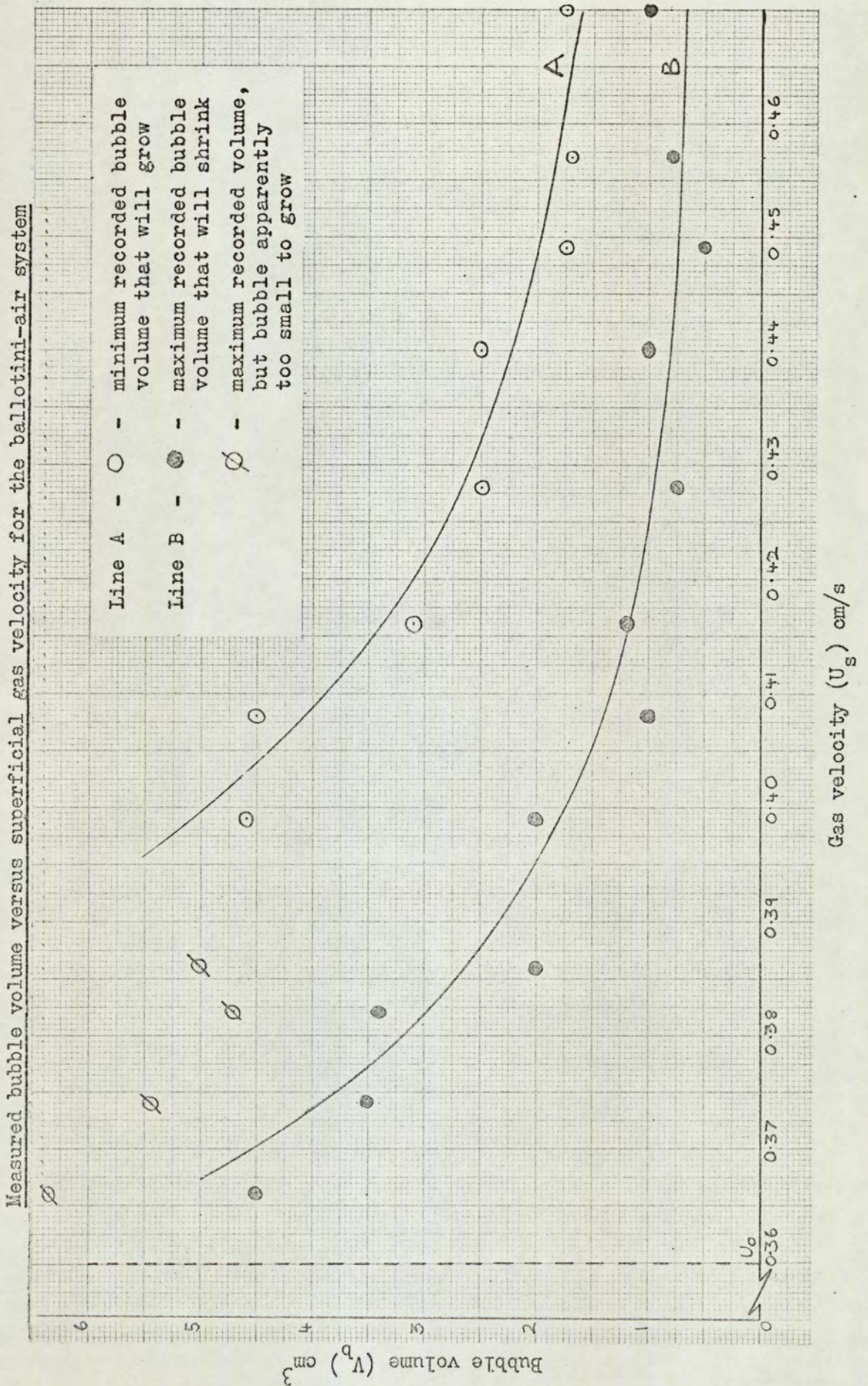


Fig. 8.4.2.(3).

Measured bubble volume versus superficial gas velocity for the ballotini-CO₂ system

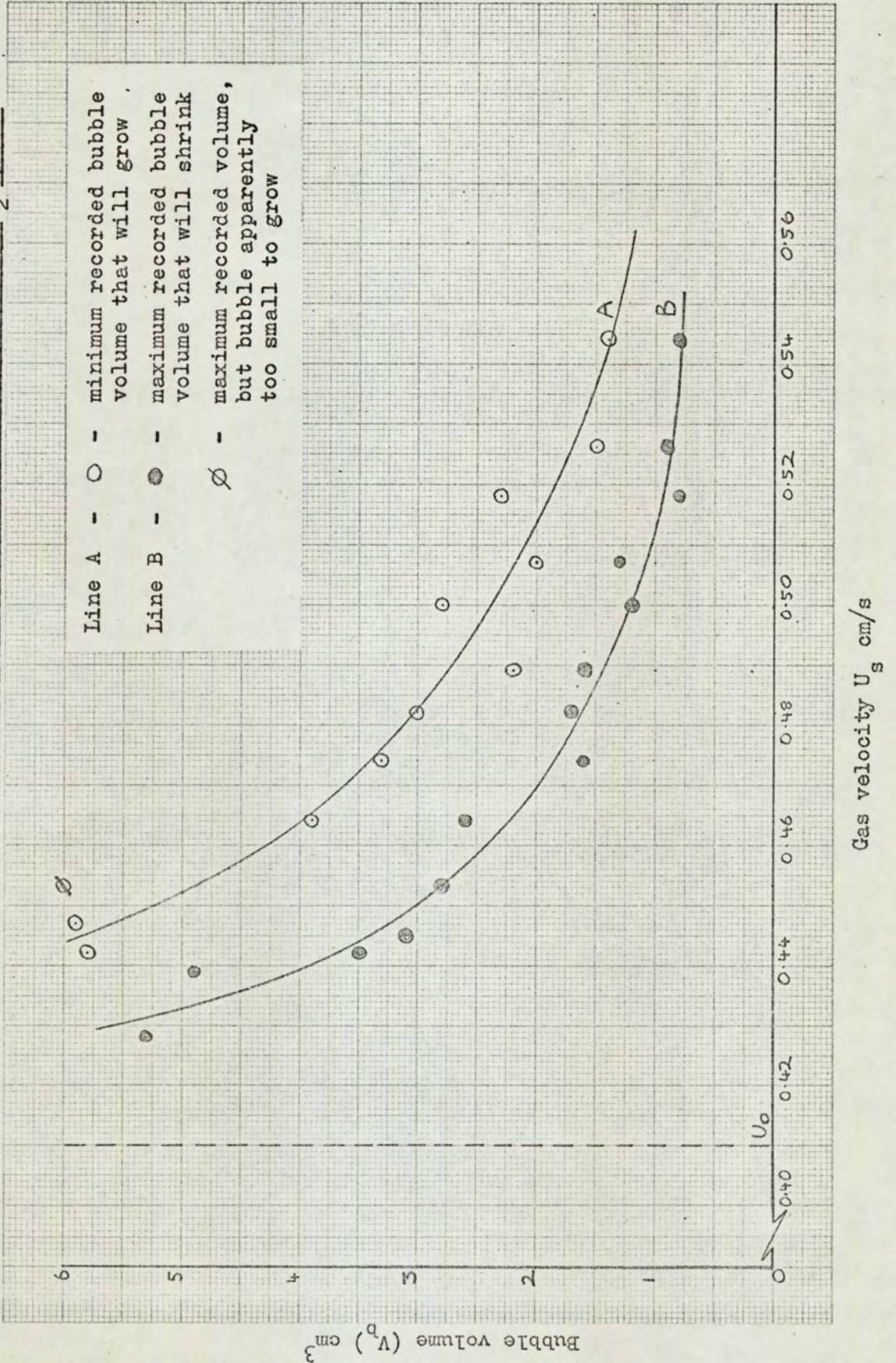


Fig. 8.4.2.(4).

Measured bubble volume versus superficial gas velocity for the catalyst-air system

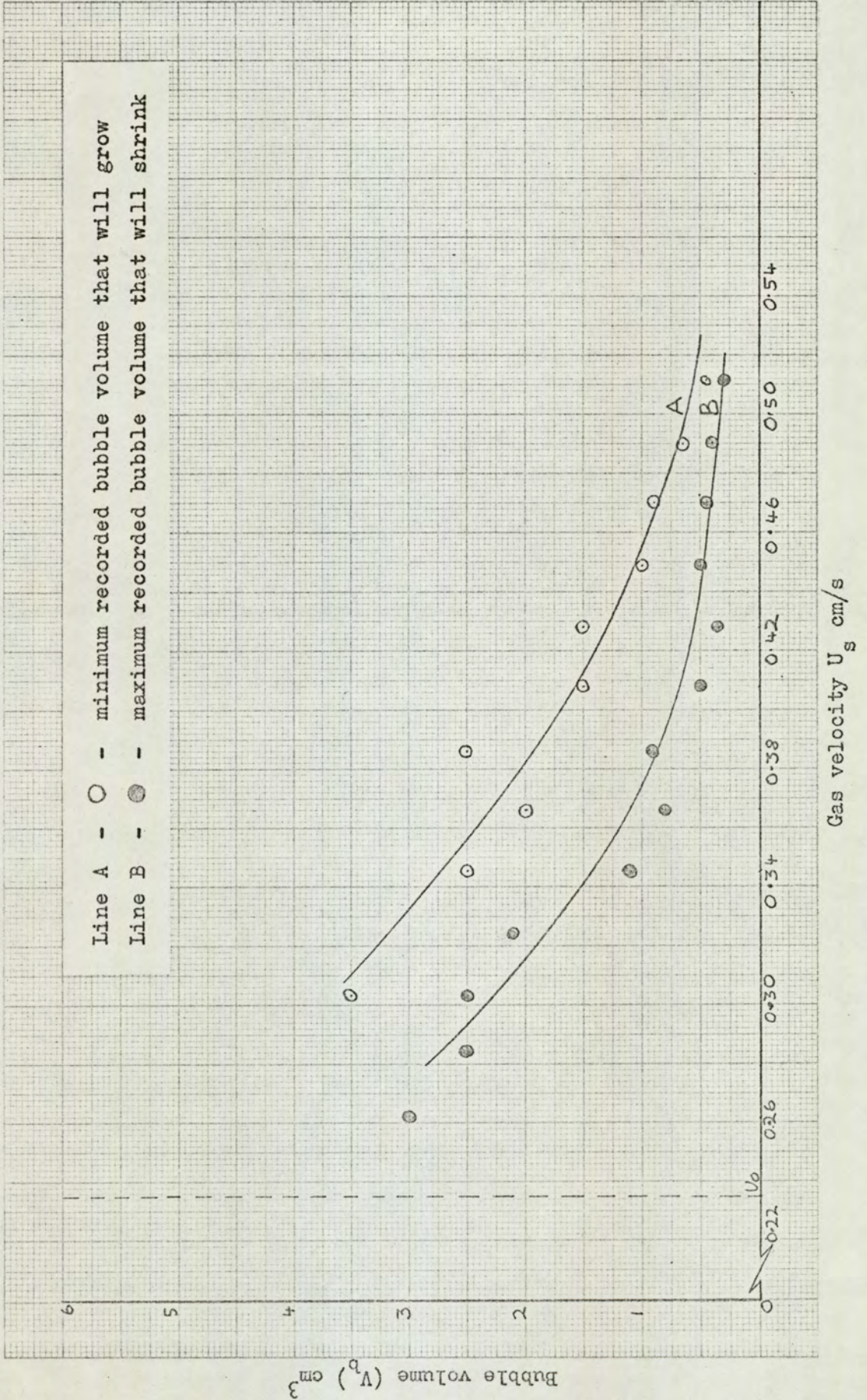


Fig. 8.4.2.(5).

Measured bubble volume versus superficial gas velocity for the catalyst-CO₂ system

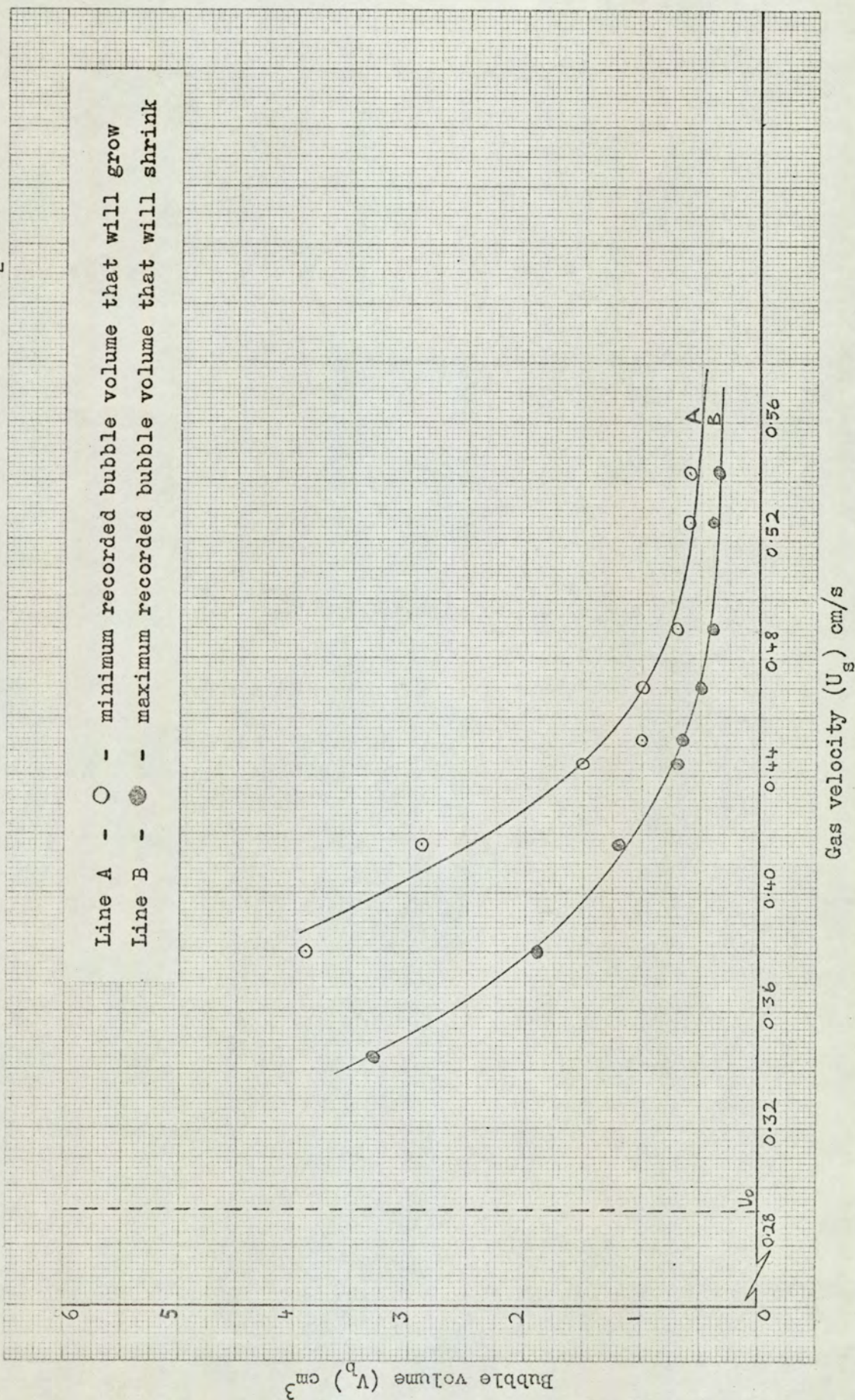


Fig. 8.4.2. (6).

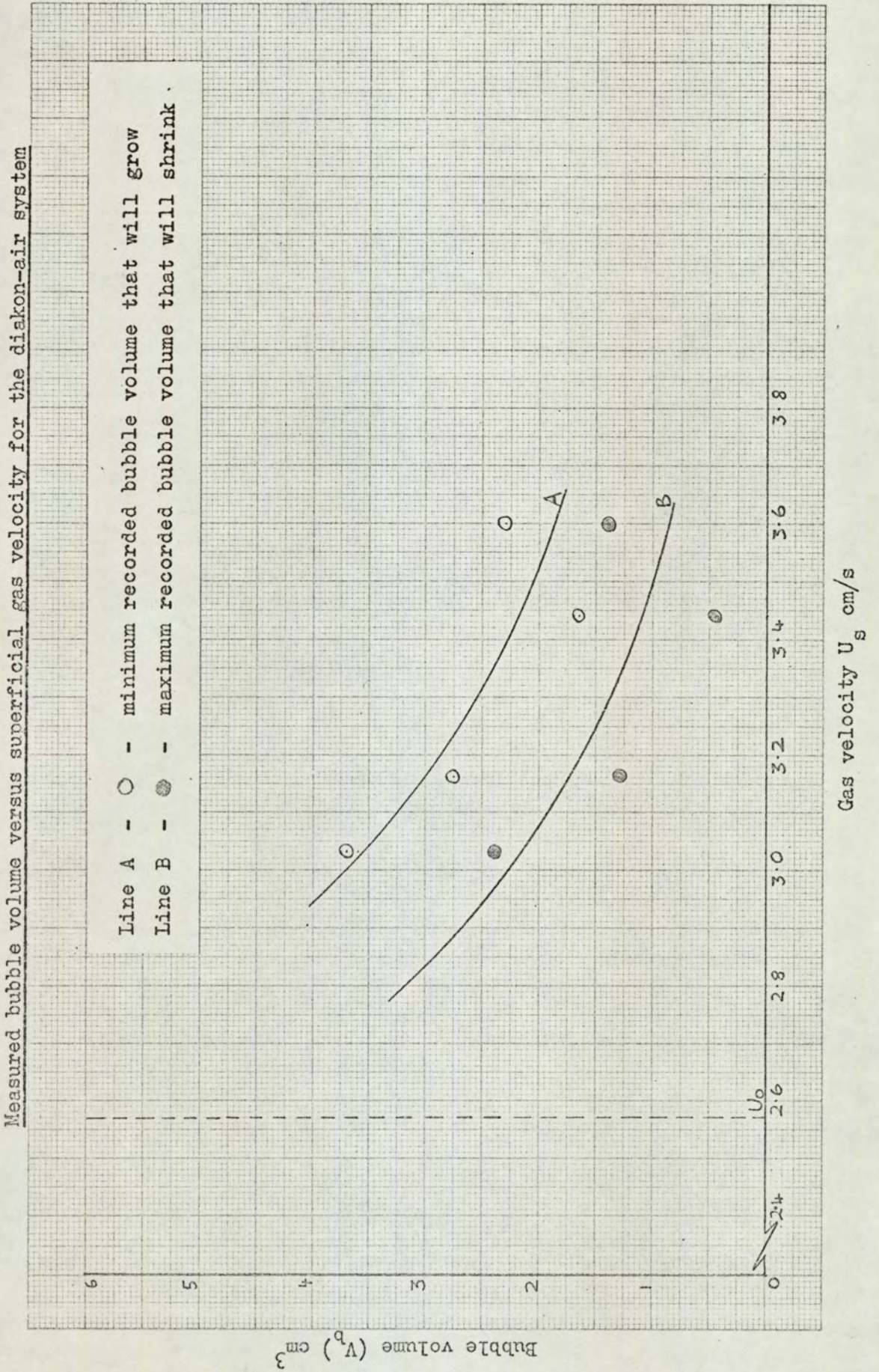


Fig. 8.4.2.(7).

Meta-stable bubble volume versus the gas velocity ratio U_s/U_0 for both ballotini systems

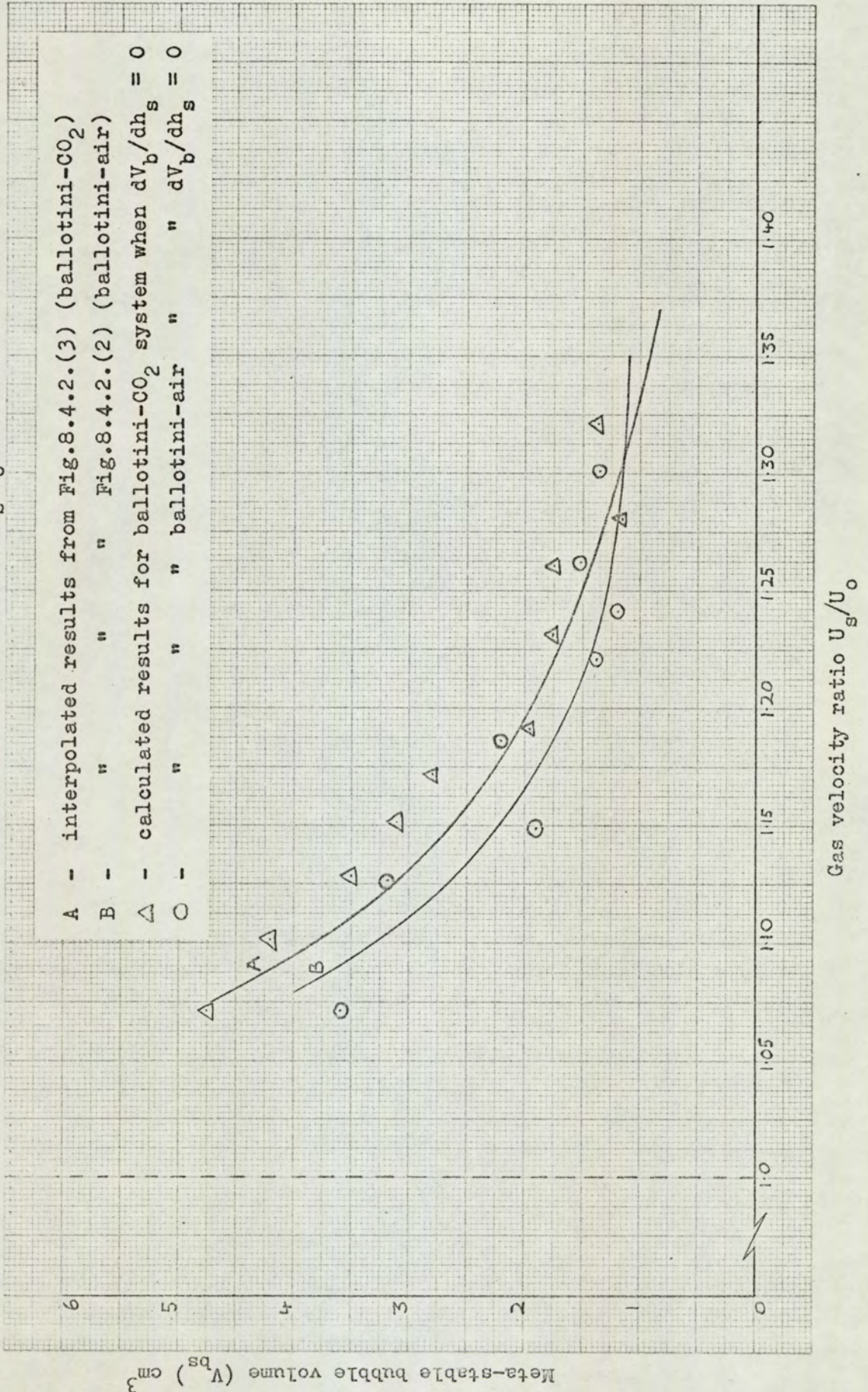
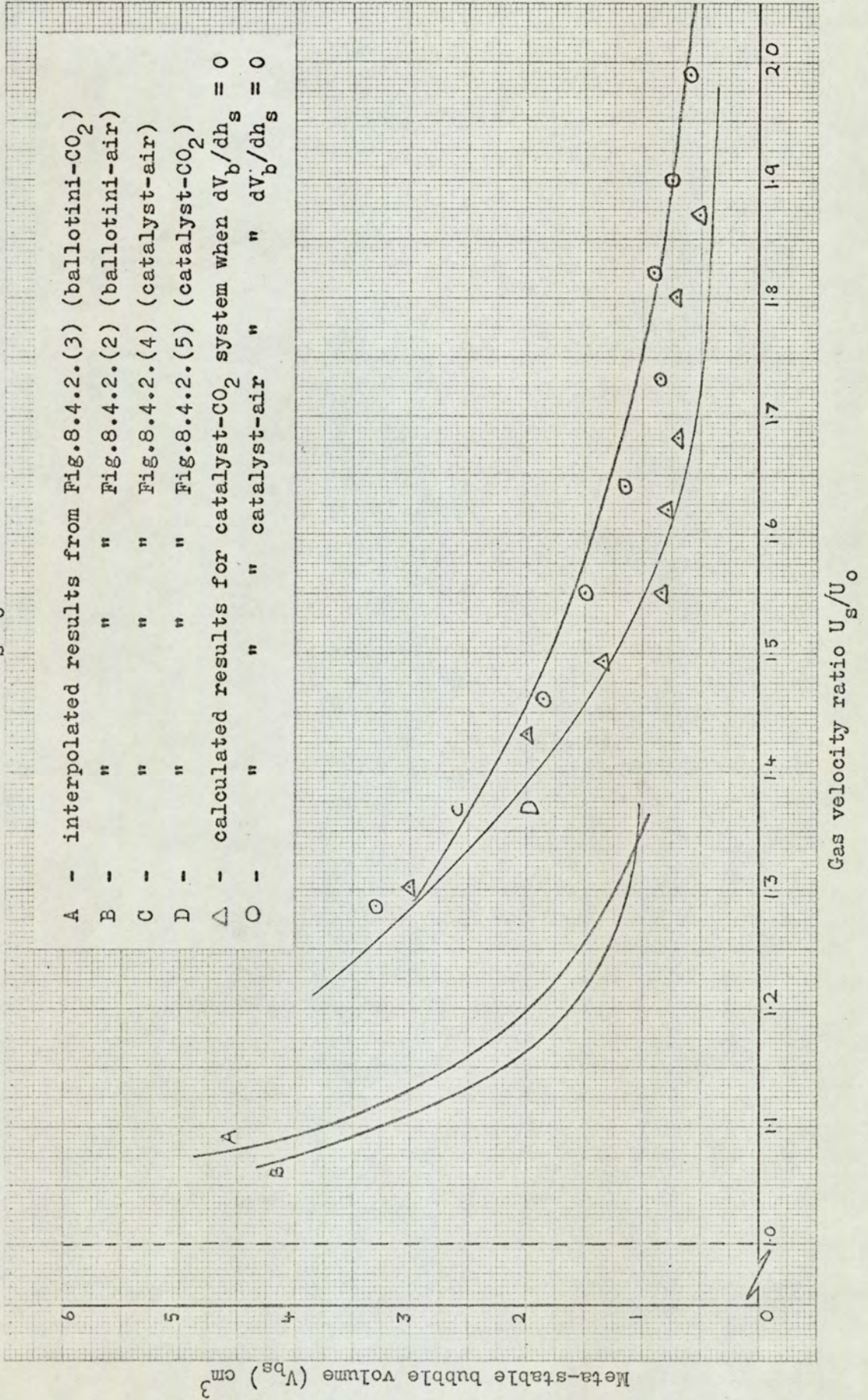


Fig. 8.4.2.(8).

Meta-stable bubble volume versus the gas velocity ratio U_s/U_0 for the catalyst and the ballotini systems

- A - interpolated results from Fig.8.4.2.(3) (ballotini-CO₂)
- B - " " " " " (ballotini-air)
- C - " " " " " (catalyst-air)
- D - " " " " " (catalyst-CO₂)
- △ - calculated results for catalyst-CO₂ system when $dV_b/dh_s = 0$
- - " " " " " catalyst-air " " $dV_b/dh_s = 0$



Gas velocity ratio U_s/U_0

8.5. VELOCITY OF A SINGLE BUBBLE

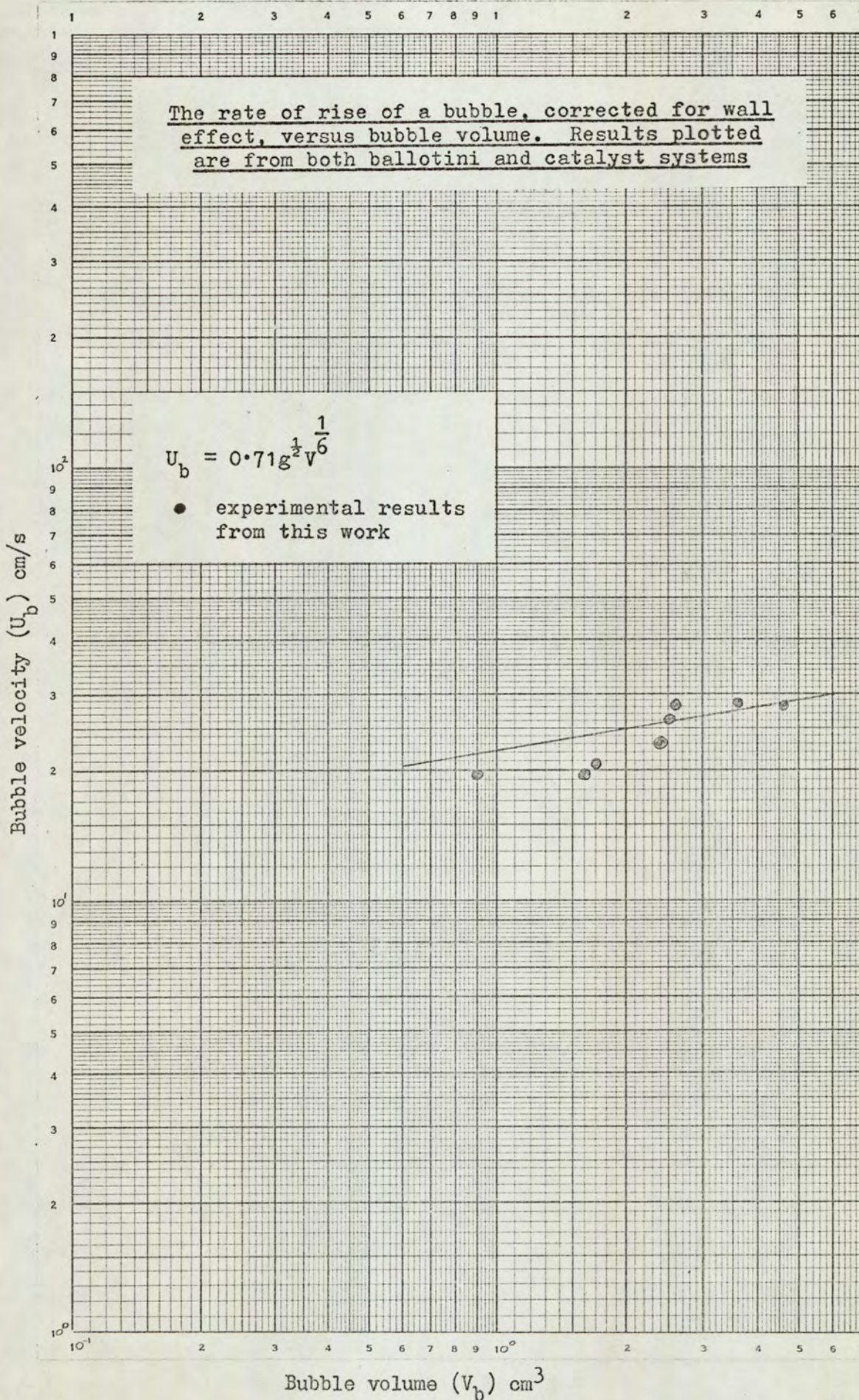
Previously the rate of rise of a gas bubble in a gas fluidised bed has been determined by injecting a known volume of gas and recording the time it took to rise a known distance (Harrison and Davidson⁽¹²⁾, Angelino et al.⁽⁴²⁾), but no precautions were taken to ensure that the bubble remained at a constant volume throughout its rise. Therefore, any correlation between the rate of rise and the bubble volume, obtained in this manner, has the inherent errors of

- i) assuming that the injected volume equals the initial bubble volume formed;
- ii) assuming that the bubble volume remains constant throughout its rise.

By studying the graphs of peak height versus background gas rate in this work, it was possible to choose results where a known injected volume had produced a bubble of constant volume at injector-to-plate distances between 8 and 18cm. The appropriate UV oscillograph chart was then referred to, and the time for the bubble of known volume to travel from 8cm to 18cm above the injector was obtained by difference.

Fig. 8.5.(1), (p.186) compares these experimentally obtained velocities, corrected for wall effect, with the theoretical ones calculated from Harrison and Leung's⁽¹³⁾ equation for the rate of rise of a bubble.

Fig. 8.5.(1).



8.6. RATE OF GROWTH OF SINGLE BUBBLES

Values of growth rates were obtained by extracting data from the graphs of peak height versus distance bubble travelled. (The procedure used to obtain these graphs is outlined in Section 8.4.1. and the data is tabulated in the Appendix Section A4.) Using Fig. 8.6.(1), (p.189) as an example, and in particular, the line with the parameter of injected volume = 3cm^3 , the peak heights at points 1, 2, 3 were converted to bubble volumes V_{b1} , V_{b2} , V_{b3} . Points 1 and 2 represent a distance of 10cm and hence the average rate of growth (with respect to distance travelled) of a bubble of mean volume (V_{b3}) at the given background gas rate was taken as

$$dV_b/dh_s = (V_{b2} - V_{b1})/10 \quad - \quad 8.6.(1)$$

The values of V_{b3} and dV_b/dh_s for each line of Fig. 8.6.(1) were plotted as a single line on Fig. 8.6.(2), (p.190), together with the other results for this system. Figs. 8.6.(3-6), (pp.191-194) show the results for the other systems.

Since the results approximate to straight lines, they may be represented by an equation of the type

$$V_b = K dV_b/dh_s + V_{bs} \quad - \quad 8.6.(2)$$

The values of the gradients (K) thus obtained are plotted against the ratio U_s/U_o in Fig. 8.6.(7), (p.195). In addition, for the air catalyst system the values of K are plotted against $(U_s - U_o)$ (Fig. 8.6.(8), (p.196) in order to compare them with the results of Davies and Richardson⁽¹⁰⁾ for a similar system.

As in Section 8.4, the diakon-air results (Fig. 8.6.(6), (p.194)) are included only for completeness because no trend was

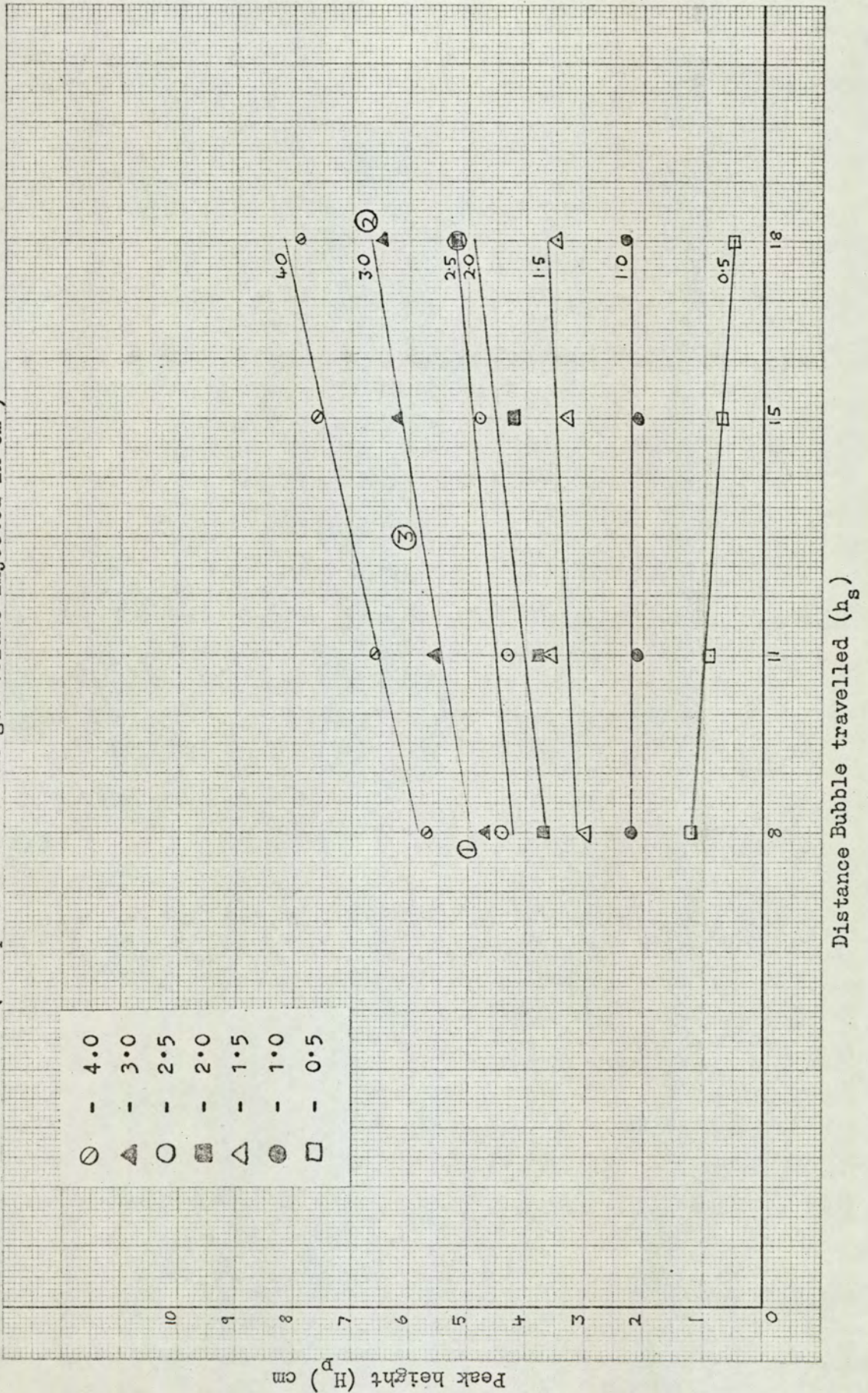
apparent from them, and therefore only the average value of K ($\approx 25\text{cm}$) has been evaluated.

Values of V_{bs} obtained from equation 8.6.(2) should be equivalent to the interpolated values obtained in Section 8.4.2. and are therefore superimposed on the results in Figs. 8.4.(7 and 8).

Fig. 8.6.(i).

Peak height versus distance bubble travelled for the ballotini-air system ($U_s = 0.440\text{cm/s}$)

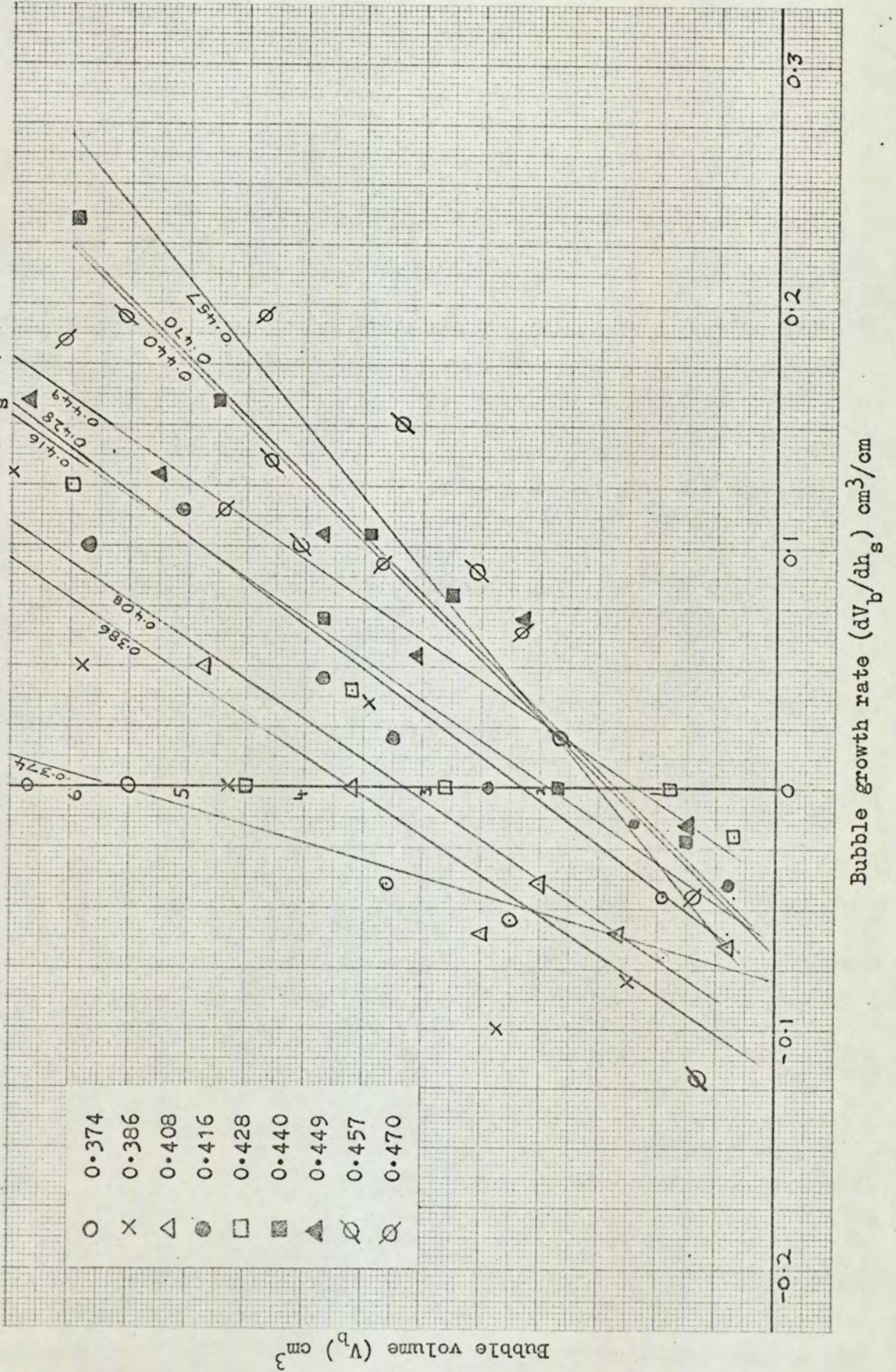
(The parameter is the gas volume injected in cm^3)



Distance Bubble travelled (h_s)

Fig. 8.6.(2).

Measured bubble volume versus bubble growth rate for the ballotini-air system
 (The parameter is the superficial gas velocity U_s cm/s)



Bubble growth rate (dV_p/dh_s) cm^3/cm

Fig. 8.6.(3).

Measured bubble volume versus bubble growth rate for the ballotini-CO₂ system
 (The parameter is the superficial gas velocity U_s cm/s)

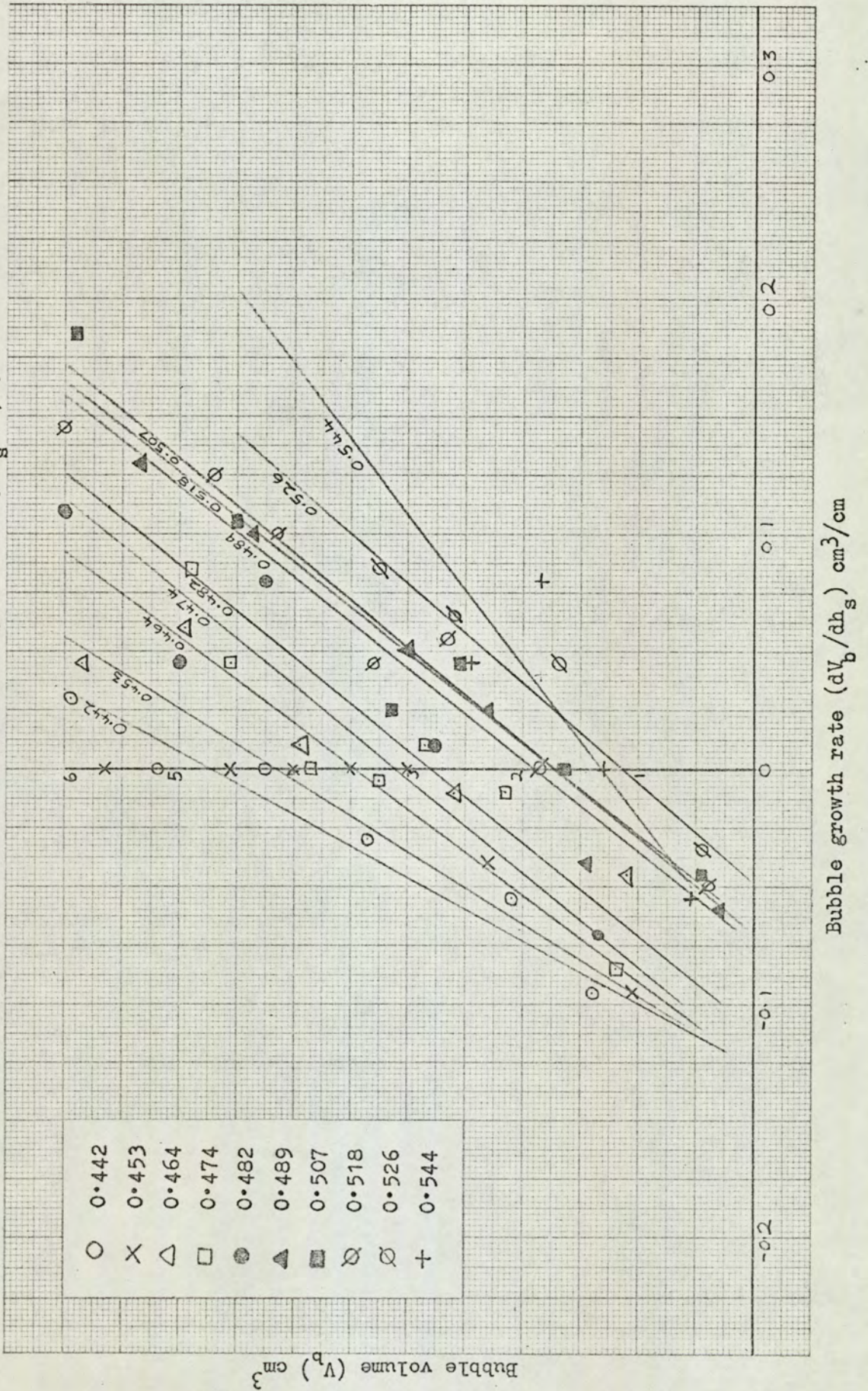
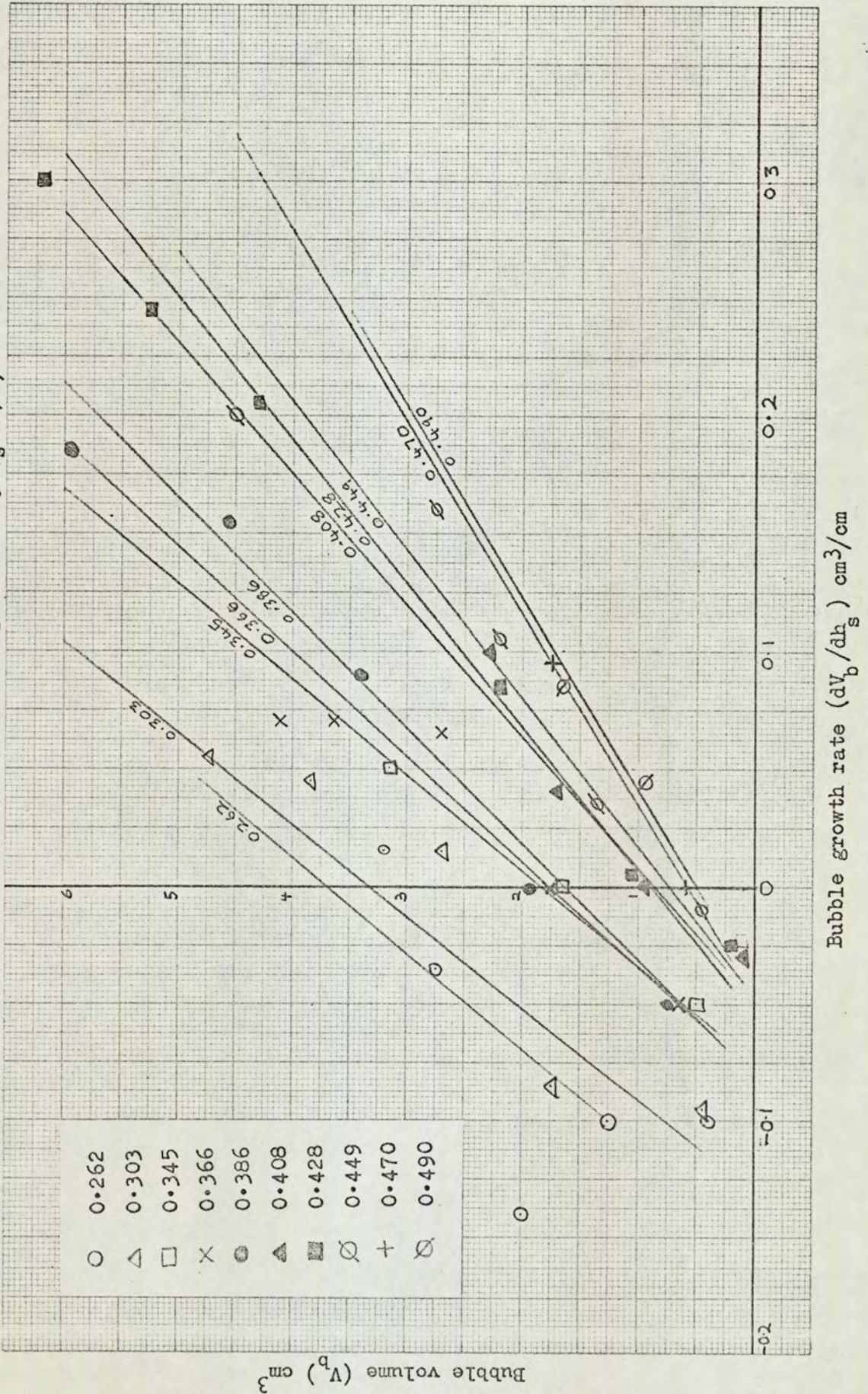


Fig. 8.6.(4).

Measured bubble volume versus bubble growth rate for the catalyst-air system
 (The parameter is the superficial gas velocity U_s cm/s)



Bubble growth rate (dV_p/dh_s) cm^3/cm

Fig. 8.6.(5).

Measured bubble volume versus bubble growth rate for the catalyst-CO₂ system
 (The parameter is the superficial gas velocity U_s cm/s)

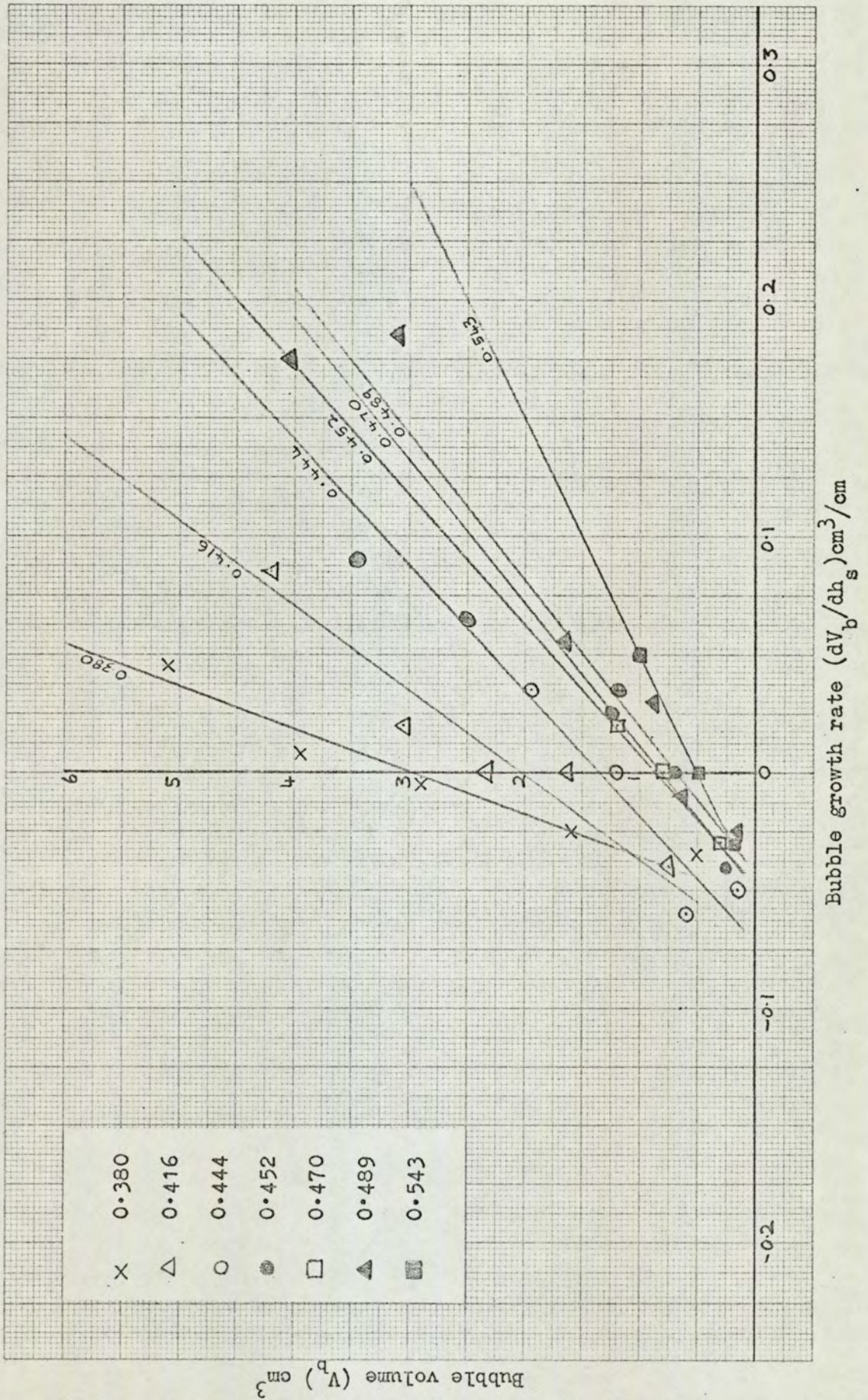
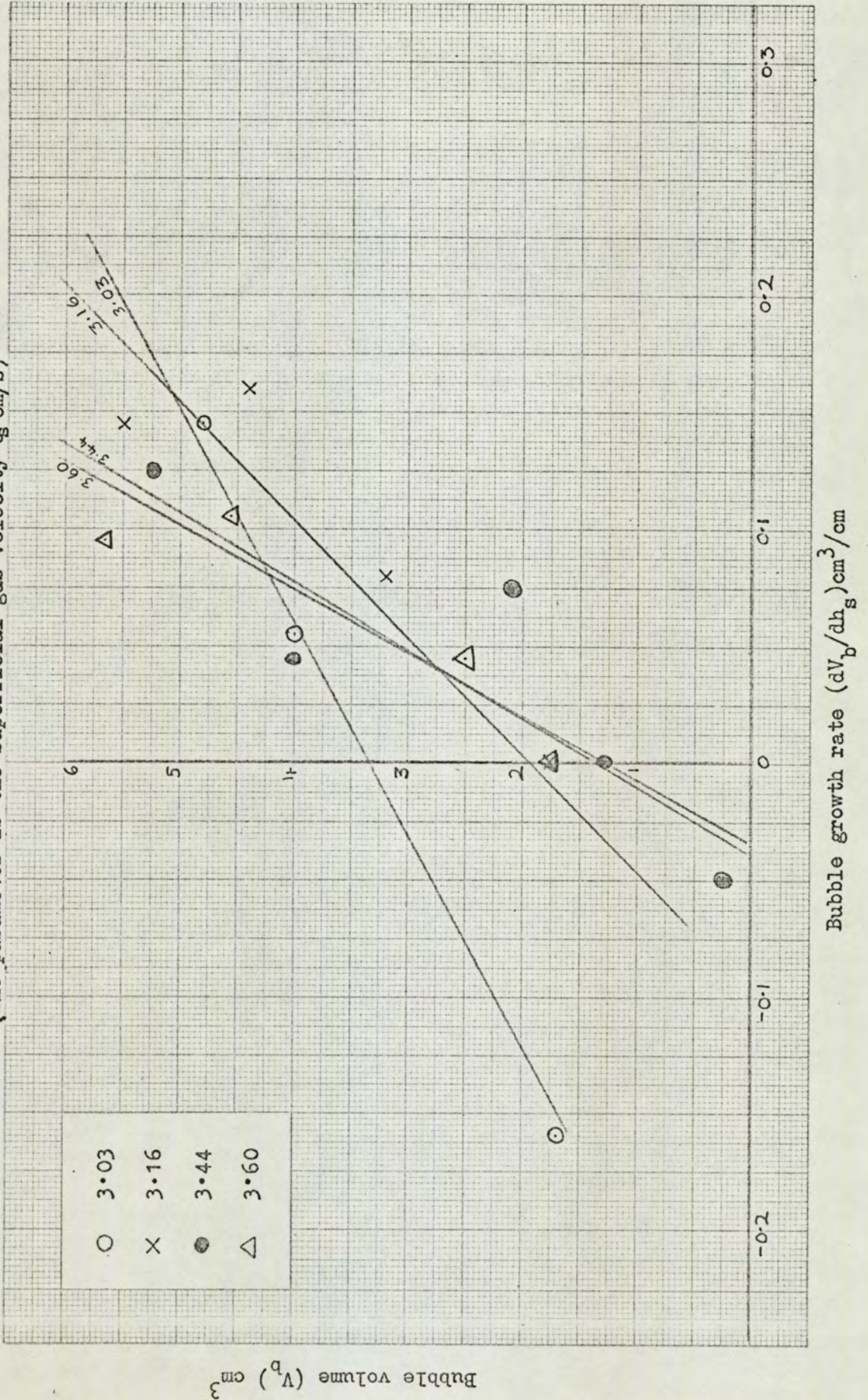


Fig. 8.6.(6).

Measured bubble volume versus bubble growth rate for the diakon-air system
 (The parameter is the superficial gas velocity U_s cm/s)



Bubble growth rate (dV_b/dh_s) cm³/cm

Fig. 8.6.(7).

Growth rate constant (K) versus gas velocity ratio (U/U_0) for the ballotini and the catalyst systems

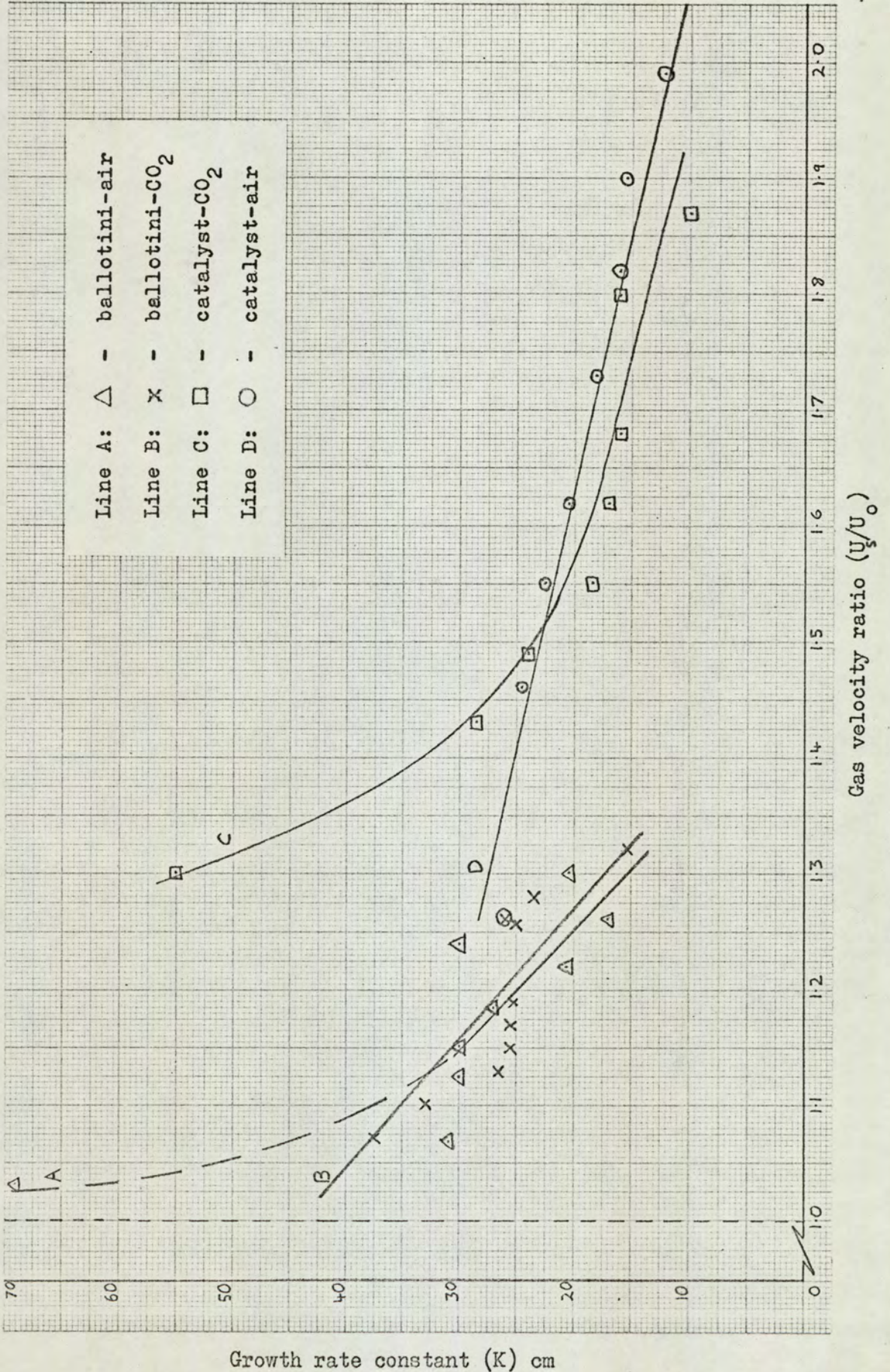
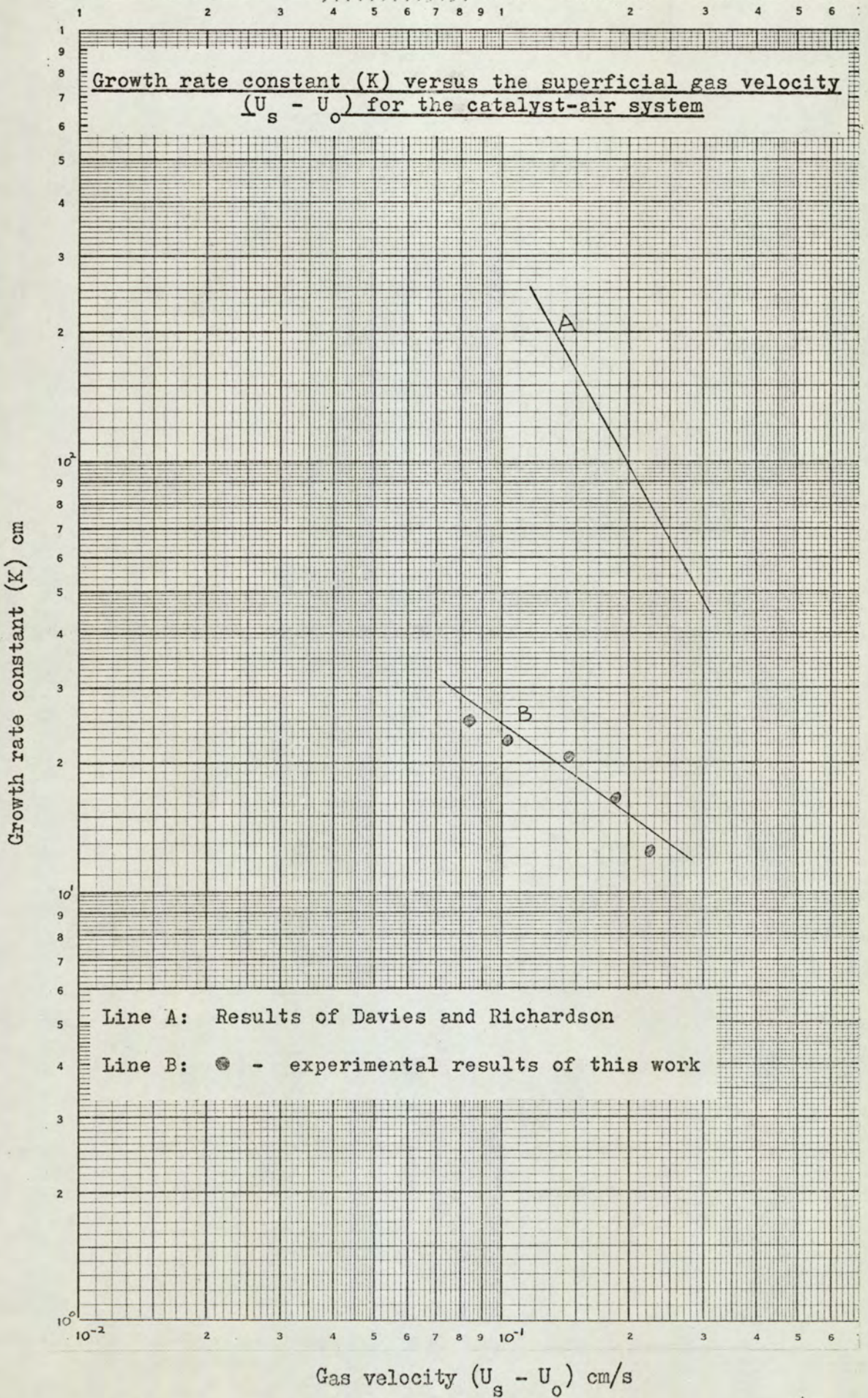


Fig. 8.6.(8).



DISCUSSION OF RESULTS

9.1. DETERMINATION OF THE INCIPIENT FLUIDISING VELOCITIES

9.1.1. Discussion of the gradient in Figs. 8.1.(1-3).

The Reynolds Numbers (Re_a) for the systems which were considered in this work (where $Re_a = (\rho_f U_s d_p) / (\mu_f (1 - e_i))$) were at least an order of magnitude less than the laminar flow limit at U_0 . The bed pressure drop should therefore have been directly proportional to the superficial gas velocity (U_s) and if the voidage of the bed had been independent of U_s , a log-log plot of ΔP versus U_s should have yielded a straight line of gradient 1.0.

However, from Fig. 8.2.1.(1), (p.168) it can be seen that the bed height (and therefore the bed voidage) increased with gas velocity at velocities less than U_0 . If the bed expanded in discrete increments, the plot of ΔP versus U_s would appear as indicated in Fig. 9.1.1.(1), (p.198), the vertical lines representing a decrease in ΔP caused by incremental increases in bed voidage and the lines of gradient 1.0, representing U_s proportional to ΔP , for a bed of constant voidage. A fluidised bed does not, of course, normally expand in such noticeable increments and the experimental results would be expected to follow the broken line, in Fig. 9.1.1.(1). Hence the gradient should be less than 1.0, as was found in practice. It would therefore appear that much more weight should be given to points near to $U_s = U_0$ than to points near to $U_s = 0$.

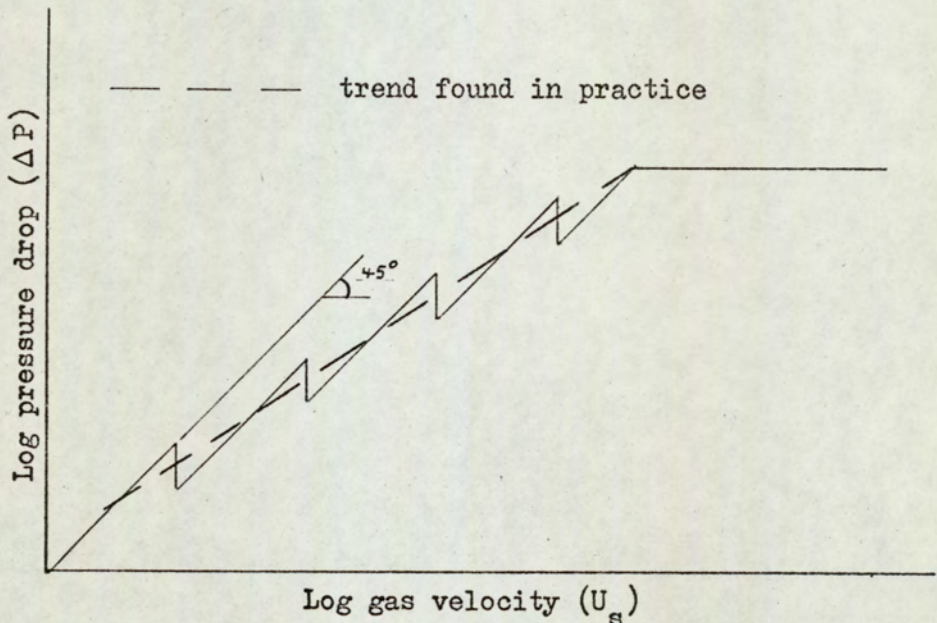
9.1.2. Discussion of the Discrepancy between Theoretical and Recorded Bed Pressure Drop at U_0

It has been shown (Section 8.1.) that the recorded bed pressure drops for the ballotini and the catalyst systems were 2-3% less than the theoretical pressure drops calculated from the bed weights.

Sutherland⁽⁶⁸⁾ predicted this effect by considering the change in distributor pressure drop due to change in fluid density (and hence velocity) at constant mass flow rate. However, for the distributor pressure drop involved in the present work, (3-6cm H_2O), his predicted error is only of the order of 0.5-1.0%. This suggests that other factors, such as particle size distribution, may also contribute to the discrepancy between the theoretical and experimental values of ΔP .

Fig. 9.1.1.(1).

Theoretical plot of bed pressure drop
versus superficial gas velocity



9.2. DISCUSSION OF BED EXPANSION RESULTS

9.2.1. Bed Expansion for Gas Velocities in the Range $U_0 < U < U_{mb}$

The experimental values of A_2 and n_2 in equation 2.3.2.(4):

$$U_s = A_2 e_i^{n_2} \quad - \quad 2.3.2.(4)$$

for the air-catalyst system in the present work and from the work of Davies and Richardson⁽¹⁰⁾ for a similar air-catalyst system are compared with the values of U_t and n_1 predicted by Richardson and Zaki⁽³²⁾ (Table 9.2.1.(1)).

In order to determine the predicted value of n_1 it was first necessary to calculate the value of the Reynolds Number for a particle under free falling conditions. Re_p was found to be 0.35 for the present work (assuming spherical particles), and was given as 0.34 for the work of Richardson and Davies⁽¹⁰⁾.

Table 9.2.1.(1).

Theoretical and Experimental Bed Expansion Constants

Author	cm/s	
Watkins	6.6 (A_2)	4.5 (n_2)
Davies and Richardson	7.6 (A_2)	6.21 (n_2)
Richardson and Zaki	8.4 (U_t)	4.5 (n_1)

From Table 9.2.1.(1) it can be seen that the value of n_2 for the present work, though less than the value found by Davies and Richardson, agrees with the value of n_1 predicted by Richardson and Zaki. However, the value of A_2 for the present work is less than the equivalent value for both the other pairs of workers.

This discrepancy may well be due to the assumption that the particles were spherical, which, as can be seen from the photo-micrograph, Fig. 7.3.2.(2), (p.152), is not really valid.

9.2.2. Bed Expansion at Gas Velocities in the Range $U_s > U_{mb}$

The observations noted in Section 8.2.2. for the ballotini and catalyst systems suggest that the bed height oscillations which occur in the range $2U_{mb} > U_s > U_{mb}$ are not due to an instability that grows from the distributor or from the free surface, but rather to an instability of the bed itself. This instability would not appear to be related to the Reynolds Number of the interstitial gas velocity because at all velocities the Reynolds Number is at least two orders of magnitude less than the limit for laminar flow. A hypothesis which explains the oscillations is that there is a critical bed expansion rate for a given voidage, which, if it is exceeded, causes the bed to collapse. The rate of bed expansion will decrease as the bed expands, but at a given voidage the rate will be directly related to the background gas velocity. This would therefore explain the decrease in the maximum bed height (line A, Fig. 8.2.1.(1), (p.168)) as the background gas rate increases, and also why the instability appears to be instantaneous throughout the bed.

9.3. INJECTION EFFECT

The injection effect appears to be more complicated than indicated by previous workers^(14, 27).

Rowe and Partridge⁽¹⁴⁾ compared the volume of a bubble formed by injection, calculated from an X-ray photograph, with the volume of gas injected but apparently, change in bubble size after formation was not considered. One photograph only was taken of each bubble, which may or may not have been at its stable size, and therefore Rowe and Partridge were able only to investigate the effect of variation of background gas rate on bubble volume as measured. Their conclusion was that it was only at a unique background gas rate that the injected volume equalled the (measured) volume of the bubble formed.

An explanation of the present results is that all bubbles gain gas from the bed while forming, but that bubbles larger than about 3cm^3 detach from the orifice before all the measured volume of gas has been delivered. The net effect for injected volumes larger than about 4cm^3 is a gas loss and smaller than about 2cm^3 is a gas gain. This is supported by the visual observations of the calibration work carried out in oils. Injected volumes less than about 3cm^3 formed single bubbles but greater volumes had several small trailing bubbles formed by gas leaving the orifice after the main bubble had detached.

9.4. BUBBLE STABILITY

9.4.1. The Limits of the Meta-stable Bubble Phenomenon

The present work has demonstrated conclusively that the meta-stable bubble phenomenon does exist. An attempt was therefore made to determine the limits of this phenomenon. It would appear that V_{bs} should approach infinity as U_s approaches U_o , since at values of $U_s < U_o$ the bed would not be fully fluidised and therefore even a large bubble should still be absorbed.

At high values of U_s the results obtained in this work suggest that V_{bs} becomes very small as U_s approaches U_{mb} and it seems reasonable that $V_{bs} = 0$ at the theoretical value of the minimum bubbling velocity since at this velocity infinitely small bubbles must be able to grow. Due to departure from ideality in the bed, the theoretical value of minimum bubbling velocity may be considerably greater than the value of U_{mb} found experimentally.

Log-log graphs of V_{bs} versus $(U_s - U_o)$ were therefore plotted (Fig. 9.4.1.(1), (p.203)) to determine if the results obtained in this work did in fact have a hyperbolic form, as suggested by the linear plots of V_{bs} versus U_s .

From Fig. 9.4.1.(1) it can be seen that:

i) the catalyst systems can be approximately represented by

$$V_{bs} (U_s - U_o)^{-1.65} = 0.06 \quad - \quad 9.4.1.(1).$$

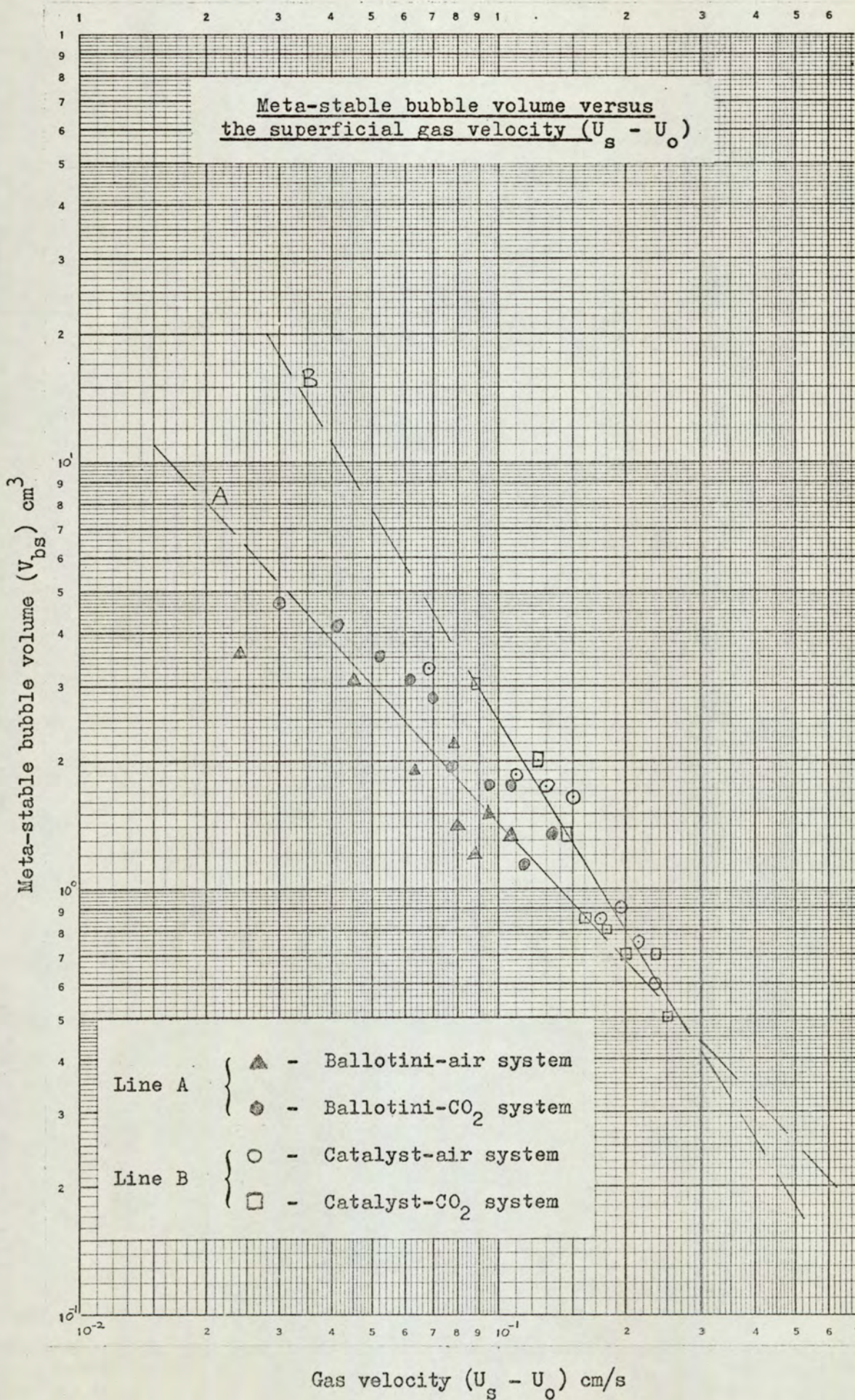
$$\text{for } 0.5\text{cm}^3 < V_{bs} < 3\text{cm}^3;$$

ii) the ballotini systems can be approximately represented by

$$V_{bs} (U_s - U_o)^{-1.1} = 0.12 \quad - \quad 9.4.1.(2).$$

$$\text{for } 1.0\text{cm}^3 < V_{bs} < 5\text{cm}^3.$$

Fig. 9.4.1.(1).



9.4.2. Physical Properties affecting the Meta-stable Volume

From Fig. 8.4.2.(8) it would appear that the meta-stable bubble volume is not extremely sensitive to changes in gas density or viscosity, though because the density and viscosity ratios for CO_2 :air are only 1.53:1 and 0.8:1 respectively, a greater range is required before a definite conclusion can be reached. There is, however, a significant difference between the catalyst and the ballotini results, though whether it is due to the difference in particle density or shape factor is not possible to determine from the present results.

9.4.3. A Theoretical Explanation of the Meta-stable Phenomenon

It is assumed that a bubble is at its stable state when the volumetric rate of gas entering the base of the bubble equals the rate at which it leaves. The rates are, of course, not equal when the bubble is growing or shrinking.

It would appear that these rates could be related to the ratio (R_v) of the dense phase voidage above a bubble (e_{ab}) to the dense phase voidage below a bubble (e_{bb}) and the ratio (R_z) of the surface area of the cap of a bubble (A_{ab}) to the surface area of the base of a bubble (A_{bb}). The smaller either of these ratios, the greater will be the rate of growth of a bubble, and if the ratios are sufficiently large the rate will be negative.

Now Davies and Richardson⁽⁶⁹⁾ have considered bubble growth only and have suggested that gas transfer from the dense phase to a bubble occurs because the voidage above a bubble remains constant at e_0 , irrespective of the background gas velocity, whilst the voidage at the base of a bubble increases with background gas rate, i.e. $R_v < 1.0$. Only hemispherical bubbles were considered, and

they concluded that all bubbles must grow in beds fluidised at velocities above U_o .

This is not the case in practice and the relationship between R_z and the included angle (in degrees) of a spherical capped bubble (w) was therefore considered. A model spherical capped bubble of volume V_b and included angle w is shown in Fig. 9.4.3.(1), (p.205).

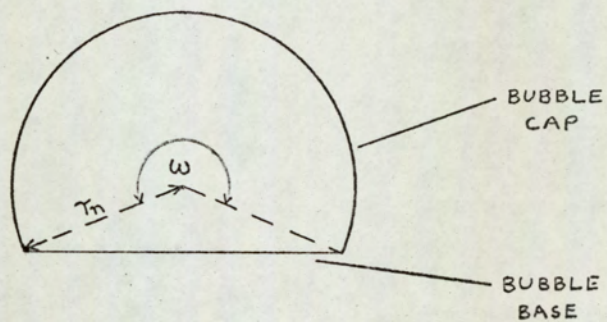
Considering Fig. 9.4.3.(1):

$$R_z = \frac{A_{ab}}{A_{bb}} = \frac{\frac{\pi w}{360} (2r_n)^2}{\frac{\pi}{4} (2r_n \left(\frac{360-w}{2}\right))^2}$$

i.e. $R_z = \frac{4}{360} \frac{w}{\sin^2 \left(\frac{360-w}{2}\right)}$ - 9.4.3.(1)

Fig. 9.4.3.(1).

A model spherical capped bubble



A plot of R_z versus w is given in Fig. 9.4.3.(2), (p.208) from which it can be seen that R_z is directly related to w .

Grace⁽¹⁶⁾ has investigated the relationship between w and the bubble Reynolds Number (Re_b) and obtained a plot of w versus Re_b for gas bubbles in liquids. He assumed that the same plot should hold for gas bubbles in gas fluidised beds in order to predict bed viscosities. By making the same assumption it was therefore possible to obtain a plot of D_b versus R_z (line A, Fig. 9.4.3.(3), (p.209)). (The values of $\mu_a = 5\text{Poise}$, $e_i = 0.475$, $\rho_p = 2.2\text{g/cm}^3$ were chosen as being realistic values for the air-ballotini system.) It can be seen from Fig. 9.4.3.(3) that D_b is inversely related to R_z . Hence, at a constant background gas rate and assuming a constant value of R_v , a small bubble could shrink whilst a big bubble could grow, merely due to the different bubble shapes, and therefore a meta-stable bubble could exist.

Having shown that a meta-stable bubble could theoretically exist, an attempt was made to predict the relationship between U_s and the stable bubble volume V_{bs} for a given system.

$$\text{Now } Re_b \propto \frac{(1 - e_i)}{\mu_a} \quad - \quad 9.4.3.(3)$$

for a fixed bubble volume in a given system, but as yet there would appear to be no published data on the relationship between e_i and μ_a for a given system. However, Sehmi⁽⁷⁰⁾ has completed some initial work which suggests that μ_a is very sensitive to e_i , such that in equation 9.4.3.(3) the change in e_i compared to the change in μ_a is negligible. Therefore equation 9.4.3.(3) can be rewritten as:

$$Re_b \propto \frac{1}{\mu_a} \quad - \quad 9.4.3.(4)$$

to the first approximation.

Assuming that a voidage increase from 0.475 to 0.5 causes a

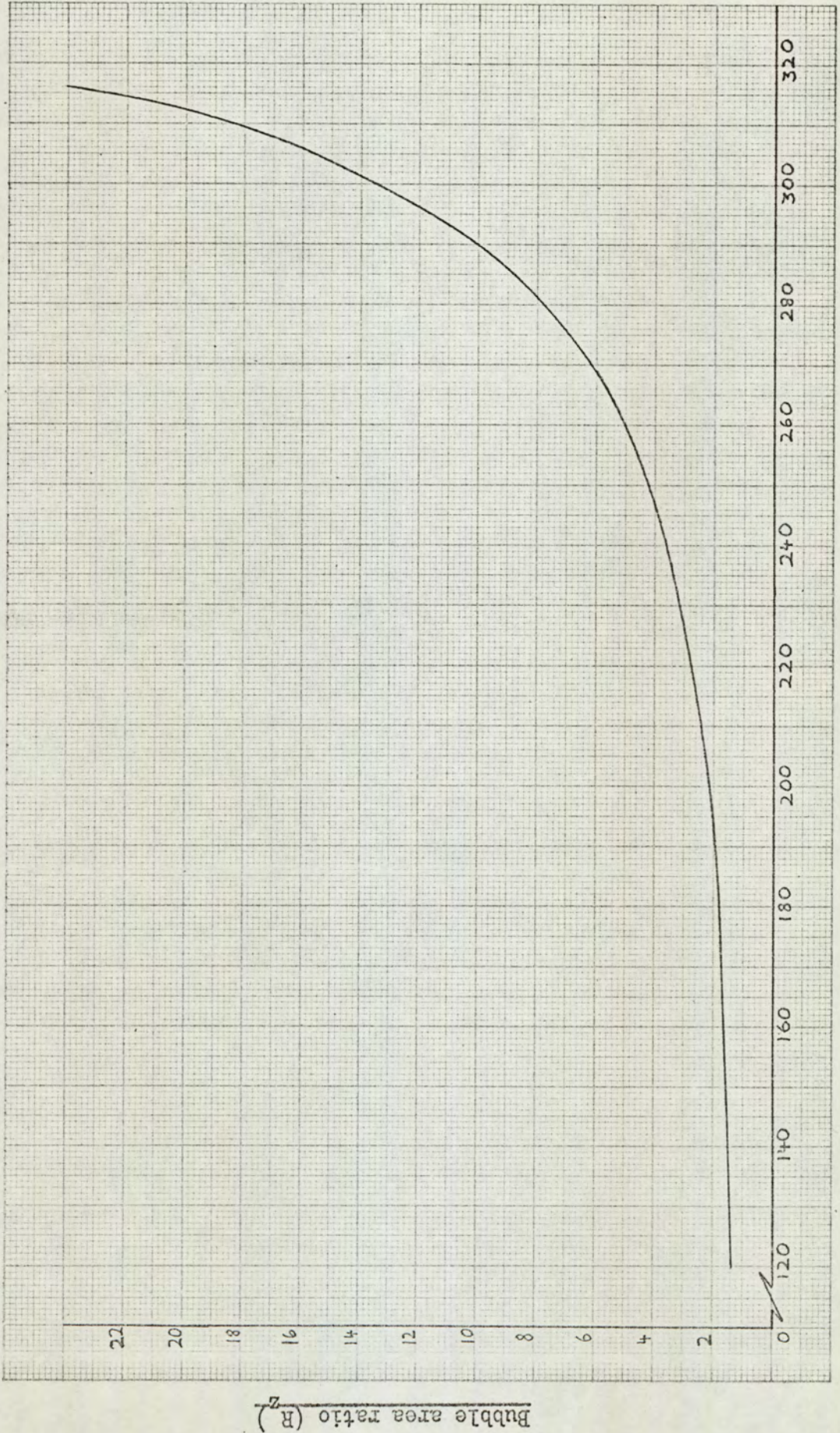
viscosity decrease from 5.0 to 2.5 for the ballotini-air system, which would appear reasonable from Sehmi's work, then plotting R_z versus D_b gives line B in Fig. 9.4.3.(3). Comparing lines A and B indicates that if stability is related to R_z , then the stable volume will decrease with increased bed voidage, as was found in practice.

The effect of R_v has so far been neglected, but consideration of the voidage trend above and below a bubble found by Lockett and Harrison⁽²⁰⁾ suggests that R_v is less than 1.0. This fits the bubble stability theory of the present work because R_z is always greater than 1.0 and therefore R_v must be less than 1.0 for bubbles to grow.

To conclude, the variation of R_z with bubble diameter and with bed viscosity for a constant bubble volume predicts results of the form found in the present work. At present, however, it is not possible to determine if the stable volumes obtained in this work fit this suggested theory, because the exact relationship between μ_a and e_i is unknown, as is the relationship between e_{ab} and e_{bb} , and R_v and U_s .

Fig. 9.4.3.(2).

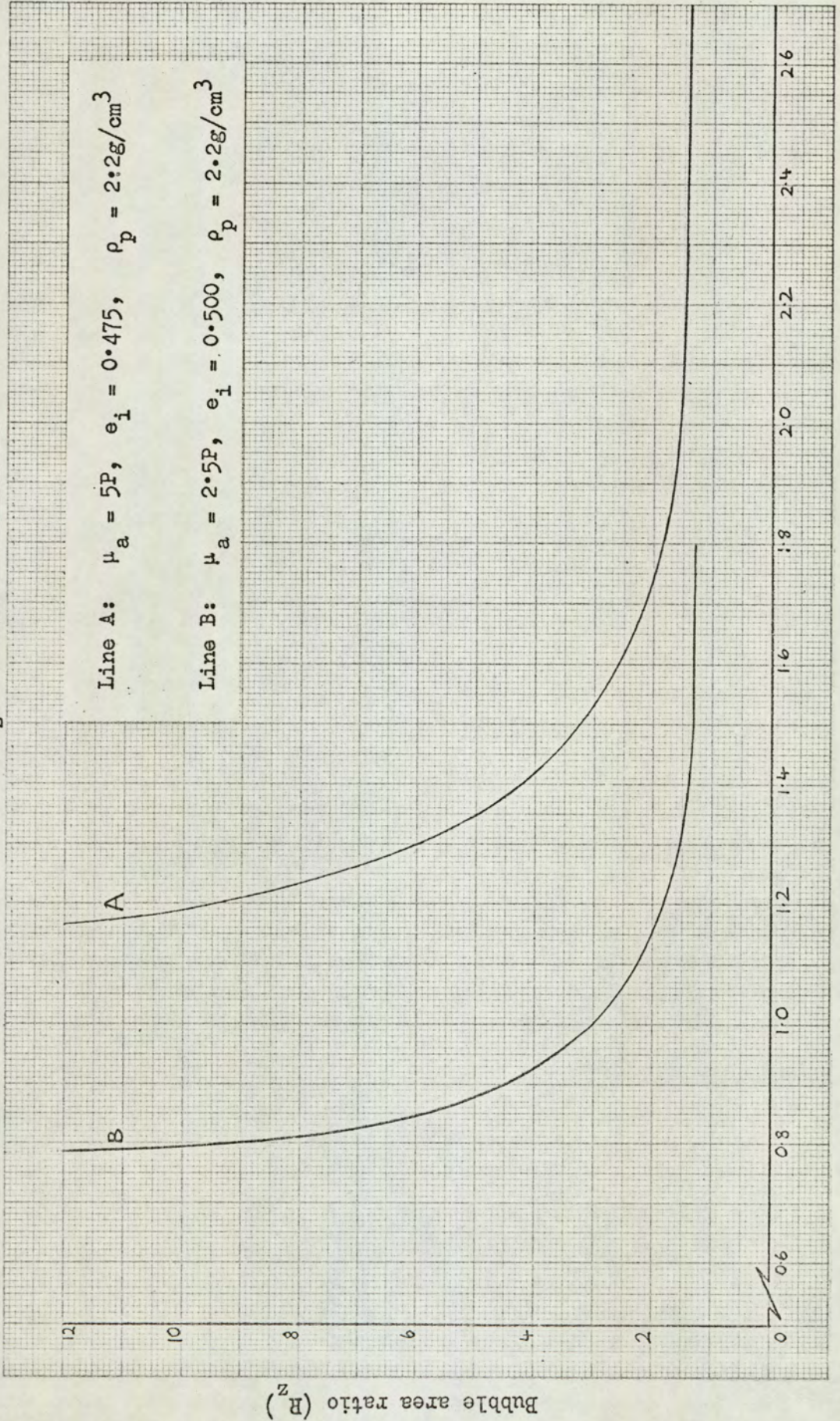
The bubble area ratio R_z versus the included angle of a bubble (equation 9.4.3.(1))



Bubble included angle (w) degrees

Fig. 9.4.3.(3).

Bubble area ratio R_z versus bubble diameter



Bubble diameter (D_p) cm

9.5. RATE OF RISE OF A BUBBLE

It must be noted that the velocity measurements were not the main aim of this work, and that the results have been included to demonstrate a method rather than produce accurate results. To conserve the expensive oscillograph paper the chart speed was considerably lower than that which would have been used for accurate velocity measurement and therefore the possible errors stated below were higher than need have been.

The distance equivalent to the time taken for an average bubble to travel 8cm was only about 0.25cm and the maximum accuracy to which the readings could be made was 0.1cm. Similarly, the 18cm measurements had an equivalent chart distance of about 0.7cm which could be read to the same accuracy. Due to the statistical cancelling of the errors the combined chart error was $(2 \times 0.05^2)^{\frac{1}{2}} = \pm 0.07\text{cm}$. The average chart distance was approximately 0.5cm and therefore the error in the velocity measurement was $\pm 14\%$. Within this error the experimental results, corrected for the effect of the bed wall, agree with the correlation of Harrison and Leung⁽¹³⁾.

9.6. RATE OF GROWTH OF SINGLE BUBBLES

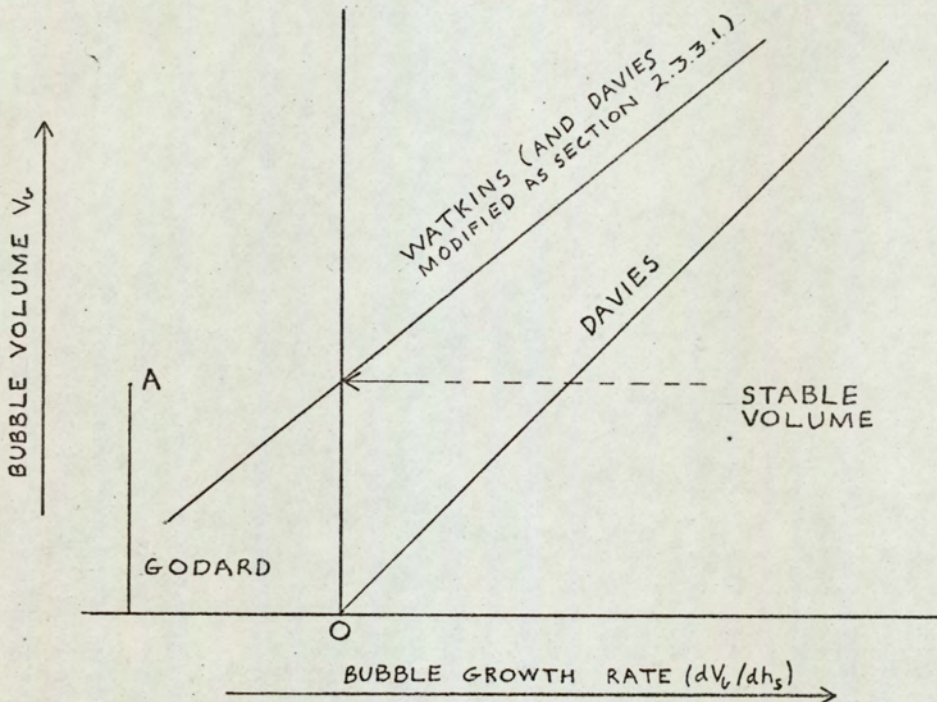
9.6.1. The Relationship between dV_b/dh_s and V_b

The results in Section 8.6. show that plots of dV_b/dh_s versus V_b do not pass through the origin, contrary to the suggestion of Davies and Richardson⁽¹⁰⁾.

This work also indicates that Godard and Richardson⁽³⁴⁾ may have been in error when they stated that dV_b/dh_s for shrinking bubbles was independent of bubble size for a given background gas rate. If this were so (and their own results for larger bubbles suggest otherwise), then the plot of dV_b/dh_s versus V_b for a given gas rate would be as indicated in Fig. 9.6.1.(1), (p.211).

Fig. 9.6.1.(1).

Qualitative graph of
bubble growth rate results



The discontinuity at A seems very unlikely and as Fig. 8.6.(6) is for the same system as used by Godard and Richardson (diakon-air) it would appear that their results could have been expressed in a like manner.

9.6.2. The Variation in K for Different Systems

The values of K for the different systems are plotted on Fig. 8.6.(7), (p.195), from which it would appear that the change in material had a marked effect but the change in fluidising gas very little. This difference caused by the change in materials could be due either to the density change or the particle shape, but without further investigation with other materials it is not possible to suggest which one.

9.6.3. The Relationship between K and V_b

Fig. 8.6.(8), (p.196) compares the values of K obtained in the present work for the air-catalyst system with those published by Davies and Richardson⁽¹⁰⁾ for a similar system, and it shows a difference of nearly an order of magnitude between the two sets of results for the same range of $(U_s - U_o)$. The only difference between the two experiments was the size of bubble being considered (Davies and Richardson considered bubbles in the range 15 - 1500cm³). It therefore suggests that perhaps K is not in fact a constant for a given background gas rate, but may depend on bubble volume or some related property such as rate of rise.

However, the good comparison (Figs. 8.4.2.(7 and 8), (pp.183-184), between the values of V_{bs} , determined by interpolation (Section 8.4.) and the values of V_{bs} , determined by equation 8.6.(2), does suggest that the relationship between V_b and

dV_{bs}/dh_s is approximately linear over the range of bubble sizes investigated in this work.

C O N C L U S I O N S

The following conclusions can be drawn from the present work:

- 1) The meta-stable bubble phenomenon can occur in the following systems:

ballotini-air

ballotini-CO₂

catalyst-air

catalyst-CO₂

diakon-air

The stable size decreases with increase in background gas velocity over the range of bubble size (5 - 0.5cm³) investigated, and is dependent on the physical properties of the particles rather than those of the fluidising gas. The experimental values of V_{bs} and $(U_s - U_o)$ for the catalyst and ballotini systems respectively can be correlated by

$$V_{bs} (U_s - U_o)^{-1.65} = 0.06 \quad - \quad 9.4.1.(1)$$

$$V_{bs} (U_s - U_o)^{-1.1} = 0.12 \quad - \quad 9.4.1.(2)$$

The meta-stable phenomenon can be explained by considering the effect on bubble shape of a Reynolds Number with respect to a bubble. Over the range of bubble volumes considered the bubble Reynolds Number is primarily a function of bed viscosity for a given particulate system.

2) An instrument has been developed which can measure the volume of small bubbles in a non-conducting bed. The accuracy is directly related to the dielectric constant of the fluidised particles, but for materials with a dielectric constant greater than about 6 (which includes glass and catalyst), the accuracy is approximately $\pm 0.01 \text{cm}^3$. The instrument can also measure voidage to an accuracy of $\pm 0.2\%$.

3) The rate of growth of bubbles over the size range investigated for a given system fluidised at a given background gas velocity can be expressed by

$$V_b = K \frac{dV_b}{dh_s} + V_{bs} \quad - 8.6.(2)$$

The value of dV_b/dh_s lies in the range $-0.15 - +0.25$ (cm^3/cm travelled) and the values of K lie in the range $10 - 70 \text{cm}$.

4) The pressure drop at U_0 was found to be 2 - 3% less than the bed weight, which is of the same order as predicted by theory.

5) The bed expansion of the catalyst-air system and the background gas velocity can be correlated by

$$U_s = 6.55e^{4.5} \quad - 8.2.1.(1)$$

which is of the form predicted by other workers.

6) A bed oscillation occurred at background gas rates between U_{mb} and about $2U_{mb}$, which suggests that for a given bed voidage there may be a critical rate of bed expansion.

7) During the formation of single bubbles by injection, the bubbles gain gas irrespective of their size, but for those larger than 3cm^3 the net effect is a gas loss due to bubble departure from the injector orifice before all the measured gas has been delivered.

8) Measured rates of rise for bubbles in the systems investigated agree with the velocities predicted by the generally accepted correlation.

SUGGESTIONS FOR FUTURE WORK

1) The rate of bed expansion at background velocities greater than U_{mb} should be studied, to determine if there is a maximum stable rate of expansion for a given voidage, as suggested in Section 9.2.2.

2) The relationship between the physical properties of the fluidising medium and the meta-stable bubble phenomenon could be investigated over a much larger range if the bed were operated under pressure and at temperatures above ambient (Section 9.4.2.). The capacitance probe can be used to determine the bed height if it is not feasible to record it visually.

The increased gas density available by working under pressure should also increase the choice of particles available for particulate fluidisation. The effect of the particle density and the shape factor on the stability phenomenon could therefore be investigated separately.

3) The initial work of Sehmi⁽⁷⁰⁾ should be extended to investigate accurately the change in bed viscosity with voidage. This would enable actual values to be calculated from the theory suggested in Section 9.4.3., and compared with the results of the present work.

4) If possible, the values of e_{ab} and e_{bb} should be determined and whether R_v is related to U_s . At present, however, the only

feasible method appears to be the capacitance technique of Lockett and Harrison⁽²⁰⁾, which has the disadvantage that the capacitance fringe effects must become significant in any bed other than a two-dimensional type.

5) The maximum permissible size of bubble in the present work was about 8cm^3 in the ballotini systems and about 5cm^3 in the catalyst systems. Bubble volumes in the range $5 - 30\text{cm}^3$ should be investigated for the following reasons:

- i) the values of stable volumes are required, corresponding to gas velocities equal to, or just greater than, U_0 . These results should substantiate or disprove the theory put forward in Section 9.4.3. that the stable volume tends to infinity as U_s tends to U_0 ;
- ii) in the present work the growth rate results can be correlated by the equation

$$V_b = K \frac{dV_b}{dh_s} + V_{bs} \quad - \quad 8.6.(2)$$

The values of K, however, do not agree with the values found by Davies and Richardson⁽¹⁰⁾ using much larger bubbles. Results for bubbles in the $5 - 30\text{cm}^3$ range would allow a direct comparison to be made and hence, determine whether K is in fact a function of

$$U_b^{\frac{n}{3}}.$$

A P P E N D I X

A 1

Derivation of the relationship between the gas flow rate at atmospheric pressure (G_a) and the flow rate indicated by the VA flow meter (G_c)

Let P_m = calibration meter operating pressure;

G_m = volumetric flow rate recorded by the calibration meter at pressure P_m ;

P_t = pressure in the VA flow meter tube when operating;

G_t = volumetric flow rate in the VA flow meter tube at pressure P_t .

Now in Section 6.10.2. the basic equation for VA flow meters was given as:

$$G_v = \frac{k_{10}}{(P_r)^{\frac{1}{2}}} \quad - \quad 6.10.2.(1)$$

The VA flow meters were calibrated with a positive displacement meter and from the calibration results, the metered volume (G_m) could be plotted against the VA flow meter scale reading.

The values of G_m were converted to G_c , the flow rate in the VA flow meter tube at pressure P_c , by applying the gas law $P_1 G_1 = P_2 G_2$, assuming isothermal expansion;

$$\text{therefore } G_c = \frac{G_m P_m}{P_c} \quad - \quad A.1.(1)$$

The pressure (P_t) in the VA flow meter tube depended on atmospheric pressure and on the fluidised bed pressure drop. The calibration chart was therefore corrected for this by applying equation 6.10.2.(1):

$$G_c (P_c)^{\frac{1}{2}} = G_t (P_t)^{\frac{1}{2}}$$

Substituting from equation A.1.(1) for G_c

$$G_t = \frac{G_m P_m}{(P_t P_c)^{\frac{1}{2}}} \quad - \text{A.1.(2)}$$

The volumetric flow rate in the tube G_t was then converted to the volumetric flow rate at atmospheric pressure G_a , by again assuming isothermal expansion and applying the gas law $P_1 G_1 = P_2 G_2$

i.e. $G_a = \frac{G_t P_t}{P_a}$

Substituting from equation A.1.(2) for G_t

$$G_a = \frac{G_m P_m (P_t)^{\frac{1}{2}}}{P_a (P_c)^{\frac{1}{2}}} \quad - \text{A.1.(3)}$$

In equation A.1.(3), the values of P_m and P_c are constant for a given calibration and therefore G_a may be expressed as

$$G_a = \frac{G_c k_{10} (P_t)^{\frac{1}{2}}}{P_a} \quad - \text{A.1.(4)}$$

where $k = \frac{P_m}{(P_c)^{\frac{1}{2}}}$

P_t can be expressed as $(P_a + \Delta P)$ where ΔP is the summation of the fluidised bed pressure drop and the pressure drop in the air line between the VA flow meter outlet and the fluidised bed. Therefore equation A.1.(4) can be rewritten as

$$G_a = \frac{G_c k_{10} (P_a + \Delta P)^{\frac{1}{2}}}{P_a} \quad - \text{6.10.2.(2)}$$

A 2

Relationship between the dielectric constant and the voidage of the dense phase of a fluidised bed

The capacitance, C, of a capacitor with rectangular plates is given by

$$C = \frac{k_7 D_k S_p}{h_g} \quad - \text{A.2.(1)}$$

(where k_7 = a constant depending only on the units used)

(D_k = dielectric constant)

(S_p = plate area)

(h_g = distance between plates)

Fig. 6.14.1.(1) shows the two extreme cases for a given voidage.

i) Parallel Capacitance

From Fig. 6.14.1.(1A) it can be seen that the width of capacitor occupied by either components = h_g .

Let S_{p1} = area of the plate occupied by component 1

S_{p2} = area of the plate occupied by component 2

From equation 6.14.1.(1):

$$e_k = \frac{h_g S_{p2}}{h_g S_p}$$

therefore, $S_{p2} = S_p e_k$ - A.2.(2)

As $S_p = S_{p1} + S_{p2}$

$$S_{p1} = S_p (1 - e_k) \quad - \text{A.2.(3)}$$

For two capacitors in parallel, the total capacitance C_T is given by $C_T = C_1 + C_2$. Substituting for C from equation A.2.(1)

$$\frac{k_7 D_{kT} S_p}{h_g} = \frac{k_7 D_{k1} S_{p1}}{h_g} + \frac{k_7 D_{k2} S_{p2}}{h_g}$$

Hence eliminating S_{p1} and S_{p2} :

$$D_{kT} = D_{k1}(1 - e_k) + D_{k2} e_k \quad - 6.14.1.(2)$$

ii) Series Capacitance

From Fig. 6.14.1.(1B) it can be seen that $S_{p1} = S_{p2} = S_p$.

Let d_1 = width of capacitor occupied by component 1

d_2 = width of capacitor occupied by component 2

From equation 6.14.1.(1):

$$e_k = \frac{d_2 S_p}{h_g S_p} = \frac{d_2}{h_g}$$

therefore, $d_2 = h_g e_k \quad - A.2.(4)$

As $h_g = d_1 + d_2$

$d_1 = h_g(1 - e_k) \quad - A.2.(5)$

For two capacitors in series, the total capacitance C_T is given by

$$\frac{1}{C_T} = \frac{1}{C_1} + \frac{1}{C_2}$$

Substituting for C from equation A.2.(1)

$$\frac{h_g}{k_7 D_{kT} S_p} = \frac{d_1}{k_7 D_{k1} S_p} + \frac{d_2}{k_7 D_{k2} S_p}$$

Hence eliminating d_1 and d_2 :

$$\frac{1}{D_{kT}} = \frac{(1 - e_k)}{D_{k1}} + \frac{e_k}{D_{k2}} \quad - 6.14.1.(3)$$

A 3

The Results of the Injection Effect Investigation

The figures tabulated in this Section are peak heights (H_p) obtained as described in Section 8.3. The peak heights are given in centimetres and each value represents the average of three recordings.

The system investigated was 45-63 micron ballotini-air.

The results obtained when $U_g = 0.386\text{cm/s}$ are plotted as Fig. 8.3.(2), (p.173) and are therefore not tabulated in this Section.

Table A.3.(1).

UV Chart No.155

Gas Velocity (U_g): 0.360cm/s

Dense Phase Capacitance: 0.468pF

Volume of gas injected, V_i (cm ³)	Distance between injector and plates (cm)									
	2	3	4	5	6	7	8	9	10	
6	6.0	5.8	6.0	6.0	7.0	6.3	7.0	6.8	7.1	
5	4.9	5.3	5.2	5.2	5.8	5.9	5.9	5.9	6.5	
4	4.7	5.0	5.1	5.0	4.8	5.2	5.1	4.8	5.2	
3	3.8	3.6	3.7	3.9	4.1	4.3	4.3	4.0	4.1	
2	3.0	2.8	2.7	2.4	2.4	2.5	2.9	3.0	2.8	
1	1.8	1.5	1.7	1.6	1.7	1.5	1.6	1.4	1.6	
0.5	0.9	0.9	0.9	0.6	0.8	0.5	0.6	0.3	0.2	

Table A.3.(2).

UV Chart No.157

Gas Velocity (U_g): 0.407cm/s

Dense Phase Capacitance: 0.450pF

Volume of gas injected, V_i (cm ³)	Distance between injector and plates (cm)									
	2	3	4	5	6	7	8	9	10	
6	5.9	5.7	5.7	5.5	6.1	6.0	6.9	6.4	7.2	
5	5.8	5.3	5.3	5.6	5.3	5.6	6.6	5.8	6.0	
4	4.8	4.6	4.3	4.7	4.7	5.6	5.2	5.0	5.0	
3	3.7	3.6	4.0	4.0	3.6	4.3	4.2	4.1	4.4	
2	2.6	2.6	2.7	2.8	3.0	3.0	3.3	3.2	3.2	
1	1.5	1.4	1.7	1.5	1.8	1.8	1.9	1.5	1.8	
0.5	0.7	1.3	1.0	0.9	0.8	0.9	0.5	0.6	0.7	

A 4

The Results of the Bubble Stability Investigation

The figures tabulated in this Section are peak heights (H_p) obtained as described in Section 8.4.1. The peak heights are given in centimetres and each value represents the average of three recordings.

This Section has been subdivided as follows:

- A 4.1. Results for the system, 45-63 micron ballotini-air;
- A 4.2. Results for the system, 45-63 micron ballotini-CO₂;
- A 4.3. Results for the system, 45-63 micron catalyst-air;
- A 4.4. Results for the system, 45-63 micron catalyst-CO₂;
- A 4.5. Results for the system, 125-250 micron diakon-air.

A 4.1. System: 45-63 micron diameter ballotini-air

Table A.4.1.(1).

UV Chart No.164

Gas Velocity (U_g): 0.366cm/s

Dense Phase Capacitance: 0.460pF

Volume of gas injected, V_i (cm ³)	Distance between injector and plates (cm)			
	8	11	15	18
1.0	1.9	2.0	1.0	0.8
2.0	3.3	3.0	2.6	1.8
2.5	3.9	3.8	3.6	2.9
3.0	4.6	4.0	3.9	3.5
3.5	5.3	4.7	4.8	3.5
4.0	5.7	5.6	5.3	4.3
5.0	7.1	6.8	7.0	6.3

Table A.4.1.(2).

UV Chart No.170

Gas Velocity (U_g): 0.374cm/s

Dense Phase Capacitance: 0.464pF

Volume of gas injected, V_i (cm ³)	Distance between injector and plates (cm)			
	8	11	15	18
1.0	1.3	1.4	1.1	0.7
2.0	3.3	2.6	2.9	2.6
3.0	4.6	4.4	4.3	4.2
4.0	5.9	6.1	6.0	6.3
5.0	7.1	7.2	7.0	7.3
6.0	8.1	8.2	7.8	7.7

Table A.4.1.(3).

UV Chart No.166

Gas Velocity (U_g): 0.382cm/s

Dense Phase Capacitance: 0.459pF

Volume of gas injected, V_i (cm ³)	Distance between injector and plates (cm)			
	8	11	15	18
0.5	0.9	0.6	0.1	0.0
1.0	1.9	1.6	0.8	0.9
1.5	2.5	2.6	1.9	2.4
2.0	3.0	3.6	2.9	2.5
2.5	4.0	3.8	3.6	3.6
3.0	4.3	4.6	4.2	3.8
4.0	6.0	5.1	6.1	5.9

Table A.4.1.(4).

UV Chart No.171

Gas Velocity (U_g): 0.386cm/s

Dense Phase Capacitance: 0.460pF

Volume of gas injected, V_i (cm ³)	Distance between injector and plates (cm)			
	8	11	15	18
1.0	2.1	1.7	1.4	1.1
2.0	3.0	3.6	3.0	2.9
3.0	4.2	4.3	4.7	4.6
4.0	6.4	5.7	6.6	5.6
5.0	6.6	7.3	8.1	7.3
6.0	7.3	8.1	8.6	7.8

Table A.4.1.(5).

UV Chart No.167

Gas Velocity (U_s): 0.399cm/s

Dense Phase Capacitance: 0.455pF

Volume of gas injected, V_i (cm ³)	Distance between injector and plates (cm)			
	8	11	15	18
0.5	1.0	0.7	0.2	0.0
1.0	1.8	1.9	1.5	1.4
1.5	2.5	2.4	2.1	2.1
2.0	3.1	3.2	2.5	3.2
2.5	3.6	3.6	4.0	3.0
3.0	4.6	4.9	4.7	4.7
4.0	5.8	5.6	6.2	6.9

Table A.4.1.(6).

UV Chart No.168

Gas Velocity (U_s): 0.408cm/s

Dense Phase Capacitance: 0.451pF

Volume of gas injected, V_i (cm ³)	Distance between injector and plates (cm)			
	8	11	15	18
0.5	0.9	0.4	0.4	0.0
1.0	2.0	1.7	1.2	1.3
1.5	2.6	2.6	2.3	2.2
2.0	3.6	3.1	2.8	2.7
3.0	4.5	4.7	4.5	4.5
4.0	5.9	5.7	5.7	6.6
5.0	6.3	6.5	7.1	7.7

Table A.4.1.(7).

UV Chart No.172

Gas Velocity (U_g): 0.416cm/s

Dense Phase Capacitance: 0.455pF

Volume of gas injected, V_i (cm ³)	Distance between injector and plates (cm)			
	8	11	15	18
0.5	0.7	0.8	0.2	0.1
1.0	1.6	2.1	1.4	1.3
2.0	3.1	2.9	3.7	3.2
2.5	4.1	4.0	4.5	4.3
3.0	4.7	5.0	4.9	5.7
4.0	5.8	5.9	6.9	7.1
5.0	6.8	6.7	7.7	7.5

Table A.4.1.(8).

UV Chart No.161

Gas Velocity (U_g): 0.428cm/s

Dense Phase Capacitance: 0.452pF

Volume of gas injected, V_i (cm ³)	Distance between injector and plates (cm)			
	8	11	15	18
0.5	0.7	0.5	0.3	0.3
1.0	1.7	1.7	1.7	1.8
2.0	3.2	3.8	3.8	3.4
3.0	4.4	4.3	4.7	4.9
4.0	5.6	5.8	5.8	5.6
5.0	6.4	7.0	7.7	7.7

Table A.4.1.(9).

UV Chart No.179

Gas Velocity (U_s): 0.440cm/s

Dense Phase Capacitance: 0.440pF

Volume of gas injected, V_i (cm ³)	Distance between injector and plates (cm)			
	8	11	15	18
0.5	1.2	0.9	0.7	0.5
1.0	2.2	2.1	2.1	2.3
1.5	3.0	3.6	3.3	3.5
2.0	3.7	3.8	4.2	5.2
2.5	4.4	4.3	4.8	5.1
3.0	4.7	5.6	6.2	6.5
4.0	5.7	6.6	7.6	7.9

Table A.4.1.(10).

UV Chart No.162

Gas Velocity (U_s): 0.449cm/s

Dense Phase Capacitance: 0.445pF

Volume of gas injected, V_i (cm ³)	Distance between injector and plates (cm)			
	8	11	15	18
0.5	0.7	1.2	1.1	0.7
1.0	1.9	2.5	2.8	2.9
2.0	3.0	3.4	3.8	3.9
3.0	4.0	4.6	5.1	5.6
4.0	4.8	5.3	6.5	7.4
5.0	6.0	6.6	7.5	9.1

Table A.4.1.(11).

UV Chart No.174

Gas Velocity (U_g): 0.457cm/s

Dense Phase Capacitance: 0.445pF

Volume of gas injected, V_i (cm ³)	Distance between injector and plates (cm)			
	8	11	15	18
0.5	1.0	1.1	0.4	0.0
1.0	2.0	2.2	2.6	2.1
1.5	2.5	3.2	3.2	3.6
2.0	2.9	3.6	4.5	4.8
2.5	4.5	4.6	4.6	5.8
3.0	4.5	4.9	5.7	6.1
4.0	5.8	6.3	6.6	7.9

Table A.4.1.(12).

UV Chart No.163

Gas Velocity (U_g): 0.470cm/s

Dense Phase Capacitance: 0.435pF

Volume of gas injected, V_i (cm ³)	Distance between injector and plates (cm)			
	8	11	15	18
0.5	1.0	0.8	0.8	0.5
1.0	2.1	2.3	2.7	2.9
2.0	3.5	3.7	4.2	4.6
3.0	4.0	4.3	5.7	6.2
4.0	4.6	5.4	5.9	6.3
5.0	5.7	6.4	7.2	7.4

A 4.2. System: 45-63 micron diameter ballotini-CO₂

Table A.4.2.(1).

UV Chart No.182

Gas Velocity (U_g): 0.428cm/s

Dense Phase Capacitance: 0.468pF

Volume of gas injected, V_i (cm ³)	Distance between injector and plates (cm)			
	8	11	15	18
1.0	1.4	1.3	0.3	0.4
2.0	3.5	3.0	2.8	2.1
3.0	4.6	4.6	3.9	4.2
4.0	6.5	5.9	5.1	5.8
5.0	7.1	7.5	7.4	6.2

Table A.4.2.(2).

UV Chart No.186

Gas Velocity (U_g): 0.439cm/s

Dense Phase Capacitance: 0.468pF

Volume of gas injected, V_i (cm ³)	Distance between injector and plates (cm)			
	8	11	15	18
1.0	1.7	1.4	0.9	0.7
2.0	3.6	3.0	3.2	2.1
3.0	5.0	5.2	4.3	3.5
4.0	6.3	6.6	5.5	5.0
5.0	6.8	7.3	7.3	5.3
6.0	8.1	8.2	7.7	7.3

Table A.4.2.(3).

UV Chart No.191

Gas Velocity (U_g): 0.442cm/s

Dense Phase Capacitance: 0.460pF

Volume of gas injected, V_i (cm ³)	Distance between injector and plates (cm)			
	8	11	15	18
1.5	2.4	1.9	1.7	1.2
2.0	3.1	2.9	3.0	2.1
3.0	4.6	4.6	4.2	4.2
4.0	6.0	6.0	4.8	5.0
5.0	6.7	7.3	6.3	6.7
6.0	7.3	7.7	7.7	7.0

Table A.4.2.(4).

UV Chart No.183

Gas Velocity (U_g): 0.445cm/s

Dense Phase Capacitance: 0.462pF

Volume of gas injected, V_i (cm ³)	Distance between injector and plates (cm)			
	8	11	15	18
1.0	1.7	1.2	1.0	0.6
2.0	3.8	3.2	3.2	2.7
3.0	4.8	4.9	4.5	4.6
4.0	6.0	6.2	5.5	5.9
5.0	7.2	7.4	6.9	6.5

Table A.4.2.(5).

UV Chart No.187

Gas Velocity (U_g): 0.453cm/s

Dense Phase Capacitance: 0.465pF

Volume of gas injected, V_i (cm ³)	Distance between injector and plates (cm)			
	8	11	15	18
1.0	1.8	1.7	1.0	0.5
2.0	3.5	3.2	3.0	2.6
2.5	4.2	4.0	4.3	3.6
3.0	5.1	4.6	4.4	4.7
3.5	5.4	5.6	5.0	4.9
4.0	6.4	5.7	6.4	5.6
5.0	7.6	7.4	6.5	7.2

Table A.4.2.(6).

UV Chart No.184

Gas Velocity (U_g): 0.464cm/s

Dense Phase Capacitance: 0.459pF

Volume of gas injected, V_i (cm ³)	Distance between injector and plates (cm)			
	8	11	15	18
1.0	1.6	1.4	1.3	1.1
2.0	3.4	3.5	3.5	3.1
3.0	5.1	5.1	5.0	5.3
4.0	6.0	5.8	7.1	6.8
5.0	7.1	7.4	7.5	7.5

Table A.4.2.(7).

UV Chart No.188

Gas Velocity (U_g): 0.474cm/s

Dense Phase Capacitance: 0.46OpF

Volume of gas injected, V_i (cm ³)	Distance between injector and plates (cm)			
	8	11	15	18
1.0	1.9	2.0	1.5	0.8
1.5	2.9	2.5	2.5	2.8
2.0	3.6	3.8	3.9	3.6
2.5	4.3	4.3	4.3	3.9
3.0	5.3	5.1	5.3	4.7
3.5	5.7	5.3	5.8	6.3
4.0	5.9	6.3	6.8	6.5

Table A.4.2.(8).

UV Chart No.185

Gas Velocity (U_g): 0.482cm/s

Dense Phase Capacitance: 0.45OpF

Volume of gas injected, V_i (cm ³)	Distance between injector and plates (cm)			
	8	11	15	18
1.0	2.0	1.7	1.5	1.0
2.0	3.5	3.4	3.9	3.0
3.0	4.8	5.4	5.4	5.9
4.0	6.0	6.1	6.5	6.4
5.0	6.8	7.2	7.6	7.9

Table A.4.2.(9).

UV Chart No.194

Gas Velocity (U_g): 0.489cm/s

Dense Phase Capacitance: 0.452pF

Volume of gas injected, V_i (cm ³)	Distance between injector and plates (cm)			
	8	11	15	18
0.5	0.7	0.4	0.1	0.0
1.0	2.0	1.9	1.8	1.3
1.5	2.7	2.8	3.2	2.9
2.0	3.4	3.8	3.9	4.0
3.0	4.9	5.2	6.1	6.0
4.0	5.9	6.8	7.1	6.5

Table A.4.2.(10).

UV Chart No.189

Gas Velocity (U_g): 0.500cm/s

Dense Phase Capacitance: 0.448pF

Volume of gas injected, V_i (cm ³)	Distance between injector and plates (cm)			
	8	11	15	18
0.5	0.9	0.8	0.8	0.0
1.0	2.2	2.4	2.2	1.9
1.5	3.2	3.1	3.3	2.6
2.0	3.7	3.8	4.3	4.2
2.5	4.4	4.6	5.1	5.1
3.0	4.8	5.4	5.9	6.0
4.0	6.0	6.2	7.6	6.9

Table A.4.2.(11).

UV Chart No.195

Gas Velocity (U_g): 0.507cm/s

Dense Phase Capacitance: 0.447pF

Volume of gas injected, V_i (cm ³)	Distance between injector and plates (cm)			
	8	11	15	18
0.5	0.8	0.6	0.6	0.0
1.0	2.0	2.3	2.0	1.9
1.5	2.9	3.1	3.5	3.2
2.0	3.8	3.9	4.1	4.0
3.0	5.1	5.0	6.2	6.1
4.0	6.2	6.6	7.7	7.8

Table A.4.2.(12).

UV Chart No.190

Gas Velocity (U_g): 0.518cm/s

Dense Phase Capacitance: 0.445pF

Volume of gas injected, V_i (cm ³)	Distance between injector and plates (cm)			
	8	11	15	18
0.5	0.7	0.7	0.3	0.1
1.0	2.0	2.5	2.5	2.0
1.5	2.9	3.1	3.4	3.6
2.0	3.7	4.3	4.4	4.2
2.5	4.7	5.0	5.5	5.3
3.0	5.0	5.9	6.4	6.3
4.0	6.5	7.3	7.6	7.1

Table A.4.2.(13).

UV Chart No.196

Gas Velocity (U_g): 0.526cm/s

Dense Phase Capacitance: 0.447pF

Volume of gas injected, V_i (cm ³)	Distance between injector and plates (cm)			
	8	11	15	18
0.5	0.7	0.8	0.4	0.1
1.0	1.8	2.0	2.3	2.3
1.5	2.8	3.2	3.5	3.5
2.0	3.6	4.2	4.3	5.0

Table A.4.2.(14).

UV Chart No.197

Gas Velocity (U_g): 0.544cm/s

Dense Phase Capacitance: 0.444pF

Volume of gas injected, V_i (cm ³)	Distance between injector and plates (cm)			
	8	11	15	18
0.5	0.9	0.9	0.7	0.2
0.75	1.6	1.7	1.7	1.1
1.0	2.1	1.9	2.4	2.5
1.5	2.8	2.9	3.5	3.1

A 4.3. System: 45-63 micron diameter catalyst-air

Table A.4.3.(1).

UV Chart No.210

Gas Velocity (U_g): 0.262cm/s

Dense Phase Capacitance: 0.580pF

Volume of gas injected, V_i (cm ³)	Distance between injector and plates (cm)			
	8	11	15	18
1.0	1.7	0.5	0.1	0.1
2.0	3.1	2.5	1.4	1.6
3.0	5.0	3.5	4.0	2.2
4.0	5.4	4.9	3.9	5.0
5.0	5.8	6.2	6.7	5.2

Table A.4.3.(2).

UV Chart No.223

Gas Velocity (U_g): 0.284cm/s

Dense Phase Capacitance: 0.598pF

Volume of gas injected, V_i (cm ³)	Distance between injector and plates (cm)			
	8	11	15	18
3.0	5.1	4.0	3.7	4.3
4.0	5.0	5.8	5.7	6.5
5.0	7.9	7.9	8.5	7.3

Table A.4.3.(3).

UV Chart No.213

Gas Velocity (U_g): 0.303cm/s

Dense Phase Capacitance: 0.575pF

Volume of gas injected, V_i (cm ³)	Distance between injector and plates (cm)			
	8	11	15	18
1.0	1.6	0.9	0.5	0.0
2.0	3.8	3.4	2.9	2.2
3.0	5.0	4.9	5.2	4.4
4.0	6.7	7.4	7.3	7.1
5.0	8.3	8.5	8.7	8.5

Table A.4.3.(4).

UV Chart No.221

Gas Velocity (U_g): 0.324cm/s

Dense Phase Capacitance: 0.006pF

Volume of gas injected, V_i (cm ³)	Distance between injector and plates (cm)			
	8	11	15	18
1.0	2.6	2.5	2.1	1.8
2.0	5.3	5.2	5.8	5.1
3.0	7.6	7.6	6.9	7.8
4.0	9.2	9.8	9.5	9.9

Table A.4.3.(5).

UV Chart No.220

Gas Velocity (U_g): 0.345cm/s

Dense Phase Capacitance: 0.590pF

Volume of gas injected, V_i (cm ³)	Distance between injector and plates (cm)			
	8	11	15	18
0.5	1.4	1.3	0.7	0.5
1.0	3.1	2.9	3.1	2.2
2.0	5.6	5.6	6.4	6.0
3.0	8.4	8.3	8.1	8.6

Table A.4.3.(6).

UV Chart No.215

Gas Velocity (U_g): 0.366cm/s

Dense Phase Capacitance: 0.537pF

Volume of gas injected, V_i (cm ³)	Distance between injector and plates (cm)			
	8	11	15	18
0.5	1.3	1.3	0.5	0.8
1.0	2.8	3.2	2.4	2.8
1.5	4.0	3.9	4.3	5.0
2.0	5.7	5.2	6.0	6.7
3.0	7.3	6.8	7.7	8.2

Table A.4.3.(7).

UV Chart No.214

Gas Velocity (U_g): 0.386cm/s

Dense Phase Capacitance: 0.532pF

Volume of gas injected, V_i (cm ³)	Distance between injector and plates (cm)			
	8	11	15	18
0.25	0.4	0.2	0.0	0.0
0.50	1.5	1.2	1.1	0.5
1.0	2.6	3.0	2.6	2.5
2.0	5.0	5.1	5.4	6.4
3.0	6.4	6.6	6.8	8.9
4.0	7.0	7.8	10.0	10.0

Table A.4.3.(8).

UV Chart No.216

Gas Velocity (U_g): 0.408cm/s

Dense Phase Capacitance: 0.542pF

Volume of gas injected, V_i (cm ³)	Distance between injector and plates (cm)			
	8	11	15	18
0.25	0.5	0.2	0.1	0.0
0.50	1.5	1.4	2.2	1.4
0.75	2.4	2.4	2.9	3.0
1.0	2.9	3.7	3.6	4.7
2.0	6.2	6.8	6.9	7.6

Table A.4.3.(9).

UV Chart No.212

Gas Velocity (U_g): 0.428cm/s

Dense Phase Capacitance: 0.513pF

Volume of gas injected, V_i (cm ³)	Distance between injector and plates (cm)			
	8	11	15	18
1.0	2.7	3.2	3.7	4.0
2.0	5.1	5.9	6.4	8.0
3.0	6.4	6.6	8.9	8.9
4.0	6.7	9.1	10.0	10.5
0.50	1.5	1.5	1.8	1.5
0.25	0.5	0.3	0.4	0.0

Table A.4.3.(10).

UV Chart No.217

Gas Velocity (U_g): 0.449cm/s

Dense Phase Capacitance: 0.535pF

Volume of gas injected, V_i (cm ³)	Distance between injector and plates (cm)			
	8	11	15	18
0.25	0.7	0.8	0.7	0.4
0.50	1.7	2.0	2.3	2.3
0.75	2.6	2.8	3.4	4.3
1.0	3.2	4.0	4.7	5.8
2.0	5.7	6.3	7.8	8.7

Table A.4.3.(11).

UV Chart No.218

Gas Velocity (U_g): 0.470cm/s

Dense Phase Capacitance: 0.516pF

Volume of gas injected, V_i (cm ³)	Distance between injector and plates (cm)			
	8	11	15	18
0.25	0.9	0.9	1.1	0.9
0.50	2.0	2.3	3.0	3.5

Table A.4.3.(12).

UV Chart No.219

Gas Velocity (U_g): 0.470cm/s

Dense Phase Capacitance: 0.520pF

Volume of gas injected, V_i (cm ³)	Distance between injector and plates (cm)			
	8	11	15	18
0.16	0.4	0.3	0.0	0.0
0.25	1.0	1.3	1.8	1.8
0.40	2.0	2.2	2.9	3.3

Table A.4.3.(13).

UV Chart No.224

Gas Velocity (U_g): 0.511cm/s

Dense Phase Capacitance: 0.502pF

Volume of gas injected, V_i (cm ³)	Distance between injector and plates (cm)			
	8	11	15	18
0.16	0.4	0.3	0.1	0.0
0.20	0.6	0.8	0.8	1.2
0.25	1.0	1.3	1.6	1.6

A 4.4. System: 45-63 micron diameter catalyst-CO₂

Table A.4.4.(1).

UV Chart No.233

Gas Velocity (U_g): 0.344cm/s

Dense Phase Capacitance: 0.655pF

Volume of gas injected, V_i (cm ³)	Distance between injector and plates (cm)			
	8	11	15	18
1.0	2.8	1.9	0.8	1.2
2.0	5.4	5.0	3.2	2.2
3.0	7.0	7.6	6.2	4.7
4.0	7.2	8.6	7.4	8.2

Table A.4.4.(2).

UV Chart No.229

Gas Velocity (U_g): 0.380cm/s

Dense Phase Capacitance: 0.660pF

Volume of gas injected, V_i (cm ³)	Distance between injector and plates (cm)			
	8	11	15	18
0.5	1.5	1.3	0.9	0.7
1.0	3.6	4.0	2.6	3.2
2.0	5.7	6.6	6.4	6.3
3.0	8.5	8.6	7.4	8.8
4.0	10.5	10.9	10.9	11.2

Table A.4.4.(3).

UV Chart No.225

Gas Velocity (U_g): 0.416cm/s

Dense Phase Capacitance: 0.670pF

Volume of gas injected, V_i (cm ³)	Distance between injector and plates (cm)			
	8	11	15	18
0.5	1.9	2.5	1.7	1.3
1.0	5.3	5.2	5.3	5.1
2.0	8.8	8.0	10.0	9.1
0.75	3.4	3.6	3.2	3.6
1.5	6.4	6.7	7.0	6.7

Table A.4.4.(4).

UV Chart No.230

Gas Velocity (U_g): 0.444cm/s

Dense Phase Capacitance: 0.615pF

Volume of gas injected, V_i (cm ³)	Distance between injector and plates (cm)			
	8	11	15	18
0.25	0.8	0.3	0.2	0.0
0.32	1.2	1.3	1.0	1.0
0.50	2.1	2.4	2.4	2.4
0.75	3.5	3.4	3.9	4.0

Table A.4.4.(5).

UV Chart No.228

Gas Velocity (U_s): 0.452cm/s

Dense Phase Capacitance: 0.612pF

Volume of gas injected, V_i (cm ³)	Distance between injector and plates (cm)			
	8	11	15	18
0.25	0.9	0.6	0.3	0.1
0.32	1.4	1.3	1.4	1.3
0.40	1.9	2.0	2.5	2.5
0.50	2.2	2.3	2.5	2.7
1.0	4.2	4.5	5.1	5.7
1.5	5.9	6.4	7.5	8.7

Table A.4.4.(6).

UV Chart No.231

Gas Velocity (U_s): 0.470cm/s

Dense Phase Capacitance: 0.590pF

Volume of gas injected, V_i (cm ³)	Distance between injector and plates (cm)			
	8	11	15	18
0.25	0.8	0.6	0.6	0.2
0.32	1.3	1.5	1.2	1.5
0.40	1.8	2.2	2.3	2.4

Table A.4.4.(7).

UV Chart No.226

Gas Velocity (U_g): 0.489cm/s

Dense Phase Capacitance: 0.605pF

Volume of gas injected, V_i (cm ³)	Distance between injector and plates (cm)			
	8	11	15	18
0.2	0.6	0.4	0.2	0.0
0.25	1.2	1.2	1.5	0.6
0.32	1.4	1.6	2.0	1.8
0.5	2.5	3.1	3.4	3.5
1.0	4.3	5.4	6.0	7.7
1.5	6.3	6.6	8.5	9.3

Table A.4.4.(8).

UV Chart No.227

Gas Velocity (U_g): 0.526cm/s

Dense Phase Capacitance: 0.582pF

Volume of gas injected, V_i (cm ³)	Distance between injector and plates (cm)			
	8	11	15	18
0.16	0.5	0.1	0.1	0.0
0.25	1.3	1.5	1.5	1.7
0.50	2.9	3.3	3.9	4.3

Table A.4.4.(9).

UV Chart No.232

Gas Velocity (U_g): 0.543cm/s

Dense Phase Capacitance: 0.560pF

Volume of gas injected, V_i (cm ³)	Distance between injector and plates (cm)			
	8	11	15	18
0.16	0.5	0.6	0.2	0.0
0.20	0.8	1.0	1.0	0.6
0.25	1.3	1.7	1.8	2.1

A 4.5.

System: 125-250 micron diameter diakon-air

Table A.4.5.(1):

UV Chart No.198

Gas Velocity (U_g): 3.03cm/s

Dense Phase Capacitance: 0.298pF

Volume of gas injected, V_i (cm ³)	Distance between injector and plates (cm)			
	8	11	15	18
2.0	1.2	1.5	1.1	0.2
3.0	1.2	1.9	1.6	1.7
4.0	2.2	2.1	2.2	2.4
5.0	2.5	2.3	3.1	4.0

Table A.4.5.(2):

UV Chart No.199

Gas Velocity (U_g): 3.16cm/s

Dense Phase Capacitance: 0.295pF

Volume of gas injected, V_i (cm ³)	Distance between injector and plates (cm)			
	8	11	15	18
2.0	1.1	0.9	1.3	0.6
3.0	1.5	1.8	2.0	2.0
4.0	1.9	2.5	2.7	2.7
5.0	2.8	2.6	3.1	3.5

Table A.4.5.(3).

UV Chart No.201

Gas Velocity (U_g): 3.44cm/s

Dense Phase Capacitance: 0.295pF

Volume of gas injected, V_i (cm ³)	Distance between injector and plates (cm)			
	8	11	15	18
1.0	0.2	0.2	0.7	0.0
1.5	0.8	0.7	1.2	0.1
2.0	1.0	1.0	1.3	1.4
3.0	2.1	2.2	2.4	2.3
4.0	2.6	2.9	2.7	3.2

Table A.4.5.(4).

UV Chart No.202

Gas Velocity (U_g): 3.60cm/s

Dense Phase Capacitance: 0.296pF

Volume of gas injected, V_i (cm ³)	Distance between injector and plates (cm)			
	8	11	15	18
1.0	0.8	0.4	0.1	0.0
1.5	1.2	0.9	1.0	0.4
2.0	1.3	1.3	1.6	1.3
3.0	2.3	2.4	2.5	3.0
4.0	2.8	3.1	3.2	3.2

N O M E N C L A T U R E

A_1	Cross sectional area of the bed.	cm^2
A_2	Constant for a given system.	cm/s
A_3	ρ_f/ρ_p	
A_b	Projected area of a bubble, measured in a vertical plane.	cm^2
A_{ab}	Surface area of the cap of a bubble.	cm^2
A_{bb}	Surface area of the base of a bubble.	cm^2
a	U_b/U_i	
B_1	Gas flow per unit cross section through bubbles at a given height in the bed.	cm^3/s
C, C_T	**Capacitance.	pF
C_1, C_2		
C_3	Capacitor (Fig. 5.5.1.(1)).	pF
C_4	Capacitor (Fig. 5.5.1.(2)).	pF
ΔC	Capacitance change.	pF
D_b	Maximum bubble diameter.	cm
D_c	Diameter of bed container.	cm
D_e	Equivalent diameter of a bubble of volume V_b .	
	$D_e = \sqrt[3]{(6V_b)/\pi}$	cm
D_k, D_{kT}	**Dielectric constant.	
D_{k1}, D_{k2}		
D_{km}	Dielectric constant of a solid-fluid mixture.	
D_s	Maximum stable arch diameter.	
d_1, d_2	**Width of capacitor plate occupied by material.	cm
d_p	Diameter of a particle.	micron $\text{cm} \times 10^{-4}$

E_s, E_u	*Voltage.	volt
e_b	Ratio of total bubble volume in the bed to the total bed volume.	
e_{ab}	Dense phase voidage above a bubble.	
e_{bb}	Dense phase voidage below a bubble.	
e_{bm}	Minimum value of e_b .	
e_i	Voidage of the dense phase.	
e_k	Voidage of a mixed phase capacitor.	
e_{mb}	Dense phase voidage of a bed fluidised at U_{mb} .	
e_o	Dense phase voidage at incipient fluidisation.	
Fr	Froude Number = $U_o^2/g d_p$	
$f(e_i)$	Function of bed voidage.	
G_a	Volumetric flow rate in the VA flow meter at pressure P_a .	cm^3/s
G_c	Volumetric flow rate in the VA flow meter at pressure P_c .	cm^3/s
G_m	Volumetric flow rate recorded by the calibration meter at pressure P_m .	cm^3/s
G_t	Volumetric flow rate in the VA flow meter at pressure P_t .	cm^3/s
G_v	Volumetric gas flow rate.	cm^3/s
g	Gravity - acceleration.	cm/s^2
H_p	Peak height; the galvanometer displacement equivalent to the bubble volume causing the capacitance change. $H_p = (h_p + x_{pf} - x_{pl})$	cm
h_c	Height of a fluidised bed.	cm
h_g	Plate gap.	cm
h_o	Bed height at incipient fluidisation.	cm
h_m	Minimum distance a bubble of volume just less than V_{bs} must travel to be completely absorbed in a bed fluidised at a given value of U_s .	cm

h_p, h_p^1	Chart distance equivalent to the decrease in capacitance when a bubble passes between the plates of the probe (Fig. 6.6.1.(1)).	cm
h_s	Distance travelled by a bubble.	cm
h_t	Plate height.	cm
h_w	Plate width.	cm
I_s, I_u	*Current.	amp
K	Bubble growth rate constant.	cm
$k_1 - k_{10}$	Constant.	
M	d_p or h_o in Romero and Johanson ⁽⁵⁰⁾ correlation.	cm
N_{1s}, N_{2s}	*Number of turns on a winding of a transformer.	
N_{1u}, N_{2u}		
$n_1 - n_3$	Constant for a given system.	
P	Pressure.	mm Hg
P_a	Atmospheric pressure.	mm Hg
P_c	Pressure in the VA flow meter at calibration.	mm Hg
P_m	Calibration meter operating pressure.	mm Hg
P_r	Pressure in a VA flow meter tube.	mm Hg
P_t	Pressure in the VA flow meter when recording flow rates.	mm Hg
ΔP	Bed pressure drop.	cm H ₂ O
Q_b	Observed bubble flow (frequency x volume).	cm ³ /s
Q_d	Gas flow through the dense phase.	cm ³ /s
q_f	Kinematic viscosity of the fluid.	cm ² /s
R_1	Resistor (Fig. 5.4.(1)).	ohm
R_{2-5}	Resistor (Fig. 5.5.1.(1)).	ohm
R_{6-8}	Resistor (Fig. 5.5.1.(2)).	ohm
Re_a	Reynolds Number for a fluidised bed fluidised at a velocity, U_s	
	$= \frac{\rho_f U_s d_p}{\mu_f (1-e_t)}$	

Re_b	Reynolds Number for a bubble. $= \frac{D_e U_b \rho_f}{\mu_f}$ for a gas bubble in a liquid. $= \frac{D_e U_b \rho_p (1-e_i)}{\mu_a}$ for a gas bubble in a fluidised bed.	
Re_p	Reynolds Number with respect to a particle $= \frac{U_t d_p \rho_f}{\mu_f}$	
R_d	Theoretical damping resistance.	ohm
R_m	Resistance equivalent to internal meter resistance.	ohm
R_s	Source resistance.	ohm
R_v	e_{ab}/e_{bb}	
R_z	A_{ab}/A_{bb}	
r_n	Radius of curvature of the nose of a bubble.	cm
S_a	Measure of stability.	
S_{ac}	Critical value of S.	
S_p	Plate area = $h_w \times h_t$.	cm ²
S_{p1}, S_{p2}	**Area of a capacitor plate occupied by material.	cm ²
T	Temperature.	Deg C
t	Time.	s
Tr_1, Tr_2	*Transformer.	
U_a	Average gas velocity through a bubble relative to the bubble.	cm/s
U_b	Rate of rise of a bubble.	cm/s
$U_{b\infty}$	Velocity of a bubble when $D_c = \infty$.	cm/s
U_f	U_f = the value of U_s at $e_i = 1$.	cm/s
U_i	Interstitial gas velocity in the dense phase.	cm/s

U_m	Superficial gas velocity equivalent to the minimum volume of gas transported by bubbles in a fluidised bed ($e_{bm} \cdot U_b$).	cm/s
U_{mb}	Maximum superficial fluidising gas velocity for a bed to behave particulate.	cm/s
U_o	Superficial fluid velocity at incipient fluidisation.	cm/s
U_s	Superficial fluid velocity.	cm/s
U_t	Terminal falling velocity of a particle.	cm/s
V_b	Volume of a bubble.	cm ³
V_{bs}	Meta-stable bubble volume.	cm ³
V_c	Volume of the cloud in the dense phase.	cm ³
V_i	Volume of gas injected.	cm ³
V_m	Minimum injected volume to reach the bed surface.	cm ³
w	Included angle of a bubble in degrees.	degree
x_{pl}, x_{pl}^1	*** Chart distance equivalent to an increase in capacitance recorded just before (x_p) or just after (x_p^1) a bubble passes between the plates of the probe.	cm
x_{pf}, x_{pf}^1		
Z_s, Z_u	*Impedance (Fig. 5.3.(1)).	ohm
ρ_f	Density of a fluid.	g/cm ³
ρ_p	Density of the particles.	g/cm ³
μ_a	Viscosity of a fluidised bed.	g/(cm s)
μ_f	Viscosity of a fluid.	g/(cm s)

* Subscript 1 refers to voltage transformer.
 " 2 " " current transformer.
 " u " " unknown side of the bridge.
 " s " " the standard side of the bridge.

** Subscript 1 refers to the discontinuous (solid) phase.
 " 2 " " " continuous (liquid) phase.
 " T " " " summation of the two phases.

*** Subscript f refers to a bubble in a fluidised bed.
 " 1 " " " " in a liquid.

B I B L I O G R A P H Y

1. DAVIDSON, J. F. and HARRISON, D., Fluidised Particles, Cambridge University Press, 1963.
2. HARRISON, D., A.I.Ch.E.-I.Chem.E. Symposium Series No.6, 6:16, (1965), (London: Instn Chem.Engrs).
3. PYLE, D. L.* Ph.D. Thesis, (1965), University of Cambridge.
4. PARTRIDGE, B. A. and ROWE, P. N., Trans.Instn Chem.Engrs 44, T349, (1966).
5. DAVIDSON, J. F. and HARRISON, D., Chem.Eng.Sci. 21, 731, (1966).
6. LOCKETT, M. J., DAVIDSON, J. F. and HARRISON, D., Chem.Eng. Sci., 22, 1059, (1967).
7. MURRAY, J. D., J.Fluid Mech., 22 part 1, 57, (1965).
8. JUDD, M. R.* Ph.D. Thesis, (1965), University of Cape Town.
9. GRACE, J. R. and HARRISON, D., Chem.Eng.Sci. 24, 497, (1969).
10. DAVIES, L. and RICHARDSON, J. F., Trans.Instn Chem.Engrs 44, T293, (1966).
11. DAVIES, R. M. and TAYLOR, G.* Proc.Roy.Soc., A, 200, 375, (1950).
12. DAVIDSON, J. F., PAUL, R. C., SMITH, M. J. and DUXBURY, H. A., Trans.Instn Chem.Engrs, 37, 323, (1959).
13. HARRISON, D. and LEUNG, L. S., Trans.Instn Chem.Engrs 40, 146, (1962).
14. ROWE, P. N. and PARTRIDGE, B. A., Trans.Instn Chem.Engrs 43, T157, (1965).
15. PYLE, D. L. and HARRISON, D., Chem.Eng.Sci. 22, 531, (1967).
16. GRACE, J. R., Can.J.Chem.Eng. 48, 30, (1970).
17. REUTER, H., Chem.Eng.Prog.Symp.Ser. No.62, 62, 92, (1966).
18. STEWART, P. S. B., Trans.Instn Chem.Engrs 46, T60, (1968).
19. ROWE, P. N., Chem.Eng.Sci. 19, 75, (1964).
20. LOCKETT, M. J. and HARRISON, D., "Proc.Int.Symp.on Fluidization", Eindhoven, 257, Netherland University Press, (1967).
21. STEWART, P. S. B., Chem.Eng.Sci. 23, 396, (1968).

22. ROWE, P. N., PARTRIDGE, B. A. and LYALL, E., Chem.Eng.Sci. 19, 973, (1964).
23. ROWE, P. N. and PARTRIDGE, B. A., Chem.Eng.Sci. 18, 511, (1963).
24. PARTRIDGE, B. A. and ROWE, P. N., Trans.Instn Chem.Engrs 44, T335, (1966).
25. HARRISON, D. and LEUNG, L. S., Symposium on the Interaction between Fluids and Particles, London: Instn Chem.Engrs, 127, (1962).
26. ROWE, P. N. and PARTRIDGE, B. A., Symposium on the Interaction between Fluids and Particles, London: Instn Chem.Engrs, 135, (1962).
27. HARRISON, D. and LEUNG, L. S., Trans.Instn Chem.Engrs 39, 409, (1961).
28. SCHUGERL, K., MERZ, M. and FETTING, F.* Chem.Eng.Sci. 15, 39, (1961).
29. SIMPSON, H. C. and RODGER, B. W., Chem.Eng.Sci. 16, 153, (1961).
30. HARRISON, D., DAVIDSON, J. F. and de KOCK, J. W., Trans. Instn Chem.Engrs. 39, 202, (1961).
31. LEUNG, L. S.*, Ph.D. Thesis, (1961), University of Cambridge.
32. RICHARDSON, J. F. and ZAKI, W. N., Trans.Instn Chem.Engrs 32, 35, (1954).
33. GODARD, K., Ph.D. Thesis, (1968), University of Wales.
34. GODARD, K. and RICHARDSON, J. F., Can.J.Chem.Eng. 47, 350, (1969).
35. ASHTON, M. D., SCHOFIELD, C. and VALENTIN, F. H. H., Chem. Eng.Sci. 21, 843, (1966).
36. WINTER, O., A.I.Ch.E.J. 14, No.3, 426, (1968).
37. OSTERGAARD, K., Chem.Eng.Sci. 21, 470, (1966).
38. MORSE, R. D. and BALLOU, C. O., Chem.Eng.Prog. 47, No.4, 199, (1951).
39. DOTSON, J. M., A.I.Ch.E.J. 5, No.2, 169, (1959).
40. LANNEAU, K. P., Trans.Instn Chem.Engrs 38, 125, (1960).
41. ORMISTON, R. M., MITCHELL, F. R. G. and DAVIDSON, J. F., Trans.Instn Chem.Engrs 43, T209, (1965).

42. ANGELINO, H., CHARZAT, C. and WILLIAMS, R., Chem.Eng.Sci. 19, 289, (1964).
43. BAKKER, P. J. and HEERTJES, P. M., Brit.Chem.Eng. 4, 524, (October 1959).
44. BAKKER, P. J. and HEERTJES, P. M., Brit.Chem.Eng. 3, 240, (May 1958).
45. BAKKER, P. J. and HEERTJES, P. M., Chem.Eng.Sci. 12, 260, (1960).
46. JACKSON, R., Trans.Instn Chem.Engrs 41, 13, (1963).
47. ANDERSON, T. B. and JACKSON, R., Chem.Eng.Sci. 19, 509, (1964).
48. RICE, W. J. and WILHELM, R. H., A.I.Ch.E.J. 4, No.4, 423, (1958).
49. WILHELM, R. H. and KWAUK, M., Chem.Eng.Prog. 44, 201, (1948).
50. ROMERO, J. B. and JOHANSON, L. N., Chem.Eng.Prog.Symp.Ser. No.38, 58, 28, (1962).
51. ROWE, P. N., Chem.Eng.Prog.Symp.Ser. No.38, 58, 42, (1962).
52. RUCKENSTEIN, E. and MUNTEAN, O., Can.J.Chem.Eng. 45, 95, (1967).
53. RIETEMA, K., "Proc.Int.Symp.on Fluidization", Eindhoven, 176, Netherland University Press, (1967).
54. ROWE, P. N., Chem.Eng.Sci. 24, 415, (1969).
55. MOLERUS, O., "Proc.Int.Symp.on Fluidization", Eindhoven, 134, Netherland University Press, (1967).
56. RIETEMA, K., "Proc.Int.Symp.on Fluidization", Eindhoven, 154, Netherland University Press, (1967).
57. RICHMOND, O. and GARNER, G. C., Chem.Eng.Sci. 17, 1071, (1962).
58. LEA, R. J., Postgraduate Course in Chem.Eng., University of Aston, (1966).
59. British Scientific Instrument Research Association, private communication, (1968).
60. Ancom Ltd., private communication, (1968).
61. UNO, S. and KINTNER, R. C., A.I.Ch.E.J. 2, No.3, 420, (1956).
62. Wayne Kerr Ltd., private communication, (1968).
63. Langes' Handbook of Chemistry, Revised 10th Edition, (1967).

64. Handbook of Chemistry and Physics, 49th Edition, (Chemical Rubber Company).
65. English Glass Company Ltd., Catalogue 33, Issue 1/866.
66. McCOY, B. J. and MADDEN, A. J., Chem.Eng.Sci. 24, 416, (1969).
67. SCHODES, D., (J. Crossfield Ltd.), private communication.
68. SUTHERLAND, J. P., Chem.Eng.Sci. 19, 839, (1964).
69. DAVIES, L. and RICHARDSON, J. F., Brit.Chem.Eng. 12, No.8, 1223, (1967).
70. SEHMI, H. S., University of Aston, Undergraduate final year project, (1971).

* These works were referred to by other authors but have not been read.